Theoretical mechanisms of information filtering in stochastic single neuron models

D I S S E R T A T I O N

zur Erlangung des akademischen Grades

doctor rerum naturalium
(Dr. rer. nat.)
im Fach Physik
mit Spezialisierung auf dem Gebiet
der Theoretischen Physik

eingereicht an der
Mathematisch-Naturwissenschaftlichen Fakultät
der Humboldt-Universität zu Berlin

von
Herrn Dipl.-Phys. Sven Blankenburg

Präsidentin der der Humboldt-Universität zu Berlin:
Prof. Dr.-Ing. Dr. Sabine Kunst

Dekan der Mathematisch-Naturwissenschaftlichen Fakultät:
Prof. Dr. Elmar Kulke

Gutachter:
1. Prof. Dr. Benjamin Lindner (HU-Berlin, Germany)
2. Prof. Dr. Lutz Schimansky-Geier (HU-Berlin, Germany)
3. Prof. Dr. Susanne Ditlevsen (University of Copenhagen, Danmark)

Tag der mündlichen Prüfung: 05.07.2016

"Was für mich wichtig ist:
ich muss verstehen.
Zu diesem Verstehen gehört
bei mir auch das Schreiben.

Das Schreiben ist noch
mit im Verstehensprozess ...
weil jetzt bestimmte Dinge
festgelegt sind."[1]

Hannah Arendt im Gespräch mit
Günter Gaus in der Sendereihe
"zur person ..." vom 26.10.1964.

[1] 'I'd say the most important thing for me is to understand. For me, writing is part of this process of understanding. Writing is an integral part of the process of understanding ... because certain things have been established.'

Zusammenfassung

Die vorrangige Aufgabe neuronaler Systeme besteht in der Informationsübertragung zeitabhängiger Signale. Diese geschieht in anregbaren Neuronen unter Verwendung von stark nichtlinearen Reaktionen, den sogenannten Aktionspotenzialen - auch 'Spikes' genannt. Diese Signalübertragung kann frequenzabhängig sein (Informationsfilterung) und ermöglichen, dass das Neuron bevorzugt Information über langsame (Tiefpassfilter), schnelle (Hochpassfilter), oder moderate (Bandpassfilter) Signalanteile überträgt.

Die vorliegende Arbeit beschäftigt sich mit Mechanismen, die in Einzelzellmodellen zu einer solchen frequenzabhängigen Informationsübertragung führen können. Um dies zu untersuchen, werden Methoden aus der theoretischen Physik (Statistische Physik) und der Informationstheorie angewandt.

Die Informationsfilterung in mehreren stochastischen Neuronmodellen, in denen unterschiedliche Mechanismen zur Informationsfilterung führen können, werden numerisch und, falls möglich, analytisch untersucht. Die Bandbreite der betrachteten Modelle erstreckt sich von reduzierten strombasierten 'Integrate-and-Fire' (IF) Modellen bis zu biophysikalisch realistischeren leitfähigkeitsbasierten Modellen.

Anhand numerischer Untersuchungen wird aufgezeigt, dass viele Varianten der IF-Neuronenmodelle vorzugsweise Information über langsame Anteile eines zeitabhängigen Eingangssignals übertragen.

Der einfachste Vertreter der oben genannten Klasse der IF-Neuronmodelle wird dahingehend erweitert, dass ein theoretisches Konzept von neuronalem 'Gedächtnis', vermittelst positiver Korrelationen zwischen benachbarten Intervallen aufeinanderfolgender Spikes, integriert wird. Dieses Model wird in zwei Varianten untersucht, die sich einzig durch das Vorhandensein der oben beschriebenen Korrelationen unterscheiden. Dieses Model erlaubt eine analytische störungstheoretische Untersuchung der Auswirkungen positiver Korrelationen auf die Informationsfilterung. Dabei stellt sich heraus, dass das Vorhandensein positiver Korrelationen die Filtereigenschaften des betrachteten Neuronmodelles von Tief- zu Bandpassfilterung verändern.

Um zu untersuchen, wie sich sogenannte 'unterschwelligen Resonanzen' auf die Signalübertragung auswirken, werden Neuronenmodelle mit verschiedenen Nichtlinearitäten anhand numerischer Computersimulationen analysiert. Als wichtige Erkenntnis wird sich dabei herausstellen, dass unterschwellige Resonanzen in nichtanregbaren (linearen) Neuronenmodellen die Signalübertragung in keinster Weise beeinflussen. Jedoch, das Zusammenspiel von unterschwelligen Resonanzen und Nichtlinearitäten, die essentiell für die Anregbarkeit von Neuronmodellen sind, ermöglicht Informationsfilterung.

Abschließend wird die Signalübertragung in einem neuronalen Kaskadensystem, bestehend aus linearen und nichtlinearen Elementen, betrachtet. Die Einfachheit dieses neuronalen Modellsystems erlaubt eine exakte analytische Untersuchung der Filtereigenschaften. Es wird sich zeigen, dass neuronalen Nichtlinearitäten bei der Ausprägung einer Informationsfilterung eine entscheidende Bedeutung zukommt.

Neuronale Nichtlinearitäten bewirken eine gegenläufige Abhängigkeit (engl. "tradeoff") zwischen qualitativer, d.h. frequenzselektiver, und quantitativer Informationsübertragung, welche in allen von mir untersuchten Neuronmodellen beobachtet und diskutiert wird. Diese Arbeit hebt daher die Gewichtigkeit von Nichtlinearitäten in der neuronalen Informationsfilterung hervor.

Abstract

Neurons transmit information about time-dependent input signals via highly nonlinear responses, so-called action potentials or spikes. This type of information transmission can be frequency-dependent and allows for preferences for certain stimulus components. A single neuron can transmit either slow components (low pass filter), fast components (high pass filter), or intermediate components (band pass filter) of a time-dependent input signal. Using methods developed in theoretical physics (statistical physics) within the framework of information theory, in this thesis, cell-intrinsic mechanisms are being investigated that can lead to frequency selectivity on the level of information transmission.

Various stochastic single neuron models are examined numerically and, if tractable analytically. Ranging from simple spiking models to complex conductance-based models with and without nonlinearities, these models include integrator as well as resonator dynamics.

First, spectral information filtering characteristics of different types of stochastic current-based integrator neuron models are being studied, including the perfect (PIF), leaky (LIF), and quadratic (QIF), as well as the exponential (EIF) integrate-and-fire (IF) model. It will be numerically demonstrated that the previous mentioned IF models preferentially encode information about slow components of a time-dependent input signal and therefore act as low pass filters on information.

Subsequently, the simple deterministic PIF model is being extended with a stochastic spiking rule, leading to positive correlations between successive interspike intervals (ISIs). In this simple model, the ISI distribution, as well as the strength of correlations between adjacent ISIs, can be controlled. It will be considered in two variants that solely differ in the presence of positive ISI correlations and therefore allow studying exclusively the effects of positive ISI correlations on the spectral information transmission characteristics. It will be shown that positive ISI correlations can alter the filtering properties of IF models from low to band pass filter.

Thereafter, models are being examined which show subthreshold resonances (so-called resonator models) and their effects on the spectral information filtering characteristics are being investigated by using two distinct neuronal responses: i) the purely (linear) subthreshold response (without spikes), and ii) the (nonlinear) spiking response (resonate-and-fire model). It will be revealed that subthreshold resonances do not change the information filter characteristics of the purely subthreshold response, whereas their effects on the frequency-dependent information transmission of the spiking response become apparent.

Finally, the spectral information filtering properties of stochastic linear-nonlinear cascade neuron models are being researched by employing different static nonlinearities (SNLs). The more 'nonlinear' the transformation gets, the more pronounced the band-pass filtering effect in the presence of subthreshold resonances becomes. This work highlights the consequences of subthreshold resonances in conjunction with cell-intrinsic nonlinearities (fire-and-reset rule, biophysical spike mechanisms, and static nonlinearities), which generally can lead to shape the information transmission characteristics of the neuron model from low to band pass filtering. The trade-off between frequency-dependent signal transmission and the total amount of transmitted information will be demonstrated in all models and constitutes a direct consequence of the nonlinear formulation of the models.

Contents

1 Introduction to single neuron models and information theory **1**
1.1 Introduction . . . 1
1.1.1 'Artificial electricity' and Maxwell's theory . . . 1
1.2 Mathematical models of single excitable neurons . . . 2
1.2.1 From 'animal electricity' to ion channels . . . 2
1.2.2 Levels of single neuron modeling . . . 4
1.3 Characteristics of responses of excitable neurons . . . 6
1.3.1 Spike train statistics . . . 6
1.4 Aspects of neural coding . . . 6
1.4.1 Experimental evidence of information filtering in single neurons . . . 7
1.4.2 Historic approaches to neural coding . . . 7
1.4.3 Concepts of information theory . . . 9
1.4.4 Signal transmission filter characteristics . . . 15
1.5 Outline of this thesis . . . 17

2 Low-pass filtering in integrate-and-fire models **19**
2.1 Introduction . . . 19
2.2 Known results for PIF, LIF, and QIF neuron models . . . 23
2.3 Information transmission characteristics of the EIF model . . . 25
2.4 Summary . . . 33

3 Information filtering effects of positive ISI correlations **35**
3.1 Introduction . . . 35
3.1.1 Experimental evidence of ISI correlations and stochastic thresholds 35
3.1.2 PIF with stochastic threshold and reset distributions . . . 38
3.1.3 Quality factor of information filter . . . 39
3.2 Approaches to model the spontaneous activity . . . 40
3.2.1 Implementing prescribed ISI distributions and correlations . . . 41
3.2.2 Exact analytical expressions for the power spectrum . . . 44
3.3 Approximated power spectra in the presence of a signal . . . 46
3.3.1 Known analytical expressions for weak signals . . . 46
3.3.2 Special choice of the input signal . . . 48
3.3.3 Coherence function between signal and spiking output (theory I) . . . 48
3.4 Comparison between analytical and numerical spectra . . . 49
3.4.1 Theory I versus theory II (regular firing) . . . 52
3.4.2 Theory I versus theory II (rather irregular firing) . . . 53

3.5 Numerical studies of the filtering characteristics . . . 55
3.5.1 The effects of threshold and reset variability . . . 55
3.5.2 The effects of the firing rate . . . 57
3.5.3 The effects of the correlation 'strength' between adjacent ISIs . . . 60
3.5.4 The effects of ISI correlations in different firing regimes . . . 63
3.6 Analytical insights on the effects of ISI correlations . . . 65
3.6.1 Spiking regimes for band-pass filtering (theory I) . . . 66
3.7 Summary & Discussion . . . 74

4 Information filtering in resonator neuron models 79
4.1 Introduction . . . 79
4.2 Neuron models with subthreshold resonances . . . 81
4.2.1 Linear model of the purely subthreshold voltage response . . . 82
4.2.2 Spiking resonate-and-fire neuron model . . . 86
4.2.3 Morris-Lecar neuron model . . . 88
4.2.4 Conductance-based Hodgkin-Huxley neuron model . . . 89
4.3 Signal transmission in the absence of a nonlinearity . . . 91
4.4 Signal transmission with discontinuous nonlinearities . . . 93
4.4.1 Resonate-and-fire neuron model . . . 93
4.5 Signal transmission with continuous nonlinearities . . . 107
4.5.1 Morris-Lecar neuron model with current noise . . . 107
4.5.2 Hodgkin-Huxley neuron model with ion channel noise . . . 111
4.6 Summary and Discussion . . . 114

5 Information filtering in linear-nonlinear cascades 119
5.1 Introduction . . . 119
5.1.1 Example static nonlinearities . . . 121
5.1.2 A measure of 'nonlinearity' . . . 122
5.2 Numerical results for resonator neurons . . . 124
5.2.1 Coherence shape and information rate depend on the nonlinearity 127
5.2.2 Subjecting voltage values to different degrees of nonlinearities . . . 129
5.3 Theoretical approaches . . . 132
5.3.1 Analytical cross-spectrum . . . 133
5.3.2 Analytical power spectrum . . . 134
5.4 Example spectra by using different static nonlinearities . . . 138
5.4.1 The identity static nonlinearity . . . 138
5.4.2 The exponential static nonlinearity . . . 138
5.4.3 The Heaviside static nonlinearity . . . 139
5.4.4 The erf-sigmoidal static nonlinearity . . . 140
5.5 Closed-form expressions for the spectra of LN-cascades . . . 140
5.5.1 Integrator-LN-cascade . . . 140
5.6 Summary & Discussion . . . 147

6 Summary and concluding remarks 149

A Richardson's integration method **155**
A.1 Introduction . . . 155
A.2 Calculation of the power spectrum via spike triggered rate . . . 155

B Information filtering effects of positive ISI correlations **159**
B.1 Raw and standardized moments of the inverse Gaussian ISI density . . . 159
B.2 Approximation of the coherence function at low frequencies . . . 160
B.3 Analytics & numerics for triangular ISI distributions . . . 160
B.3.1 Moments of the triangular ISI density . . . 160
B.3.2 Exact spontaneous power spectrum (max. correlations) . . . 162
B.3.3 The effects of threshold and reset variability . . . 162

C Information filtering in resonator neuron models **165**
C.1 Numerical values of the model parameter sets . . . 165
C.2 Gradually changing the impedance quality . . . 166

D Information filtering in linear-nonlinear cascades **169**
D.1 Frequently used functions . . . 169
D.1.1 Pochhammer symbols . . . 169
D.1.2 Hermite polynomials . . . 169
D.1.3 Gamma function . . . 170
D.1.4 Error functions . . . 170
D.1.5 Hypergeometric functions . . . 170
D.1.6 Incomplete beta function . . . 171
D.2 Generalized expression . . . 171
D.2.1 Cross-correlation . . . 171

Bibliography **173**

Index **194**

1 Introduction to single neuron models and information theory

Abstract | In this chapter, a short but comprehensive overview of the subject of computational neuroscience is given. This overview includes biophysical aspects of excitable neurons and their mathematical modeling as well as an introduction to information theory, which serves as a proper framework to analyze the signal transmission characteristics of those neuron models.

1.1 Introduction

Theoretical physics returns the insights and observations obtained by experiments to mathematical frameworks and models. Those models are then used to explain (qualitatively, and/or quantitatively) and predict real systems. Due to the complexity of the scientific models, computer become the primary tool of modern physicists to falsify those theories. A typical example from theoretical physics is Maxwell's theory of electromagnetism (Maxwell, 1865), which unifies electric as well as magnetic phenomena very elegantly and is able to predict the existence of electromagnetic waves but failed in describing the quantal interaction between electromagnetic waves and matter[1]. 'Although modeling is a central component of modern science, scientific models at best are approximations of the objects and systems that they represent - they are not exact replicas. Thus, scientists always are working to improve and refine models.'(Rogers, 2006)

1.1.1 'Artificial electricity' and Maxwell's theory

When James Clerk Maxwell (1831-1879) published in 1864 his theory on electromagnetism, he referred to the facts collected by several scientists in uncountable hours of

[1]This formulation was later done by Sin-Itiro Tomonaga (1906-1979), Julian Schwinger (1918-1994), and Richard Feynman (1918-1988) culminating in quantum electrodynamics.

experimental and theoretical work. Starting[2] with Hans Christian Oersted's (1977-1851) experimental finding in 1806 that electric currents create magnetic fields and its theoretical description by André-Marie Ampère (1775-1836) fourteen years later and by Carl Friedrich Gauss (1777-1855) in 1855. In 1832, Michael Faraday (1791-1867) discovered that a moving magnet near a loop of wire causes the flow of an electric current - a phenomenon called 'electrical induction'. More than 'just' compiling all results into a set of 20 dynamical equations, Maxwell's theory predicted the phenomenon of generation of electromagnetic waves by the theoretical mechanism of oscillating electrically charged particles (ions). Nine years after Maxwell's death, Heinrich Hertz (1857-1894) were able to discover experimentally those electromagnetic waves in 1888. Ever since, the human race makes daily use of Hertz' discovery in different types of wireless communication ranging from radio, television, to mobile phones.

1.2 Mathematical models of single excitable neurons

1.2.1 From 'animal electricity' to ion channels

Just one year before Hertz' discovery of the 'artificial electromagnetic waves', the Spanish neuroscientist[3] Santiago Ramón y Cajal (1852-1934) explored that cells within the grey matter of the brain are connected with each other via cables - called 'axons' (according to Rudolph A. von Kölliker, 1817-1905) and 'dendrites' (according to Wilhelm His, 1831-1904). This experimental finding by Cajal heralds an era of the so-called 'neuron doctrine'. 65 Years later, the two physiologists Alan Lloyd Hodgkin (1914-1998) and Andrew Huxley (1917-2012) compiled, similar to James Clerk Maxwell, the experimentally observed facts by numerous scientists into a mathematical neuron model. Starting from the very early idea of 'animal electricity' by Luigi Galvani (1737-1798) in the 1780s, which states that the activity in muscles is based on electric currents ('bioelectricity'). Numerous experiments by Alessandro Volta (1745-1827) and Alexander von Humboldt (1769-1859) confirmed Galvani's hypothesis. About the same time as Faraday discovered electrical induction, the Czech anatomist Jan Evangelista Purkyně (1787-1869) described 'drop-like' cells with elongated fiber-like structure in neural tissue. This was the starting signal for modern neuroscience and paved the way for scientists like Cajal and ultimately led to the formulation by Hodgkin and Huxley in 1952(Hodgkin and Huxley, 1952e).

Nowadays, the 'neuron doctrine', which states that neural tissue consists of single elements, the neurons[4] ($\nu\epsilon\tilde{\nu}\rho o\nu$, Greek for nerf, fibre) is verified to high precision. Many neurons are excitable in the presence of external electrical current stimuli, such that a stereotypical elongations (first recorded by Hodgkin and Huxley (1939)), the so-called

[2]This historical overview is based on the article by Sengupta and Sarkar (2003). Biographical data were found in Hoffmann et al. (2004).

[3]This historical overview is based on the works by Costandi (2006); Llinás (2003); Schuetze (1983); Schwiening (2012); Sourkes and Stevenson (1967). Biographical data were found in Hoffmann et al. (2004).

[4]The term 'neuron' for nerve cells is believed to be used for the first time by Heinrich Wilhelm von Waldeyer (1836-1921) in 1891(von Waldeyer-Hartz, 1891).

action potential, of the membrane voltage across the membrane layer[5] is elicited if the input current is strong enough with respect the all-or-none principle[6] of neural excitability. In 1888, Walther Hermann Nernst (1864-1941) derived from basic principles of thermodynamics, that the neuron's equilibrium potential depends on the ratio between ion concentration inside (intracellular) and outside (extracellular) the neuron (Debye et al., 1914), which led to the first (but incorrect[7]) biophysical description of the action potential(Bernstein, 1902). Based on Overton (1902), Hodgkin and Huxley(Hodgkin and Huxley, 1939) were able to publish the first recording of the action potential in the year 1939. In the very same year, the Hertzian dipole was used to announce the illegal invasion of Poland by German troops, which led to the second world war. Hodgkin and Huxley stopped working together and were commissioned to military research (see for example the wonderful book Squire (2011)). After the war, Hodgkin and Huxley published, in what one can call an annus mirabilis of (computational) neuroscience, five influential papers (Hodgkin and Huxley, 1952a,b,c,d,e), which establish a quantitative model of a single neuron including a probabilistic description of the permeability of the neuron's membrane. Similar to Maxwell's equations of electrodynamics, the Hodgkin-Huxley model was able to describe the all-or-non-principle as well as relative refractory periods of neural excitability. The biophysical interpretation of neuronal excitability in terms complex proteins embedded in the membrane layer was first given by Cole and Baker (1941). Nowadays, over 300 different ion channels are known(Hille, 2001). Their interplay between each other and the membrane voltage results in different neuronal mechanisms, such as[8]:

- subthreshold adaptation (resonances),
- suprathreshold adaptation,
- stochastic excitability (in absence of a stimulus),
- short-term memory,
- variable thresholds (relative refractoriness).

Sir John Eccles (1903-1997) and Wilfrid Rall (1922-today) identified the biophysical mechanisms how electrical signals (action potentials) from the neuron's membrane are passed to neighboring neurons via the axon (cable theory by Wilfrid Rall) and synapses

[5]The ion permeable membrane theory dates back to Julius Bernstein (1839-1917) and his influential publication(Bernstein, 1868).

[6]The all-or-none principle seems to date back to Henry Pickering Bowditch (1840-1911), who studied in 1871 the heart muscle by electrical injections(Bowditch, 1871). A historical review about the all-or-none principle can be found in Pareti (2007). It is not known (to the best of my knowledge), why the all-or-none principle is often referred to Lucas (1909) (or even later to Adrian and Zotterman (1926a)) instead of Bowditch (1871).

[7]Bernstein's formulation was incorrect because he neglected in influence of cellular sodium concentration, and thus was not able to describe the upstroke of the action potential completely.

[8]This list is just a selection of neuronal mechanisms that can be modeled within the Hodgkin-Huxley model framework and does not claim to be complete.

(Sir John Eccles), which permit neurons to 'communicate' by exchanging chemical substances, so-called neurotransmitter. Thus, neuronal communication is based on electrical as well as chemical reactions.

1.2.2 Levels of single neuron modeling

As described in the previous section, the biophysical mechanisms behind neural excitability are quite complex. The Hodgkin-Huxley (HH) model offers a phenomenological model, which can be used to study neuronal excitability numerically, i.e. with the help of numerical computer simulations. There exists a whole hierarchy of single neuron modeling, ranging from very realistic multicompartmental neuron models (Level I in Fig. 1.1a) to very reduced firing rate models, so-called black-box neuron models (Level V in Fig. 1.1a). As often observed in science, increasing model complexity comes to the cost of analytical tractability of the model and its consequences(Fig. 1.1b).

A reasonable trade-off between model complexity and numerical as well as analytical tractability is offered by using phenomenological neuron models as the HH model and a simplified variant of it, the so-called Morris-Lecar(Morris and Lecar, 1981) (ML) model. Both neuron models have in common that they exhibit a biophysical plausible dynamical mechanism to generate action potentials. We, therefore, refer those excitable conductance-based neuron models as continuous nonlinear neuron models. A more drastic reduction of neural excitability is done by using so-called fire-and-reset models, in which no dynamical spike mechanisms is implemented, but instead is imposed onto the model by postulating a hard voltage threshold, such that each threshold crossing from below is identified as the beginning of an action potential and is marked as a spike. The voltage dynamic is subsequently reset to a value below the threshold. This procedure mimics the qualitative time course of an action potential. Several variants of reduced fire-and-reset models as well as the complex conductance-based HH and ML models are used to study the signal transmission characteristics of those models in the presence of theoretical mechanisms such as:

- integrator characteristics without memory (Chapter II),
- integrator characteristics with memory (Chapter III),
- resonator characteristics without memory (Chapter IV),
- integrator & resonator characteristics in LN-models (Chapter V).

An even more drastic simplification is done by using so-called linear-nonlinear (NL) cascade neuron models(Ostojic and Brunel, 2011), which involves a transformation of the output of a linear system (L) with a static nonlinearity (N, also abbreviated by SNL). Those NL cascade models can accurately describe the time-dependent firing rate due to a complex time-dependent stimulus(Ostojic and Brunel, 2011). These NL cascade models (see Level IV in Fig. 1.1a) are rather quantitative than qualitative models.

The studies presented in this thesis reveal that the signal transmission in these models depends strongly on the presence of the above-mentioned characteristics in the presence of a nonlinearity (fire-and-reset, biophysical AP mechanism, static nonlinearity). In the

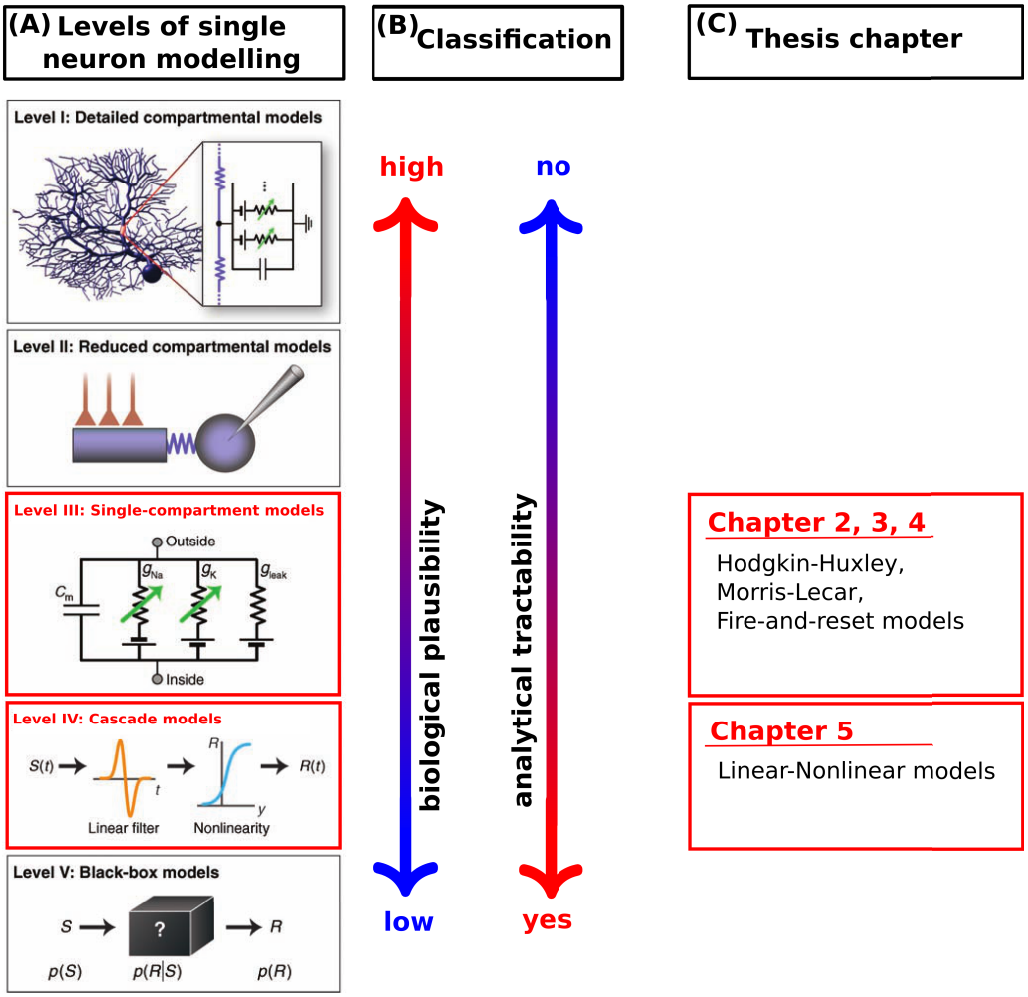

Figure 1.1: Levels of neuronal descriptions and their behavioral relevance. Behavioral goals (A) described by the level of single neuron modeling (B). The subject of this thesis is the understanding of information transmission in single neuron models with moderate biological plausibility and analytical tractability (C). Adopted and modified from Herz et al. (2006). Copyright © 2006, The American Association for the Advancement of Science

next section, we will briefly introduce the reader to the basic concepts of information theory and its application in the field of computational neuroscience.

1.3 Characteristics of responses of excitable neurons

1.3.1 Spike train statistics

Because the shape of an action potential (AP) is believed to be stereotypical for a certain class of neurons, it is very unlikely that the exact form of the AP encoded any information. Thus, one can without loss of generality replace the continuous and non-linear response of the neuron (series of APs) with a binary sequence of delta pulses, so-called spike trains:

$$z(t) = \sum_i \delta\left(t - t_i\right), \tag{1.1}$$

where spikes occur at time points t_i. The reduction of a series of APs to a spike train allows the usage of theoretical concepts of point processes(Cox, 1962). The time-difference between two successive spikes $T_i = t_{i+1} - t_i$ is called the Inter-Spike-Interval (ISI). The two important measures that quantify neuronal activity are the mean firing rate r and the coefficient of variation C_V. In terms of ISIs, the firing rate r:

$$r = \frac{1}{\langle T_i \rangle}, \tag{1.2}$$

and the coefficient of variation C_V:

$$C_V = \frac{\sqrt{\langle \left(T_i - \langle T_i \rangle\right)^2 \rangle}}{\langle T_i \rangle}, \tag{1.3}$$

are obtained by computing the first two moments of the ISI distribution. Where $\langle \cdot \rangle$ means an average over spikes. If the C_V is zero, then the spike-train $z(t)$ is regular (pacemaker cell). A C_V around one indicates a very irregular (almost random) spike train. Bursting activity, which means a multi-modal ISI-distribution is associated with C_V values larger than one.

1.4 Aspects of neural coding

Neurons receive, process, and transmit information about external stimuli (signals) in the brain via pulses of action potentials, which can be reduced to binary responses, so-called spike-trains(Borst and Theunissen, 1999; Rieke et al., 1996). Thus, it seems of importance to answer the question whether neurons can select specific features of a stimulus to feed forward to the information transmission process. A simple classification for time-dependent stimuli, such as natural sounds, is whether a neuron can transmit information preferentially about slow or fast components of the stimulus, or put differently about low or high-frequency components of the time-dependent input signal.

Such frequency selectivity on information can occur as a theoretical mechanism at the single cell level (Droste et al., 2013; Oswald et al., 2004; Vilela and Lindner, 2009), as well as the network level (Middleton et al., 2009; Sharafi et al., 2013). The ability to select

specific components of a stimulus is of great importance in biological environments, such as the electro-sensory system of the paddle fish (Chacron et al., 2003), which enables the paddle fish to distinguish between prey and fellow species in very muddy environments (examples are depicted in Fig. 1.2).

1.4.1 Experimental evidence of information filtering in single neurons

Processing of signals in neuronal systems is in general inherently frequency dependent due to the dynamical properties of the underlying biochemical and biophysical mechanisms. As a result, signals entering a biological subsystem (like a nerve cell) are filtered in the subsystem's response (consisting, for example, the membrane potential of a nerve cell). Often, one encounters low-pass filtering of signals, i.e. the responses to time-dependent signals exhibit largest amplitudes for lower frequencies and attenuate for higher frequencies of the incoming signal. Alternatively, signals can also be high-pass filtered or show band-pass characteristics, i.e. response amplitudes peak in a preferred range of frequencies and decline for lower as well as higher surrounding frequencies. The latter case is also termed "resonant". In neuronal systems, all three signal transmission characteristics are observable, and it is believed that these filtering properties have behavioral consequences (see for example the neural systems depicted in Fig. 1.2 and the references therein).

1.4.2 Historic approaches to neural coding

All living animals are confronted with the problem of gathering information about their environment via sensory organs and processing those input-signals and transferring them into patterns of neuronal activity (ultimately of motor neurons), which results in complex behavior ranging from escaping from predators to finding mating partners. This flow of information about an incoming stimulus often involves the interplay of several hundreds of thousand neurons. However, information transmission in insects often involves only a few hundreds of neurons, and it was recently found out that even single cell stimulation can evoke a change of an animal's behavior. One can classify three approaches to understanding neural coding:

- tuning curve approach,
- Wiener stochastic approach,
- reverse construction approach.

the **tuning curve approach** dates back to the classical works of Adrian and Zotterman (1926a,b), who studied the response of a frog's (R. temporaria) sciatic nerve under physical tension: "For stimulating the end-organs in the muscle we have used weights of 1/4, 1/2, 1, 2, 3 and 5 gram attached to the thread from the muscle and allowed to hang over a light pulley."(Adrian and Zotterman, 1926a) They found out that the now-called firing rate of the sciatic nerve is dependent on the loaded weight, i.e. the stimulus intensity. This classical experiment can be seen as the first formulation of a tuning curve, in

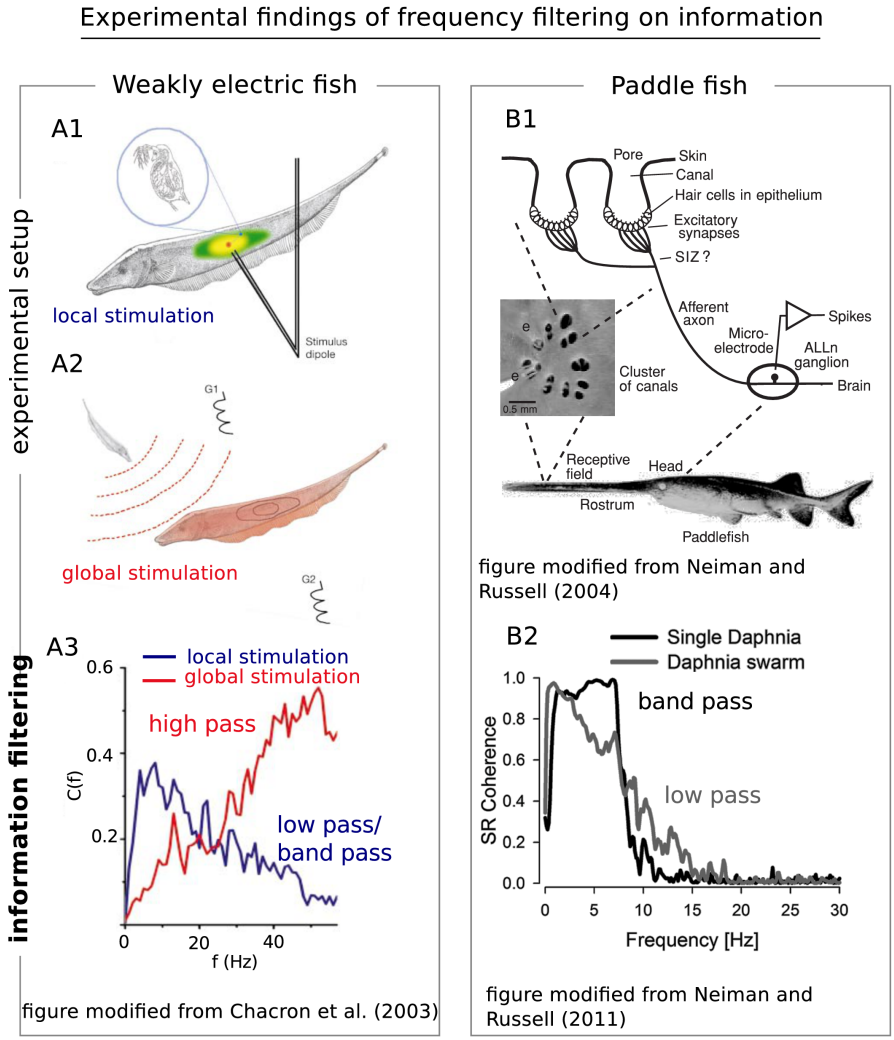

Figure 1.2: Experimental evidence of frequency-dependent information transmission. A1-A3) experiments involving weakly electric fish (Chacron et al., 2003) under local stimulation (mimicking a typical daphnia pray, see A1), and under global stimulation (mimicking a typical conspecific, see A2). Both stimulations lead to different filtering properties of the input signal by using spiking output response (pyramidal neurons). Similar experimental findings (see B1 and B2) in the Paddle fish (Neiman and Russell, 2004, 2011) by using single Daphnia stimuli (black line in B2) and Daphnia swarm stimuli (gray line in B2). Both findings indicate frequency-dependent information transmission for specific natural stimuli (based on the spectral (stimulus-response) coherence function, see Eq.(1.13).

which a map is developed between a static stimulus property (like weight or the direction of moving bars) and the output, often measured as spikes per second, i.e. as firing rate.

Although crucial conclusions were drawn by using the tuning curve approach, like the all-or-non-principle (Adrian, 1926; Bowditch, 1871; Lucas, 1909), it involves two drastic assumptions: i) that static properties of a stimulus are important to "pass on" information about a stimulus to the nervous system, and ii) that this information is encoded (mapped) to a single variable: the firing rate, for example.

A less restricted approach on neural coding is the so-called **Wiener method** (Wiener, 1966) and was introduced to the field of neuroscience by Marmarelis and Marmarelis (1978); Marmarelis and Naka (1972). The aim of the method is to predict the response of a general non-linear system (neuron model) under stimulation with a stochastic input signal (Gaussian white noise), "since with such an input, there is a non-zero probability that any given function over a finite interval of time will be closely represented by some sample of this noise, and therefore, the system will effectively be tested with all possible inputs."(Marmarelis, 1972)

This method involves the so-called Volterra series (Volterra, 2005) expansion of the system's output function (for example the membrane voltage) in terms of linear and non-linear integral operators (consult for example Marmarelis (2012)). Therefore, the task is to identify these integral operators (see for example the classical works Marmarelis (1972); Marmarelis and Udwadia (1976); Udwadia and Marmarelis (1976)) and thus how a time-dependent input signal is encoded into the neuron's output.

Although mathematically equivalent, the third method does not approach the coding question from the how-perspective, but rather from the what-perspective. The **reverse construction approach** (Rieke et al., 1993) asks which spectral components of the stimulus can be reconstructed given the neuron's response, i.e. a frequency resolved input-output characteristics. This approach allows qualitatively, and more important, quantitatively estimations of the encoded information about a time-dependent stimulus in the neuron's output within the framework of information theory(Shannon, 1948).

1.4.3 Concepts of information theory

In order to study the information transmission(Shannon, 1948) characteristics of neurons, we use standard methods in frequency space (Fourier space), which involve the power spectrum of a neuronal output (membrane voltage or spike train), the cross-spectrum between the neuronal output and the time-dependent stochastic input signal, as well as the power spectrum of the input signal. These spectra are the 'building blocks' in order to study the spectral information transmission properties with the help of the stimulus-response coherence function or the response-response coherence function. These spectral measures can (in some rare cases) be approximated analytically[9] (see sec. 3 and sec. 5).

In the following, we will define and discuss all necessary measures to study in an approximate way the spectral information characteristics of neuronal response.

[9]Note that analytical closed form expressions for simple IF neuron models driven by Gaussian white noise can be obtained (see for example the review by Burkitt (2006a)).

Spectral measures of neuronal responses

Because we are interested in the information transmission(Cover and Thomas (1991); Hartley (1928); Shannon (1949, 2001, 1948)) of the neuron model in the frequency domain, we will work in the following only in the frequency domain. Let $x(t)$ be the output of the neuron subjected to the signal $s(t)$. The Fourier transformation of the output will be denoted by a tilde and is for a finite time window of length T defined as:

$$\tilde{x}_T(f) = \int_0^T dt x(t) e^{2\pi i f t}, \tag{1.4}$$

Given the output $x(t)$ and the signal $s(t)$, the power spectrum of $x(t)$ and the cross-spectrum between the output- and the input-signal is given by:

$$S_{\mathrm{x,x}}(f) = \lim_{T\to\infty} \frac{\langle\langle \tilde{x_T}(f)\tilde{x_T}^*(f)\rangle_\eta\rangle_s}{T}, \tag{1.5a}$$

$$S_{\mathrm{x,s}}(f) = \lim_{T\to\infty} \frac{\langle\langle \tilde{x_T}(f)\tilde{s_T}^*(f)\rangle_\eta\rangle_s}{T}, \tag{1.5b}$$

where the star denotes the complex conjugated and the average is performed two-fold. Once for realizations with fixed stimuli (average over the internal noise $\eta(t)$ and once with fixed internal noise (average over external stimuli $s(t)$).

Entropy, Information and the coherence function

Claude E. Shannon's (1916-2001) surprising insight to information transmission states that there is a close connection between the amount of information carried by a technological device and disorder, which is captured in statistical physics(Gibbs, 2014; Jaynes, 1957) by the entropy (Ludwig Boltzmann's (1844-1906) H-theorem, 1872). This connection seems to be counter-intuitive, because in the age of an information society, we are used to gaining information to reduce our uncertainty about our surrounding. However, Shannon did not study the semantical notion of information but the technical one exclusively.

Think of a kitchen with all the tools needed to cook[10]. If the kitchen is very ordered, then from knowing the location of the spoons, one can predict the location of the knives, for example, with a high accuracy. The site of the knives does not encode any further information about the kitchen. In contrast, if the kitchen is in a very messy (disordered) state, then one have to guess from the location of the spoons the place of the knives. One is very surprised when one has found the knives in an ordered kitchen, because of the correlation between the spoons and the knives in an ordered kitchen. In Shannon's viewpoint, it is the randomness which does not surprise. The reason why Shannon's perspective seems to be counter-intuitive is that we, as living animals, are living in a world full of correlations (family, friends, society). However, we have to keep in mind

[10]The following example and interpretation was found in Baecker (2005).

that coherences, in general, are very unlikely. The point of Shannon's information theory is "that the actual message is one selected from a set of possible messages"(Shannon, 1948). Thus, Shannon's measure of information captures the uncertainty of an event. This measure of information increases with increasing disorder.

Shannon would have said, that an unordered kitchen can transmit more information than an ordered one, whereas Boltzmann would have said that the entropy of an unordered kitchen is higher than that of an ordered one. In neuronal context, discussed in this thesis, the set of messages is constituted by Fourier components of a time-dependent input signal (frequency-dependent signal transmission).

According to Boltzmann's H-theorem(Boltzmann, 1872, 2003):

$$S = -k_B \sum_i p_{\mathrm{i}} \log\left(p_{\mathrm{i}}\right), \tag{1.6}$$

where S is called the entropy, k_B is the Boltzmann constant and p_{i} the probability of a microstate with energy E_i, Shannon proposed the Shannon entropy given by(Shannon, 1948):

$$H(P) = -\sum_i p_{\mathrm{i}} \log_2\left(p_{\mathrm{i}}\right). \tag{1.7}$$

This so-called probability mass function $H(P)$ of a set P, where events happen with probability p_{i}, satisfies the following important properties:

$H(P) \geq 0$ (non-negative information),
$H(1) = 1$ (a certain event does not transfer information),
$H(p_1 p_2) = H(p_1) + H(p_2)$ (information due to indep. probabilities is additive).

Given two random variable (x, s), one can define the **joint entropy** (see for example the textbook by Fazlollah (1961)):

$$H(X, S) = -\sum_{x \in X, s \in S} p(x, s) \log_2\left(p(x, s)\right), \tag{1.8}$$

and the **conditional entropy**:

$$H(X|S) = -\sum_{x \in X, s \in S} p(x|s) \log_2\left(p(x|s)\right), \tag{1.9}$$

where $p(x, s)$ is the joint probability function of measuring x and s together. The conditional probability $p(x|s)$ determine the likelihood of observing x given s. To define how much information can be obtained from a random variable (for example a signal, s) by measuring a second variable (for example the response, x), one defines the mutual information between x and s as:

$$I_{\mathrm{x,s}} = H(X) - H(X|S) = \sum_{x \in X, s \in S} p(x, s) \log_2\left(\frac{p(x, s)}{p(x)p(s)}\right). \tag{1.10}$$

In technical as well as natural devices, one encounters the presence of noise $\eta(t)$, which can reduce the mutual information. This noise is additive in the simplest model, i.e. $x = s + \eta$. In the case that the variables x and s are Gaussian distributed with mean $\mu_{\mathrm{x,s}}$ and variance $\sigma_{\mathrm{x,s}}$, one can show that the mutual information (see Eq.(1.10)) is given by(Fazlollah, 1961):

$$I_m = \frac{1}{2}\log_2\left(1 + \frac{\sigma_s^2}{\sigma_\eta^2}\right), \tag{1.11}$$

where $\frac{\sigma_s^2}{\sigma_\eta^2}$ is called the signal-to-noise ratio (SNR).

However, in technical devices as well as in natural circumstances, one does not often measure random variables, but rather time series (Eq.(1.1)). Thus, one can generalize Eq.(1.11) to a stochastic time series $x(t) = s(t)+\eta(t)$, which leads to a lower bound (LB) of the mutual information rate (mutual information per time window) as follows(Borst and Theunissen (1999); Gabbiani (1996)):

$$MI_{LB} = -\int_0^\infty df \log_2\left(1 - C_{\mathrm{x,s}}(f)\right), \tag{1.12}$$

in units of $bits/s$.

Spectral Stimulus-Response coherence function The function $C_{\mathrm{x,s}}(f)$ is called the spectral stimulus-response (SR) coherence function (see for example Rieke et al. (1996); Roddey et al. (2000)), which is defined(Borst and Theunissen (1999)) as:

$$C_{x,s}(f) = \frac{|S_{x,s}(f)|^2}{S_{x,x}(f)S_{s,s}(f)}, \tag{1.13}$$

where $S_{x,x}(f)$ is the power-spectrum of the neuronal output (graded voltage trace or discontinuous spike train) and $S_{x,s}(f)$ the cross-spectrum of the neuron's output and the input signal. The coherence function is a dimensionless quantity, which is bounded to the region $[0, 1]$. It measures which spectral components of the input signal are represented in the response. A value nearby one at a certain frequency indicates that the output carries almost all information of this spectral component of the stimulus, whereas a value close to zero can be interpreted that almost no information of the frequency component of the stimulus is present (encoded) in the output. In Fig. 1.3, a sketch of how signal transmission characteristics in single neuron models can be obtained by using the spectral coherence function. The frequency resolved lower bound mutual information rate density $MI_{LB}(f) = \log_2\left(1 - C_{SR}(f)\right)$ (the integrand in Eq.(1.12)) is a monotonic function of the coherence function. Thus, if the coherence function displays a band-pass filter property, this band-pass filter is also a band-pass filter on information (according to the lower bound expression, see Eq.(1.12)). Eq.(1.12) serves as an upper bound in the linear coding scheme (linear filter). That leads to the question, what

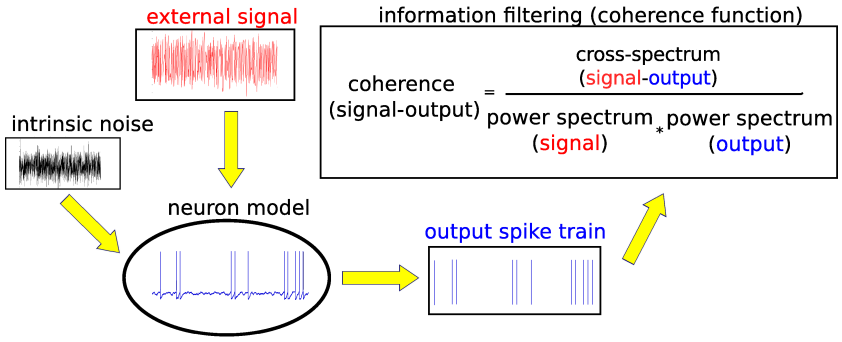

Figure 1.3: Signal transmission in single neuron models based on the spectral SR-coherence function. The interplay between intrinsic neuronal noise sources (ion channel noise, synaptic noise, thermal noise, ...) with a time-dependent external signal leads to a specific neuronal output (spike train, if the neuron is excitable). Based on Fourier transforms, one can measure the signal transmission characteristics with the help of the spectral Stimulus-Response (SR) coherence function (Eq.(1.13)).

one means by saying that the neuron encodes information linear or non-linear? One might be tempted to think that the response of a linear model encodes information linearly, whereas the non-linear spiking response of a neuron encodes non-linearly. This is not true in general. Here, linear and non-linear refers to the characteristics that the best estimate of the stimulus, which for example leads to the elicitation of two spikes, is constructed by using the best estimate for each spike separately and adding up the result. If this is true, then one says that the system encodes information about a time-dependent stimulus linearly. This superposition principle holds true for linear system per definition. For a non-linear system the superposition principle can be fulfilled in certain activity regimes. One can say that if neurons fire at a high rate and very regularly ($CV \approx 0$) then they encode information about a time-dependent stimulus rather linearly, whereas the low-firing and very irregular ($CV \approx 1$) firing activity regime is related to non-linear coding on information. The linear or non-linear coding characteristics has a priori little in common with the linear or non-linear description of neuron models.

Spectral Response-Response coherence function The linear stimulus-response (SR) coherence function Eq.(1.13) can be used to construct a lower bound on the mutual information rate and characterizes an optimal linear filter (Roddey et al., 2000). The spectral response-response (RR) coherence function is defined as (Chacron, 2006; Massot

et al., 2011; Neiman and Russell, 2011; Roddey et al., 2000):

$$C_{\mathrm{RR}}^{s_i(t)}(f) = \frac{\left| \frac{2}{(K-1)K} \sum_{k=1}^{K} \sum_{j=1}^{k} P_{kj}(f) \right|^2}{\left(\frac{1}{K} \sum_{k=1}^{K-1} P_{kk}(f) \right)^2}, \tag{1.14}$$

where $P_{kj}(f)$ is the cross spectrum between the k-th and j-th responses within a frozen stimulus setup (K repetitions of the same stimulus current $s_i(t)$). The RR coherence function in the form of Eq.(1.14) measures the response variability that does not originate from the stimulus. The RR coherence is than afterwards averaged over the set of presented stimuli $s_1(t), ..., s_N(t)$ and reads:

$$C_{\mathrm{RR}}(f) = \frac{1}{N} \sum_{i=1}^{N} C_{\mathrm{RR}}^{s_i(t)}(f). \tag{1.15}$$

The RR coherence function Eq.(1.14) and Eq.(1.15) is bounded to the region from zero to one and satisfies(Neiman and Russell, 2011; Roddey et al., 2000) the following inequality:

$$C_{\mathrm{SR}}(f) \leq \sqrt{C_{\mathrm{RR}}(f)}, \tag{1.16}$$

and thus can be used as an **estimate** of an upper bound (est. UB) of the mutual information rate via (Chacron, 2006; Marsat and Pollack, 2004; Massot et al., 2011; Middleton et al., 2009):

$$MI_{\text{est. UB}} = -\int_0^\infty df \log_2 \left(1 - \sqrt{C_{RR}(f)}\right), \tag{1.17}$$

in units of $bits/s$, as long as the intrinsic noise is Gaussian distributed (Borst and Theunissen, 1999; Massot et al., 2011). One can show, that the following relation between the RR and SR coherence for linear Gaussian stochastic processes holds(Roddey et al., 2000):

$$C_{\mathrm{SR}}(f) = \sqrt{C_{\mathrm{RR}}(f)} \qquad \text{(linear coding)}. \tag{1.18}$$

Please note that the RR coherence is generally not a strict upper bound of the mutual information rate, but is used here rather as a rough estimate of the upper bound of mutual information rate and as an alternative measure of information transfer besides the SR coherence. It will be demonstrated in sec. 3 and sec. 4 (in the discussion) that the RR coherence gives consistent results although counter examples Bernardi and Lindner (2014) exists (in which Eq.(1.16) is violated). A more rigorous approach that leads to a more sophisticated **direct method** in order to calculate a frequency resolved mutual information rate density was developed by Bernardi and Lindner (2014). However, this approach developed by Bernardi and Lindner (2014) is more numerically involved as the

indirectly obtained lower and estimated upper bound of the mutual information rate density via the SR Eq.(1.13) and the RR Eq.(1.14) coherence function, and is thus not applied in this thesis.

1.4.4 Signal transmission filter characteristics

As described above, the coherence function can be utilized in order to classify the frequency-filtering characteristics of a dynamical system. One distinguishes three classes of filters: **i)** a low pass filter, which is characterized by a monotonically decreasing coherence function; **ii)** a band pass filter, which is characterized by a single peak in the cohrence function; and **iii)** a high pass filter, which preferentially encodes information about fast components of a time-dependent signal. These three classes are shown schematically in Fig. 1.4.

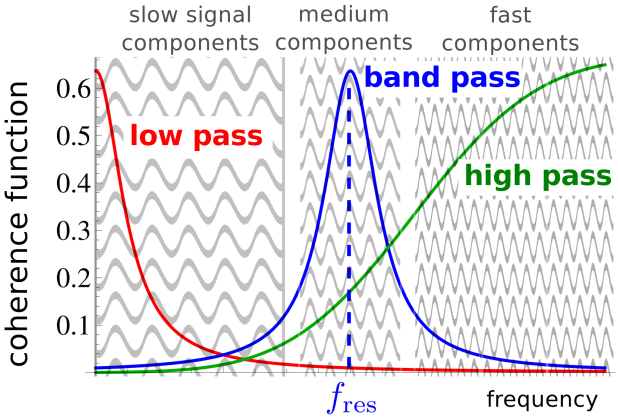

Figure 1.4: Filter characteristics based on the coherence function. Shown are three different information filter characteristics: low pass filter (red), band pass filter (blue), and high pass filter (green) on signal transmission. Slow, medium, and fast components of a time-dependent signal are sketched as Fourier components.

Next, we will briefly discuss two measures in order to describe the phenomenon of frequency-dependent signal transmission (information filtering), namely **i)** the quality factor, and **ii)** the curvature of the coherence function at zero frequency.

A measure to distinguish low from band/high pass filters I: quality factor

We will use throughout this thesis the **quality factor** as a measure of 'peakedness' of an uni-modal spectral function $F(f)$. The quality factor is defined as:

$$Q_{\mathrm{F}} = \frac{F(f_{\mathrm{res}})}{F(f=0)}, \tag{1.19}$$

where the spectral quantity F attains its maximal value at $f = f_{\text{res}}$ (see Fig. 1.5). Quality factors close to one indicate that the frequency of maximum spectral quantity $F(f)$ is close to zero, and thus describe the effect of low-pass filtering, whereas a quality factors much larger than one suggest a filter property different from low pass, i.e. a band pass (a preferred frequency band within an intermediate frequency range) or a high pass filter, which favors high frequencies and attenuates signal transmission for low and intermediate frequencies. In this thesis, low or high frequencies always refers to the inverse time scale of the underlying dynamics of the neuron model and changes with changing time scale. We will use the quality factor in cases, where the coherence

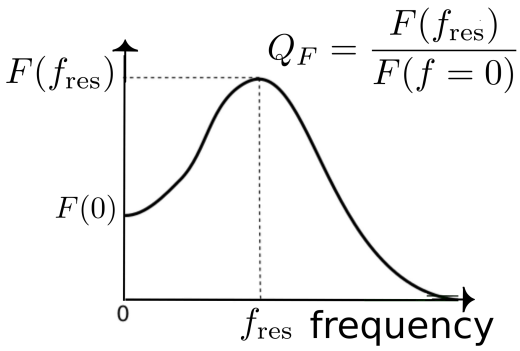

Figure 1.5: Quality factor of a spectral unimodal characteristics. The quality factor measures the deviations from low-pass filtering, i.e. the presence of band- or high-pass filtering properties.

function is described by a rather simple closed form expression, in which an analytical localization of the peak of the coherence function is feasible as well as in numerical studies (see sec. 4).

A measure to distinguish low from band/high pass filters II: curvature

The coherence quality (Eq.(1.19)) relies on the localization of a maximum. An analytical solution of this task is in general very difficult. Thus, in order to classify the filtering properties of single neurons, we will use a measure, that relies solely on the coherence function $C(f)$ at a single frequency, here at zero frequency, and its first ($C^{(1)}(f)$) and second (($C^{(2)}(f)$)) derivative in order to construct the curvature κ_C of the coherence function at zero frequency:

$$\kappa_C\big|_{f=0} = \frac{C^{(2)}(f)}{\left(1 + C^{(1)}(f)C^{(1)}(f)\right)^{3/2}}\Bigg|_{f=0}. \tag{1.20}$$

Because the spectral coherence function is a symmetric function (with respect to zero frequency), its first derivative at zero frequency vanishes identically. Consequently, the

curvature of the coherence function at zero frequency is solely determined by the second derivative of the coherence function at this location, i.e

$$\kappa_{\mathrm{C}}\big|_{f=0} = C^{(2)}(f)\Big|_{f=0}. \tag{1.21}$$

Low pass filters (see red line in Fig. 1.5) are described by a negative curvature at zero frequency (concave function), whereas a positive curvature (convex function) is a sufficient condition for a band pass (see blue and green line in Fig. 1.5). The curvature of the coherence function will be utilized in analytical approaches (see sec. 2, sec. 3 and sec. 5). A theoretical analysis of a resonance in the coherence is presented in sec. B.2.

1.5 Outline of this thesis

First, in sec. 2 the class of integrate-and-fire (IF) type neuron models, ranging from the perfect integrate-and-fire (PIF) to the exponential integrate-and-fire (EIF) is discussed and their signal transmission characteristics is explored by means of numerical and semi-numerical approaches.

Secondly, it is motivated in sec. 3 that an elementary representative of the class of IF neuron models can be modified such that a theoretical mechanism is integrated into the model, which allows studying the effects of positive interspike interval (ISI) correlations on the signal transmission characteristics of the model. These effects are studied with the aid of numerical as well as analytical approaches for the deterministic PIF neuron with a stochastic fire-and-reset rule. It is shown that positive ISI correlations lead to a frequency-specific signal transmission (information filtering).

Having established the effects of positive ISI correlations on the neuronal information filtering characteristics in sec. 3, the effects of so-called subthreshold resonances on the information filtering properties of neuron models is shown and discussed employing extensive numerical studies. These numerical studies involve single neuron models with different nonlinearities, which include a simple fire-and-reset rule (resonate-and-fire) as well as biophysical realistic dynamical spike mechanisms (Morris-Lecar, Hodgkin-Huxley). The effects of several intrinsic and extrinsic single neuron model parameters on the signal transmission characteristics are revealed and discussed.

Next, in sec. 5 rather simplified neuron models: linear-nonlinear cascade models (LN) are introduced, and their signal transmission characteristics are explored using numerical and analytical approaches. Numerical results for the spectra, necessary in order to study the information filtering characteristics, of linear-nonlinear models in the presence of subthreshold resonances are shown and the vital role of static nonlinearities (SNLs) in form of: i) an exponential, ii) a hard threshold (Heaviside step function), and iii) a soft threshold (sigmoidal) is demonstrated. The mathematical simplicity of the single neuron model allows studying the signal transmission characteristics analytically (based on perturbative approaches). In the case of integrator LN cascade models, based on exact analytical expressions for the power and cross-spectrum between the input signal

and the output of the LN model, the signal transmission characteristics is investigated analytically. This exact expressions results in very general predictions of the information filtering characteristics of LN models with and without subthreshold resonances.

Finally, in sec. 6 the results obtained in this thesis are summarized, and a brief outlook on future work regarding the signal transmission characteristics of single neuron models is presented.

2 Low-pass filtering in integrate-and-fire models

Abstract | Here, a brief review of known numerical results of the information filtering characteristics of stochastic integrate-and-fire neuron models (ranging from the perfect, leaky, and quadratic integrate-and-fire models) is shown. By motivating that the exponential integrate-and-fire (EIF) model can reproduce experimentally observed neuronal spiking characteristics, the EIF neuron model and its signal transmission characteristics is studied using numerical and semi-analytical approaches.

2.1 Introduction

Integrate-and-fire (IF) type neuron models (see (Burkitt, 2006a,b) for reviews) have been successfully utilized in order to model single neuron activity (see for example Badel et al. (2008a,b); Rauch (2003)) as well as phenomena observed in in vivo experimental circumstances, by using networks of connected IF models (see for example Brunel and Hakim (1999); Richardson (2008). IF models date back to Lapicque (1907) and their widespread application can be explained by the insight that two timescales govern neuronal behavior. First, the slower subthreshold membrane voltage response, and second, the very fast mechanism that generates suprathreshold (stereotypical) action potentials APs (often reduced to spikes, which translates the series of APs to a point process (Johnson, 1996; Perkel et al., 1967)). Because of the linear subthreshold description and the usage of a hard threshold concept (in order to mimic spikes), one is able to calculate analytically the moments of the interspike interval distribution (ISI), which results in analytical expressions for the firing rate of this neuron model as well as the coefficient of variation C_V (see for example volume 2 of Tuckwell (1988)).

All IF models are commonly described via a first order differential equation (1st order ODE):

$$\tau_m \frac{d}{dt} V(t) = \mu + F(V), \tag{2.1}$$

where $V(t)$ denotes the time-dependent membrane voltage with an intrinsic time scale τ_m and μ the baseline current (constant drift). The nonlinearity functions $F(V)$ are used to model different aspects of subthreshold neuronal behavior. Nonlinear pulsatile (spiking) neuronal responses are mimicked by using a threshold-and-reset concept, such that if the voltage crosses a threshold V_{thresh} from below, a spike (a pointed version of a biophysical action potential, AP) is triggered (fired) and the membrane voltage V is reset to a specific value V_{reset} (below the threshold). This threshold-and-reset concept justifies the notion of an excitable system, which is nonlinear per construction(Izhikevich, 2007).

Specific choices of nonlinearity functions $F(V)$ result in different types of IF neuron models(Burkitt, 2006a), for example:

- perfect IF (PIF):$F(V) = 0$,
- leaky IF (LIF):$F(V) = -V(t)$,
- quadratic IF (QIF):$F(V) = (V(t) - V_0)(V(t) - V_T)$,
- exponential IF (EIF):$F(V) = -V(t) + \Delta_T e^{(V-V_T)/\Delta_T}$,

where $V(t)$ denotes the membrane voltage, V_0 the resting/steady state of V and V_T acts as an effective threshold at which spike initiation cannot be reversed, Δ_T determines the sharpness of this spike initiation. IF models, ranging from the simple PIF (Gerstein and Mandelbrot, 1964), LIF (Lapicque, 1907; Stein, 1965, 1967), QIF (Hansel and Mato, 2001; Izhikevich, 2007; Latham et al., 2000) (which is closely related to the canonical type-I Θ-neuron (Ermentrout, 1996; Latham et al., 2000)), and more realistic EIF (Fourcaud-Trocme et al., 2003) neuron models, are able to reproduce various forms of single neuron spiking statistics. In Fig. 2.1 the experimental findings of Badel et al. (2008b) for the EIF with and without relative refractory period (rEIF and EIF) are shown. Badel et al. (2008b) suggest that the EIF neuron model is well suited to describe neuronal activity (see Fig. 2.1A,B,C) of pyramidal cell activity in mice (see Fig. 2.1D,E). This motivates the study of the the signal transmission characteristics of the EIF neuron model, which is explored within different regimes of neuronal activity, ranging from very regular ($C_V \approx 0$ to very irregular spiking activity ($C_V \approx 1$), in this chapter.

Because of stochasticity (often observed by trial-to-trial variability, see Destexhe and Rudolph-Lilith (2012); van Steveninck et al. (1997)) in neuronal responses, one introduces an additive stochastic current noise, modeled with the help of Gaussian White noise current (see for example Kohn (1997); Ricciardi and Sacerdote (1979); Stein (1967); Tuckwell (1988); Tuckwell and Cope (1980)), onto the membrane voltage dynamics Eq.(2.1). This simple stochastic single neuron model combines different stochastic phenomena observed in real neurons: i) ion channel noise (White et al., 2000), ii) synaptic noise (Hubbard et al., 1967), and iii) thermal noise(Johnson, 1928; Nyquist, 1928), into one stochastic noise current. The stochastic IF neuron models are described by the following subthreshold dynamics:

$$\tau_m \frac{d}{dt} V(t) = \mu + F(V) + \sqrt{D}\eta(t), \tag{2.2}$$

where D is the amplitude of the stochastic input current and $\eta(t)$ is normally distributed with zero mean and uncorrelated, i.e. $< \eta(t)\eta(t') >= \delta(t-t')$. In addition to the purely subthreshold description of the single neuron model (Eq.(2.2)), a simple nonlinearity in form of a fire-and-reset rule is implemented such that a fixed membrane voltage threshold V_T is introduced. If the membrane voltage $V(t)$ exceeds this voltage threshold V_T, then a spike is elicited and the neuron model dynamics is reset. This results in a 'pulsatile' neuron response (spike train, see Fig. 2.1A,B), which mimics biophysical action potentials (APs).

Although highly simplified, such stochastic versions of the IF neuron models offer theoretical insights even in analytical perturbation approaches (diffusion approximation, see for example Brunel and Hakim (1999); Johannesma (1968); Lindner et al. (2005); Stein (1965); Tuckwell (1988)). These analytical studies focus mainly on analytical expressions for the first-passage time and the associated interspike interval (ISI) density (Darling and Siegert, 1953; Lindner, 2004) and its moments (Lindner et al., 2003), and spectral quantities like the spike train power spectrum of stochastic IF models by using Fokker-Planck equations(Lindner et al., 2002).

Two important statistics regarding the regime of spiking neuronal responses are i) the mean firing rate r, and ii) the coefficient of variation CV (see sec. 1.4.3). Both, firing rate and CV, are statistics of the ISI distribution and quantify the strength of neuronal response (firing rate) and the variability of a neuronal spike train (CV):

$$r = \frac{1}{< ISI >}, \qquad CV = \frac{\sigma_{\mathrm{ISI}}}{< ISI >}, \tag{2.3}$$

where σ_{ISI} denotes the standard deviation of the ISI distribution. Large variability in the spike train (phasic firing is described by a CV close to one ($CV \approx 1$), whereas very regular (tonic) firing patterns are described by a CV close to zero (vanishing ISI variability). Both firing regimes are relevant in neuronal systems. Regular firing activity describes a neuronal 'clock'(Jaeger, 2011), whereas very phasic spiking activity can account for neuronal variability(Schaette et al., 2005; Stein, 1967; van Steveninck et al., 1997).

To study the spectral information filtering properties of stochastic IF neuron models, we will study the spectral stimulus-response coherence function (Eq.(1.13)) between the output spike train (or short spike) and the input signal (short signal):

$$C_{\mathrm{spike,signal}}(f) = \frac{S_{\mathrm{spike,signal}}(f)}{S_{\mathrm{spike,spike}}(f) \cdot S_{\mathrm{signal,signal}}(f)}. \tag{2.4}$$

Here, $S_{\mathrm{spike,signal}}(f)$ denotes the cross-spectrum between the response and the signal, and $S_{\mathrm{spike,spike}}(f)$ as well as $S_{\mathrm{signal,signal}}(f)$ refers to the power spectrum of the spike train and the power spectrum of the input signal respectively. As described in sec. 1.4.3, the stimulus-response coherence function can be used as a lower bound of spectral signal transmission. The coherence function is a normalized spectral characteristic between zero and one. Very low values within a certain frequency range indicate that the signal transmission (in this frequency band) is very low. If the coherence function is close to one in a certain frequency region, then the signal transmission is enhanced within this

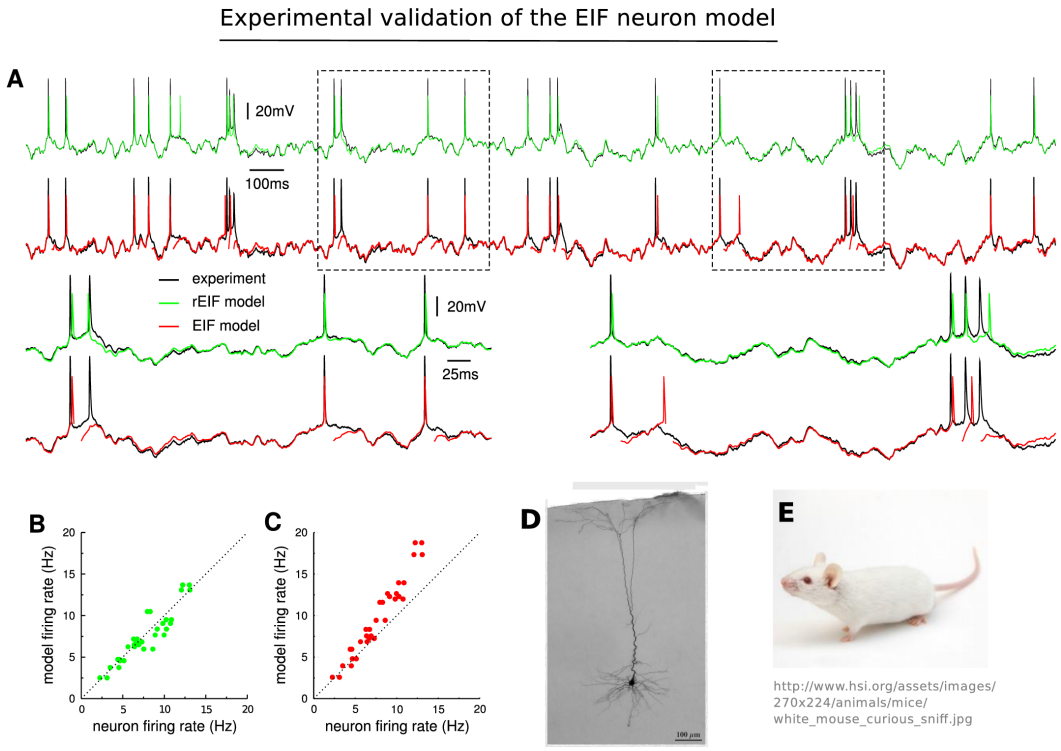

Figure 2.1: Experimental validation of the EIF neuron model. A) example voltage traces for recorded data from layer 5 pyramidal neurons in mice (black line) and EIF with relative refractory period (rEIF, green line) and the standard EIF Eq.(2.5) (red line) are shown. Inset shows the zoomed in voltage traces. The steady state firing rate of the rEIF (B) and the EIF (C) matches the recorded data. An example pyramidal cell of layer 5 (D) in the mice (E) cortex is shown. A,B,C are adopted from Badel et al. (2008b), D is adopted from Hattox and Nelson (2007).

frequency region. One classifies three types of signal transmission characteristics (see Fig. 1.4):

- low pass (transfer about slow freq. components is preferred),
- band pass (transfer about interm. freq. components is preferred),
- high pass (transfer about high freq. components is preferred).

A rigorous mathematical classification between the filtering characteristics involves the identification of global maxima of the coherence function. Here, we will use the curvature of the coherence function at zero frequency as a proxy of the transmission characteristics to distinguish low from band/high pass filter. If the curvature is negative, then this measure suggests a low pass filter on information, whereas a positive curvature at zero frequency indicates a deviation from low-pass filtering, i.e. a band/high pass filter characteristics. This measure between a band- and a low-pass filter is not mathematically

rigorous, but is rather an approximation of a stringent classifier between the two classes of filtering characteristics. An analytical measure to distinguish a band pass filter from a low pass filter is in general difficult to obtain, because it involves an analytical expression for the coherence function, and therefore for the necessary spike train power spectrum and the squared cross-spectrum. Those spectra are tough to be obtained and are only for a few examples (PIF and LIF driven by weak Gaussian white noise) known(Burkitt, 2006a).

All statistics, r, CV (see Eq.(2.3)), spectral coherence function Eq.(2.4) and its associated information theoretical characteristics. Namely, the lower bound of mutual information (see Eq.(1.12)), and its curvature at zero frequency will be used in the following to study the spectral information filtering properties of these IF neuron models in different firing activity regimes (from very phasic to very tonic firing activity).

First, we will recapitulate in sec. 2.2 known theoretical results regarding the spectral signal transmission properties of the PIF, LIF, and QIF obtained by Vilela and Lindner (2009). We will extend this study in sec. 2.3 to the EIF neuron model variants.

2.2 Known results for PIF, LIF, and QIF neuron models

Here, we will briefly review the theoretical results obtained by Lindner (2012); Vilela and Lindner (2009) concerning the information transmission characteristics of the stochastic perfect (PIF, also called Wiener Process), leaky (LIF, also called Ornstein-Uhlenbeck model(Kostal et al., 2007; Lánský and Rospars, 1995; Ricciardi and Sacerdote, 1979; Shinomoto et al., 1999; Uhlenbeck and Ornstein, 1930)), and the quadratic integrate-and-fire (QIF) neuron models based on the spectral coherence function between the output spike train and the stochastic input signal Eq.(2.4).

Fig. 2.2 shows the main findings obtained by Vilela and Lindner (2009) for the stochastic PIF, LIF, and QIF neuron models Eq.(2.2). As one can infer from Fig. 2.2A-I, all three neuron models, which are driven by Gaussian white current noise, act as a low pass filter on information. This filtering property is irrespective of the spiking activity regime, i.e. from very regular firing activity ($CV \approx 0.1$) to more irregular spike patterns, characterized by a CV close to one. Consequently, the PIF, LIF, and QIF transmit information about a time-dependent (here stochastic) input current preferentially at low frequencies.

The structure of Fig. 2.2 is such that the firing rate is held constant in each row, and the CV varies from regular to more irregular spiking activities (see Fig. 2.2A-C,D-F,G-I. The coherence function is always a decreasing function of frequency and consequently, characterizes a low pass filter on information, i.e. most information is transmitted about slow components of the input signal, whereas the signal transmission for faster components is attenuated. Thus, the PIF, LIF, and QIF neuron models do not show a preferred frequency of signal transmission. This lowpass filtering is due to the integrating behavior, which is a key feature of the one-dimensional description of the neuron model (see Eq.(2.1)).

In the next section, we will study in more detail the information transmission char-

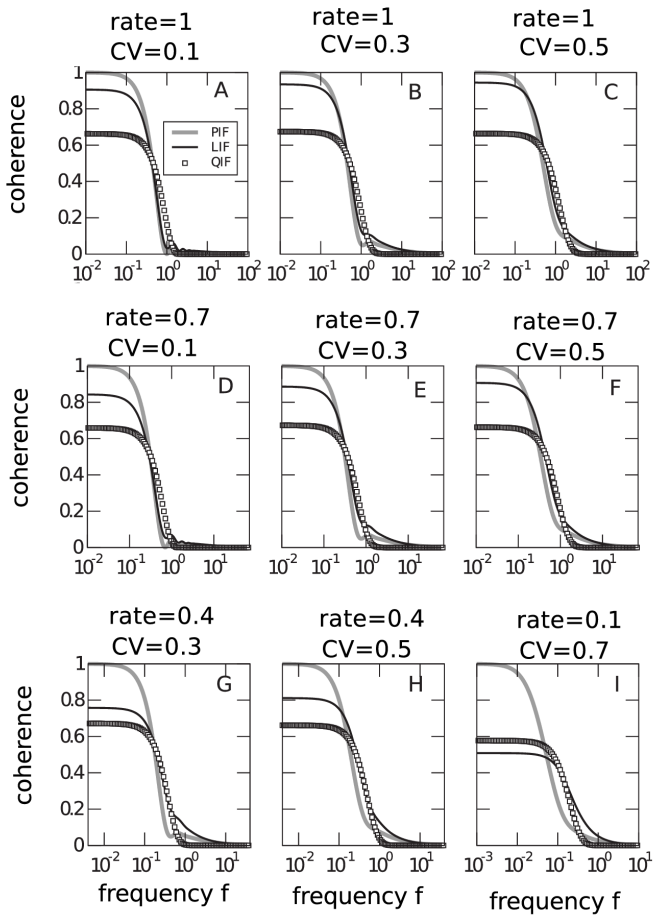

Figure 2.2: Signal transmission of PIF, LIF, and QIF. Shown are coherence functions of the PIF, LIF, and QIF in different firing activity regimes. From top to bottom: the firing rate (in units of inverse membrane time constant) decreases, whereas the CV is kept almost constant in each column. All three neuron models show low-pass filter characteristics of information, irrespective of the spiking activity (regular versus irregular) measured by the CV. Figure is abstracted from Vilela and Lindner (2009).

acteristics of the exponential integrate-and-fire (EIF) driven by Gaussian white noise current (similar setup as shown in Fig. 2.2). We verify the above mentioned statement that the low-pass characteristic on information transmission is inherently connected to the one-dimensional description of the neuron model and cannot be altered by changing the nonlinearity function $F(V)$.

2.3 Information transmission characteristics of the EIF model

The exponential integrate-and-fire (EIF) neuron model (Fourcaud-Trocme et al., 2003)

$$\tau_m \frac{d}{dt} V(t) = \mu - V(t) + \Delta_T e^{(V-V_T)/\Delta_T} + \sqrt{2\tau} D\eta(t) \tag{2.5}$$

describes cortical neuronal activity at a high precision (Badel et al., 2008a,b; Brette and Gerstner, 2005). When the current drives the potential beyond V_T (effective threshold potential), then the exponential term actuates a positive feedback, which leads to the upstroke of the action potential. The parameter Δ_T sets the slope of the onset of the action potential and thus, is often referred as spike slope parameter.

Two Schemes exist to study the information transmission properties of integrate-and-fire neuron models. First, a time discretization scheme to simulate the stochastic ordinary differential equation Eq.(2.5) (including the fire-and-reset rule) and the use of numerical Fourier transforms(Frigo and Johnson, 2005) of the resulting spike train to calculate the spectral statistics necessary to study the coherence function. Second, direct numerical calculations of the first-order dynamics via the associated Fokker-Planck equation (Risken, 1989). The first approach is called the Monte-Carlo (MC) method, whereas the latter method, which was developed by Magnus Richardson(Richardson, 2007, 2008) for IF neuron models, is called Richardson's integration method (see also sec. A). The MC method is always applicable and can be easily extended to reduce the numerical accuracy by adjusting the time-discretization step-size as well as the number of independent realizations (the statistical error of a Monte Carlo simulation scales inversely proportional to the square root of the number of independent trials). However, the numerical integration of Eq.(2.5) can be very time-consuming, especially if one is interested in spectral characteristics in the very low firing regime. The Richardson integration method(Richardson, 2007, 2008) allows us to obtain analytical approximations of the spectral characteristics, for example, the power spectrum of the spike train, and the cross-spectrum between spike train and an input signal. Both are necessary to study the information transmission characteristics of IF models (see Eq.(2.4)). The Richardson integration method is less computationally demanding and is therefore ideally suited for numerical studies that involve the exploration of a broad parameter space. Thus, we will use the Richardson method to study the information filtering effects of the EIF model. We will validate the results obtained by Richardson's method to results received by employing MC simulations (see Fig. 2.4 and Tab. 2.1).

First, we want to take a close look at example trajectories of the EIF model (resulting from numerical MC simulations of Eq.(2.5)) in order to establish an intuition for the different model parameters. Scaling the spike slope factor Δ_T from very low values to very high values leads to a gradual shift from a LIF ($\Delta_\mathrm{T} \to 0$) to a QIF ($\Delta_\mathrm{T} \to \infty$) model characteristics. Fig. 2.3 shows example trajectories for different EIF models (by using different values of the threshold slope factor Δ_T, shown in each column of Fig. 2.3) and different signal parameters (DC-input μ and signal strength D, shown in each row of Fig. 2.3). The corresponding parameter sets are listed in Tab. 2.1. The DC input

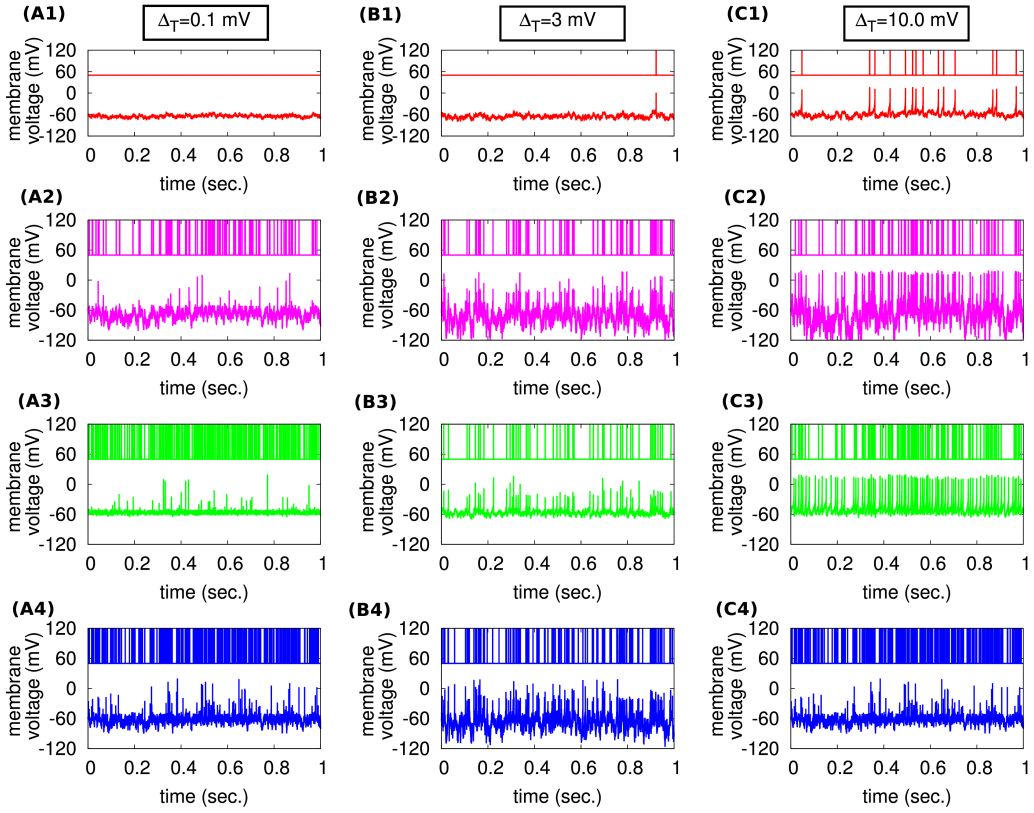

Figure 2.3: Time course of the EIF neuron model ($\Delta_T = 0.1$ mV,$\Delta_T = 3.0$ mV,$\Delta_T = 10.0$ mV) for different μ and D. Shown are results from numerical Monte Carlo simulations of Eq.(2.5) for different values of Δ_T in different regions of spiking activity (see Tab. 2.1 for numerical values). The color-coding stands for: low μ and low D (red), low μ and high D (magenta), high μ and low D (green), and high μ and high D (blue) in (A1–A4,B1–B4, and C1–C4).

μ and the stochastic signal strength D leads the classification of four different spiking activity regimes: **i)** low DC input and low signal strength result in a very irregular firing activity with low firing rate (see Fig. 2.3A1,B1,C1 and Tab. 2.1), **ii)** low DC and high signal strength lead to a higher firing rate and a more irregular spiking activity (see Fig. 2.3A2,B2,C2 and Tab. 2.1), **iii)** a high DC input and a low signal strength lead to high firing rates and very regular spike trains (see Fig. 2.3A3,B3,C3 and Tab. 2.1), and **iv)** a high DC input and a high signal strength result in a very high firing rate and very irregular spiking activities (see Fig. 2.3A4,B4,C4 and Tab. 2.1). Thus, the EIF model variants are able to describe different aspects of neuronal dynamics, ranging from very phasic (low firing rate and very irregular spike trains) to very tonic (high firing rate and very regular spiking activity) firing activities.

Having established an intuition of the spiking dynamics of the EIF neuron model in different activity regimes, we want to study now the signal transmission characteristics

Table 2.1: Example paramter sets for the EIF model with different Δ_T and output statistics concerning the dynamics of the EIF models: spike train firing rate and spike train coefficient of variation. The color-coding is adopted from Fig. 2.3.

Δ_T	0.1	3.0	10.0	threshold slope factor
V_{res}	-60	-60	-60	reset value
V_{th}	$+20$	$+20$	$+20$	threshold value
V_T	-53	-53	-53	effective threshold potential
τ	0.005	0.005	0.005	membrane time constant
τ_{ref}	0	0	0	abs. refractory period
μ_1	-65	-65	-65	DC input
D_1	3.16	5.01	5.01	signal strength
r_1	0.1	1.3	10.48	firing rate
$C_{V,1}$	1.00	1.00	0.90	coefficient of variation
μ_2	-65	-65	-65	DC input
D_2	12.68	19.95	25.11	signal strength
r_2	125.7	91.5	75.80	firing rate
$C_{V,2}$	1.43	1.22	1.08	coefficient of variation
μ_3	-50	-55	-55	DC input
D_3	3.16	5.01	5.01	signal strength
r_3	180.6	56.3	81.83	firing rate
$C_{V,3}$	0.57	0.76	0.44	coefficient of variation
μ_4	-50	-55	-55	DC input
D_4	12.68	19.95	25.11	signal strength
r_4	354.5	151.7	113.34	firing rate
$C_{V,4}$	1.27	1.16	1.01	coefficient of variation

of the EIF model within different firing activity regimes. Thus, we study the spectral coherence function and its corresponding meta statistics, like the lower bound of the mutual information rate and the resulting frequency filter characteristics (low, band, or high pass). In Fig. 2.4 (same parameter sets were used as in Fig. 2.3, see Tab. 2.1), example spectra for the three different EIF variants (by varying Δ_T) for four different input signal parameter sets (see color coding in Fig. 2.4) are shown (by employing Richardson's method(Richardson, 2007, 2008)).

Fig. 2.4 displays the numerical results concerning the spectral statistics (squared cross-spectrum, power spectrum, and coherence function) for different variants of the EIF neuron model ($\Delta_T = 0.1$, $\Delta_T = 3.0$, and $\Delta_T = 10.0$ mV) and different baseline currents μ and stochastic input signal strengths D (see magenta, blue, red, and green line in Fig. 2.7). The squared cross-spectrum between the input signal (Gaussian white noise) and the output, as well as the resulting spike train power spectrum for different EIF

model variants, are shown in Fig. 2.4A1–C1.

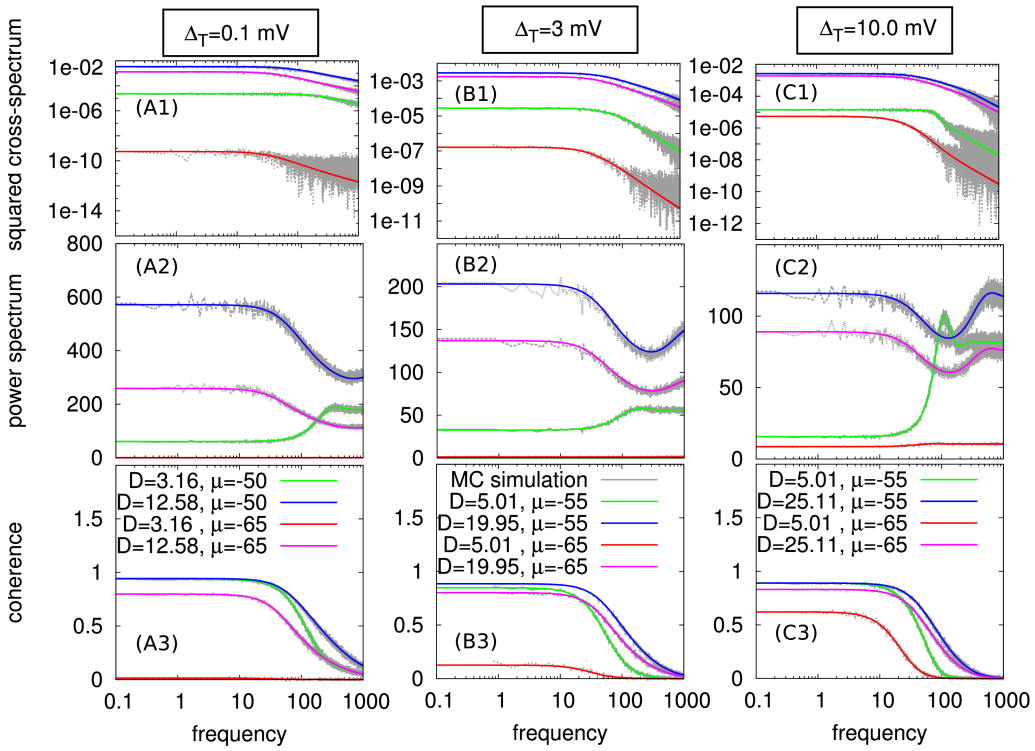

Figure 2.4: Spectral characteristics of the EIF neuron model ($\Delta_T = 0.1$ mV,$\Delta_T = 3.0$ mV,$\Delta_T = 10.0$ mV.) for different μ and D. Shown are numerical results of the squared cross-spectrum (A1, B1, C1), the spike-train power spectrum (A2, B2, C2), and the spectral coherence function (A3, B3, C3) at different DC-inputs μ and signal strength D and model parameter Δ_T ($\Delta_T = 0.1$ mV,$\Delta_T = 3.0$ mV, $\Delta_T = 10.0$ mV. The color coding of the spectra corresponds to Fig. 2.3.

From Fig. 2.4A1–C1, one can infer that the squared cross-spectrum decreases with increasing frequency. The power spectrum of the output spike train (shown in Fig. 2.4A2–C2) is flat and low in the very irregular firing regime (red curve, Poissonian limit), which is characterized by a CV close to one. The peak in the spike train power spectrum of the 'QIF-like' EIF ($\Delta_T = 10.0$ mV) is very pronounced in the tonic firing regime (green line in Fig. 2.4C2). Because the squared cross spectrum is a decreasing function of frequency (see Fig. 2.4A1–C1), the coherence function decreases with increasing frequency (negative curvature of the coherence function at zero frequency). Therefore, this coherence characterizes a low pass filter on information, irrespective of the firing activity regime (from very regular activity, see red lines in Fig. 2.4 to very irregular activity, see blue lines in Fig. 2.4). These example spectra indicate that the stochastic EIF neuron models also acts as a low pass filter on information, similar to the PIF, LIF, and QIF (see Fig. 2.2). In the following, we will discuss the signal transmission characteristics of the EIF model

variants in more detail. This exploration involves the meta statistics regarding the dynamical measures (firing rate and CV) as well as the information theoretic measures (curvature of the coherence function (see Eq.(1.13)) at zero frequency and the lower bound of the mutual information rate, see Eq.(1.12)). Fig. 2.5 shows the meta statistics of the coherence function of the EIF driven by Gaussian white noise (see Eq.(2.5)). In Fig. 2.5A and B, it is demonstrated that the chosen parameter space, which is spanned by the DC input μ and the signal strength D is large enough to cover different firing activity regimes of the EIF model variants: from low and irregular firing to high and very regular firing activity (see Fig. 2.3 and Tab. 2.1). In Fig. 2.5A, the firing rate of the EIF neuron model (with parameters chosen such that it acts similarly as the LIF neuron model ($\Delta_{\mathrm{T}} = 0.1$)) is shown with respect to the signal strength D and the baseline current (DC-current) μ. As one can infer from Fig. 2.5A, the firing rate increases with increasing signal strength D and DC input μ. Fig. 2.5A shows that the firing rate is very sensitive to changes of the input current μ and the signal strength D. In Fig. 2.5B it is shown that the CV decreases with increasing μ and increases with increasing stochastic input signal strength D. This dependency can be understood intuitively because one increases the noise in the system if one increases the signal strength D. The DC input μ controls the speed of the trajectory from reset to the threshold value. The higher the DC input, the higher faster goes the system from reset to the threshold. Thus, threshold crossings in this regime are dominantly influenced by the deterministic drift, instead of the stochastic diffusion due to the signal. The colored points in Fig. 2.5A1–A3 correspond to example spectra shown in Fig. 2.3 and example membrane voltage trajectories and resulting spike trains shown in Fig. 2.3A1–A3 (parameters are shown in Tab. 2.1).

The meta statistics of the EIF ($\Delta_T = 0.1$) regarding the information filtering characteristics as a function of the signal strength and DC-input are shown in Fig. 2.5C,D. Namely the curvature of the coherence function at zero frequency as a proxy between low-pass or band/high-pass filtering on information (Fig. 2.5C) and the lower bound of the mutual information rate (Fig. 2.5D). The curvature of the coherence function at zero frequency (Fig. 2.5C) is always negative, indicating that the EIF model variant ($\Delta_T = 0.1$) acts as a low pass filter on information irrespective of the firing regime (from phasic to tonic firing activity). The magnitude of the curvature becomes close to zero (red data point in Fig. 2.5C) in the phasic firing regime (red data point in Fig. 2.5B). This phasic firing regime is characterized by a very low coherence function (see red line in Fig. 2.4A3, B3). Consequently, the lower bound of the mutual information rate (Eq.(1.12)) is close to zero (Fig. 2.5D) in this phasic regime. Thus, one can conclude from the data shown in Fig. 2.5 that the EIF model variant ($\Delta_T = 0.1$ mV) always acts as a low pass filter on information (based on the spectral coherence function). This filtering characteristic is manifested by a monotonically decreasing coherence function with frequency (negative curvature of the coherence function at zero frequency). Performing the same analysis for the two other EIF model variants ($\Delta_T = 3.0$, $\Delta_T = 10.0$ mV), leads to the conclusion that this low-pass filtering on information is a generic feature of the EIF model (see Fig. 2.6C and Fig. 2.7C).

As Fig. 2.6C suggests, the curvature of the coherence at zero frequency is always

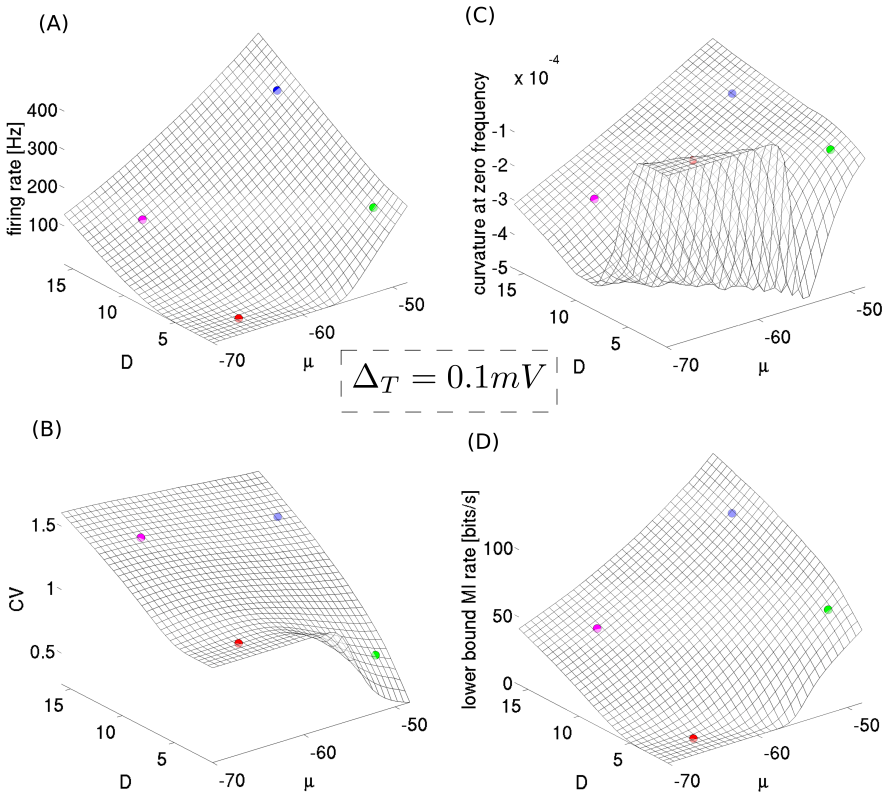

Figure 2.5: Meta statistics of the EIF neuron model with $\Delta_T = 0.1$ mV. Shown are the firing rate (A), the coefficient of variation (B), as well as the information theoretic measures: lower bound of the mutual information rate (C), and the curvature of the spectral coherence function (D) as a discriminator between low-pass and band-pass filter properties on information in different activity regimes, which are achieved by varying the stochastic signal strength D and the DC input current μ. Results were obtained by using Richardson's method(Richardson, 2007, 2008). Example spectra corresponding to the colored data points are displayed in Fig. 2.4A1–A3.

negative, which is the hallmark of a low pass filter on information. The curvature approaches zero from below, as soon as the EIF model operates in the very low firing rate and irregular spiking activity regime ($r \approx 0$, $CV \approx 1$, see red data point in Fig. 2.6C). The irregular firing activity is accompanied with a total reduction of the coherence function (see red data point in Fig. 2.6D and corresponding red curve in Fig. 2.4A3). Thus, the meta statistics of the EIF ($\Delta_T = 3.0$) suggests that this EIF model variant also acts as a low pass filter on information irrespective of the spiking regime. This statement holds true also for the QIF-limit-EIF model with a spike slope factor of $\Delta_T = 10$ mV (see Fig. 2.7A–D) as well. Fig. 2.5 and Fig. 2.7 show the meta statistics (dynamical, as well as information theoretic) corresponding to EIF variants that are closely related to the leaky integrate-and-fire (LIF) model ($\Delta_T \approx 0$ mV), and to the quadratic integrate-

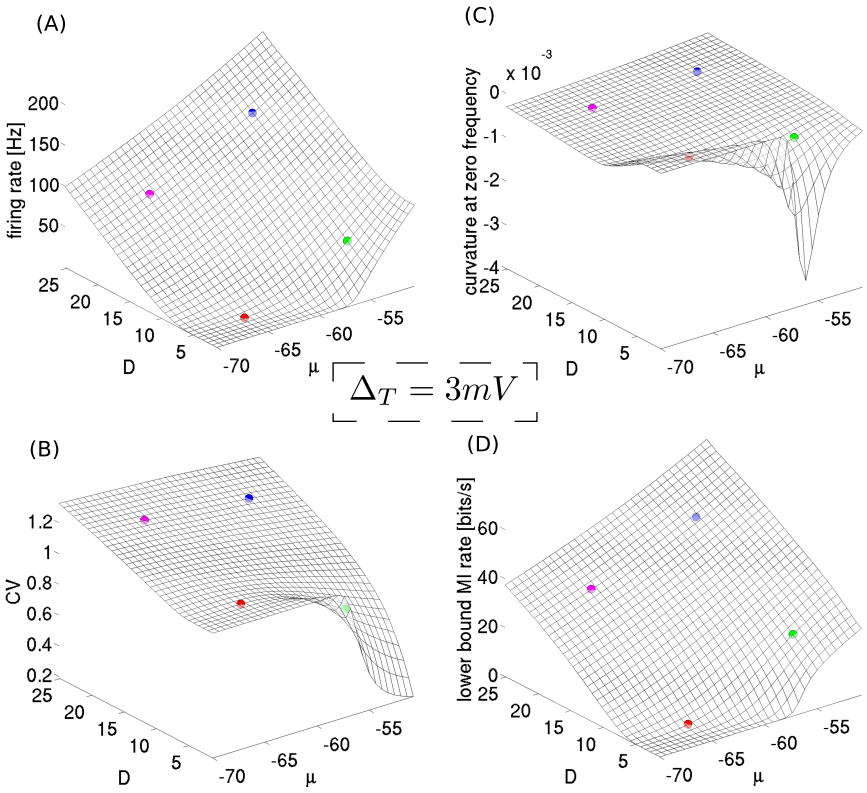

Figure 2.6: Meta statistics of the EIF neuron model with $\Delta_T = 3.0$ mV. Shown are the firing rate (A), the coefficient of variation (B), as well as the information theoretic measures: lower bound of the mutual information rate (C), and the curvature of the spectral coherence function (D) as a discriminator between low-pass and band-pass filter properties on information in different activity regimes, which are achieved by varying the stochastic signal strength D and the DC input current μ. Results were obtained by using Richardson's method(Richardson, 2007, 2008). Example spectra corresponding to the colored data points are displayed in Fig. 2.4B1–B3.

and-fire (QIF) model (in the limit $\Delta_T \to \infty$ mV). The respective model variant behaves very similarly to the LIF model (see Fig. 2.5) across the whole range of spiking activity (see Fig. 2.5A,B). Consequently, this model acts as a low pass filter on information (see Fig. 2.5C), which is indicated by a negative curvature of the coherence function at zero frequency. The lower bound of mutual information rate scales with the firing rate of the model (compare Fig. 2.5A and Fig. 2.5D).

Thus, we can conclude that the PIF, LIF, QIF, and EIF model acts as a low pass filter on information, based on the spectral stimulus-response coherence function, which serves as a lower bound on the mutual information rate. The described models do not show any model intrinsic theoretical mechanism to establish a qualitative (frequency-selective) filtering characteristics on information. This phenomenon of low-pass filtering

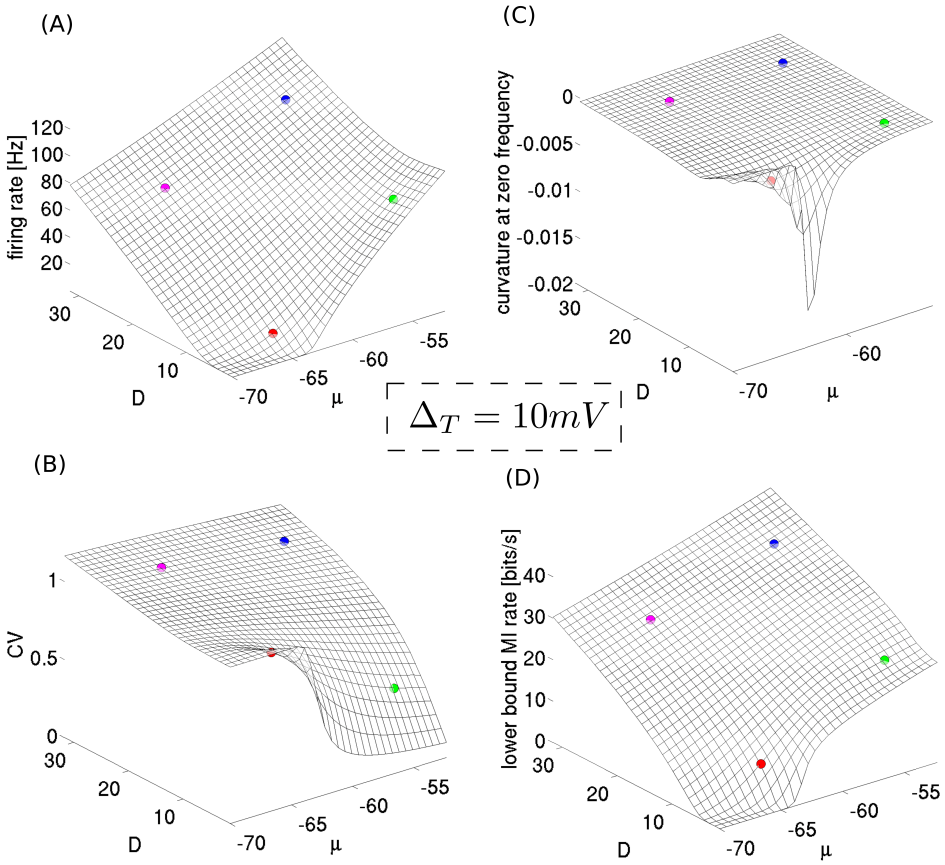

Figure 2.7: Meta statistics of the EIF neuron model with $\Delta_T = 10.0$ mV. Shown are the firing rate (A), the coefficient of variation (B), as well as the information theoretic measures: lower bound of the mutual information rate (C), and the curvature of the spectral coherence function (D) as a discriminator between low-pass and band-pass filter properties on information in different activity regimes, which are achieved by varying the stochastic signal strength D and the DC input current μ. Results were obtained by using Richardson's method(Richardson, 2007, 2008). Example spectra corresponding to the colored data points are displayed in Fig. 2.4C1–C3.

on information in IF neuron models was shown in a whole range of spiking activities, ranging from very phasic to very tonic firing activities.

2.4 Summary

In this chapter, previously obtained results obtained by Lindner (2012); Vilela and Lindner (2009) concerning the signal transmission characteristics of the perfect, leaky, and quadratic integrate-and-fire (PIF, LIF, QIF) driven by Gaussian white noise were reviewed. Lindner (2012); Vilela and Lindner (2009) have shown that all three (PIF, LIF, QIF) integrate-and-fire neuron models act as low pass filter on information, i.e. their coherence function attains its global maximum at zero frequency and decreases monotonically with increasing frequency.

Here, the exponential IF (EIF) neuron model and its signal transmission characteristics were explored numerically (based on Monte Carlo simulations) as well as semi-analytically, by employing Richardson's method(Richardson, 2007, 2008) to obtain power and cross-spectrum of the spike train. This approach, developed by Richardson (2007, 2008), allows us to explore the characteristics of the chosen IF models within a large parameter set very efficiently. This method does not rely on numerical averaging of independent model response realizations, which is an integral part of every Monte Carlo simulation of a stochastic process. In agreement with the results of the stochastic PIF, LIF, and QIF obtained by Lindner (2012); Vilela and Lindner (2009). Here, it was demonstrated that the stochastic EIF driven by Gaussian white noise Eq.(2.5) acts as a low-pass filter on information too. This low-pass filtering on information has been observed throughout the whole parameter range of the model, irrespective of the spiking activity regime (from very phasic to very tonic firing activities). Thus, integrate-and-fire neuron models (PIF, LIF, QIF, and EIF) are not able to filter specific frequency components of a time-dependent stimulus, but rather encode information about slow components of the signal. This low-pass filtering on information can be understood by the insight, that only slow components of a signal can lead to large excursions of the trajectory in the phase space, spanned by the variables V and dV/dt, from its resting state. Whereby fluctuations in the signal (dominantly seen via contributions at higher frequencies) cannot affect the information processing in single IF neuron models drastically.

To conclude, the numerical and analytical results presented in this chapter suggest that the low pass filter on information is a generic characteristic of integrate-and-fire-type neuron models. Thus, the nonlinearity (fire-and-reset rule) of the neuron model alone does not shape the information filtering characteristics of the model. Several mechanisms have to interfere with the nonlinearity, which is inherent in excitable neuron models, to shape the filtering characteristics of the neuron model from low- to band-pass filtering on information.

Although the EIF model describes cortical activity very accurately (Badel et al., 2008b; Platkiewicz and Brette, 2010; Rossant et al., 2011), it lacks the capacity of modeling for example ISI correlations within the spontaneous (without signal) activity. Also, IF models are not able to model complex subthreshold dynamics, such as resonances, which will be the subject of the next chapter (see sec. 3 and sec. 4).

3 Information filtering effects of positive ISI correlations

Abstract | Here, the effects of positive interspike interval (ISI) correlations on the neuronal information filtering characteristics are pointed out. By using the deterministic perfect integrate-and-fire neuron model with a stochastic threshold and reset rule, the spectral coherence function is studied numerically as well as analytically. Two variants of the model are investigated: a) without ISI correlations (renewal variant) and b) with positive ISI correlations (non-renewal variant). Both variants differ solely in the presence or absence of ISI correlations and show commonly observed experimental findings such as i) threshold variability and ii) skewed ISI distributions (often modeled with the help of an inverse Gaussian). Additionally, the non-renewal variant includes a third frequently experimentally measured phenomenon: iii) positive ISI correlations between adjacent ISIs. Based on numerical and analytical studies, it is shown that the presence of positive ISI correlations leads to a change of the frequency-dependent signal transmission characteristics from low-pass (renewal) to band-pass (non-renewal) filtering on information.

3.1 Introduction

3.1.1 Experimental evidence of ISI correlations and stochastic thresholds

According to the fundamental 'all-or-none'-principle in neuroscience, a neuron elicits a stereotypical response, so-called action potential (AP) or spike, if the neuron is excitable. The time scale of an AP is typically very fast and hence allow the neuron to respond very quickly to temporal changes in the input signal (Rieke et al., 1996). It is believed that neurons encode information via sequences of such spikes (Koch, 1999; Rieke et al., 1996). It is very subtle, to define or identify rigorously an action potential, i.e. a spike, in biophysical realistic conductance-based neuron models (see for example Koch et al. (1995); Platkiewicz and Brette (2010)). Traditionally, one uses the concept of a fixed threshold value such that a membrane voltage crossing (from below) marks the

beginning of an action potential, i.e. the realization of a spike. It will be motivated that the concept of a variable (here stochastic) membrane voltage threshold concept can be found in experiments and offers for example the possibility to incorporate the concept of memory via correlations between interspike spike intervals (ISIs) even in very simplified neuron models, such as the perfect integrate-and-fire (PIF), which was discussed in sec. 2.

ISI correlations

A simple concept of 'memory' on the level of the spiking output can be established via correlations between ISIs. A memoryless spiking output has the signature of no ISI correlation and is called renewal output (Cox, 1962). In contrast, the presence of ISI correlations (either short or long range) leads to short or long term memory. Several experimental studies suggest that ISI correlations exist in neuronal in vivo as well as in vitro environments (please consult for example Avila-Akerberg and Chacron (2011) for an overview article). One classifies roughly four types of ISI correlations i) positive decaying ISI correlations, ii) negative decaying ISI correlations (anti-correlations), iii) alternating decaying ISI correlations and iv) seemingly stochastic ISI correlations.

Postive ISI correlations can be found in the grasshopper's auditory neurons (Fisch, 2011; Schwalger et al., 2010) (see Fig. 3.1g), and in the spontaneous activity of neocortical cells in primary sensory cortex (S1) of long evans rats (Nawrot et al., 2007) (see Fig. 3.1e,f), as well as the cat medullary sympathetic neurons (Lewis et al., 2001).

Negative ISI correlations (dominantly seen between adjacent ISIs) seem to be very common as well and can be found in many experimental studies, ranging from the Honeybee's mushroom neurons (Farkhooi et al., 2009), the rat's entorhinal cortical pyramidal neurons (Engel et al., 2008), as well as human's motoneurons (Hagiwara, 1949).

Examples of the third type of ISI correlation structure, alternating decaying ISI correlations, have been found experimentally in the paddlefish's electroreceptors (Neiman and Russell, 2001, 2005) and the weakly electric fish's electroreceptors (Chacron et al., 2000, 2005; Longtin and Racicot, 1997). The fourth type of ISI correlations, which are seemingly rather chaotic in their distribution over lags, have been identified in experimental studies, for example in the Paddlefish electroreceptor (Neiman and Russell, 2004; Neiman et al., 2011), and their theoretical explanation was provided in Bauermeister et al. (2013).

Several biophysical mechanisms can result in ISI correlations such as i) neural refractoriness (Câteau and Reyes, 2006), ii) cell intrinsic slow and stochastic adaptation currents (Fisch et al., 2012; Schwalger and Lindner, 2010, 2013; Shiau et al., 2015), and iii) correlations of the input signal (Baddeley et al., 1997; Schwalger et al., 2015). In the theoretical study by Lindner et al. (2005) it was shown, that negative ISI correlations do not change the spectral information transmission characteristics of a simple neuron model. Thus, an inherent low pass filter neuron model (for example the PIF) equipped with negative ISI correlations (between successive ISIs) does not show a frequency preference in information coding. In this chapter, we will study the effect of positive ISI correlations between adjacent ISIs, i.e. at lag one, on the information filtering properties based on the spectral stimulus-response coherence function (see Eq.(1.13) in sec. 1.4.3) by means of a very simplified neuron model, the deterministic perfect integrate-and-

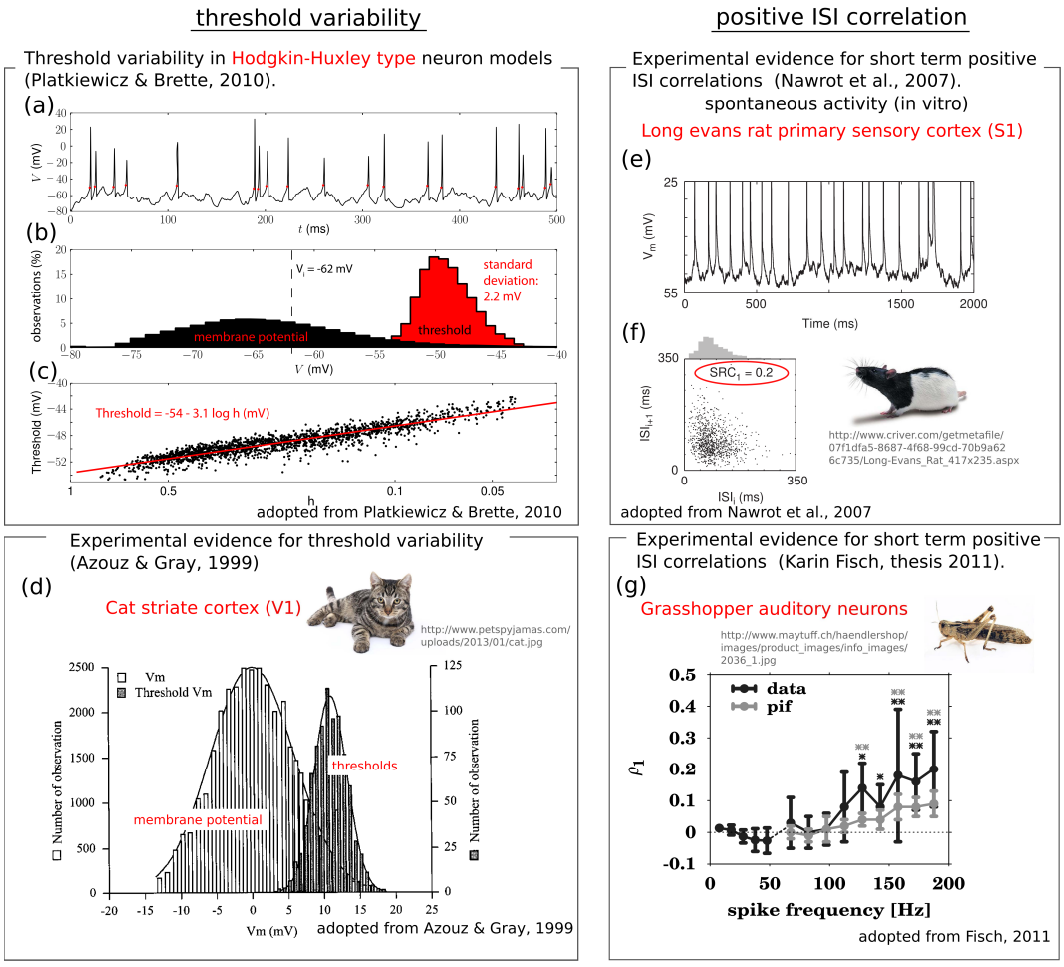

Figure 3.1: Phenomenological and experimental evidences for variable spike-thresholds and for positive ISI correlations. Threshold variability (red dots in the trajectory (a) mark the identified membrane voltage spike thresholds) can be seen in classical conductance-based neuron models such as the Hodgkin-Huxley model(Hodgkin and Huxley, 1952e) (a–c) as well as in Cat visual (V1) striate cortex neurons (d). Experimental evidence for positive correlations between adjacent ISIs from the spontaneous activity of Long evan's primary sensory (S1) cortex neurons (e–f) and Grasshopper's auditory neurons (g).

fire (PIF) equipped with a stochastic threshold and reset concept (based on the model proposed by Lindner et al. (2005)) that lead to positive ISI correlations between successive ISIs. Also, this model allows to fine tune the strength of the correlations between successive ISIs in the range from zero to one-half.

Stochastic thresholds

It has been shown that one can construct a biologically motivated threshold criterion that is more appropriate than the fixed threshold crossing concept, such that the resulting threshold distribution is not sharp but rather broadly distributed (see for example Lecar and Nossal (1971a); Naundorf et al. (2006); Platkiewicz and Brette (2010)). This broadening can be due to i) cell intrinsic adaptation mechanisms (Schwalger and Lindner, 2013), or ii) intrinsic noise (ion channel noise, conductance noise, synaptic noise) (Lecar and Nossal, 1971b). The biophysical origin of those threshold variability is an old and an ongoing debate (Azouz and Gray (1999, 2000); Chacron et al. (2007); Holden (2013); Koch et al. (1995); Lecar and Nossal (1971a); Platkiewicz and Brette (2010); Stein (1967); Weiss (1966)) in neuroscience and can be observed in vitro as well as in vivo (Henze and Buzsaki, 2001) experiments.

Additionally, it has been shown experimentally that stochastic threshold models can reliably predict cortical neuronal spiking responses (Jolivet et al., 2006) and can account for trial-to-trial spike-train variability of neuronal responses (Calvin, 1974; Schlue et al., 1974; Schwindt and Crill, 1982; Stafstrom et al., 1984). Although the underlying mechanisms for threshold variability are still an ongoing debate, beneficial effects of stochastic threshold has been observed in auditory (Escabí et al., 2005; Fisch, 2011), in visual (Azouz and Gray, 1999; Priebe and Ferster, 2008), as well as in sensory (Aizenman et al., 2003) areas of cortex (see Fig. 3.1d).

As one can infer from Fig. 3.1b,d, the spiking threshold distribution is not sharp but rather broad. Fig. 3.1b suggests an inverse Gaussian distribution (Folks and Chhikara, 1978) for thresholds, which is rather skewed. The overlap of the distributions of membrane voltage and thresholds in Fig. 3.1b,d advises also that not every stochastic threshold crossing leads to the release of an action potential, but is rejected in a small percentage (close to 1% in Fig. 3.1b) and high percentage (close to 50% in Fig. 3.1d).

3.1.2 PIF with stochastic threshold and reset distributions

Here, we will study the effects of threshold variability (such that they result in correlations between subsequent interspike intervals (ISIs)) on the information transmission properties. Therefore we will use a very simplified neuron model, the perfect integrate-and-fire (PIF) (Knight (1972); Stein (1965)) with threshold-and-reset variability (extension of the model proposed by (Lindner et al., 2005)), which leads in a specific variant of the stochastic threshold-and-reset model to positive correlations of subsequent ISIs. Positive correlations between successive ISIs have been observed experimentally for example in i) neurons of the primary sensory cortex of rats (Nawrot et al., 2007) and in ii) auditory receptor neurons in grasshopper (lat. locusta migratoria) (Fisch et al., 2012)).

We will use the deterministic PIF neuron model, which is governed (until a voltage threshold is reached) by the following deterministic differential equation:

$$\frac{dv(t)}{dt} = \mu + s(t), \tag{3.1}$$

where $v(t)$ describes the time course of the membrane potential and μ is a constant drift term, which acts as a bifurcation parameter between non-excitable and excitable activity. The (external) time-dependent signal $s(t)$ modulates the rate of change of the membrane voltage linearly, i.e. acts as a current input. The dynamics of the neuron model is described by Eq.(3.1). In addition to the subthreshold dynamics, on introduces a fire-and-reset concept to model excitable neurons. If the voltage $v(t)$ crosses a threshold v_{th} from below then the voltage is reset to v_{reset} and will follow Eq.(3.1) until the voltage threshold is crossed again. As described above, we will not use a constant threshold and reset value here, but a stochastic fire-and-reset rule, in such a way that the threshold and reset values are drawn from a probability distribution (with finite mean and variance). Two variants of the model can be distinguished: i) if the threshold and reset value are drawn **independently** from each other then threshold and reset values are uncorrelated and therefore, subsequent ISIs are uncorrelated as well (**renewal variant**), ii) if the magnitude of the reset value is the same (or a scaled version) of the previous threshold value then both are maximally correlated with each other, which translates[1] to correlations among adjacent ISIs (**non-renewal variant**). Thus, this approach to model autonomous[2] correlations among subsequent ISIs is based on correlations between successive threshold and reset values, which allows studying the effects of positive ISI correlations (similar to model proposed by Lindner et al. (2005)) on frequency-dependent signal transmission analytically. In Fig. 3.2 the basic effects of these 'autonomous' correlations between adjacent ISIs on the signal transmission characteristics of the two model variants: i) with ISI correlations (non-renewal), and ii) without ISI correlations (renewal) is shown. Positive ISI correlations can lead to band-pass filtering on information (see Fig. 3.2), which is manifested by a peak in the spectral coherence function at intermediate frequencies.

3.1.3 Quality factor of information filter

The quality factor Q_C of the coherence function ($C(f)$) will be used throughout this chapter to quantify the 'strength' of the band pass filter on information (see Fig. 1.5):

$$Q_{\mathrm{C}} = \frac{C(f_{\mathrm{res}})}{C(f=0)}, \tag{3.2}$$

where the coherence function attains its maximum at f_{res}. A quality factor larger than one indicates a band/high pass filter on information, whereas a value of one marks the presence of a low pass filter on information.

[1] Here the specific choice of the deterministic PIF dynamics guarantees that correlations between threshold and reset values are translated directly to ISI correlations. The presence of current noise diminish the correlations between ISIs.

[2] Because the correlation structure is inherent in the neuronal model and is not induced for example by correlations in the input signal (see for example Middleton et al. (2003); Moreno et al. (2002); Sompolinsky et al. (2001)).

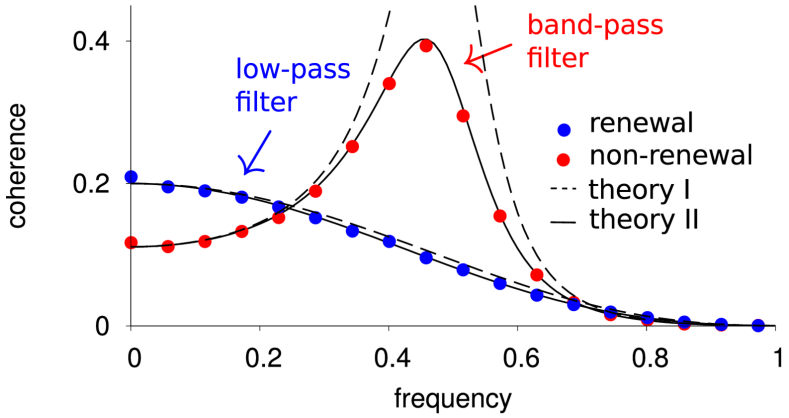

Figure 3.2: Information filtering of the two model variants with an inverse Gaussian ISI distribution. Numerical results (symbols) compared to theory I (dashed lines, see Eq.(3.20)) and theory II (solid lines, see Eq.(3.21a)) for $C_{\mathrm{V},0} = 0.1$ of the spontaneous activity and a weak input signal $s(t)$ ($\varepsilon^2 = 0.01$). Theory I predicts a maximum of the coherence at much higher values ($C_I(f_{\mathrm{res}}) \approx 0.7$), which is not shown.

3.2 Approaches to model the spontaneous activity

The specific choice of the deterministic PIF model for the subthreshold dynamics is twofold motivated. First, by noticing that IF neuron models act as low pass filter on information (see sec. 2). Second, by the fact that the specific choice of the deterministic PIF in addition to threshold noise results in an analytically tractable neuron model (similar to the model proposed by Lindner et al. (2005)). Therefore, a prescribed ISI density, the correlation coefficient between adjacent ISIs, and all relevant spectral measures, which are necessary to study the information filtering properties (based on the spectral coherence function) of the model, can be obtained analytically.

To characterize the statistical dependency among the ISIs, one uses the serial correlation coefficient (SCC) (Perkel et al., 1967):

$$\rho_k = \frac{\langle (T_{i+k} - T_i)\,(T_i - \langle T_i \rangle_i) \rangle_i}{\langle (T_i - \langle T_i \rangle_i)^2 \rangle_i}. \tag{3.3}$$

The SCC of the renewal model is zero for higher lags than zero, because threshold and reset values are independent of each other, which implies:

$$\rho_{\mathrm{R,k}} = 0, \qquad k > 0. \quad \text{(renewal variant)} \tag{3.4}$$

3.2.1 Implementing prescribed ISI distributions and correlations

In this part, it will be described how one can use the deterministic PIF model with a stochastic threshold and reset concept such that the resulting ISIs are distributed according to a prescribed density (here an inverse Gaussian density), and positive 'autonomous' correlations between adjacent ISIs are observed.

Inverse Gaussian distributed ISIs

Experimentally observed ISI densities are often modeled with the help of inverse Gaussian distributions. In the model studied here (deterministic PIF)), the ISI density can be written as the convolution of the threshold and the reset distribution. The choice of an inverse Gaussian distribution (Chhikara, 1988; Tweedie, 1957) for threshold and reset values results in an inverse Gaussian ISI distribution $F_{1,0}(T)$ (in the absence of an external signal) for the renewal and the non-renewal model variant. This effect is due to the fact that the convolution of two inverse Gaussians with the same mean and variance results in an inverse Gaussian (Chhikara, 1988)).

The inverse Gaussian distribution of the ISI (see Fig. 3.3c) can be conveniently parametrized in terms of its inverse mean value, i.e. the firing rate r_0, and its coefficient of variation C_V as follows:

$$F_{1,0}(T) = \sqrt{\frac{1}{2\pi r_0 C_\mathrm{V}^2 T^3}} \exp\left[-r_0 \frac{(T - 1/r_0)^2}{2C_\mathrm{V}^2 T}\right]. \tag{3.5}$$

Using the above discussed relation between threshold and reset distributions on the one hand and the ISI distribution on the other hand, one can prescribe the C_V and the rate of the spontaneous (in the absence of a time-dependent input signal) output spike train by drawing the threshold v_T and reset values v_R from the following distributions:

$$p_\mathrm{T}(v_T) = \sqrt{\frac{\mu}{8\pi r_0 C_\mathrm{V}^2 v_T^3}} \exp\left[-r_0 \frac{(v_T - \mu/(2r_0))^2}{2C_\mathrm{V}^2 v_T \mu}\right], \quad p_\mathrm{R}(v_R) = p_\mathrm{T}(-v_R). \tag{3.6}$$

Maximal positive correlations between adjacent ISIs

In contrast to the renewal variant, the non-renewal exhibits correlations between threshold and reset values such that each reset value is a flipped version of the foregoing threshold value (compare Fig. 3.3a,b). This correlation between threshold and successive reset value leads to a pronounced positive correlation exclusively between adjacent ISIs of the form (see Fig. 3.3d):

$$\rho_\mathrm{NR,k} = \frac{1}{2}\delta_{1,k}, \qquad k > 0. \quad \text{(non-renewal variant)} \tag{3.7}$$

In Fig. 3.3 the dynamics of the two models (renewal and non-renewal) is displayed. Both models are similar in their output statistics, except for the presence of ISI correlations.

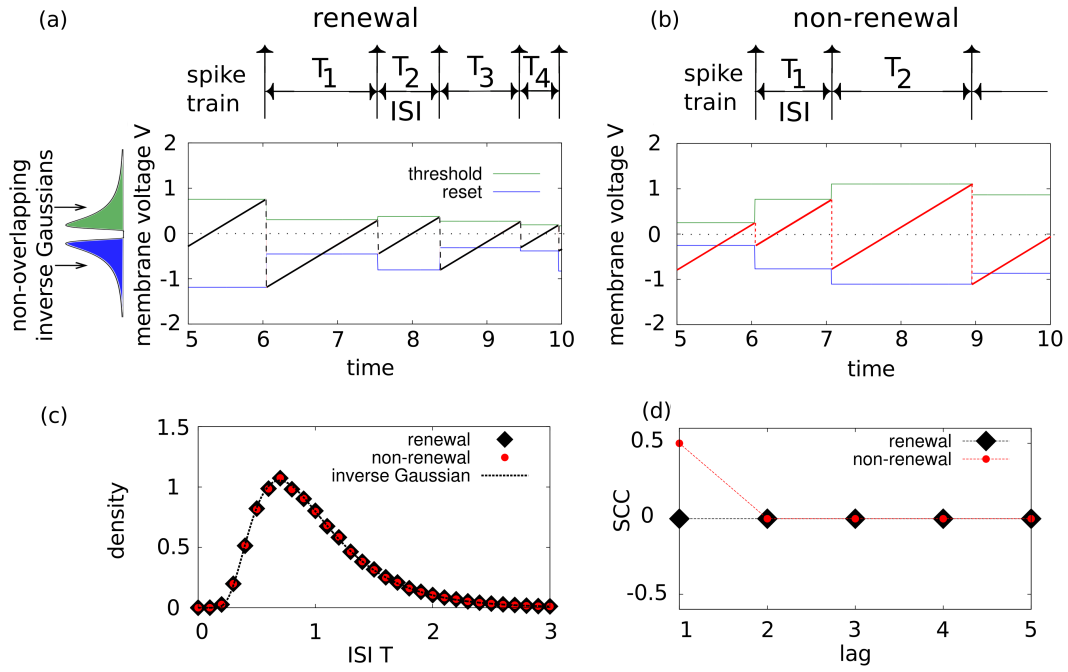

Figure 3.3: Spontaneous activity of the two model variants studied in this chapter. Shown are: time course of the membrane voltage of the integrate-and-fire model with threshold noise in the renewal version (a) and the non-renewal variant (b). In the renewal variant (a), the threshold (green) and reset (blue) values are drawn independently from an inverse Gaussian distribution (indicated on the top left and given in Eq.(3.5)). In the non-renewal variant (b), each reset value is a flipped version of the previous threshold value (which is mirrored along the time axis), giving rise to positive correlations between adjacent ISIs (d). Both model variants display exactly the same ISI distribution (c) (see Eq.(3.5) below) which is an inverse Gaussian though with different mean and variance than the ones used for threshold and reset.

This allows us to study the effects of positive ISI correlations between adjacent ISIs on the frequency-dependent signal transmission of the neuron model.

Variable correlations between successive ISIs

The above described variant of constructing positive correlations between adjacent ISIs can be seen as a special case, in which threshold and reset values are maximally correlated to each other, due to the fact that the subsequent reset value is the mirrored (with respect to zero) version of the previous threshold value. In order to vary the ISI correlation at lag one, I introduce an asymmetry factor α, such that the reset value, drawn from the mirrored distribution of threshold (in the renewal case) or exactly the same value of the previous threshold (in the non-renewal variant), is scaled by this factor α.

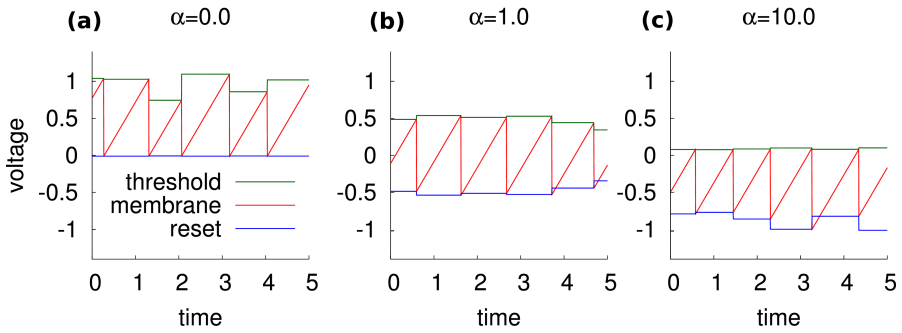

Figure 3.4: By reallocating the ISI variability among threshold and reset value distribution, one can change gradually the correlation between successive ISIs. Three example trajectories for different scaling parameter α are shown. a) low scaling factors leads to low ISI correlations and manifests itself by the fact that all intrinsic variability is due to the threshold variability. increasing α leads to shifting the variability from threshold to reset values. For $\alpha = 1$ (b), threshold and reset variability is equal and the ISI correlation is maximal and decreases in the regime in which all the reset variability is the dominant intrinsic noise source (c). Here the firing rate was set to one and the CV of the ISI distribution was fixed to $C_V = 0.125$ (in a,b,c).

This approach leads to SCCs at lag one, i.e. between adjacent ISIs, of the following form:

$$\rho_{\mathrm{NR,k}} = \frac{1}{2}\left(\frac{(1+\alpha)^2}{1+\alpha^2} - 1\right)\delta_{1,k}. \qquad k > 0. \tag{3.8}$$

The above described asymmetry approach leads to positive correlations between successive ISIs in the range from zero to one-half (see Fig. 3.5b). The maximal value ($\rho_{\mathrm{NR},1} = 1/2$) is obtained by using the symmetric (between threshold and resets) implementation ($\alpha = 1$) (see Fig. 3.3b,d).

This general model variant is able to discriminate between the renewal and non-renewal model variant continuously. The limits $\alpha \to 0$ and $\alpha \to \infty$ are characterized by the absence of ISI correlations, and thus describe a renewal process(Cox, 1962). The correlation coefficient between adjacent ISIs (Eq.(3.8)) of this model is invariant under the transformation $\alpha \to 1/\alpha$, which reflects the fact that one could scale the threshold value instead of the following reset value in order to change the correlation between adjacent ISIs.

By introducing a scaling factor α of the reset value, one also changes the resulting ISI density, or put differently, the resulting characteristic function of the ISI distribution, which takes the form:

$$\tilde{F}_{1,0}(f;\alpha) = \tilde{\phi}_{\mathrm{T}}(f)\tilde{\phi}_{\mathrm{R}}(\alpha f). \tag{3.9}$$

From Eq.(3.9) one can draw the conclusion[3]. that with the help of the α scaling factor,

[3]Because of the simple connection between the characteristic function $\tilde{F}(f)$ and the central moments

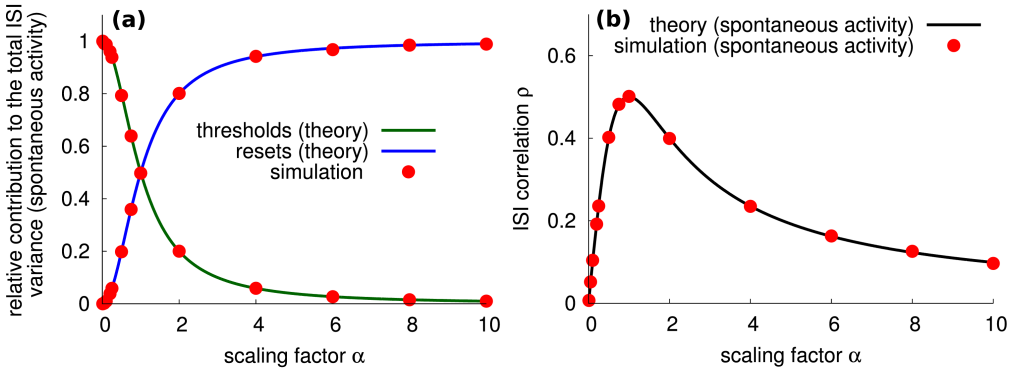

Figure 3.5: The scaling factor α of the reset value gradually change the noise distribution from threshold to reset variability and the ISI correlation coefficient. The scaling factor α as an asymmetry factor for threshold and reset distribution leads to a shift of the intrinsic variability from threshold to reset distribution (a). b) the factor α allows to control the ISI correlation ρ continuously from zero to one-half. The analytically obtained SCC (Eq.(3.8)) with respect to α (black solid line in b) is compared with numerical results (red data points in b). Here the firing rate was set to one and the CV of the ISI distribution was fixed to $C_V = 0.125$ (in a,b).

one redistributes the total variance of the ISI density among the underlying threshold distribution $p_{\mathrm{T}}(V_{\mathrm{T}})$ and the reset distribution $p_{\mathrm{R}}(V_{\mathrm{R}})$ (see Fig. 3.5a and Fig. 3.4a–c) from dominantly threshold stochasticity to primarily reset variability.

3.2.2 Exact analytical expressions for the power spectrum

In Fig. 3.6 a schematic description of the analytical approach, i.e. the decomposition of ISIs into two time intervals, from reset to zero ($\hat{\tau}_i$) and from zero the the threshold (τ_i) is shown. Many of these sub-intervals are pairwise identical because of the mirroring rule ($\tau_i = \hat{\tau}_{i+1}$), leading to the following expression for the n-th order interval $\bar{T}_n$:

$$\bar{T}_n = \hat{\tau}_1 + \tau_1 + \hat{\tau}_2 + \tau_2 + \cdots + \hat{\tau}_n + \tau_n = \tau_1 + \tau_n + 2\sum_{j=1}^{n-1} \tau_j. \tag{3.10}$$

In the last step I have expressed $\bar{T}_n$ by a sum of independent variables, the probability density of which is given by the convolution of the probability densities of the single variables and the characteristic function of which is given by the product of the single characteristic functions:

$$\tilde{F}_n = \tilde{F}_\tau(f)^2 \tilde{F}_{2\tau}(f)^{n-1} = \tilde{F}_\tau(f)^2 \tilde{F}_\tau(2f)^{n-1}, \tag{3.11}$$

of this distribution ($\langle T^n \rangle$) via $\frac{d^n}{df^n} \tilde{F}(f)|_{f=0} = (2\pi i)^n \langle T^n \rangle$.

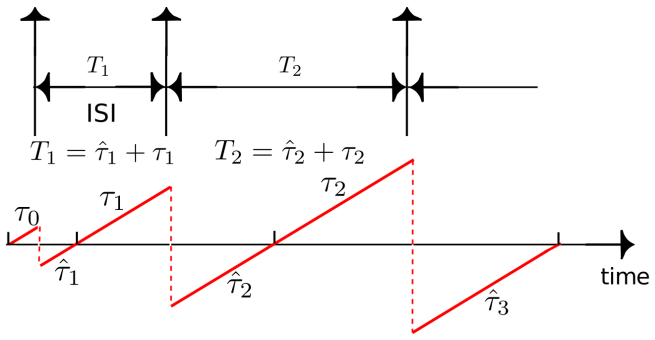

Figure 3.6: Schematic presentation of the non-renewal model variant with maximal positive correlations between adjacent ISIs. In order to derive the serial correlation coefficient more easily, one divides the interspike interval from the reset value to zero ($\hat{\tau}_i$) and from zero to threshold (τ_i).

where I have used $\tilde{F}_{2\tau}(f) = \tilde{F}_{\tau}(2f)$.

In order to calculate analytically the power spectrum of the spontaneous activity (without a time-dependent input signal) I use the well-known result from the theory of point processes(Holden, 1976):

$$S_0(f) = r_0 \left(1 + \sum_{n=1}^{\infty} \tilde{F}(f) + \tilde{F}(-f) \right), \tag{3.12}$$

where $\tilde{F}(f)$ describes the Fourier transform of the probability density of the n-th order interval $\bar{T}_n$ and is given by Eq.(3.11).

Vanishing correlations between adjacent ISIs

For a renewal process one has that $\tilde{F}_n(f) = \left(\tilde{F}_1(f)\right)^n$. In the absence of a signal (which we indicate in the following by the index '0'), we obtain the well-known renewal formula(Stratonovich, 1967):

$$S_{\mathrm{R},0}(f) = r_0 \frac{1 - |\tilde{F}_{1,0}(f)|^2}{|1 - \tilde{F}_{1,0}(f)|^2} = r_0 \frac{1 - \tilde{F}_{1,0}(f)\tilde{F}_{1,0}(-f)}{\left(1 - \tilde{F}_{1,0}(f)\right)\left(1 - \tilde{F}_{1,0}(-f)\right)}, \tag{3.13}$$

where we have used that $\tilde{F}^*_{1,0}(f) = \tilde{F}_{1,0}(-f)$.

Maximal correlations between adjacent ISIs

For the nonrenewal model studied here one has that $\tilde{F}_n(f) = \tilde{F}^2_{\tau}(f)\tilde{F}_{\tau}(2f)^{n-1}$, where $\tilde{F}_{\tau}(f)$ denotes the characteristic function of the probability density of threshold and reset values. The expression for the spontaneous power spectrum of the spike train (Eq.(3.12))

can be significantly simplified and reads:

$$S_{\mathrm{NR},0}(f) = r_0 \frac{\left|1-\sqrt{\tilde{F}_{1,0}(2f)}\right|^2 + 2\Re\left[\tilde{F}^*_{1,0}(f)\left(1-\sqrt{\tilde{F}_{1,0}(2f)}\right)\right]}{|1-\sqrt{\tilde{F}_{1,0}(2f)}|^2}, \tag{3.14}$$

where $\Re[...]$ denotes the real part of a complex number.

Variable correlations between adjacent ISIs

The general expressions ($\alpha \neq 1$) for the power spectrum of the spontaneous spiking activity (similar to Eq.(3.13) and Eq.(3.14)) for the two model variants (renewal, non-renewal) thus reads:

$$S_{\mathrm{R},0}(f;\alpha) = r_0 \frac{1-|\tilde{F}_{1,0}(f;\alpha)|^2}{|1-\tilde{F}_{1,0}(f;\alpha)|^2}, \tag{3.15}$$

and

$$S_{\mathrm{NR},0}(f;\alpha) = r_0 \left(1 - \frac{\tilde{\phi}_{\mathrm{T}}(-f)\tilde{\phi}_{\mathrm{R}}(-\alpha f)}{\tilde{\phi}_{\mathrm{R}}(-(\alpha+1)f)-1} - \frac{\tilde{\phi}_{\mathrm{T}}(f)\tilde{\phi}_{\mathrm{T}}(\alpha f)}{\tilde{\phi}_{\mathrm{R}}((\alpha+1)f)-1}\right), \tag{3.16}$$

where $\tilde{\phi}_{\mathrm{T}}(f)$ is the characteristic function of the threshold distribution and $\tilde{\phi}_{\mathrm{R}}(\alpha f)$ respects the asymmetric distribution of reset values with respect to the thresholds by a scaling factor α.

The power spectrum at zero frequency of a spike train with firing rate r_0 and coefficient of variation C_V and ISI correlations ρ_k, where k denotes the lag, can be written as:

$$S(f \to 0) = r_0 C_V \left(1 + 2\sum_{k=1}^{\infty} \rho_k\right). \tag{3.17}$$

Using Eq.(3.8) for the SCC of our nonrenewal variant, the spontaneous power spectrum at zero frequency can be written as:

$$S_{\mathrm{NR},0}(f \to 0) = r_0 C_V \frac{(1+\alpha)^2}{1+\alpha^2}. \tag{3.18}$$

3.3 Approximated power spectra in the presence of a signal

3.3.1 Known analytical expressions for weak signals

In this section we will briefly recapitulate the theoretical approaches in order to obtain the spectral densities of the deterministic PIF model with stochastic threshold and reset. The approaches presented below were obtained by Lindner et al. (2005). We will use a simple approach (theory I developed by Lindner et al. (2005)) to discriminate between low and band pass filter based on the curvature of the coherence function, i.e. its second

derivative, at zero frequency. Additionally, we will use both theories (theory I and theory II) to compare the simulated results with theoretical approximations and thus verify the analytical expressions based on Lindner et al. (2005) as well as the correct implementation of the procedures to simulate the model numerically.

Cross-spectrum between signal and spike-train

The susceptibility $\chi(f)$ for the perfect IF model with threshold noise is a constant with respect to frequency (Lindner et al., 2005)

$$\chi(f) = \chi_0 = r_0/\mu, \tag{3.19}$$

where r_0 denotes the firing rate in absence of a signal, i.e. spontaneous activity and μ is the constant drift (see Eq.(3.1)). Thus, due to Eq.(1.13) in sec. 1.4.3 the spectral information transfer resonance effect, i.e. a peak in the spectral coherence is shaped solely by the spike train power spectrum (a local minimum) of the evoked activity.

Spike-train power spectrum in the presence of a signal (theory I)

The spike-train power spectrum in presence of a weak broadband stimulus can be approximated by this following simple expression (theory I from Lindner et al. (2005)):

$$S_{\mathrm{I}}(f) = S_0(f) + |\chi(f)|^2 S_{\mathrm{s,s}}(f) = S_0(f) + \frac{r_0^2}{\mu^2} S_{s,s}(f). \tag{3.20}$$

Where $\chi(f) = r_0/\mu$ denotes the constant susceptibility of the PIF. Thus, the only frequency modulation of the evoked power spectrum due to the time-dependent signal $s(t)$ is supported by the power spectrum of the input signal $S_{s,s}(f)$. In our setup, a band-limited Gaussian white noise (for simplicity) was used and thus, its power spectrum is flat and non-zero for frequencies smaller than the cut-off frequency and identical zero otherwise. It seems therefore proper to modify the linear response approach in order to obtain a more reliable approximation of the frequency modulation within the power spectrum of the evoked activity. This calculation was performed by Lindner et al. (2005) and will be briefly presented next.

Spike-train power spectrum in the presence of a signal (theory II)

For the perfect IF model with threshold noise and external driving, an alternative theory for the power spectrum (in the following called theory II) has been developed by Lindner et al. (2005). It turns out that the following formula can be applied in our setup as well:

$$S_{\mathrm{II}}(f) = r_0 + |\chi(f)|^2 S_{\mathrm{s,s}}(f) + \int_{-\infty}^{\infty} df' \left(S_0(f') - r_0\right) I(f, f'), \tag{3.21a}$$

$$I(f, f') = \frac{4\left(af'^2\right)^3}{\left[a^2 f'^4 + 4\pi^2 \left(f - f'\right)^2\right]^2} + 2\Re\left[\frac{\left(af'^2 - 2i\pi f\right)^2}{\left[af'^2 - 2i\pi\left(f - f'\right)\right]^2} \int_{-\infty}^{\infty} d\tilde{f} \frac{S_{\mathrm{s,s}}\left(\tilde{f}\right)/\mu^2}{af'^2 - 2i\pi\left(f - f' - \tilde{f}\right)}\right], \tag{3.21b}$$

with the abbreviation $a = \pi^2\varepsilon^2/(\mu^2 f_c)$. Theory II is valid for a weak noise only but still captures nonlinear effects of the signal on the power spectrum. It can quantitatively describe(Lindner et al., 2005), how a band-limited signal (having power only up to a cut-off frequency f_c) broadens a spectral peak that is outside the signal band, e.g. a peak at $f > f_c$.

3.3.2 Special choice of the input signal

For the input signal $s(t)$ a band-limited Gaussian white noise with a variance $\langle s^2 \rangle = \varepsilon^2$ and a cut-off frequency f_c is used, such that its power spectrum reads

$$S_{\mathrm{s,s}}(f) = \frac{\varepsilon^2}{2f_c}\Theta(f - f_c), \tag{3.22}$$

where $\Theta(f)$ is the Heaviside function. Note that this model includes two kinds of variability: the random values of threshold and reset, and the randomness of the external stimulus as a simple model for a complex time-dependent signals. If not stated otherwise, a cut-off frequency $f_c = 2.0$, i.e. twice the firing rate of the spontaneous activity is used.

3.3.3 Coherence function between signal and spiking output (theory I)

Because of the special choice of the input signal, i.e. a band-limited Gaussian white noise signal, the coherence function between the input signal and the spiking output can be described in the following form (by assuming a weak input signal):

$$C_I(f) = \left[1 + \gamma S_{0,I}(f)\right]^{-1}, \tag{3.23}$$

with the abbreviation $\gamma = \frac{2f_c\mu^2}{r_0^2\varepsilon^2}$ and $S_0(f)$ denotes the spontaneous spike train power spectrum of the renewal or nonrenewal variant (by using theory I).

3.4 Comparison between analytical and numerical spectra

Here, the numerically and analytically obtained results of the model and its variants ($\alpha = 1$, as discussed above) are shown and discussed. The necessary methods, to study the information transmission characteristics of the model and its variants, are described in detail in sec. 1.4.3. The phenomenon of band-pass filtering in the non-renewal model variant, as described and analyzed theoretically, are displayed in Fig. 3.7. The peak in the coherence function of the model with positive correlations between successive ISIs (shown in Fig. 3.7c) is due to the shaping of the power spectrum of the evoked activity of the model (displayed in Fig. 3.7b), whereas the squared cross-spectrum (see Fig. 3.7a) between the input signal (band-limited Gaussian white noise with a cut-off frequency of two (in units of the membrane time constant)) and the evoked spike-train as well as the power spectrum of the signal are constant (with respect to frequency). In contrast to the renewal model, which shows a monotonically decreasing coherence function (low pass filter), the non-renewal model acts as a band pass filter on information. Both variants show the typical fluctuations in the squared cross-spectrum for frequencies close to the firing rate (here one) (see Fig. 3.7a).

The peak of the coherence function, i.e. the local minimum of the power spectrum of the evoked spike-train is close to half the firing rate (here $r_0 = 1$). Both effects of low-pass filtering (renewal model, i.e. without ISI correlations) and band-pass filtering (non-renewal model, i.e. positive correlations between adjacent ISIs) are captured by both theoretical approaches (theory I and theory II). Although theory I predicts the emergence of a peak of the coherence function qualitatively, the coherence function (obtained by using theory I) overestimates the simulated coherence function. In contrast to theory I, theory II describes the coherence function surprisingly well (see the solid line in Fig. 3.7c). These example spectra indicate, that theory I can be used to obtain a reliable estimation of the peak of the coherence function. However, the coherence quality (see Eq.(3.2) will not be well approximated by using theory I. Note also that the coherence function at zero frequency and also its curvature at this point is very similar between theory I and theory II and is in good agreement with numerically simulated results.

Here, the phenomenon of band-pass filtering on information based on positive ISI correlations is numerically analyzed in more detail. For the sake of validation of the numerical procedure, we also compare the numerical results with theoretical predictions (using the approach developed by Lindner et al. (2005)). In Fig. 3.8, example spectra obtained by numerical simulations for different signal strengths and rather regular firing patterns ($C_V = 0.1$) are shown and compared to theoretical predictions (theory I).

The most prominent difference between the renewal and the non-renewal variant of the deterministic PIF with a stochastic threshold and reset concept (using an inverse Gaussian distribution for both) is the filtering effect measured by the coherence function

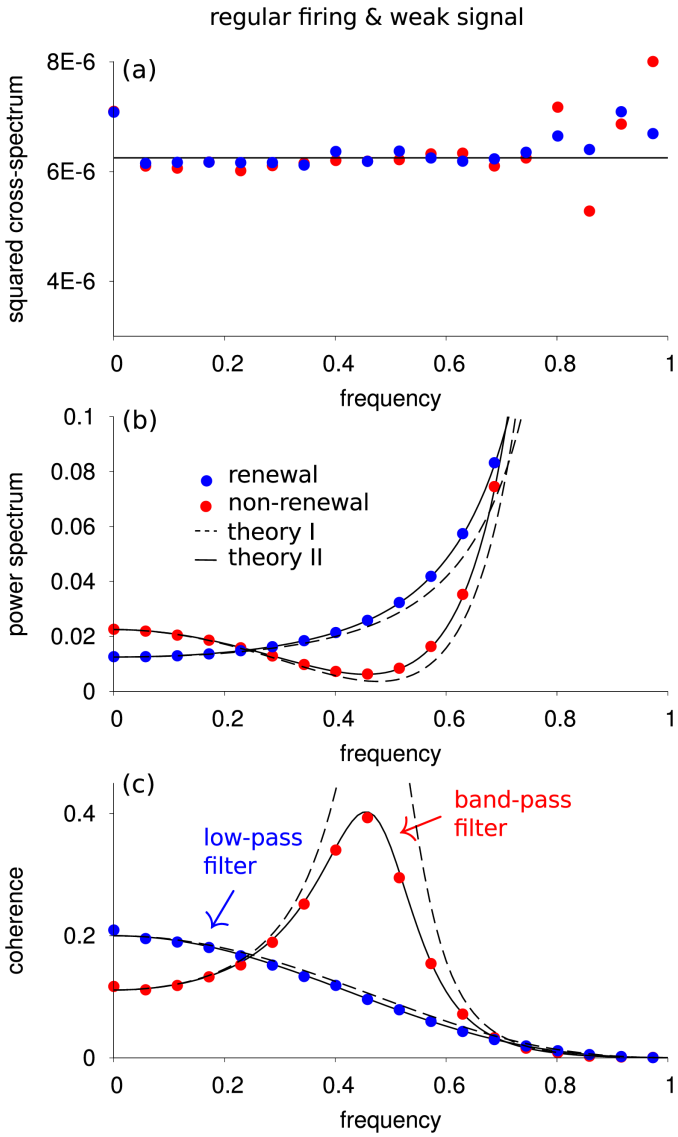

Figure 3.7: Information filtering of the two models with an inverse Gaussian ISI distribution. Numerical results (symbols) compared to theory I (dashed lines, see Eq.(3.20)) and theory II (solid lines, see Eq.(3.21a)) for $C_{V,0} = 0.1$ of the spontaneous activity and a weak input signal $s(t)$ ($\varepsilon^2 = 0.01$). Theory I predicts a maximum of the coherence at much higher values ($C \approx 0.7$), which is not shown.

(seen in Fig. 3.8c,f). The renewal version (left panel of Fig. 3.8) acts as a low pass filter on information within the region of regular firing (spontaneous $C_V = 0.1$) for different input signal intensities $\varepsilon^2 \in \{0.01, 0.1, 0.5\}$. Thus, the coherence function of the renewal model does not exhibit any significant peak (see Fig. 3.8c). In contrast to the

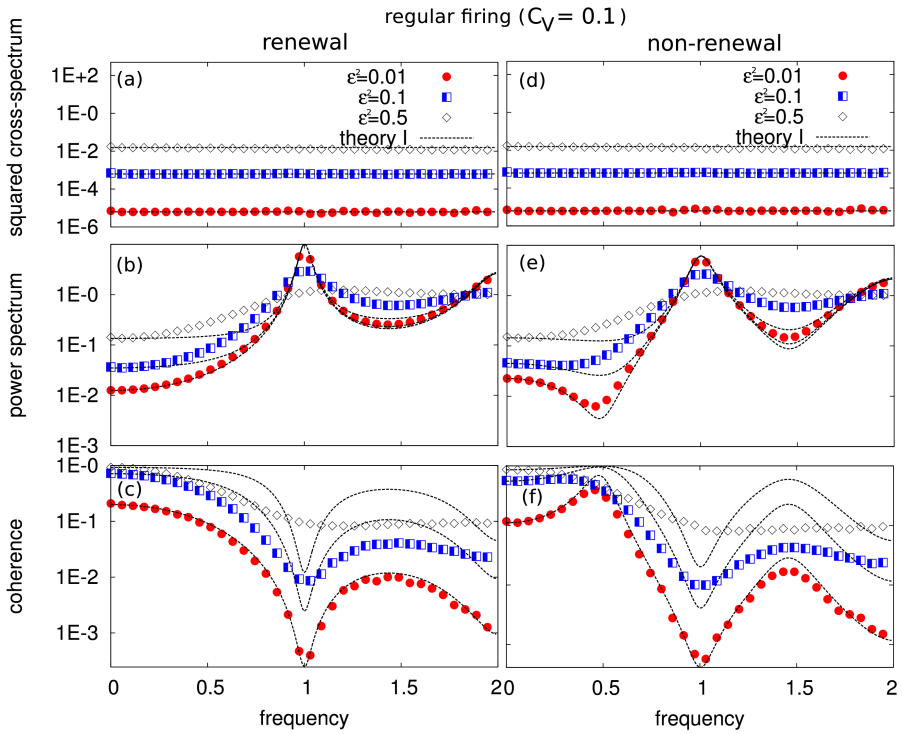

Figure 3.8: Spectral measures for low intrinsic variability ($C_V = 0.1$) and different values of the signal variance $\epsilon^2 \in \{0.01, 0.1, 0.5\}$. Comparison between the spectra of the renewal (first column) and non-renewal (second column): squared cross-spectrum (a,d), spike train power spectrum (b,e) and the coherence function (c,f) to theoretical estimations by using theory I (dashed lines, see Eq.(3.20)).

renewal variant, the non-renewal version (right panel of Fig. 3.8) exhibits a band-pass filtering effect on information, because the coherence function (displayed in Fig. 3.8f) shows a significant peak located around $f = 0.5$, which is half the firing rate of the spontaneous activity ($r_0 = 1$). This effect is most pronounced for very weak signal variances ($\varepsilon^2 = 0.01$, see red data points in Fig. 3.8) and is attenuated for larger signal strengths. This effect of band-pass filtering in the non-renewal variant of the stochastic model (resulting in positive correlations between adjacent ISIs) is due to the modulation of the power spectrum by the input signal and *not* due to modulations of the squared cross-spectrum (compare Fig. 3.8d and Fig. 3.8e).

The local minimum in the power spectrum, which is close to half the firing rate of the spontaneous activity, causes the peak in the coherence function of the non-renewal variant. This local minimum is due to the presence of correlations between adjacent ISIs and is not visible in the renewal variant (model without adjacent ISI correlations).

A second, more technical conclusion can be drawn from Fig. 3.8, which demonstrates that theory I describes the filtering effects (low-pass in the case of the renewal variant

and band pass in the case of the non-renewal version) quantitatively only for very low input signal variances (here $\varepsilon^2 \leq 0.01$).

3.4.1 Theory I versus theory II (regular firing)

As have been demonstrated in Fig. 3.8, the use of the 'basic' approach (theory I, see Eq.(3.20)) to obtain the power spectrum of the evoked activity is only valid for small signal strengths. Next, a direct comparison of theory I and theory II within this parameter regime (regular firing rate) will be performed. As one can see in Fig. 3.9b,e, theory

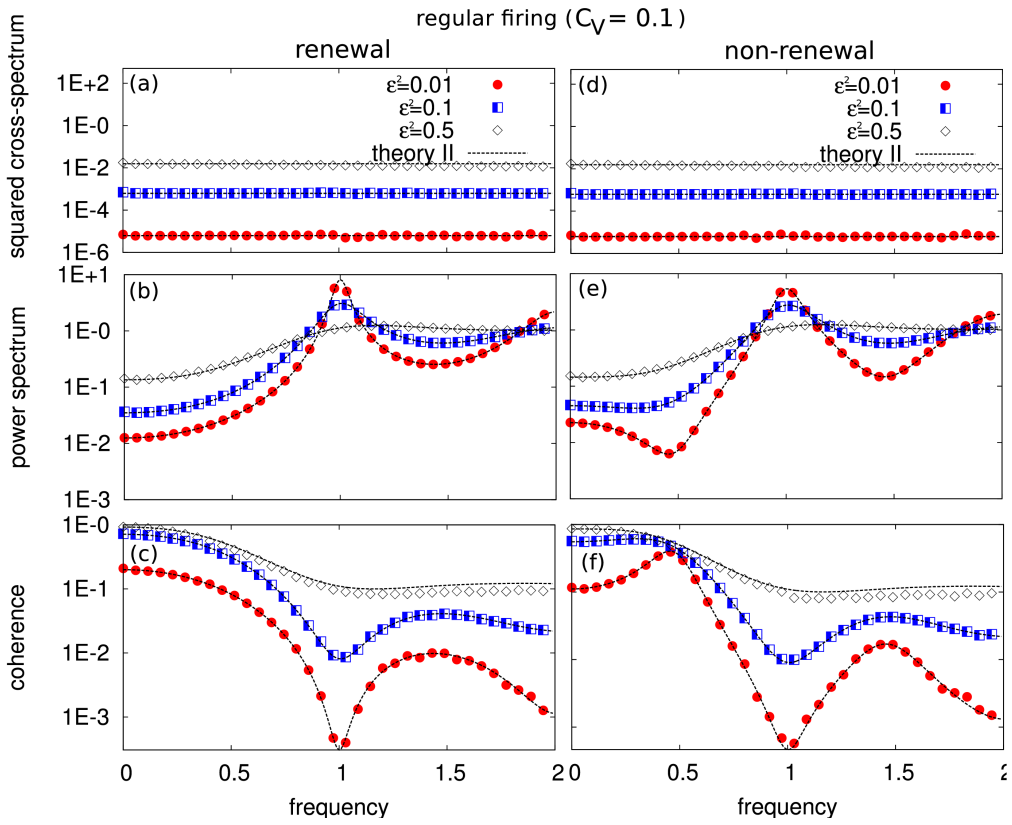

Figure 3.9: Spectral measures for low intrinsic variability ($C_V = 0.1$) and different values of the signal variance $\varepsilon^2 \in \{0.01, 0.1, 0.5\}$. Comparison between the spectra of the renewal (first column) and non-renewal (second column): squared cross-spectrum (a,d), spike train power spectrum (b,e) and the coherence function (c,f) to theoretical estimations using theory II (dashed lines).

II (dashed line, see Eq.(3.21a)) describes the power spectrum at low as well as at high signal strengths very accurately. Therefore, the coherence function (consult Fig. 3.9c,f is veraciously described by theory II for a large range of signal strengths as well.

3.4.2 Theory I versus theory II (rather irregular firing)

As have been demonstrated above, theory I (see Eq.(3.20)) is only applicable for small signal strengths (there $\varepsilon^2 \leq 0.01$) within the regular spiking activity regime (small intrinsic noise due to a narrow threshold and reset distributions). In contrast, theory II (see Eq.(3.21a)) characterizes the band-pass filtering effect quantitatively for a large range of signal strengths. How does the effect of band-pass filtering on information change, when the firing activity becomes more irregular, i.e. $C_V > 0.1$? To answer this question, one has to increase the noise strength in the model system, i.e. one has to broaden the threshold and reset distribution. Fig. 3.10 presents the numerically and analytically

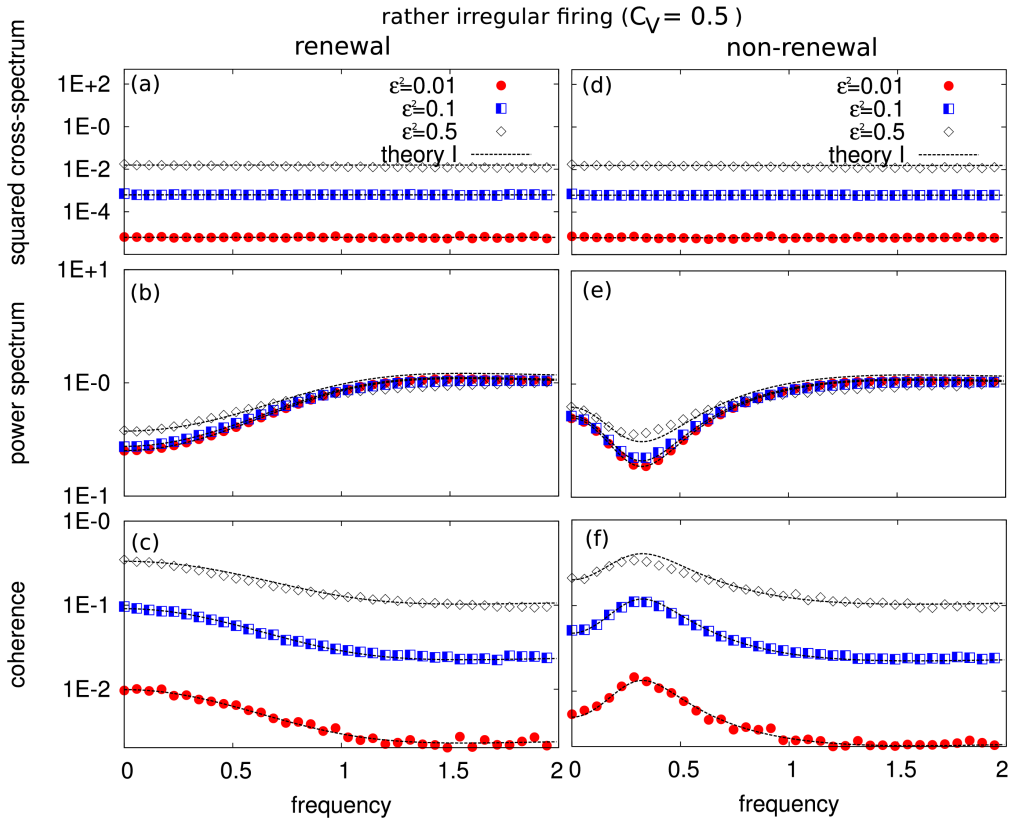

Figure 3.10: Spectral measures for moderate intrinsic variability ($C_V = 0.5$) and different values of the signal variance $\epsilon^2 \in \{0.01, 0.1, 0.5\}$. Comparison between the spectra of the renewal (first column) and non-renewal (second column): squared cross-spectrum (a,d), spike train power spectrum (b,e) and the coherence function (c,f) to theoretical estimations using theory I (dashed lines).

obtained squared cross-spectrum (Fig. 3.10a,d), power spectrum (Fig. 3.10b,e) as well as the coherence function (Fig. 3.10c,f) for the renewal variant (first column of (Fig. 3.10) and the non-renewal (second column of (Fig. 3.10) version by using an inverse Gaussian

distribution for threshold and reset values, which results in a spontaneous activity that is classified as rather irregular ($C_V = 0.5$). The band-pass filtering effect in the non-renewal variant, visible in regular firing regimes (see for example Fig. 3.9), is also present in the rather irregular firing regime. One can see that the band pass filter on information is more pronounced at large signal strengths (see Fig. 3.10f) compared to band pass filters observed in the rather regular firing regime (see Fig. 3.9f). This markedness of the band-pass filter is due to an increase of the intrinsic variability of the system (threshold and reset noise), which results in a smaller signal-to-noise ratio (SNR) of the model. Thus, small SNRs are of advantage in establishing a band pass filter on information. The theory I predicts the simulated power spectrum for all shown signal strengths very well, because of the higher intrinsic noise, which effectively lowers the signal strength. Fig. 3.11 shows the same numerical results as in Fig. 3.10, i.e. within the rather irregular

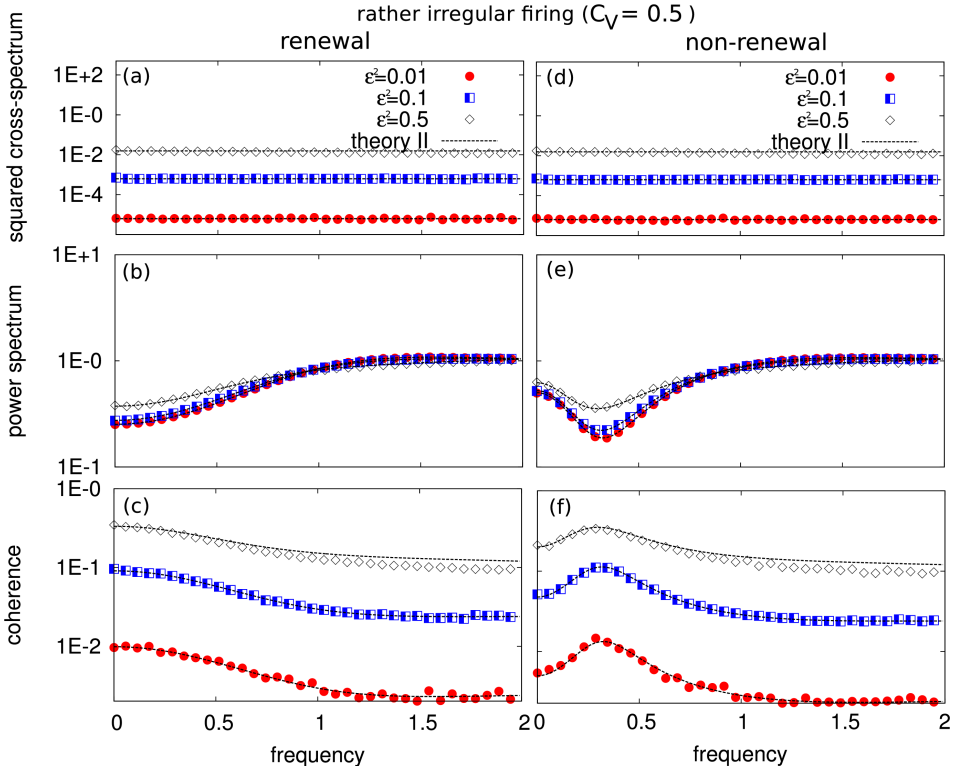

Figure 3.11: Spectral measures for moderate intrinsic variability ($C_V = 0.5$) and different values of the signal variance $\epsilon^2 \in \{0.01, 0.1, 0.5\}$. Comparison between the spectra of the renewal (first column) and non-renewal (second column): squared cross-spectrum (a,d), spike train power spectrum (b,e) and the coherence function (c,f) to theoretical estimations using theory II (dashed lines).

firing region ($C_V = 0.5$) of the two model variants, but in comparison with theory II. As expected, for large signal strengths the more refined approach for the power spec-

trum of the evoked power spectrum (see Eq.(3.21a)) describes the spectra more accurate compared to the 'basic' approach: theory I (see Eq.(3.20)).

3.5 Numerical studies of the filtering characteristics

In the following section, the effects of the threshold and reset variability on the information filtering characteristics of both variants (renewal, non-renewal) of the symmetric model ($\alpha = 1$), i.e. with strongest correlations for the non-renewal model, as well as the effects of the steady state firing rate r_0 are discussed. Then the effects of the strength of the correlations (varied by varying α) of adjacent ISIs on information filtering properties of the general model, which includes renewal variant as special cases ($\alpha \to 0$,$\alpha \to \infty$), are analyzed by means of extensive numerical simulations (50.000 parameter sets), which cover different regimes of spiking activity (from phasic to tonic firing).

3.5.1 The effects of threshold and reset variability

As have been demonstrated above, the intrinsic variability due to the threshold and reset value variability is essential to establish (and enhance) the band-pass filtering characteristics on information of the non-renewal model. Here, the effects of this intrinsic variability in the two model variants (renewal, non-renewal) are explored and discussed in more detail. This exploration in based on numerical studies.

Fig. 3.12 shows the meta statistics obtained by analyzing numerical spectra of the renewal and non-renewal model variant. The relationship between information theoretic characteristics like: the frequency of the local maximum of the coherence function, i.e. the band-pass filtering frequency (Fig. 3.12a,e), the quality of the coherence function (Fig. 3.12b,f) ,and the lower bound of the mutual information rate (Fig. 3.12c,g) using the coherence function, and the coefficient of variation (CV) of the evoked spiking activity (Fig. 3.12d,h), is illustrated.

The variability of the evoked activity stems from two sources: i) variability of threshold and reset (spontaneous CV), and ii) variability due to the stochastic input signal (band-limited Gaussian white noise with a cut-off frequency of two). The renewal model, which does not show any ISI correlations at all, acts primarily as a low pass filter on information, which is manifested by a coherence quality of one (see Fig. 3.12b) and consequently a maximum of the coherence function at zero frequency (see (Fig. 3.12a). In contrast, the non-renewal model, which exhibits positive correlations between adjacent ISIs, can act as band pass filter on information, i.e. a non-zero band-pass filter frequency (see (Fig. 3.12e) and consequently a coherence quality larger than one (Fig. 3.12f).

(Fig. 3.12f) suggests that weak signals are favored concerning band-pass filtering on information (see red data points in Fig. 3.12f). The band-pass filter effect is most pronounced for weak signals, for which the coherence quality obtains its maximum of around five (see red data points in Fig. 3.12f) for rather regular spiking activity ($C_V \approx 0.15$). However, the lower bound of the mutual information rate is very low in this activity regime (see Fig. 3.12g), because it decreases very fast with increasing ISI variability,

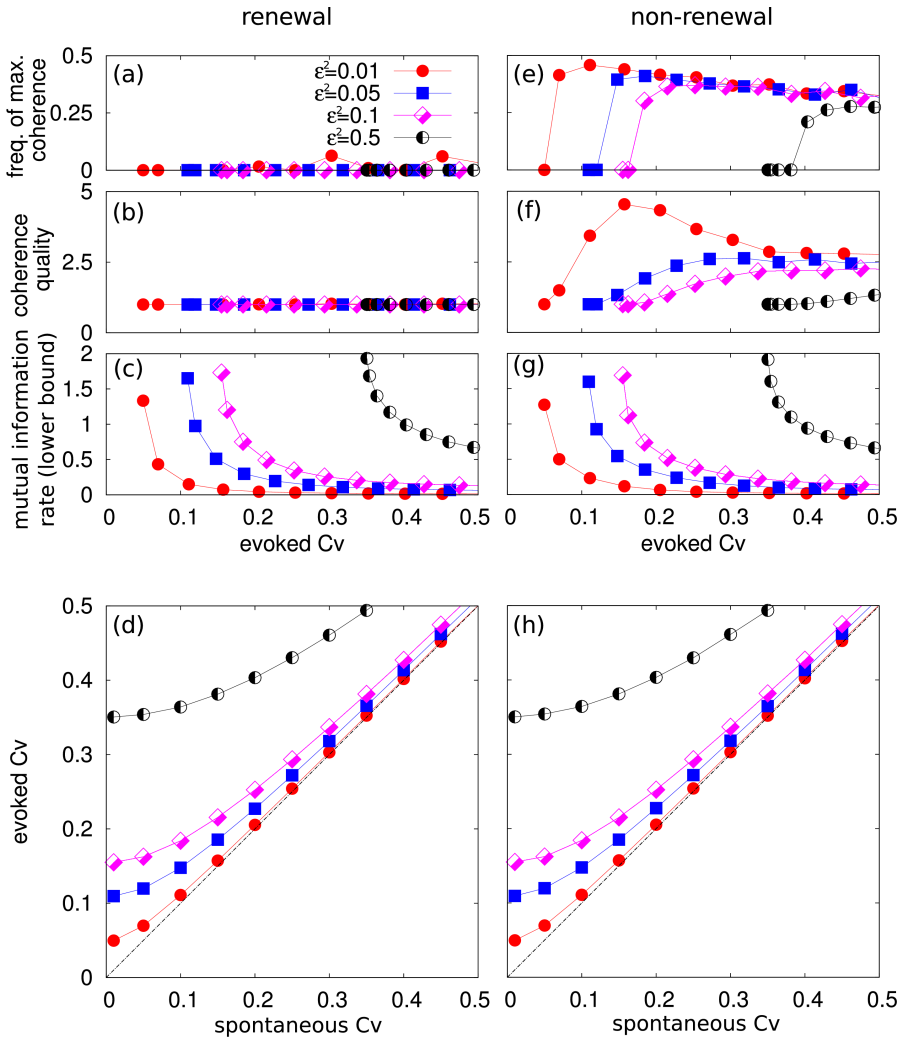

Figure 3.12: Characteristics of the information transmission and filtering as functions of spiking variability for renewal model (left) and non-renewal model (right) using an inverse Gaussian distribution for thresholds and resets. Shown are: the frequency at which the coherence has its global maximum (a, e), quality of coherence, Eq.(3.2) (b, f), and lower bound on the mutual information rate, Eq.(1.12) (c, g). All statistics are determined from simulation data and plotted vs. evoked coefficient of variation (CV in the presence of broadband stimulus), which is also measured in simulations. The evoked CV was varied by changing the CV of the spontaneous activity, a parameter that enters the model through the distributions of threshold and reset, Eq.(3.6). Evoked CV is shown as a function of spontaneous CV in (d, h). All data are obtained from numerical simulations of the models.

measured by the CV. A further increase of the ISI variability results in less pronounced band pass filter (smaller Q value for the non-renewal variant) and less transmitted information (see Fig. 3.12g). As expected from data shown above (see Fig. 3.12a), the renewal variant acts within the explored firing regime ($C_V \in (0, 0.5)$) as low pass filter on information.

Interestingly, the comparison between the mutual information rate of the renewal and the non-renewal variant reveals a remarkable similarity between the two variants (compare Fig. 3.12c and Fig. 3.12g). This effect is due to the fact that the renewal model has a lower signal-to-noise (SNR) ratio compared to the non-renewal model because threshold and reset values are drawn independently in the renewal model. The relationship between the evoked and spontaneous activity is shown in Fig. 3.12d,h and reveals that the variability of the evoked activity is almost equal to the variability of the spontaneous activity for weak signals (see red data points in Fig. 3.12d,h). However, the linear relationship between the spontaneous CV and the evoked CV is no longer fulfilled in cases of moderate and high signal strengths (see blue, magenta and black data points in Fig. 3.12d,h).

We conclude that the intrinsic variability is indeed of pivotal importance to establish a band-pass filter on information in the non-renewal variant of the model, such that an optimal amount of intrinsic variability exists, at which the band-pass filtering characteristics is very pronounced (see red data point in Fig. 3.12f). The numerical data are shown in Fig. 3.12 suggest that the band pass filter on information (of the non-renewal variant) is most pronounced at weak signal strengths and a rather regular firing regime. In the region explored ($C_V \in (0, 0.5)$), the renewal model variant acts primarily as low pass filter on information.

3.5.2 The effects of the firing rate

Besides the variability of the spiking activity, measured by the CV, another important classification is whether the neuron spikes very often or is rather silent. This activity signature is usually covered by the firing rate, i.e. the number of spikes within a unit time window, or put differently, the inverse of the mean ISI. Here we will investigate, how the firing rate of the neuron model influences the information theoretic characteristics (quality factor of the coherence) of the band pass filter on information. For this reason, one has to fix the spontaneous CV, and the signal strength ε and vary the firing rate r_0, i.e. the distance between the mean values of the threshold and reset distribution respectively.

Fig. 3.13 displays the numerically obtained results of the information theoretic meta statistics for the renewal (left side of Fig. 3.13) and the non-renewal (right side of Fig. 3.13) variant of the model with stochastic threshold-and-reset values (inverse Gaussian). As demonstrated in Fig. 3.13a the renewal variant shows a coherence quality of one, regardless of the firing rate, ranging here from zero to five (in units of frequency). Thus, the renewal version (without ISI correlations) acts as a low pass filter on information in the explored activity regime. Consequently, the resonance frequency of the coherence function is zero (see Fig. 3.13c). The lower bound of the mutual information

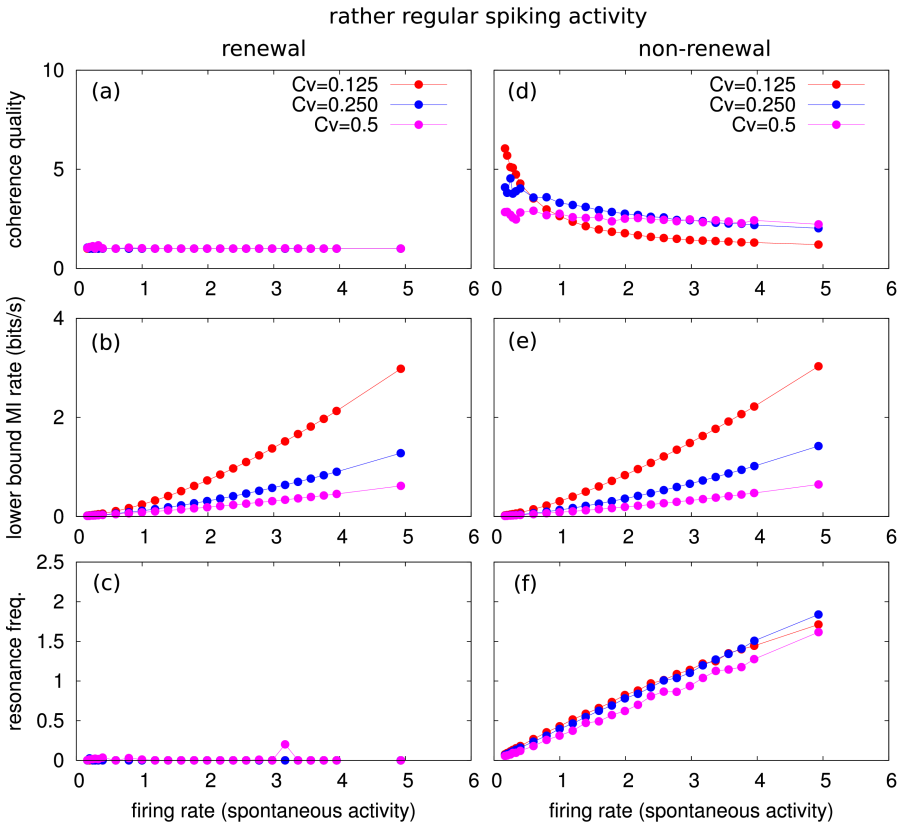

Figure 3.13: Characteristics of the information transmission and filtering as functions of spiking variability (rather regular, i.e. $C_V \leq 0.5$) for renewal model (left) and non-renewal model (right) using an inverse Gaussian distribution for thresholds and resets. Shown are: quality of coherence, Eq.(3.2) (a, d), the lower bound on the mutual information rate, Eq.(1.12) (b, e), and frequency at which the coherence attains its global maximum (c, f). The CV of the spontaneous was varied by changing the CV of the distributions of threshold and reset, Eq.(3.6). The signal strength of the band-limited Gaussian white noise with cut-off frequency of 10 was set to $D = 0.1$.

rate (Fig. 3.13b) increases with increasing firing rate and is maximal for very regular spiking activity ($CV = 0.125$, see red data points in Fig. 3.13b). In contrast to the renewal variant (right side of Fig. 3.13), the non-renewal version can act as a band pass filter on information, which is indicated by a coherence quality larger than one (see Fig. 3.13d). At low firing rates (here: smaller than two), the non-renewal model variant has a pronounced peak in the coherence function, i.e. coherence quality above one (see Fig. 3.13d) at approximately half the firing rate of the spontaneous activity (see Fig. 3.13f) irrespective of the regularity of irregularity of the activity, measured by the CV (see red, blue and pink data in Fig. 3.13). As discussed before, the lower bound of

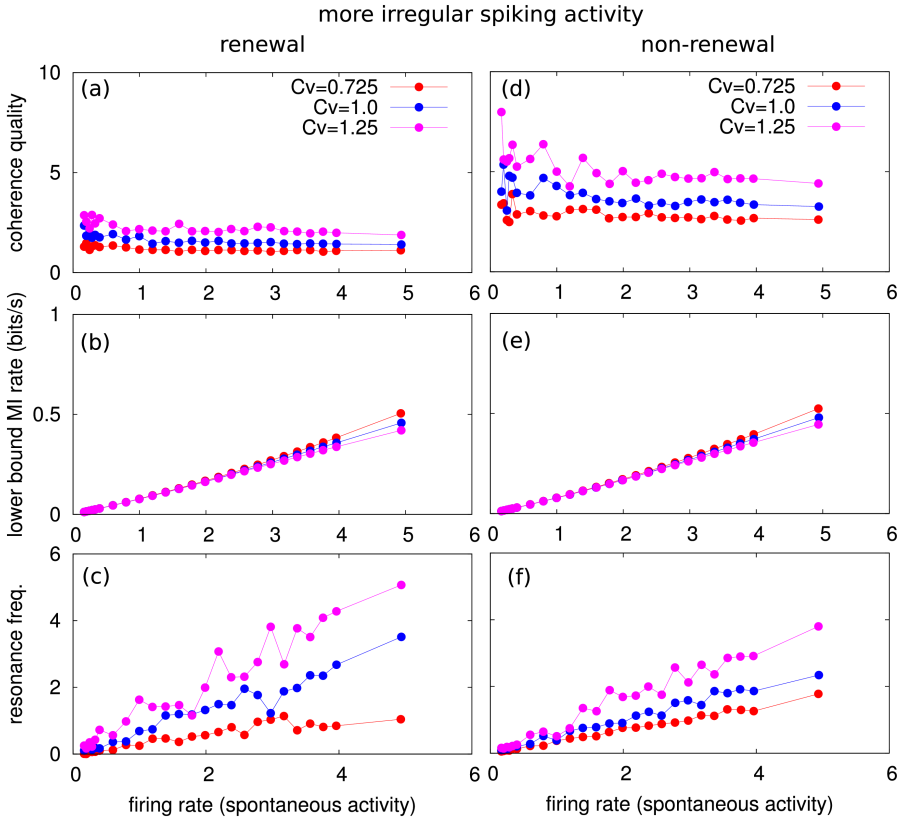

Figure 3.14: Characteristics of the information transmission and filtering as functions of spiking variability (more irregular, i.e. $C_V > 0.5$) for renewal model (left) and non-renewal model (right) using an inverse Gaussian distribution for thresholds and resets. Shown are: quality of coherence, Eq.(3.2) (a, d), the lower bound on the mutual information rate, Eq.(1.12) (b, e), and frequency at which the coherence has its global maximum (c, f). The CV of the spontaneous was varied by changing the CV of the distributions of threshold and reset, Eq.(3.6). The signal strength of the band-limited Gaussian white noise with cut-off frequency of 10 was set to $D = 0.1$.

the mutual information rate is very similar for the renewal and the non-renewal model variant (compare Fig. 3.13b and Fig. 3.13e). Fig. 3.14 shows the same meta statistics of the information filtering characteristics as shown in Fig. 3.13, but for higher values of the CV. One can infer from Fig. 3.14a that the renewal variant can display band-pass filtering characteristics, manifested by a coherence quality larger than one, if the intrinsic variability due to threshold and reset noise is very large (compared to the input signal). Here, very irregular spiking activity, which stems from intrinsic variability, leads to band-pass filtering on information in the absence of ISI correlations (renewal variant). However, this band pass filter on information is not very pronounced (coherence qualities

are smaller than two, see Fig. 3.14a) and the information transfer is very reduced (compare Fig. 3.14b,e with Fig. 3.13b,e). This effect of band-pass filtering on information in the renewal variant of the model can be explained analytically (see Eq.(3.29) in sec. 3.6).

We conclude that the firing rate of the spiking activity of the model has a major impact on the information transfer characteristics of the non-renewal model variant, i.e. the model variant with positive ISI-correlation between successive ISIs such that the quality factor of the coherence function decreases with increasing firing rate. The resonance frequency of the coherence function, i.e. the band-pass filter frequency increases with increasing firing rate approximately linear (see Fig. 3.14c) with a slope-factor of approximately of one-half. For very high intrinsic variability, the renewal variant also shows a band-pass filtering characteristics, which will be explained analytically in sec. 3.6.

3.5.3 The effects of the correlation 'strength' between adjacent ISIs

As described in sec. 3.2.1, the introduction of a scaling factor α between threshold and reset value leads to a variation of the serial correlation coefficient at lag one, i.e. ρ_1 (for $\alpha \in (0, \infty)$). By adapting the mean and the coefficient of variation (CV) of the threshold and reset distribution, one can fix the firing rate and the CV of the spike train of the spontaneous activity, i.e. without the presence of a time-dependent signal $s(t)$. Consequently, this holds true in the presence of for weak signals.

Fig. 3.15 and Tab. 3.1 show the numerical results concerning the effects of the scaling parameter α on the dynamical (firing rate, CV) and information theoretical characteristics of the general model. Shown are: example trajectories (Fig. 3.15a), squared cross spectrum between spike train and input signal (Fig. 3.15b), spike train power spectrum (Fig. 3.15c), and the coherence function (Fig. 3.15d) for three different values of ISI correlation ($\rho_1 = (0.4, 0.5, 0.23)$). From Fig. 3.15a one can draw the conclusion that the

Table 3.1: Above the dashed line, three different parameter sets for the nonrenewal variant of the PIF model with inverse Gaussian distributed thresholds and resets with different degree of adjacent ISI correlations (ρ_1. The corresponding numerical values of the information theoretic measures (coherence quality, resonance frequency of the coherence function, and the lower bound of the mutual information rate) for the example spectra shown in Fig. 3.15b–d are shown below the dashed line.

α	0.4	1	4	scaling factor
ρ_1	0.4	0.5	0.23	adjacent ISI correlation
r	0.99	0.99	0.99	mean firing rate
CV	0.11	0.11	0.11	spike train coefficient of variation
Q_C	1.8	3.25	1.09	quality factor of coherence
f_{res}	0.43	0.45	0.35	resonance freq. of coherence
MI_{LB}	0.15	0.18	0.13	lower bound of mutual information rate

firing rate and the CV is (in first approximation) constant for the three model param-

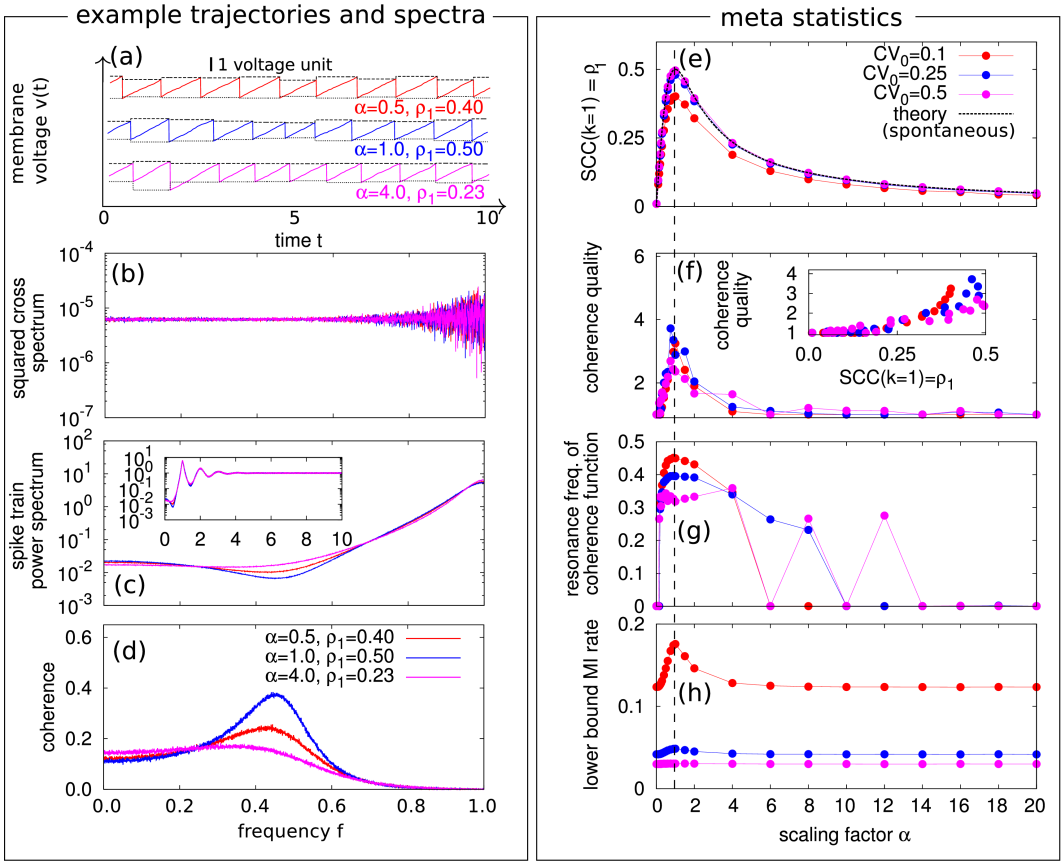

Figure 3.15: Characteristics of information transmission under variations of the magnitude of adjacent ISI correlations I. Shown are: numerical simulation results by using the stochastic threshold PIF model for scaling factors $\alpha \in (0, 20]$, which results in a gradual change of the correlations of successive ISIs in the range $\rho_1 \in (0, 0.5]$. Example trajectories for three different values of ISI correlations (a) and the corresponding squared cross spectrum between weak signal and output spike train (b), as well as the spike train power spectrum (c) and the coherence function (d). Positive ISI correlations lead to the emergence of a band pass filter on information (d). The corresponding meta statistics by varying $\alpha \in (0, 20]$ for three different values of spiking activity ($CV \approx (0.1, 0.25, 0.5)$ with fixed spontaneous firing rate of $r_0 = 1.0$) are shown in the right column. SCC at lag 1 (ρ_1) of the evoked activity (simulation results compared with analytical predictions based on Eq.(3.8)) (e), coherence quality (as a function of ρ_1 in the inset in f) (f), band-pass filter frequency of the coherence function (g), and the lower bound of the mutual information rate as a function of α (h). Numerical parameters and meta statistics can be found in Tab. 3.1.

eters ($\alpha \in \{0.5, 1.0, 4.0\}$). The different ISI correlation coefficients cannot be identified by the naked eye, but are hidden in the statistics of the spike trains (see Fig. 3.15c,e). A direct comparison between theoretically obtained ISI correlations (see Eq.(3.8)) with numerical results (see Fig. 3.15e) leads to the conclusion that the SCC of the evoked activity (numerical results) is well approximated by the SCC of the spontaneous activity (theory, dotted line in Fig. 3.15e) for weak signals, i.e. moderate to high intrinsic variability.

The coherence function (see Fig. 3.15d) shows a pronounced peak, which is located approx. at half the firing rate (here $r_0 = 1$) for a scaling factor $\alpha = 1.0$, i.e. for maximal value of $\rho_1 = 0.5$. The band-pass filtering effect on information is attenuated for scaling factors α different from one, i.e. for weaker ISI correlations. This effect of frequency selectivity on the level of information transmission is solely due to a local minimum of the spike train power spectrum (see Fig. 3.15c), because the squared cross-spectrum (see Fig. 3.15b) is always flat (for weak signals) and shows the typical (for this model system) numerical fluctuations (see Fig. 3.15b) at frequencies close to the firing rate (here $r_0 = 1$).

Fig. 3.15 also shows the corresponding meta statistics of the serial correlation coefficient at lag 1 (ρ_1) (e) , the quality factor of the spectral coherence function (f), the resonance frequency of the coherence function (g), and the lower bound of the mutual information rate (h) of input signal and output spike train for three different values of the CV of the spontaneous spike train (CV_0).

The SCC of the evoked activity is close to SCC of the spontaneous activity (compare simulation results in red, blue and magenta with theoretical predictions indicated by the dashed line in Fig. 3.15e) for more irregular firing activities (here $CV > 0.1$). The disagreement between evoked and spontaneous SCC for very regular firing activities (here $CV \leq 0.1$) can be understood by considering that for regular firing activities, the influence of the signal is very strong. Therefore, the distinction between strong and weak stochastic signals depends on the regularity or irregularity of the spontaneous activity (c.f. Fig. 3.8 and Fig. 3.10 and their corresponding interpretation and discussion). The band-pass filter effect on information (based on the spectral coherence function) is most pronounced for large ISI correlations (see Fig. 3.15f and Fig. 3.16a) and is a monotonical increasing function with respect to the serial correlation coefficient ρ_1 (shown in the inset of Fig. 3.15f and in and Fig. 3.16a). The stronger the correlation between successive ISIs, the stronger becomes the phenomenon of band-pass filtering on information. For very strong ISI correlations, the resonance frequency, i.e. the frequency of maximal coherence, is close to half the mean firing rate (here $r_0 = 1$) and decreases with decreasing ISI correlation (compare Fig. 3.15f and Fig. 3.15g).

The manifestation of a band pass filter on information comes along with a decrease of the mutual information rate (based on the lower bound formula Eq.(1.12)) and is maximal for a scaling factor of $\alpha = 1$ (symmetry between threshold and reset distribution, indicated by the dashed line in Fig. 3.15e-h). This effect is referred as **trade-off** between selective and total signal transmission.

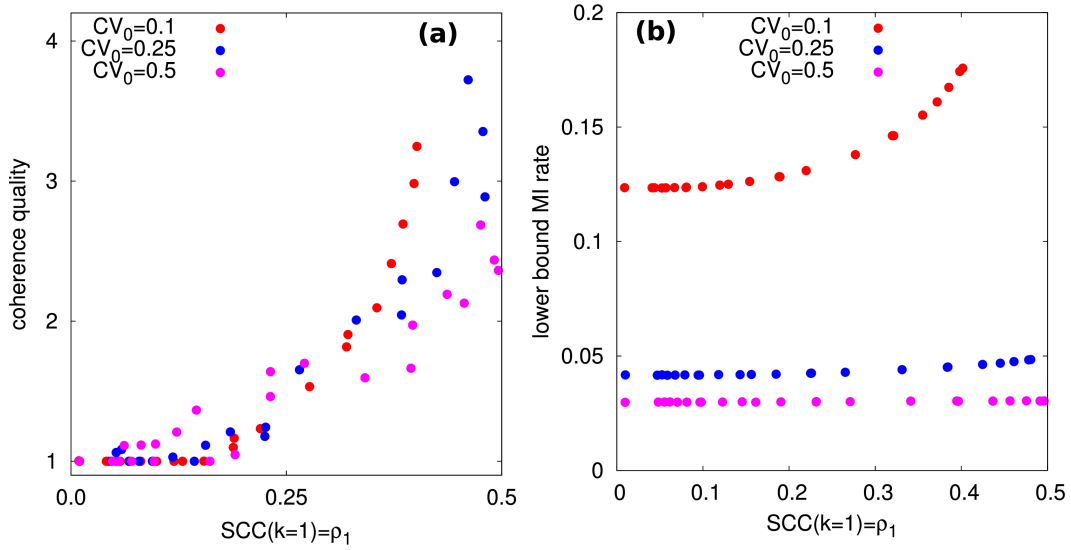

Figure 3.16: Characteristics of information transmission by under variations of the degree of adjacent ISI correlations II. Shown are: a) coherence quality Q_C and b) lower bound of the mutual information rate as a function of adjacent ISI correlation coefficient ρ_1 for three different values of coefficient of variation $CV = (0.1, 0.25, 0.5)$ and fixed spontaneous firing rate of $r_0 = 1$ in the presence of a weak time-dependent stochastic input signal (band-limited ($f_{\text{cut}} = 10$) Gaussian white noise). The quality of the band pass filter on information is positively correlated (a) with the degree of ISI correlations ρ_1. More pronounced band pass filters on information lead to higher information rates (b) based on the lower bound mutual information rate.

3.5.4 The effects of ISI correlations in different firing regimes

Here we will study the general features regarding the information filtering characteristics of the model with continuously varying ISI correlations, which includes the limits: $\alpha \to 0$ and $\alpha \to \infty$ the renewal variant (no ISI correlations at all).

How do ISI correlations influence the information transmission in different regimes? To answer this question, one has to study the stochastic threshold and reset PIF numerically in a parameter space, which is spanned by the CV and the correlation coefficient of successive ISIs ρ_1 and fixing the firing rate: $r_0 = 1$. As shown previously (see Fig. 3.16a), the quality factor of the coherence function increases with increasing serial correlation coefficient of adjacent ISIs for constant firing rate and CV. Surprisingly, the data shown in Fig. 3.16 suggest that both coherence quality and lower bound of the mutual information rate increases with increasing ISI correlations (for fixed firing rate and CV). Does this mean that the emergence of a band pass filter on information increases the mutual information rate in general? If that would be true, then there would be no disadvantage (regarding information theoretic characteristics) in establishing a band pass filter on information. This conclusion seems to be counter-intuitive because on could think of the

simplest way to establish a band pass filter on information by simply reducing the information transfer (coherence function) in frequency bands outside the desired frequency band. This procedure would imply a reduction of the total transmitted information, and thus a trade-off between the markedness of the band pass filter on information on the one hand, and the total transmitted information, measured by the lower bound of the mutual information rate, on the other hand.

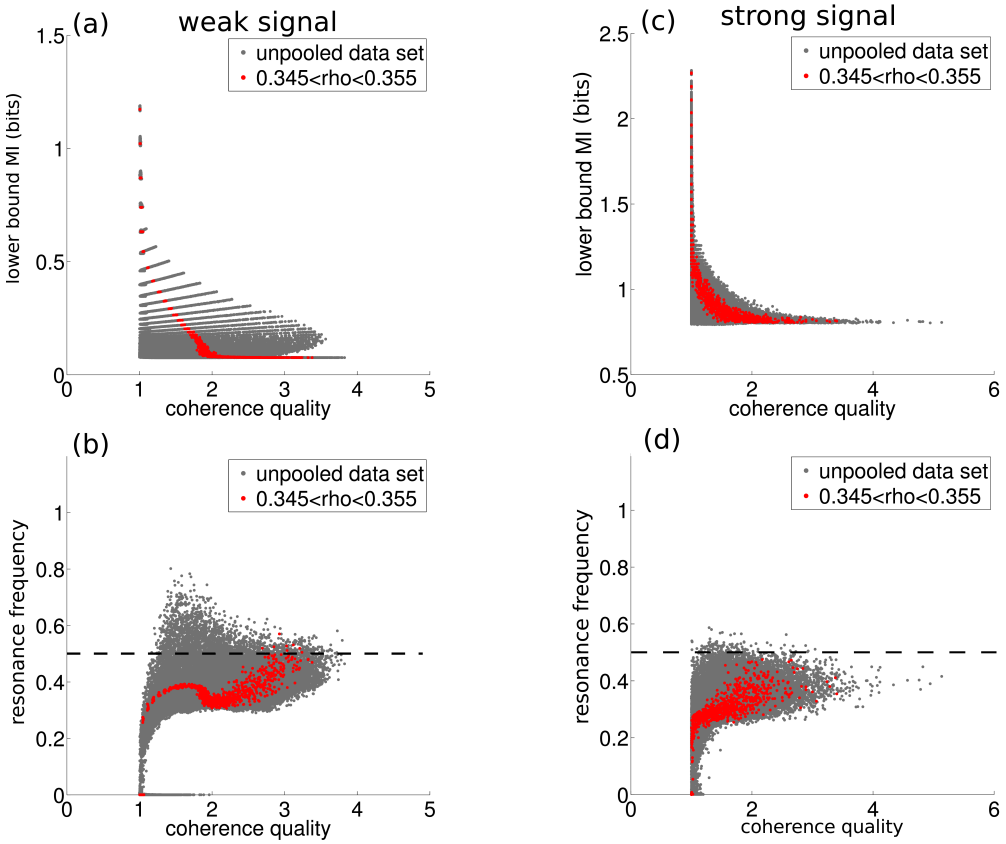

Figure 3.17: Meta statistics of information transmission characteristics under variations of ISI (IG distributed) correlations and CV for weak and strong stochastic input signal. Shown are numerical results (50.000 parameter sets) by using a weak signal (a-b) and a strong input signal (c-d). The lower bound of the mutual information with respect to coherence quality (a,c), the resonance frequency of the coherence function with respect to the coherence quality (dashed line indicates half the firing rate) (b,d). The trade-off between band-pass filtering and total transmitted information is present in both weak (a) and strong (c) signals. The center frequency, also called resonance frequency of the coherence function, is close to half the firing rate (b,d), which was set to one here. The red data points correspond to ISI correlations $0.345 < \rho < 0.355$.

To test this hypothesis, the model variant with gradual ISI correlations is explored in more detail by employing extensive numerical computer simulations (50.000 parameter sets for weak and strong signal), which cover a wide range of activity regimes (from very regular to very irregular activity). Fig. 3.17 displays the results of these simulations for a weak and a strong signal (band-limited Gaussian white noise). The numerical results suggest that the realization of a band pass filter comes to the 'cost' of reducing the mutual information rate (lower bound). Thus, the chosen model describes a trade-off between frequency selective information transmission (measured by the coherence quality) and the total amount of transmitted information (see Fig. 3.17a,c). The red data points in Fig. 3.17 correspond to almost constant ISI correlations with $\rho \approx 0.35$.

The resonance frequency of the coherence with respect to the coherence quality is shown in Fig. 3.17b,d for weak and strong signals. These numerical results suggest that the resonance frequency lies in the vicinity of half the firing rate (here $r_0 = 1$), which is indicated by the horizontal dashed line in Fig. 3.17b,d. The resonance frequency approaches zero in the limit of low-pass filtering on information, i.e. coherence qualities close to one (see Fig. 3.17b,d).

Having explored numerically the trade-off between the mutual information rate and the coherence quality, as well as the relative robustness of the resonance frequency, the question arises, whether the band-pass filtering on information is most pronounced in regular (tonic) or irregular (phasic) firing regimes? By using the same numerical data set as shown in Fig. 3.17 and a projection of the coherence quality on the CV, one can answer the question insistently.

Fig. 3.18 displays the dependency of the coherence quality with respect to the CV for weak (Fig. 3.18a) and strong (Fig. 3.18b) signals. For weak signals, there exists an optimal CV in the rather regular firing regime ($C_V < 0.5$), for which the coherence quality is maximal ($Q_C \approx 3.5$). The 'resonance' in the coherence quality with respect to the CV is very pronounced for strong correlations between successive ISIs and is diminished for weak ISI correlations, note that the red data points in Fig. 3.18a,b correspond to moderate ISI correlations, i.e. $\rho \approx 0.35$). The optimal CV within the rather regular firing regime is close to 0.2 (see also Fig. 3.12f). If the spiking output becomes more irregular, then the quality of the coherence function first decreases and increases again within the highly irregular firing regime ($C_V \approx 1$). This effect on the coherence quality is diminished for strong signal strengths (see Fig. 3.18b).

3.6 Analytical insights on the effects of ISI correlations

Here, the analytical results of the stochastic threshold-and-reset PIF with positive correlations between adjacent ISIs are presented. An approximate classifier to distinguish between low and band-pass filtering on information is proposed and analyzed. This classifier is based on the curvature of the coherence function at zero frequency (see sec. 3.6.1). Extensive numerical analyses demonstrate (see Fig. 3.19) that this approach is justified. This study culminates in an analytically obtained phase diagram for low- and band-pass filtering on information depending on the ISI correlation and the coefficient of varia-

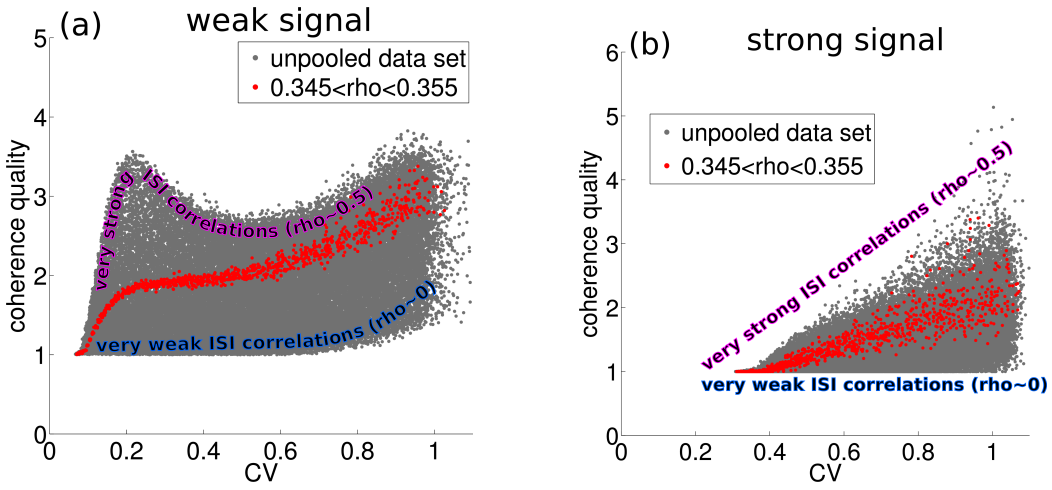

Figure 3.18: Metastatistics of information transmission characteristics under variations of ISI (IG distributed) correlations and CV for weak and strong stochastic input signal. Same parameter set as used in Fig. 3.17. For strong ISI correlations ($\rho = 0.5$) and weak signals (a), the band pass filter on information is most pronounced for rather regular ($C_V \approx 0.2$) and for very irregular firing activity ($C_V \approx 1$). However, the mutual information rate (lower bound) in the very irregular firing regime is very low. For strong signals (b), the quality resonance (shown in a) is not visible. The red data points correspond to ISI correlations $0.345 < \rho < 0.355$.

tion (CV) (see Fig. 3.19), which includes in essence qualitatively all previously obtained numerical results.

3.6.1 Spiking regimes for band-pass filtering (theory I)

Even in the simple theory I (see Eq.(3.20)) with inverse Gaussian distributed ISIs, the expression for the coherence function is rather involved Eq.(3.23) and it seems unfeasible to determine the global maximum of the coherence function analytically.

One can take the second derivative of the coherence, $C_I^{(2)}(0)$, i.e. its curvature, at zero frequency as a proxy in order to classify information filtering characteristics[4]. For example, if the curvature is positive then the coherence does not have a global maximum at zero frequency, i.e. it is not a low pass filter. On the other hand, if the curvature is negative then it is an indication that the information transmission drops with increasing frequency, which is the hallmark of a low pass filter of information. It is clear that with this locally defined measure one cannot make strict statements about global maxima of a function. However, specifically in the studied system, I have observed numerically that the curvature at zero frequency is a reliable characteristic to distinguish low pass from

[4]Note that the coherence is an even function, which implies that all odd derivatives of the coherence function vanish at zero frequency.

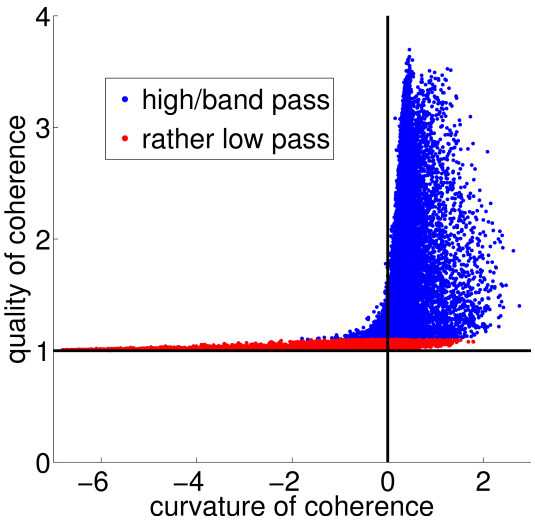

Figure 3.19: Relationship between the quality of the coherence function and its curvature at zero frequency. Shown are numerical results (50.000 parameter sets as used in Fig. 3.18 and Fig. 3.17) by using a weak input signal signal. Band-pass filtering on information is characterized by i) a quality factor larger than one and/or ii) a positive coherence curvature at zero frequency. The classification between low pass and band/high pass filter based on the curvature is justified for pronounced band pass filters (high quality factors). The red data points correspond to quality factors smaller than 1.1, i.e. weak band pass filters. A theoretical motivation that a positive curvature leads to an emergence of a resonance frequency can be seen in sec. B.2.

band pass filter on information (see Fig. 3.19). Furthermore, with a view on Fig. 3.7c it seems to be justified to use theory I for the coherence function at low frequencies, where its agreement with simulations is better than around the maximum of the coherence function.

How can we calculate $C_I^{(2)}(0)$? Because of the fact that the only frequency dependence of the coherence function results from the (non-trivial) power spectrum, in the approximation of theory I (see Eq.(3.20)) determined by $C_I(f) \sim S_0^{-1}(f)$, the curvature of the coherence can be expressed by the power spectrum of the spontaneous activity and its derivatives, $S_0(0), S_0^{(1)}(0), S_0^{(2)}(0)$. The latter in turn are related to the derivatives of characteristic function of the ISI density at zero frequency, which are given by the moments of the ISI in the absence of a stimulus according to:

$$\frac{d^n}{df^n}\tilde{F}_{1,0}(f)|_{f=0} = (2\pi i)^n \langle T^n \rangle. \tag{3.24}$$

Using this approach for the renewal and non-renewal model variants and employing the expressions for the power spectra, given in Eq.(3.13) and Eq.(3.14), one can express the curvature of the coherence function at zero frequency by the moments of the ISI density.

We will use the abbreviation $\mu_n =< T^n >$ (not to be confused for the base current μ).

Maximal positive correlations between adjacent ISIs

For the renewal model variant, the coherence function (theory I) at zero frequency is given by:

$$C_{\mathrm{R}}^{(0)}(0) = \frac{1}{1+\gamma r_0 C_V^2}, \tag{3.25}$$

which confirms that $S_{\mathrm{R},0}(f=0) = r_0 C_V^2$. The curvature of the coherence function at zero frequency of the renewal variant reads

$$C_{\mathrm{R}}^{(2)}(0) = \frac{2\pi^2\gamma\left(3\mu_2^3 - 4\mu_1\mu_3\mu_2 + \mu_1^2\mu_4\right) r_0}{3\left(\mu_1^2\left(1-\gamma r_0\right) + \gamma\mu_2 r_0\right)^2}. \tag{3.26}$$

The sign of the curvature is determined by the sign of the numerator of the fraction, i.e.

$$\begin{aligned} \operatorname{sign}\left(C_{\mathrm{R}}^{(2)}(0)\right) &= \operatorname{sign}\left(3\mu_2^3 - 4\mu_1\mu_2\mu_3 + \mu_1^2\mu_4\right) \\ &= \operatorname{sign}\left(-1 - \left(3+\beta_2\right)C_V^2 - 4\beta_1 C_V^3 + 3C_V^4\right). \end{aligned} \tag{3.27}$$

In the last line the moments were expressed in terms of the coefficient of variation (C_V), the skewness (β_1), and the kurtosis (β_2) (see Eq.(B.1)). From these expressions, which are valid for arbitrary distributions of threshold and reset, one can conclude that for low spike variability ($C_V \to 0$) the renewal model acts as a low pass filter on information because in this limit $\operatorname{sign}\left(C_{\mathrm{R}}^{(2)}(0)\right) \to \operatorname{sign}(-1)$. If one uses an inverse Gaussian ISI density then one can express skewness and kurtosis of the density solely by the mean and the C_V (see Eq.(B.3)). For an inverse Gaussian ISI density the sign of the curvature of the coherence function at zero frequency reads:

$$\operatorname{sign}\left(C_{\mathrm{R}}^{(2)}(0)\right) = \operatorname{sign}\left(-1 + 6C_{\mathrm{V}}^4\right). \tag{3.28}$$

Consequently, the analytical condition for low-pass information filtering (negative curvature) of the renewal model can be expressed with the following inequality:

$$C_{\mathrm{V}} < C_{\mathrm{V,crit}} = (1/6)^{1/4} \approx 0.6389. \tag{3.29}$$

If the C_V of the spontaneous activity (of the renewal model variant) is below the critical value $C_{\mathrm{V,crit}}$, then the model will act as a low pass filter of information, whereas for larger spiking variability a mild form of a band pass filter appears (see Fig. 3.20). The same calculation can be performed easily for the non-renewal variant. This results in analytical expressions of coherence function at zero frequency:

$$C_{\mathrm{NR}}^{(0)}(0) = \frac{\mu_1^2}{\mu_1^2\left(1-2\gamma r_0\right) + 2\gamma\mu_2, r_0}, \tag{3.30}$$

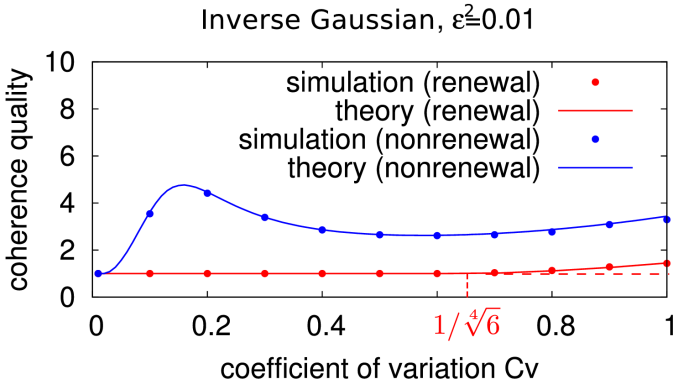

Figure 3.20: Coherence quality versus evoked coefficient of variation for small signal variance. The non-renewal blue line variant with leads to pronounced band pass filter characteristics on information, i.e. a coherence quality larger than one. The renewal variant (red line) acts primarily as a low pass filter on information. However, a very weak band pass filter in the renewal model appears for $C_V > 1/\sqrt[4]{6}$. In this regime, due to the high variability, the mutual information rate (lower bound) is very diminished. Theory refers to a numerical evaluation of theory II.

which can be expressed in terms of the r_0 and C_V as follows:

$$C_{\mathrm{NR}}^{(0)}(0) = \frac{1}{1 + 2\gamma r_0 C_V^2}. \tag{3.31}$$

This confirms that the spontaneous power spectrum at zero frequency of the non-renewal variant is twice as large as compared to the renewal case, i.e. $S_{\mathrm{NR},0}(f=0) = 2r_0 C_V^2 = 2S_{\mathrm{R},0}(f=0)$.

Similarly, the curvature of the coherence for the non-renewal variant can be expressed as:

$$C_{\mathrm{NR}}^{(2)}(0) = \frac{8\pi^2\gamma\left(3\mu_3\mu_1^3 + \left(2\mu_4 - 3\mu_2^2\right)\mu_1^2 - 8\mu_2\mu_3\mu_1 + 6\mu_2^3\right) r_0}{3\left(\mu_1^2\left(1 - 2\gamma r_0\right) + 2\gamma\mu_2 r_0\right)^2}. \tag{3.32}$$

The sign of the curvature is determined solely by the sign of the numerator:

$$\begin{aligned} \operatorname{sign}\left(C_{\mathrm{NR}}^{(2)}(0)\right) &= \operatorname{sign}\left(3\mu_3\mu_1^3 + \left(2\mu_4 - 3\mu_2^2\right)\mu_1^2 - 8\mu_2\mu_3\mu_1 + 6\mu_2^3\right) \\ &= \operatorname{sign}\left(+1 + 3\beta_3 C_V + \left(2\beta_4 - 9\right)C_V^2 - 8\beta_3 C_V^3 + 6C_V^4\right). \end{aligned} \tag{3.33}$$

The higher moments in the last line were replaced by the higher cumulants (β_3, β_4, see Eq.(B.1)) of the ISI density. Here one can already detect an important difference to the renewal case: the curvature is positive in the limit of low spiking variability ($C_{\mathrm{V}} \to 0$). In case of the inverse Gaussian probability density used in our model, the curvature

Eq.(3.33) can be further simplified (see Eq.(B.2) and Eq.(B.3)) to:

$$\text{sign}\left(C_{\text{NR}}^{(2)}(0)\right) = \text{sign}\left(2 + 6C_{\text{V}}^2 + 12C_{\text{V}}^4\right). \tag{3.34}$$

The curvature is positive for all positive values of the C_{V}, which implies that the non-renewal variant acts generically as a band pass filter on information, irrespective of the spiking variability (phasic or tonic firing regimes). Thus, maximal positive correlations between adjacent ISIs ($\rho_1 = 1/2$) leads generically to a band pass filter on information (see Fig. 3.20). Is this a general feature of positive correlations between adjacent ISIs?

Gradual positive correlations between adjacent ISIs

The coherence function and its curvature at zero frequency of the general model ($\alpha \neq 1$), which is given by Eq.(3.9), can be expressed analytically and reads for the renewal variant:

$$C_{\text{R}}^{(0)}(f \to 0; \alpha) = \frac{1}{\gamma r_0 C_V^2 + 1}, \tag{3.35}$$

and

$$\begin{aligned} C_{\text{R}}^{(2)}(f \to 0; \alpha) &= \frac{2\pi^2\gamma\left(3\mu_2^3 - 4\mu_1\mu_3\mu_2 + \mu_1^2\mu_4\right) r_0}{3\left(\mu_1^2 + \gamma\left(\mu_2 - \mu_1^2\right) r_0\right)^2} \\ &= \frac{2\pi^2\gamma r_0 C_V^2\left(C_V^2\left(\beta_4 - 4\beta_3 C_V + 3C_V^2 - 3\right) - 1\right)}{3\left(\gamma r_0^2 C_V^2 + r_0\right)^2}. \end{aligned} \tag{3.36}$$

Thus, the coherence function at zero frequency as well as its curvature at zero frequency of the renewal variant are independent of the scaling factor α. This plausible because the model does not show any ISI correlations at all. This analytical result confirms the previously obtained results (Eq.(3.31) and Eq.(3.32)).

Similarly, one can include the scaling factor α in the coherence function at zero frequency and its curvature (see Eq.(3.31) and Eq.(3.32)) for the general non-renewal variant of the model by using Eq.(3.16). The coherence function at zero frequency reads:

$$C_{\text{NR}}^{(0)}(f \to 0; \alpha) = \frac{\nu_1^2}{\nu_1^2(1 - \gamma r_0) + \gamma\nu_2 r_0}. \tag{3.37}$$

The corresponding curvature of the coherence at zero frequency of the general non-renewal model variant takes the form:

$$\begin{aligned} C_{\text{NR}}^{(2)}(f \to 0; \alpha) &= \frac{2\pi^2\gamma r_0}{3\left(\nu_1^2\left(1 - \gamma r_0\right) + \gamma\nu_2 r_0\right)^2}\Big(12\alpha\nu_3\nu_1^3 + \nu_1^2\left((\alpha+1)^2\nu_4 - 12\alpha\nu_2^2\right) - ... \\ &\quad -4(\alpha+1)^2\nu_2\nu_3\nu_1 + 3(\alpha+1)^2\nu_2^3\Big), \end{aligned} \tag{3.38}$$

where ν_k is the k-th moment of the threshold distribution. Because the characteristic function of the ISI density is related to the characteristic function of the threshold distri-

bution via Eq.(3.9) and Eq.(3.24), one can express the moments of the ISI distribution by the moments of the threshold distribution in the general (symmetric, non-symmetric model variant) as follows:

$$\begin{aligned}
\mu_1 &= (\alpha+1)\nu_1, && (3.39)\\
\mu_2 &= \left(\alpha^2+1\right)\nu_2 + 2\alpha\nu_1^2, && (3.40)\\
\mu_3 &= (\alpha+1)\left(3\alpha\nu_1\nu_2 + ((\alpha-1)\alpha+1)\nu_3\right), && (3.41)\\
&\vdots && (3.42)
\end{aligned}$$

These formula imply that the mean (μ_1) and the $C_{\mathrm{V,ISI}} = \sqrt{\mu_2/\mu_1^2 - 1}$ of the ISI density can be expressed in terms of mean (ν_1) and $C_{\mathrm{V,thresh}} = \sqrt{\nu_2/\nu_1^2 - 1}$ of the threshold distribution as follows:

$$\begin{aligned}
\mu_1 &= (\alpha+1)\nu_1, && (3.43)\\
C_{\mathrm{V,ISI}}^2 &= \frac{\alpha^2+1}{(\alpha+1)^2} C_{\mathrm{V,thresh}}^2. && (3.44)
\end{aligned}$$

We have to choose the mean and the CV of the threshold distribution according to Eq.(3.43) and Eq.(3.44) in order to fix the mean and the CV of the ISI density such that:

$$\begin{aligned}
\nu_1 &= \frac{1}{(\alpha+1)}\mu_1, && (3.45)\\
C_{\mathrm{V,thresh}}^2 &= \frac{(\alpha+1)^2}{\alpha^2+1} C_{\mathrm{V,ISI}}^2. && (3.46)
\end{aligned}$$

Expressing these equations in terms of the first four standardized moments $\beta_2, ..., \beta_4$ of the resulting ISI density (see Eq.(B.1)) results in:

$$C_{\mathrm{NR}}^{(0)}(f \to 0; \alpha) = \frac{1}{1 + \frac{(1+\alpha)^2}{1+\alpha^2} C_V^2 \gamma r_0}, \quad (3.47)$$

and

$$C_{\mathrm{NR}}^{(2)}(f \to 0; \alpha) = \frac{\left(2\pi^2\gamma\mu_1^2 r_0 C_V^2\right)\left(A_0 + A_1 C_V^1 + A_2 C_V^2 + A_3 C_V^3 + + A_4 C_V^4\right)}{3((\alpha-1)\alpha+1)\left(\alpha^2+1\right)\left(\alpha^4+1\right)\left(\alpha^2+(\alpha+1)^2\gamma r_0 C_V^2+1\right)^2}, \quad (3.48)$$

with the abbreviations:

$$A_0 = -((\alpha-10)\alpha+1)((\alpha-1)\alpha+1)\left(\alpha^2+1\right)^2\left(\alpha^4+1\right), \tag{3.49a}$$

$$A_1 = 12\alpha\left(\alpha^2+1\right)^3\left(\alpha^4+1\right)\beta_3 \tag{3.49b}$$

$$A_2 = 3(\alpha+1)^2((\alpha-1)\alpha+1)\left(\alpha^2+1\right),(\alpha((\alpha-1)\alpha+1)(\alpha(\alpha(\alpha+7)+9)+6)+1)+... \\ +(\alpha+1)^2((\alpha-1)\alpha+1)\left(\alpha^2+1\right)\left(\alpha^3+\alpha^2+\alpha+1\right)^2\beta_4, \tag{3.49c}$$

$$A_3 = -4(\alpha+1)^4\left(\alpha^2+1\right)^2\left(\alpha^4+1\right)\beta_3, \tag{3.49d}$$

$$A_4 = 3(\alpha+1)^6((\alpha-1)\alpha+1)\left(\alpha^4+1\right). \tag{3.49e}$$

Important to note here is the fact that the value of the coherence function at zero frequency (see Eq.(3.47)) within the theory-I-approximation (see Eq.(3.23)) is independent of the specific threshold and reset distribution and depends solely on the CV and the firing rate of the spiking activity as well as the correlation coefficient at lag one ρ_1, i.e. the correlation between successive ISIs.

For example, if one uses an inverse Gaussian threshold distribution (see Eq.(3.5)) in Eq.(3.47) and Eq.(3.48), as well as Eq.(B.2), one obtains:

$$C^{(0)}_{\mathrm{NR,IG}}(f\to 0;\alpha) = \frac{1}{1+\frac{(1+\alpha)^2}{1+\alpha^2}C_V^2\gamma r_0} = \frac{1}{1+(1+2\rho_1)\,C_V^2\gamma r_0}, \tag{3.50}$$

where we have used Eq.(3.8) in the last step and the abbreviation $\rho=\rho_1=SCC(1)$. The curvature of the coherence function, i.e. its second derivative with respect to frequency at zero frequency, takes the form:

$$C^{(2)}_{\mathrm{NR,IG}}(f\to 0;\alpha) = \\ = \frac{2\pi^2\gamma r_0 C_V^2 A}{3\left(\alpha^2+1\right)\left(\alpha^2-\alpha+1\right)\left(\alpha^4+1\right)\left(\alpha^2+\alpha^2\gamma\mathrm{Cv}^2 r_0+2\alpha\gamma\mathrm{Cv}^2 r_0+\gamma\mathrm{Cv}^2 r_0+1\right)^2}, \tag{3.51}$$

where A in the numerator of Eq.(3.51) is given by:

$$\begin{aligned} A \;=\; & -((\alpha-10)\alpha+1)((\alpha-1)\alpha+1)\left(\alpha^2+1\right)^2\left(\alpha^4+1\right)+ \\ & +12\alpha\left(\alpha^2+1\right)\left(\alpha^4+1\right)(\alpha(\alpha(\alpha(2\alpha-1)+6)-1)+2)C_V^2+ \\ & +6(\alpha+1)^4(\alpha(\alpha(\alpha(\alpha(\alpha(\alpha((\alpha-2)\alpha+6)-7)+12)-7)+6)-2)+1)C_V^4. \end{aligned} \tag{3.52}$$

The denominator of Eq.(3.51) is always positive for positive scaling factor α and C_V. Consequently, the sign of the curvature of the coherence function at zero frequency is

determined solely by the sign of the numerator in Eq.(3.51), i.e. the sign of Eq.(3.52). A straightforward calculation reveals that the sign of the curvature of the coherence

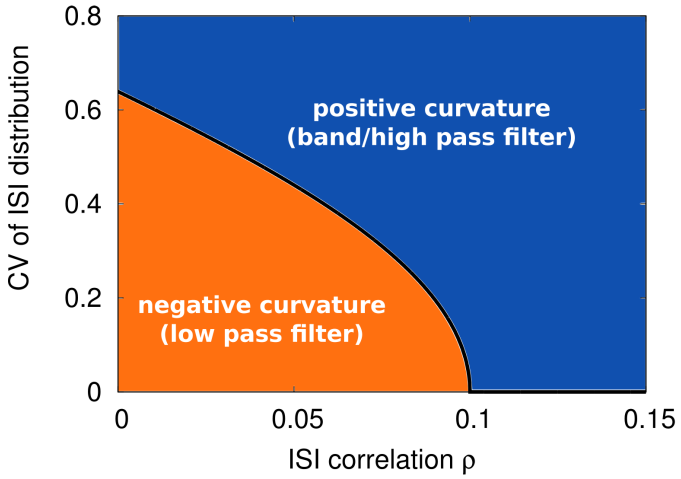

Figure 3.21: Analytically obtained phase diagram of information filtering based on positive correlations between adjacent ISIs for an inverse Gaussian ISI distribution. Based on the curvature of the coherence function at zero frequency (Eq.(3.51)) by using an inverse Gaussian ISI distribution in the α-non-renewal model Eq.(3.8), one can discriminate between low and band/high pass filter. If the coefficient of variation (CV) of the ISI distribution is below a critical value (Eq.(3.54), black solid line), then the model acts as a low pass filter on information (indicated by the orange area). Whereas a CV above the critical value leads potentially to band/high-pass filtering on information (indicated by the blue area).

function is positive, i.e. indicating band-pass filtering on information, if the following inequality is fulfilled (see Fig. 3.21):

$$C_{\mathrm{V}} \geq C_{\mathrm{V,crit}}, \tag{3.53}$$

where the critical CV is defined by:

$$C_{\mathrm{V,crit}} = \frac{\Re\left(\sqrt{\Re\left(\frac{6\rho(2\rho^2-1)(\rho(2\rho-1)+2)+\sqrt{6}\sqrt{(1-2\rho^2)(\rho(\rho(\rho(4\rho(8\rho^3-15\rho-12)+3)+17)+10)-9)+1)}}{(2\rho+1)^2(\rho(\rho(2\rho-1)+2)-2)+1)}\right)}\right)}{\sqrt{6}}, \tag{3.54}$$

with the abbreviation $\rho = \rho_1 = SCC(1)$. Expression Eq.(3.54) reduces in the limit of vanishing correlations, i.e. the renewal variant, to

$$\lim_{\rho\to 0} C_{\mathrm{V,crit}} = \frac{1}{\sqrt[4]{6}} \approx 0.638943, \tag{3.55}$$

which is in line with previously obtained analytical results (see Eq.(3.29)). In the limit of maximal ISI correlations (here $+1/2$) Eq.(3.54) reduces to:

$$\lim_{\rho \to 1/2} C_{\mathrm{V,crit}} = 0, \tag{3.56}$$

which was also discussed previously (see Eq.(3.34)). I conclude that the analytical analysis of the sign of the curvature of the coherence function at zero frequency (using an inverse Gaussian distribution for threshold and reset values) suggests that significant positive ISI correlations lead to band-pass filtering on information, irrespective of the firing pattern activity, i.e. very regular or very irregular. Whereas weak ISI correlations $\rho < 1/10$ can lead to band-pass filtering on information only if the spike train has a minimum variability, i.e. the coefficient of variation (CV) must fulfill Eq.(3.53). Thus, ISI correlation induced band-pass filtering on information (based on correlations of subsequent threshold and reset values) is a robust phenomenon for irregular spiking activities. The magnitude of the curvature increases with increasing correlation, which suggests that the stronger the ISI correlation between successive ISIs becomes, the more pronounced will be the band-pass filtering effect on information (i.e. the quality of the coherence function, see Eq.(3.2)).

3.7 Summary & Discussion

In this chapter a single neuron model based on a deterministic dynamics (without leakage) within the subthreshold regime in combination with a stochastic threshold and reset concept was developed and analyzed numerically and analytically. This model allows studying the effects of positive ISI correlations due to correlations between thresholds and a subsequent reset value: i) the renewal variant, in which threshold and reset values are not correlated, and ii) the non-renewal version, which exhibits positive ISI correlations.

The specific distribution of threshold and reset values determine the shape of the ISI density. For the sake of simplicity, the ISI density was chosen to be an inverse Gaussian distribution, which was established by using an inverse Gaussian distribution for threshold and reset values. The renewal variant acts primarily as low pass filter on information, which is also true in the case of negative correlations(). In contrast to the renewal variant, the non-renewal variant with maximal positive correlations can act as a band pass filter on information irrespective of the firing regime (from phasic to tonic). This insight is obtained by numerical studies of the model variants and is supported by analytical approaches.

The simple formulation of the mathematical neuron model with positive ISI correlations (based on correlations between threshold and subsequent reset value) allows an analytical study of the relevant spectra to study the information transmission characteristics (based on the spectral coherence function). This theoretical investigation was done by applying linear response theory to estimate the power spectrum of the evoked activity based on exact expressions of the spontaneous activity of the model variants.

As it was pointed out by Lindner (2005), the squared cross-spectrum is constant with respect to frequency, and thus, the shaping of the coherence function is solely due to the frequency modulations of the spike train power spectrum. This frequency modulation leads to a local minimum in the power spectrum of the non-renewal variants used here, which 'translates' to a local maximum of the coherence function nearby half the firing rate of the neuron model. The derived analytical expressions for the power and cross spectrum of the model variants were compared with numerical results.

It was demonstrated numerically that the quality of the band-pass filter depends on the regularity or irregularity of the spiking response, measured by the coefficient of variation (CV). It exists an optimal level of intrinsic variability, for which the band pass filter is very pronounced. This markedness of the bandpass filter is usually observed for rather regular firing activities ($CV \approx 0.1 - 0.2$). Neither strict regular ($CV \approx 0$) nor highly irregular ($CV \approx 1$) spiking activities give rise to the emergence of a band pass filter on information. Rather regular spiking activities lead to frequency selectivity on information transmission for frequencies in the vicinity of half the neuron model's firing rate r_0.

By changing the mean of the threshold and reset distribution, one can easily change the output firing rate of the neuron model. The effects of the firing rate on the information filtering characteristics were analyzed numerically (see Fig. 3.13 and Fig. 3.14). The resonance frequency of the coherence function (in the presence of positive correlations between successive ISIs) is close to half the firing rate of the model.

These numerical observations, that the renewal variant, in contrast to the non-renewal version, does not act as a band pass filter on information for low and moderate intrinsic variability (measured by the CV) were underpinned by theoretical investigations based on the curvature of the coherence function at zero frequency (see Eq.(3.26), Eq.(3.32), and Eq.(3.48)). A positive curvature indicates the appearance of a band pass or high pass filter, whereas a negative curvature rather indicates a low pass filter on information. This analytical investigation leads to a simple inequality for the CVs, for which band-pass filtering on information based on positive ISI correlations ($\rho \in \{0, 1/2\}$) can be achieved. The presence of positive correlations between adjacent ISIs leads to pronounced band-pass signal transmission for rather regular firing activities ($C_V \leq 0.2$). Because of the trade-off between coherence quality and mutual information rate, the presence of positive correlations between successive ISIs can lead to band-pass filtering characteristics on information at rather moderate rates of mutual information between the output and the input signal. This **trade-off** between coherence quality and mutual information rate was shown with the help of extensive numerical computer simulations (50.000 parameter sets, see Fig. 3.17 and Fig. 3.18).

Does the model encodes information about a time-dependent input current rather linearly or non-linearly? As mentioned in sec. 1.4.3, the response-response (RR) coherence function (Eq.(1.14)) can be used as an **estimation** of an upper bound for the mutual information rate, and by neglecting synergy effects among frequencies, this proxy holds true also on the frequency-dependent mutual information rate. The comparison between RR and the stimulus-response (SR), which is usually utilized in

this thesis, can hint at non-linear filtering characteristics. Fig. 3.22 shows the numerical results of the SR and the RR coherence function for the general non-renewal model variant for different firing regimes: i) rather regular activity ($C_V = 0.25$, see Fig. 3.22a–c), and ii) rather irregular activity ($C_V = 0.5$, see Fig. 3.22d–f). We have chosen different ISI correlations: $\alpha = 0.01$, which leads to $\rho_1 = 0.01$ (see Fig. 3.22a,d); $\alpha = 0.5$, which leads to $\rho_1 = 0.4$ (see Fig. 3.22b,e); $\alpha = 1.0$, which leads to $\rho_1 = 0.5$ (see Fig. 3.22f,g). The

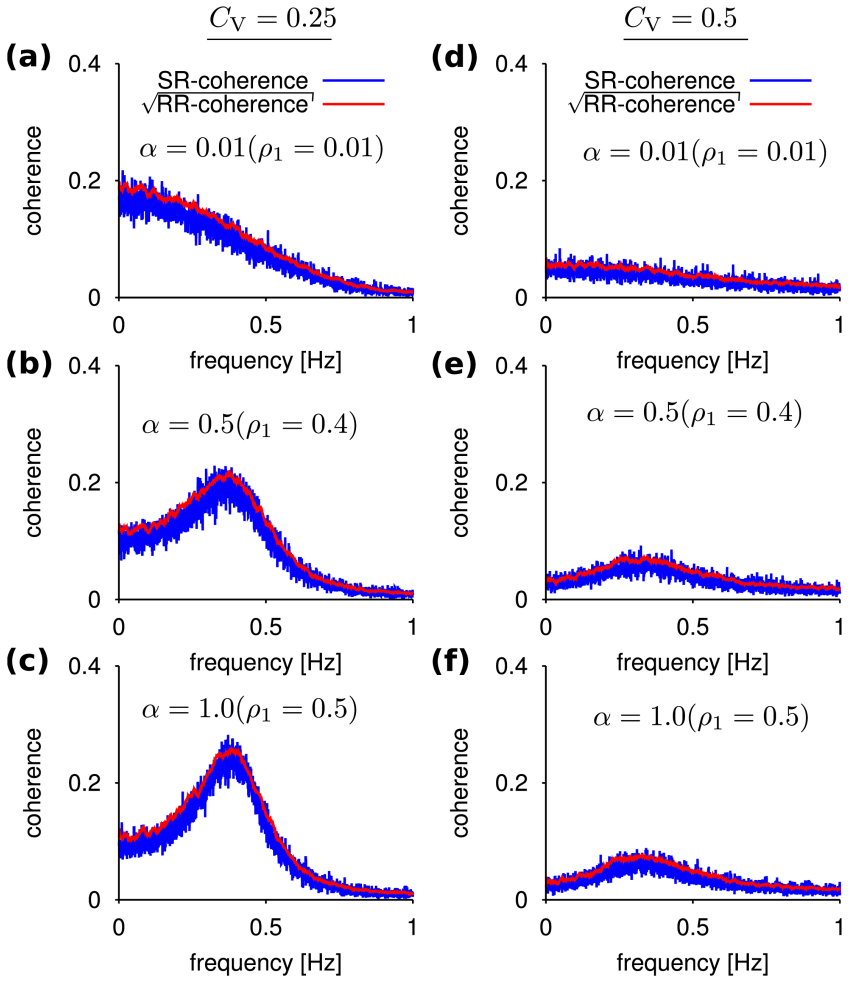

Figure 3.22: RR vs. SR coherence function for the general α-non-renewal model variant. Shown are numerical results for a fixed firing rate ($r_0 = 0$) and weak signal variance ($\varepsilon^2 = 0.002$) with a cut-off frequency $f_c = 10$ in the rather regular activity regime (a–c) and the rather irregular activity (d–e) at different values of ISI correlation coefficient. The good concordance between SR (shown in blue) and RR (shown in red) coherence indicates linear coding on information of the model.

surprising similarity between SR and RR coherence suggests that the simple PIF with a

stochastic threshold and reset noise encodes information about a time-dependent input stimulus linearly (see Eq.(1.18)). This observation justifies the usage of the SR coherence function in the numerical and analytical studies concerning the signal transmission characteristics of the chosen model.

Is the PIF the 'perfect' choice to model highly irregular spiking activity? Although (via construction) best suited to model rather regular spiking activity, the proposed PIF model with stochastic threshold and reset concept shows a band-pass filter property for the **renewal variant** at very irregular activity ($CV \approx 1$), which turns into a **very weak** band pass filter on information for CVs larger than one. Thus one can conclude here, that the presence of positive correlations between successive ISIs results in the emergence of a band pass filter on information within the region of regular and rather regular spiking activity ($0 \leq CV \leq 0.5$), i.e. an activity regime, in which the used neuron model (PIF) can be successfully utilized.

How to implement long-range ISI correlations? Although the serial correlation structure of ISIs is very drastic, i.e. only successive ISIs are positively correlated, the question arises whether the band-pass filtering effect due to this short-range correlation structure holds true for a more realistic, i.e. a prolonged (long-ranged) correlation structure across faraway ISIs. These long-range correlations are often modeled with the help of an exponential decaying ISI correlation coefficient with respect to the lag k. One can simply extend this model (PIF with threshold noise) in order to model long-range ISI correlations by using a stochastic process for the threshold values (the reset value can be fixed to zero for example), which leads to exponentially correlated threshold values. The simplest discrete stochastic process, which shows exponentially correlated outputs, is the autoregressive process of the first kind (AR1-process). Using a general AR1-process (see for example Hamilton (1994)): $v_{th,n+1} = \rho \cdot v_{th,n} + \varepsilon_n$, one can show that the resulting serial correlation coefficient at lag k ($SCC(k)$) is of exponential decaying form(Abraham and Balakrishna, 1999)

$$SCC(k) = \rho^k, \tag{3.57}$$

where ρ is a parameter between zero and one, and k denotes the lag between ISIs. The noise (ε_n) of the AR1-process can be constructed such that the resulting ISI density follows an inverse Gaussian distribution. However, a detailed numerical and analytical exploration of this model is beyond the scope of this thesis[5].

What are the effects of additional current Gaussian noise? By including intrinsic white current noise on top of the PIF dynamics, one increases the CV and reduces the ISI correlations. The firing rate is not affected by the intrinsic current noise, due to the absence of a leak term in the PIF dynamics. A straightforward calculation, where one makes use of the fact that the ISI density of the PIF model with constant

[5]The interested reader might be referred to the Master's thesis by Leonidas Eleftheriou (TU Berlin 2016, co-supervised by S.B.), where numerical, as well as analytical investigations on the information filtering properties of the PIF model with stochastic AR1-process-thresholds, are performed. Positive and exponentially decaying long-range ISI correlations show qualitatively the same effects on the information filtering characteristics as short-range positive ISI correlations (investigated in this chapter)

threshold driven by Gaussian white noise follows an inverse Gaussian distribution, leads to modifications of the CV and the serial correlation coefficient as follows[6]:

$$C_V' = \sqrt{\frac{2r_0}{\mu} D + C_V^2}, \qquad \rho_1' = \left(\frac{1}{1 + \frac{2r_0 C_V^2}{\mu} D} \right) \rho_1, \tag{3.58}$$

where C_V' and ρ_1' denote the CV and the correlation of adjacent ISIs in the presence of intrinsic Gaussian white current noise with respect the CV and correlation in the absence of white current noise (C_V, ρ_1). D stands for the intrinsic noise strength, and μ denotes the constant drift term (baseline current) of the PIF model.

Negative ISI correlations in this model variant lead preferentially to low-pass filtering on information(Lindner et al., 2005). This insight can be understood by taking into account that the spike train power spectrum at zero frequency $S(0)$ is given in terms of the mean and the CV of the ISI density as well as the sum of all correlations:

$$S(0) = r_0 C_V^2 \left(1 + 2 \sum_{k=1}^{\infty} \rho_k \right) = r_0 C_V^2 \left(1 + 2\rho_1 \right). \tag{3.59}$$

In the case of maximal negative ISI correlations, i.e. $\rho_1 \approx -1/2$, the power spectrum at zero frequency is close to zero. On the other hand, the high-frequency limit is $S(f \to \infty) = r_0$. Therefore, the power spectrum increases with frequency (for small CV ($CV < 1$) and low frequencies. Consequently, the coherence decreases with frequency.

[6] I thank Leonidas Eleftheriou, who addressed this issue and performed this calculation.

4 Information filtering in resonator neuron models

Abstract | In this chapter, we will study the effects of subthreshold resonances, induced by subthreshold membrane potential oscillations (MPOs), on the frequency-dependent signal transmission about a time-dependent input signal. This study highlights the role of nonlinearities in conjunction with subthreshold resonances to achieve a bandpass filter on information. The filtering properties of several single neuron models with different nonlinearities: i) discontinuous nonlinearity (fire-and-reset rule), and ii) continuous nonlinearities (biophysical spike mechanisms) are investigated with the help of numerical simulations. The chosen single neuron models cover different biophysical levels of neuronal modeling ranging from simple resonate-and-fire neuron model (with and without nonlinearity) to more realistic conductance-based Morris-Lecar and Hodgkin-Huxley single neuron models, which offer realistic modeling approaches to intrinsic neuronal variability in terms of stochastic ion channel dynamics.

4.1 Introduction

In the previous chapters (see sec. 2 and sec. 3) it was demonstrated (through numerical and analytical studies) that various integrate-and-fire (IF) neuron models act primarily as low pass filters on information, i.e. they transmit preferentially information about slow components of a time-dependent input signal. These IF neuron models (driven by uncorrelated stochastic input signals, Gaussian white noise) do not exhibit correlations among interspike intervals (ISIs). To study the effects of such correlations on the signal transmission characteristics, a simple modification of the PIF model (presented in sec. 2) was proposed in sec. 3. The presence of positive ISI correlations can lead to band-pass filtering on information close to half the mean firing rate of the neuron model. The higher the 'strength' of positive ISI correlations (measured by the serial correlation coefficient at lag one), the more pronounced is the band pass filter on information. Here, the impact of a different theoretical mechanism: subthreshold resonance on the signal transmission characteristics of the neuron model is analyzed.

Many cortical neurons can be described by integrator neuron models (see Fig. 2.1) very accurately (Badel et al., 2008c; Rauch et al., 2003). However, these integrator models lack the ability to describe more complex subthreshold dynamics like subthreshold membrane potential oscillations (MPOs, see Fig. 4.1D) and closely related subthreshold resonances(I. Lampl, 1997). Here, the term resonance refers to effect that the voltages response $V(t)$ of a *non-excitable neuron* shows a maximum, for frequencies close to the oscillator frequency of the MPOs.

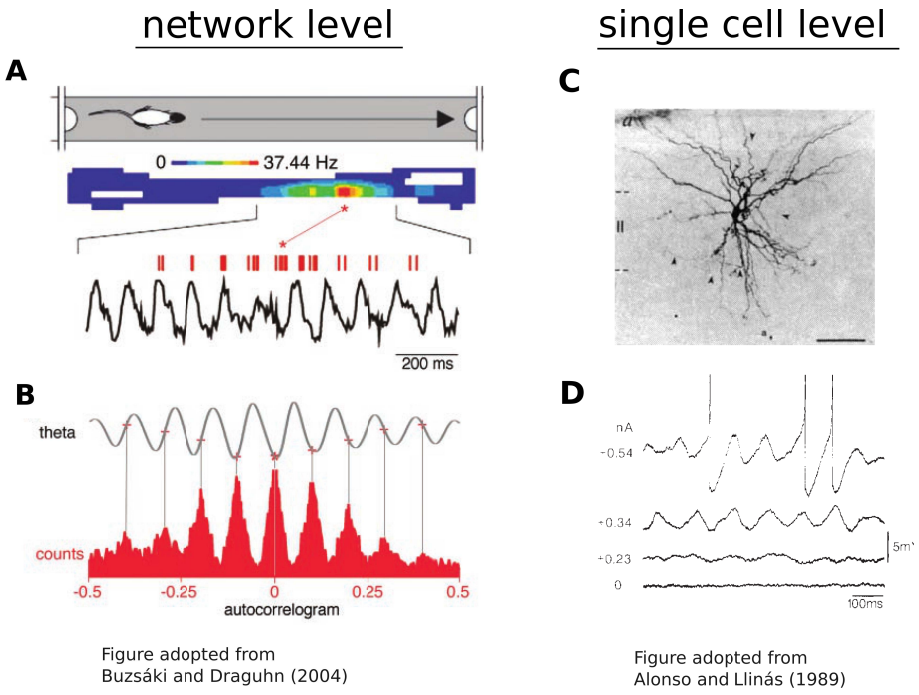

Figure 4.1: Experimental evidence of neuronal oscillations on the network and single cell level. Oscillations can be observed on the network level (A, B): EEG theta rhythm and place-cell firing (red ticks in A) on a single run and averaged over several runs (A). Peak firing occurs on the trough of the theta cycle. A spike-triggered average of theta waves and auto-correlogram of spikes (B); and the single cell level (C, D): typical morphology of a stellate cell of entorhinal cortex layer II in rats (C). The rhythmic activity of the membrane voltage response depends on the amount of injected constant current (D). High values of the DC leads to subthreshold oscillations (resonances) of approx. 8 Hz and to spiking activity (excitable neuron). Figures A, B were adopted from Buzsáki and Draguhn (2004). Figures C, D were adopted from Alonso and Llinás (1989).

Throughout the central nervous system rhythmic activity is often encountered (see for example Engel et al. (1992); Hermann (1905); Kreiter and Singer (1992); Salinas and Sejnowski (2001)). There exist two levels of description of cortical rhythmic activity: i)

the network level (see Fig. 4.1A,B and consult for example Buzsáki (2006); Buzsáki and Draguhn (2004); Gielen et al. (2010); J. Huxter and O'Keefe (2003); Wang and Buzsáki (1996)), and ii) the single cell level (see Fig. 4.1C,D and for example Alonso and Llinás (1989); Engel et al. (2008); Gloveli et al. (1997); Schreiber et al. (2004)).

The former model: the attractor network model, explains coherent neural rhythmic activity by specific recurrent connectivities between single neurons. Whereas the second level of description states, that rhythmic network activity is due to the coupling of rhythmic neurons, i.e. neural oscillators. On the network level, subthreshold resonances can be accounted for synchronous spiking behavior(I. Lampl, 1993). Rhythmic neuronal activity has been identified experimentally on both levels: on the level of neuronal network activity as well as on the level the single neurons(Alonso and Llinás, 1989; Hutcheon and Yarom, 2000; I. Lampl, 1997; Schreiber et al., 2004; Wang, 1993) (subthreshold resonances).

It is a well-known fact that this rhythmic activity establishes a frequency preference (based on power filtering, see Hutcheon and Yarom (2000)) between the neuronal subthreshold output and the input signal. It is also known that subthreshold oscillations translate to firing-rate resonances(Brunel et al. (2003),Richardson et al. (2003)), i.e. the firing rate displays a resonance, i.e. enhanced firing rate for input frequency components close the subthreshold resonance frequency (Richardson et al., 2003). However, this band pass filter on power(Hutcheon and Yarom, 2000) does not necessarily imply that the neuron model acts as a band pass filter on information, measured by the spectral stimulus-response (Eq.(1.13)) or the response-response ((see Eq.(1.14))) coherence function.

Here we want to study the effects of subthreshold resonances on the frequency-dependent signal transmission (information transmission) in spiking and non-spiking neuron models. We investigate the filtering properties with respect to model-intrinsic parameters (absolute refractory period, frequency of the subthreshold resonances, as well as the 'strength' of the subthreshold resonance) and external neuronal parameters (like the signal strength of the time-dependent input current as well as the DC input, very similar to).

Additionally, the link between subthreshold resonances and band-pass filtering on information is studied for a large set of model parameters numerically (see sec. 2).

4.2 Neuron models with subthreshold resonances

Following the neuronal modeling approach of this thesis, the simplest way to extent integrate-and-fire (IF) neuron models (discussed in sec. 2 and sec. 3) such that subthreshold resonances occur, is by introducing a subthreshold feedback mechanism in terms of a coupling between two IF neuron model dynamics(Izhikevich, 2007). The resulting linear equations (see Eq.(4.1a) and Eq.(4.1b)), which resembles a damped harmonic oscillator, are then supplemented with a fire-and-reset rule (Izhikevich, 2007) such that the linear neuron model becomes non-linear and excitable. We first consider the simplest case of the purely subthreshold response, i.e. in the absence of a threshold-and-reset rule. This

linear model is able to describe subthreshold resonances (damped harmonic oscillations of the membrane voltage) and has the advantage that all dynamical and spectral measured necessary to study the signal transmission properties of the purely subthreshold neuronal response can be calculated analytically(Rice, 1944).

4.2.1 Linear model of the purely subthreshold voltage response

We consider the following model(Engel et al., 2008; Schreiber et al., 2004) that displays subthreshold resonances (linear resonator model):

$$C\frac{d}{dt}V(t) = -\frac{1}{R}V(t) - I_L(t) + \xi_1(t) + s(t) + I_0 \tag{4.1a}$$

$$L\frac{d}{dt}I_L(t) = -R_{\mathrm{L}}I_L(t) + V(t) - \left(\frac{R_{\mathrm{L}}}{R} + 1\right) \times V_{rest} \tag{4.1b}$$

Here $V(t)$ denotes the membrane potential and I_L is a slow membrane current, C stands for the membrane capacitance, R and R_{L} are resistances, L is an inductance and V_0 is the battery term. We will study the above stated neuron model within three different parameter sets: i) a parameter set that refers to a hypothetical but 'biologically plausible' (see sec. C.2) **resonator cartoon** variant, which shows a well pronounced impedance resonance, ii) a parameter set, which corresponds to experimentally observed subthreshold resonances observed in **stellate cell** neurons in the entorhinal cortex of rats(Engel et al. (2008); Schreiber et al. (2004)), and iii) the experimentally observed(Engel et al. (2008); Schreiber et al. (2004)) non-resonant subthreshold responses (similar to the subthreshold response modeled by IF neuron models) of **pyramidal neurons** (see Tab. C.1 for numerical values). The model-intrinsic current noise(see for example Destexhe and Rudolph-Lilith (2012)), originating from ion channel noise for example, is modeled with the help of Gaussian white noise(Dorval and White, 2005; Faisal et al., 2008; Goldwyn and Shea-Brown, 2011; White et al., 2000) with intensity D and correlation function $\langle \xi_1(t)\xi_1(t')\rangle = 2D\delta(t-t')$.

In order to model 'complex'[1] time-dependent input signal currents $s(t)$ (see for example Rudolph and Destexhe (2003)), we use the well-known Ornstein-Uhlenbeck process (Uhlenbeck and Ornstein, 1930; Wang and Uhlenbeck, 1945) described by:

$$\tau_{OU}\frac{d}{dt}s(t) \quad = \quad -s(t) + \xi_{OU}(t), \tag{4.2}$$

with intensity D_{OU}, exponentially decaying correlation function:

$$\langle s(t)s(t')\rangle = \frac{D_{\mathrm{OU}}}{\tau_{OU}} e^{-\frac{|t-t'|}{\tau_{OU}}}. \tag{4.3}$$

Consequently (due to the Wiener-Khinchin theorem, see for example (Risken, 1989;

[1] The term 'complex' refers here to the observation, that neuronal input signals are often variable in time, i.e. stochastic in their nature.

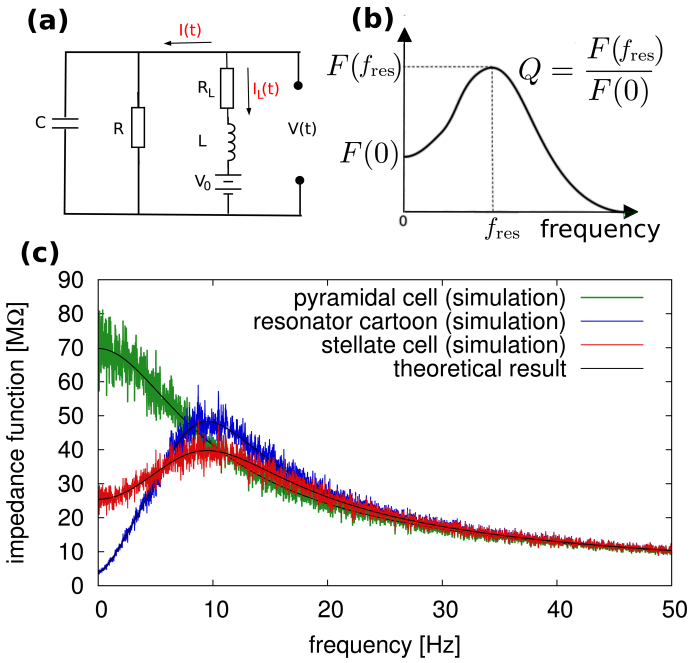

Figure 4.2: Resonator model and spectral characteristics. Shown are: circuit description of the linear resonator model (a), definition of the quality of a function (b), and impedance functions for the linear resonator model (c) (parameter are given in Tab. C.1). The theoretical results refers to Eq.(4.11).

Tuckwell, 1989)), the power spectrum of the OU-process is given by:

$$S_{s,s}(f) = \frac{2D_{\mathrm{OU}}}{1 + (2\pi f \tau_{ou})^2}. \tag{4.4}$$

To avoid correlations between the intrinsic (ion channel) noise of the neuron model and the input signal, we ensure by construction that all noise sources are independent of each other, i.e. the following equations are fulfilled:

$$\begin{aligned} \langle \xi_{ou}(t)\xi_{OU}(t')\rangle &= 2D_{\mathrm{OU}}\delta(t-t'), \\ \langle \xi_1(t)\xi_1(t')\rangle &= 2D\delta(t-t'), \\ \langle \xi_1(t)\xi_{OU}(t')\rangle &= 0. \end{aligned} \tag{4.5}$$

Thus, the cross-correlation between different independent Wiener processes $\xi_j(t)$ vanishes identically. The equivalent circuit to our chosen model is presented in Fig. 4.2a.

To characterize the 'strength'[2] of subthreshold resonances, one introduces the following

[2]Later, we will replace the term 'strength' by the more refined 'quality factor', which allows quantitative statements.

characteristics of the model with subthreshold resonances. The **damping factor** of the resonance reads:

$$\zeta = \frac{\frac{1}{R} + \frac{R_{\mathrm{L}}C}{L}}{2\sqrt{\frac{C}{L}\left(1 + \frac{R_{\mathrm{L}}}{R}\right)}}, \tag{4.6}$$

as well as the **natural frequency** (or damped frequency) f_{nat} of the underlying MPOs:

$$f_{\mathrm{nat}} = \frac{1}{4\pi}\sqrt{\frac{4}{CL} - \left(\frac{1}{RC} - \frac{R_{\mathrm{L}}}{L}\right)^2}. \tag{4.7}$$

The damping factor determines the 'strength' of the impedance quality and leads to a resonance, i.e. a peak in the impedance function, if the following inequality holds true:

$$\zeta < \frac{1}{\sqrt{2}} \quad \text{(subthreshold resonance condition)}, \tag{4.8}$$

whereas the emergence of MPOs take place, if:

$$\zeta < 1 \quad \text{(subthreshold oscillation condition)}. \tag{4.9}$$

The purely subthreshold response of neuron model to external current stimulation is characterized by the complex-valued impedance function $Z(f)$(Gimbarzevsky et al., 1984)

$$Z(f) = \frac{\tilde{V}(f)}{\tilde{s}(f)} = \frac{S_{V,s}(f)}{S_{s,s}(f)}, \tag{4.10}$$

where in the last step we have multiplied the numerator and denominator with $s^*(f)$.

For the linear model described by Eq.(4.1a) and Eq.(4.1b), the impedance function takes the form:

$$Z(f) = \frac{(2\pi i f)\, L + R_{\mathrm{L}}}{\left(\frac{R+R_{\mathrm{L}}}{R} - (2\pi f)^2\, LC\right) + (2\pi i f)\left(\frac{L}{R} + R_{\mathrm{L}}C\right)}. \tag{4.11}$$

For a stimulus $s(t) = I_s \cos(2\pi f t)$, for instance, the mean voltage (averaged over all noise sources) is given by $\langle v(t)\rangle = Z(f) I_s \cos(2\pi f t - \phi(f))$, whereas the phase lag $\phi(f) = \arg(Z(f))$ is the complex argument of the impedance.

In the resonance parameter regime ($\zeta < \frac{1}{\sqrt{2}}$), the impedance has a pronounced maximum at the resonance frequency:

$$f_{\mathrm{res}} = \frac{1}{2\pi}\sqrt{\sqrt{\frac{1}{C^2L^2} - \frac{2R_{\mathrm{L}}}{CL^2}\left(\frac{R_{\mathrm{L}}}{L} + \frac{1}{RC}\right)} - \frac{R_{\mathrm{L}}^2}{L^2}},$$

which is in general different from the natural frequency f_{nat} in Eq.(4.7).
In order to measure the strength (sharpness) of a resonance, we use the quality factor of a spectral function $F(f)$ as follows (see Fig. 4.2 and for example Erchova et al. (2004)):

$$Q_F = \frac{F(f_{res})}{F(f=0)}, \tag{4.12}$$

where $F(f)$ is a spectral function that displays a peak at the frequency f_{res}.
The quality of the impedance function can be expressed as:

$$Q_{\mathrm{ZAP}} = \frac{\left(1+\frac{R}{R_{\mathrm{L}}}\right)}{\sqrt{1+\left(\sqrt{L+2L\frac{R_{\mathrm{L}}}{R}+2CR_{\mathrm{L}}^2}-1\right)\frac{2CR^2}{L}-\left(\frac{CRR_{\mathrm{L}}}{L}\right)^2}}.$$

In the limit of large conductivity L the quality of the impedance function takes the simple form:

$$\lim_{L\to\infty} Q_{\mathrm{ZAP}} = \left(1+\frac{R}{R_{\mathrm{L}}}\right). \tag{4.13}$$

The MPO induced impedance resonance Eq.(4.13) is most pronounced for strongly underdamped MPOs ($\zeta < \frac{1}{\sqrt{2}}$, see resonator and stellate cell parameter set in Tab. C.1) and is diminished in the case of overdamped MPOs ($\zeta \geq \frac{1}{\sqrt{2}}$, see pyramidal cell parameter set in Tab. C.1). As one can see in Fig. 4.2c, the quality factor of the impedance function (Q_{ZAP}) of the chosen model with pronounced MPOs (resonator cartoon parameter set) is higher than the quality factor obtained by using the stellate cell parameter set. The usage of the pyramidal cell parameter set leads to an impedance function that is characterized by an absence of a peak. Thus, the resonating parameter sets lead to larger amplitude responses for frequency components close to 10 Hz, i.e. in the vicinity of the resonance frequency f_{res}. It is important to remember that the information filter properties of a system (based on the spectral coherence function, see Eq.(1.13) and Eq.(1.14)) have to be distinguished from the power filtering properties (described by the gain modulation or impedance function, see Eq.(4.10)) of the signal described by the cross-spectrum between stimulus and output and the power spectrum of the stimulus.

In order to characterize the dynamics of the chosen model, we will use the variance of the purely subthreshold membrane voltage $V(t)$ of the form:

$$\sigma_V^2 = \frac{\Delta_{\mathrm{eff}}}{2C}\frac{1+\frac{R_{\mathrm{L}}}{R}\left(\frac{R_{\mathrm{L}}+L}{R}\right)}{\left(\frac{R_{\mathrm{L}}+L}{R}\right)\left(1+\frac{R_{\mathrm{L}}}{R}\right)}L, \tag{4.14}$$

where the variance can be described due to an effective Gaussian fluctuating white noise source ($\eta_{\mathrm{eff}}(t)$) of amplitude Δ_{eff} and autocorrelation function $\langle \eta_{\mathrm{eff}}(t)\eta_{\mathrm{eff}}(t')\rangle = \Delta_{\mathrm{eff}}\delta(t-t')$. The amplitude can be calculated to:

$$\Delta_{\mathrm{eff}} = D + D_{\mathrm{OU}}\frac{1+\frac{R_{\mathrm{L}}}{R}\left(1+\frac{R_{\mathrm{L}}}{L}\right)\left(1+\tau_{ou}\frac{R_{\mathrm{L}}}{L}\right)}{\left(\frac{R_{\mathrm{L}}^2}{L^2}+\frac{1}{LC}\left(\frac{R_{\mathrm{L}}}{L}+1\right)\right)\left[LC+\tau_{ou}\left(\frac{R_{\mathrm{L}}+L}{R}\right)+\tau_{ou}^2\left(\frac{R_{\mathrm{L}}}{R}+1\right)\right]} \tag{4.15}$$

If the correlation time (τ_{ou}) of the external Ornstein-Uhlenbeck signal (Eq.(4.2)) is small in comparison to the time scale of the neuronal voltage dynamics ($\tau_V = RC$), Eq.(4.15) simplifies to:

$$\lim_{\tau_{ou}\to 0} \Delta_{\text{eff}} = D + D_{\text{OU}}. \tag{4.16}$$

To explore the information filtering properties of the chosen neuron model (Eq.(4.1a) and Eq.(4.1b)) in the presence of a threshold-and-reset rule, which will be the subject of the following section, we will next calculate the fixed points of the linear system (Eq.(4.1a),Eq.(4.1b)).

A straight forward[3] calculation leads to analytical expressions of the fixed points of the membrane voltage V_{FP} and the slow current variable I_{FP} as follows:

$$V_{\text{FP}} = \frac{R_{\text{L}}}{\left(\frac{R_{\text{L}}}{R}+1\right)} I_0 + V_{\text{rest}}, \tag{4.17a}$$

$$I_{FP} = \frac{1}{\left(\frac{R_{\text{L}}}{R}+1\right)} I_0 - \frac{V_{\text{rest}}}{R}. \tag{4.17b}$$

The fixed points of the linear system (without fire-and-reset rule) scales linearly with the input-DC I_0. This effect will be of great importance in order to tune the firing regime of the excitable (non-linear) neuron model: resonate-and-fire (RF) from phasic to tonic firing activities.

4.2.2 Spiking resonate-and-fire neuron model

It is believed that information between neurons is transmitted via action potentials (Borst and Theunissen (1999)), i.e. spike-trains and not via the linear subthreshold membrane potential response. Thus, we have to introduce in our linear neuron model (Eq.(4.1a),Eq.(4.1b)) the concept of a spike. This is usually done by using a fixed voltage threshold (Kistler et al., 1997) and a reset concept, which states that whenever the membrane voltage crosses a threshold from below, a spike is initiated and is followed by a reset-rule. This procedure leads to so-called generalized integrate-and-fire (GIF) neuron models (Gerstner and Naud (2009)). Such a nonlinear spike-rule results in a nonlinear model, which is difficult to treat analytically. Two different reset-rules have been applied in the literature:

- if V reaches a threshold V_{th} then V is reset to $V_{\text{reset}} < V_{\text{th}}$ (I_L is not affected),
- if V reaches a threshold V_{th} then V and I_L are reset to $V_{\text{reset}} < V_{\text{th}}$ and $I_L = I_{\text{L,reset}}$.

The first reset-rule (in which I_L is not directly affected) is used in the GIF models(Brunel et al. (2003); Richardson et al. (2003)). We use the reset-value of the auxiliary variable

[3]This is due to the linear description of the neuron model and the fact that the baseline current enters linearly the membrane voltage dynamics (Eq.(4.1a)).

I_L as follows(Engel et al., 2008):

$$I_{\mathrm{L,reset}} = I_0 - \frac{V_{\mathrm{reset}}}{R}. \tag{4.18}$$

This specific reset rule implies that the derivative of the membrane voltage (of the deterministic system) at the reset value V_{reset} is zero. This is motivated twofold. First, by the observation that a real neuron generates action potentials via an upstroke followed by a hyper-polarization. At the minimum of the hyper-polarization of the membrane potential the first derivative of the membrane potential with respect to time is always zero. Second, by the observation that this fire-and-reset-rule leads to non-correlated ISIs and thus ensures that any frequency-dependent signal transmission characteristics of the neuron model is solely due to the presence of subthreshold resonances and **not** due to ISI correlations (as described in sec. 3).

The above described fire-and-reset rule generates point processes(Cox and Isham, 1980): spike trains of the form:

$$z(t) = \sum_i \delta\left(t - t_i\right), \tag{4.19}$$

with spikes at time points t_i. In Fig. 4.3a1,a2 the dynamics of the nonlinear resonate-and-fire model is shown for the resonator cartoon parameter set.

With the help of the previously determined fixed points (Eq.(4.17a) and Eq.(4.17b)) of the linear *noisy* resonator neuron model, one can classify three distinct regimes of neuronal activity in terms of the location of the membrane voltage fixed point V_{FP} in comparison the the voltage threshold V_{th} as follows(see for example Longtin (2000)):

- V_{FP} is below the threshold: $I_0 < (V_{\mathrm{th}} - V_{\mathrm{rest}}) \times \left(\frac{1}{R_{\mathrm{L}}} + \frac{1}{R}\right)$,
- V_{FP} is nearby the threshold: $I_0 \approx (V_{\mathrm{th}} - V_{\mathrm{rest}}) \times \left(\frac{1}{R_{\mathrm{L}}} + \frac{1}{R}\right)$,
- V_{FP} is beyond the threshold: $I_0 > (V_{\mathrm{th}} - V_{\mathrm{rest}}) \times \left(\frac{1}{R_{\mathrm{L}}} + \frac{1}{R}\right)$.

In the first regime, the appearance of a threshold crossing is mostly dominated by the stochastic components of the neuron model, i.e. by the intrinsic variability and the stochastic input signal. If both stochastic processes have very small variances (compared to the distance between voltage threshold and fixed point) then threshold crossing are very rare and very irregular, i.e. a phasic spiking activity. The second regime is characterized by a larger firing rate of the neuron model. For larger DC inputs, smaller signal strengths are needed for membrane voltage threshold crossings. Therefore, this regime is characterized by more frequent threshold crossings (in the presence of a weak stochastic input signal) and a more regular spiking activity compared to the phasic firing regime. The third activity regime, threshold crossings are dominantly influenced by the strong DC current, which drives the membrane voltage very fast from the reset value to the threshold, such that a weak or moderate stochastic input signal $s(t)$ cannot influence

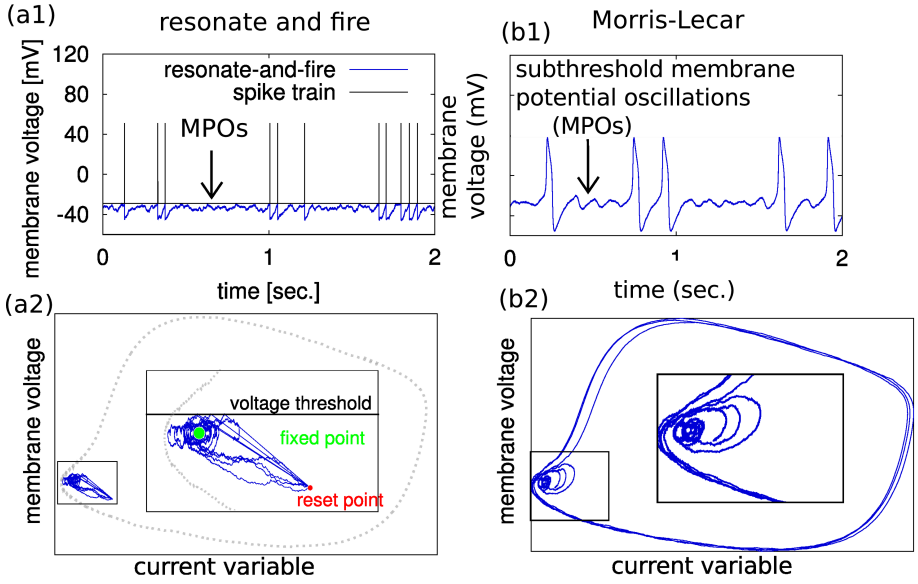

Figure 4.3: Nonlinear spiking neuron models with subthreshold resonances. Shown are: membrane voltage trace and spike train for the resonate-and-fire neuron model (a1), and for the Morris-Lecar model (b1), as well as phase portraits of the resonate-and-fire neuron model (a2) and of the Morris-Lecar model (b2). The grey dotted line in a2 corresponds to a typical phase portait of the Morris-Lecar model. Model parameter are given in Tab. C.1 and Tab. 4.3.

to threshold crossings as strongly as in the two previously characterized firing regimes. This regime is characterized by tonic firing patterns (low ISI variability, $C_V \approx 0$).

4.2.3 Morris-Lecar neuron model

In contrast to the resonate-and-fire neuron model, the Morris-Lecar (ML) model(Morris and Lecar, 1981) is a conductance-based two-dimensional nonlinear neuron model that exhibits an internal (continuous) mechanism to generate action potentials (APs), aka spikes. The parameters of the ML model can be tuned such that class I (non-resonant neurons) and class II (resonant neurons) excitabilities(Gutkin and Ermentrout, 1998; Izhikevich, 2007; Rinzel and Ermentrout, 1989) can be achieved. Firing in type I neuron models results from a saddle-node bifurcation, whereas a subcritical Hopf bifurcation underlies the type II firing onset. Thus, no explicit fire-and-reset rule is needed in this model. In addition to the continuous spike mechanism, the ML neuron model can show subthreshold resonances(Rinzel and Ermentrout, 1989). The nonlinear dynamics

is described by the following equations (Morris and Lecar, 1981):

$$\begin{aligned} C\frac{dV}{dt} &= -g_{\mathrm{Ca}} m_\infty(V)\,(V - E_{\mathrm{Ca}}) - g_{\mathrm{K}} w\,(V - E_{\mathrm{K}}) - \\ &\quad -g_L\,(V - E_{\mathrm{L}}) + \eta(t) + s(t), \qquad (4.20) \\ \frac{dw}{dt} &= \Phi \frac{w_\infty(V) - w}{\tau_w(V)}, \qquad (4.21) \end{aligned}$$

where $V(t)$ is the fast variable (membrane potential) and w the slow recovery variable, $g_{\mathrm{Ca}}, g_{\mathrm{K}}, g_{\mathrm{L}}$ and $E_{\mathrm{Ca}}, E_{\mathrm{K}}, E_{\mathrm{L}}$ are the peak conductances and the reversal potentials for calcium, potassium and the leak current. The spike generation is due to the calcium and potassium dynamics, which is given by:

$$m_\infty(V) = 0.5\left(1 + \tanh\left(\frac{V - V_1}{V_2}\right)\right), \qquad (4.22a)$$

$$w_\infty(V) = 0.5\left(1 + \tanh\left(\frac{V - V_3}{V_4}\right)\right), \qquad (4.22b)$$

$$\tau_w(V) = \frac{1}{\cosh\left(\frac{V - V_3}{2V_4}\right)}, \qquad (4.22c)$$

where m_∞ describes the voltage dependent Ca^{2+} current activation curve and w_∞ the steady state potassium activation and τ_w the corresponding time constant, which is also voltage dependent. The functions $m_\infty(V), w_\infty(V)$ are non-dimensional whereas the voltage-dependent time scale $\tau_w(V)$ is given in ms. As in the resonate-and-fire neuron model, we use three parameter sets (see Tab. 4.3): resonator cartoon, resonating type II and non-resonating type I. Sample Trajectories of the ML neuron model (resonator cartoon parameter set) are displayed in Fig. 4.3a2,b2.

To transfer the voltage trace into a spike-train (sum of Dirac pulses) we identify spikes in the voltage trace by finding the maximum of the action potential. To prevent noise fluctuations to be misidentified as spikes, we set a lower threshold for the maximum of an action potential of 0 mV. The position in time of the maximum of the action potential is then identified with the spike-time t_i. The purely subthreshold behavior is modeled by using a linear expansion around the fixed point of the ML model without any concept of a fire-and-reset rule.

The results of the numerical studies, as well as the specific parameter set of the ML neuron model we have used, can be found in sec. 4.5.1.

4.2.4 Conductance-based Hodgkin-Huxley neuron model

Similar to the previously discussed ML neuron model (see sec. 4.2.3) the continuous excitable neuron model presented here exhibits a biophysical nonlinear continuous spike mechanism. The Hodgkin-Huxley (HH) neuron model(Hodgkin and Huxley, 1952e) is a standard conductance-based neuron model which describes excitability in single neurons very accurately and biologically plausible. It is, in its standard form, described by a

four-dimensional system of deterministic ordinary nonlinear differential equations. This system describes the dynamics of the membrane voltage $V(t)$ as well as the dynamics of the cell intrinsic dynamics of the sodium and potassium ion channels (for a detailed description of ion channel dynamics, please consult the standard textbook (Hille, 2001) on this matter). These ion channel dynamics are nonlinear in nature and lead to a detailed mathematical description of the nonlinear phenomenon of action potentials(Hodgkin and Huxley, 1952e).

The dynamics of the classical HH neuron model is described by the following dynamical equations(Hodgkin and Huxley, 1952e):

$$\begin{aligned} C\frac{d}{dt}V(t) &= -I_{\text{total}}(t) \\ &= -\left(I_{\text{Na}}(t) + I_{\text{K}}(t) + I_{\text{L}}\right), \end{aligned} \tag{4.23}$$

where the time-dependent currents of the sodium (Na), potassium (K) are described by:

$$I_{Na}(t) = m(t)h(t)^3\gamma_{Na}\left(V(t) - E_{Na}\right), and \tag{4.24a}$$

$$\frac{d}{dt}m(t) = \alpha_m\left(1 - m(t)\right) - \beta_m m(t) \tag{4.24b}$$

$$\frac{d}{dt}h(t) = \alpha_h\left(1 - h(t)\right) - \beta_h h(t), \tag{4.24c}$$

where $m(t), h(t)$ denote the activation and in-activation dynamics respectively of a general sodium channel and are called 'gating variables'(Hodgkin and Huxley, 1952e). The potassium dynamics is very similar to the sodium channel dynamics but lacks an in-activation phenomenon and is thus described solely by

$$\begin{aligned} I_K(t) &= n(t)^4\gamma_K\left(V(t) - E_K\right), and \\ \frac{d}{dt}n(t) &= \alpha_n\left(1 - n(t)\right) - \beta_n n(t). \end{aligned} \tag{4.25}$$

It is the nature of the dynamics of the rates: $\alpha_n, \alpha_m, \alpha_h, \beta_n, \beta_m, \beta_h$ that leads to a description of an excitable neuron model, i.e. the presence of action potentials as follows:

$$\alpha_m = \frac{0.1(V+40)}{1 - e^{-\frac{V+40}{10}}}, \quad \beta_m = 4e^{-\frac{V+65}{18}}, \tag{4.26a}$$

$$\alpha_h = 0.07e^{-\frac{V+65}{20}}, \quad \beta_m = \frac{1}{1 + e^{-\frac{V+35}{10}}}, \tag{4.26b}$$

$$\alpha_n = \frac{0.01(V+55)}{1 - e^{-\frac{V+55}{10}}}, \quad \beta_m = 0.125e^{-\frac{V+65}{80}}. \tag{4.26c}$$

The specific choice of the ion-channel density of sodium and potassium leads to different dynamics of the HH model, which can show type-I (integrator-like) and type-II

(resonator-like) behavior(Lundstrom et al., 2008) similar to the Morris-Lecar model described earlier (see sec. 4.2.3).

Because the HH model acts as a standard model for neuronal excitability, different stochastic versions of the HH model were developed that range from i) current noise approximations (Gerstein and Mandelbrot, 1964), ii) conductance noise (Goldwyn et al., 2011), iii) subunit noise (Fox and LU, 1994), iv) as well as a full stochastic version via Monte-Carlo-Markov-Chain (MCMC) algorithms (see for example the comparative study of Sengupta et al. (2010) between different levels of stochastic versions of the HH model). Ion-channel noise can be seen in most circumstances to be the most dominant source of noise in single neurons and thus to single neuron variability (see for example the following reviews by White et al. (2000), Faisal et al. (2005), Dorval (2006), Goldwyn and Shea-Brown (2011)).

Because of its plausible biological approach and its success in modeling especially ion channel conductance variability within single neurons(Goldwyn and Shea-Brown, 2011; Sengupta et al., 2010), we will use the MCMC description of ion channel variability in the HH neuron model. Because of the simulation of MCMC algorithms is in general very time consuming, a fast and precise MCMC approximation of ion channel noise developed by Schmandt and Galán (2012) is used to simulate the stochastic HH model efficiently. The reader might be referred to consult Schmandt and Galán (2012) (and the supplementary material) for a detailed description of the Markov schemes that will be used here.

The results of the numerical studies concerning the signal transmission characteristics, as well as the specific parameter sets of the HH neuron model, can be found in sec. 4.5.2.

4.3 Signal transmission in the absence of a nonlinearity

If one would neglect nonlinearities in neuronal models with subthreshold resonances then the output of this neuronal would be determined solely by its underlying stochastic differential equations (SDEs)[4]. If the structure of these SDEs is linear, then the neuronal response can be referred as a purely linear subthreshold response, because of the absence of a threshold or nonlinear spike mechanism. The simplest mathematical system, which can exhibit subthreshold resonances is the damped linear harmonic oscillator. Because noise is present in almost all neuronal environments, it seems necessary to include noise also in the neuronal models. Here we study the effects of subthreshold resonances by including current noise onto the dynamics of the damped harmonic oscillator (see Eq.(4.1a) and Eq.(4.1b)) as well as more realistic models of intrinsic noise (ion channel noise) by using a conductance-based Hodgkin-Huxley neuron model with an efficient Monte-Carlo-Markov-Scheme algorithm(Schmandt and Galán, 2012) of ion-channel activity.

In the case of current noise, one can analytically calculate the coherence function between the linear output, i.e. the membrane voltage $V(t)$ and the current input signal

[4] A fire-and-reset rule leads to boundary conditions of the voltage probability distribution.

$s(t)$ as:

$$C_{\mathrm{V,s}}(f) \;=\; \frac{1}{1+\frac{D}{D_{\mathrm{OU}}}\left(1+(2\pi\tau_{\mathrm{ou}}f)^2\right)} \quad \text{(without threshold)}. \tag{4.27}$$

This result is rather surprising, because of two reasons. First, the coherence function is a monotonically decreasing function of frequency f. Thus, the frequency preference of the purely subthreshold response (subthreshold resonance), described by the impedance function (see Eq.(4.11)) is not translated to the level of information transmission (described by the coherence function). Second, the intrinsic properties of the neuron model (subthreshold resonances) are not reflected in the coherence function Eq.(4.27). The latter observation is because of the fact that the intrinsic noise and the external signal $s(t)$ enters in the same way (as currents to the membrane voltage $V(t)$) into the neuronal model system, as studied here. Therefore, only the signal-to-noise ratio (SNR). As a consequence, the quality (Eq.(1.19)) of the coherence function (Eq.(4.27), as a measure of 'markedness' of a specific frequency selectivity (band pass filter, see Fig. 4.2b) on the signal transmission, attains its minimal value of one in the absence of a threshold (nonlinearity):

$$Q_{\mathrm{sub,C}} \;=\; 1 \quad \text{(without threshold)}, \tag{4.28}$$

implying a low pass filter characteristic of the information transmission from the input (low pass OU process) to the output (continuous voltage trace). The coherence function Eq.(4.27) leads to a lower bound of total transmitted information rate $MI_{\mathrm{sub,exact}}$ of the purely subthreshold linear voltage response (described in sec. 1.4.3):

$$MI_{\mathrm{sub,exact}} = \frac{\sqrt{1+D_{\mathrm{OU}}/D}-1}{2\ln(2)\tau_{\mathrm{OU}}} \quad \text{(without threshold)}. \tag{4.29}$$

Hence, the lower bound of the total mutual information rate increases with increasing SNR. It was shown analytically that the linear purely subthreshold response of a neuron model, which exhibits subthreshold oscillations, acts a low pass filter on information, i.e. the coherence function between its linear membrane voltage response and its current input signal is a monotonically decreasing function of frequency. On the level of total transmitted information, based on the lower bound approximation of the mutual information rate, the presence or absence of subthreshold resonances does not show any effects. Thus, subthreshold resonances have no advantages for the signal transmission characteristics of the purely subthreshold response (without spikes). However, neurons are believed to encode information about a time-dependent input stimulus with the help of spikes (excitable neuron model) and not via the purely subthreshold membrane voltage responses. We will analyze the effects of the interplay between subthreshold resonances and nonlinearities (fire-and-reset rule as well as continuous spike mechanism) on the signal transmission characteristics of the neuron model in the next section.

4.4 Signal transmission with discontinuous nonlinearities

As described above (see sec. 4.2.3 and sec. 4.2.4) there exist two kinds of neural nonlinearities: i) discontinuous nonlinearities (fire-and-reset rules), and ii) continuous nonlinearities (dynamical spike mechanism in conductance-based neuron models (for example Eq.(4.21), Eq.(4.21)). First, we want to explore the effects of the interplay between subthreshold resonances and a discontinuous nonlinearity in the form of a fire-and-reset rule for the resonator neuron model described by Eq.(4.1a) and Eq.(4.1b).

4.4.1 Resonate-and-fire neuron model

The resonate-and-fire model is a minimal mathematical neuron model, which exhibits subthreshold resonances. We modify this linear neuron model by a fire-and-reset rule, such that it can produce pulsatile temporal outputs, i.e. spikes. This introduction of a fire-and-reset rule leads to an excitable spiking neuronal model in which the spike times can be influenced by the subthreshold dynamics, for example, the presence or absence of subthreshold resonances. This nonlinearity leads to a more realistic neuron model in such a way that its response mimics natural neuronal responses, i.e. action potentials (see Fig. 4.3). We employ in the following extensive numerical Monte-Carlo simulations of the stochastic differential equations Eq.(4.1a) and Eq.(4.1b) (with threshold-and-rest) to explore the signal transmission characteristics.

To study the nonlinear resonate-and-fire neuron model numerically, we will use three distinct parameter sets given in Tab. C.1. The first parameter set is chosen in such a way that the subthreshold resonance in the impedance function is very pronounced, i.e. with a Q_{ZAP}-value of about 16 (*resonator cartoon*). In order to study biological more realistic amplitude responses, we use the parameter set (*stellate cell*) that was fitted (Schreiber et al., 2004) to experimental observations that include a moderate resonance of the impedance function with $Q_{\mathrm{ZAP}} \approx 2$ (see Tab. 4.1). As a third parameter set (Schreiber et al., 2004), we use parameters that lead to an integrator like behavior, i.e. the absence of an impedance resonance and is referred in the following as *pyramidal cell*.

The output characteristics of the purely subthreshold voltage response (without threshold) by using these three parameter sets in the absence of a threshold are given in Tab. 4.1. In order to achieve a meaningful comparison of the output statistics of the different parameter sets (resonator cartoon, stellate cell and pyramidal cell), the input-DC (see Tab. C.1 (below the dashed line)) was chosen as such that similar firing rates were obtained. In addition, for the two stochastic processes $\eta(t)$ (intrinsic noise) and $s(t)$ (signal), the intensities were chosen such that the total variance of the voltage response without threshold (given in Eq.(4.14)) is approximately equal in all three cases. This also results in similar values of the coefficient of variation CV (see Tab. 4.2). The signal-to-noise contribution to the voltage variance was chosen to be 2/3. This fraction can be extracted from Eq.(4.15). The input signal correlation time was set to $\tau_{\mathrm{OU}} = 10$ ms for all three parameter sets. Having ensured that the dynamical output characteristics of the three different parameter sets are roughly equal in rate and CV, the question arises, whether the information filtering properties differ from the resonator cartoon, stellate

Table 4.1: Characteristics of the ZAP-response (above the dashed line) and of information filtering (below the dashed line) in the system without threshold.

parameter	resonator cartoon	stellate cell (EC-II)	pyramidal cell (EC-III)	parameter description
f_{nat} $[Hz]$	7.9	7.99	*none*	natural frequency (MPOs)
$f_{\mathrm{res}}^{\mathrm{Z}}$ $[Hz]$	8.25	8.9	*none*	freq. of max. impedance
Q_{Z}	16.1	1.5	1.0	quality factor of impedance
$f_{\mathrm{res}}^{\mathrm{sub,C}}$ $[Hz]$	0.0	0.0	0.0	freq. of max. coherence
$Q_{\mathrm{sub,C}}$	1.0	1.0	1.0	quality of coherence
$MI_{\mathrm{sub,exact}}$ $[bits/s]$	145.26	143.49	116.66	LB mutual info rate (purely subthreshold response)

Table 4.2: Parameter values and numerical results of spike train and coherence statistics (below the dashed line) for the resonate-and-fire neuron model with OU stimulation.

parameter	resonator cartoon	stellate cell (EC-II)	pyramidal cell (EC-III)	parameter description
r [Hz]	3.78	3.92	3.70	firing rate, inverse mean ISI
CV	0.78	0.70	0.63	ISI oefficient of variation
$f_{\mathrm{spike,C}}$ $[Hz]$	9.3	8.17	0	freq. of max. coherence
$Q_{\mathrm{spike,C}}$	40.8	1.6	1.0	quality of coherence
$MI_{\mathrm{spike,LB}}$ $[bits/s]$	9.80 $6.7\%MI_{\mathrm{sub}}$	10.05 $7.0\%MI_{\mathrm{sub}}$	8.35 $7.2\%MI_{\mathrm{sub}}$	LB of mutual info rate (spiking response)

cell and pyramidal cell parameter set? In Fig. 4.4 the spectral statistics of the spiking neuron model in the three different parameter regimes are shown: the coherence function (Fig. 4.4a1,b1,c1), the cross-spectrum (Fig. 4.4a2,b2,c2), and the spike train power spectrum (Fig. 4.4a3,b3,c3).

In all three regimes, power and cross-spectra expose a peak close to 8 Hz. However, a peak in the coherence function of the spiking response can be only observed for the resonator parameter sets (Fig. 4.4a1,b1). This indicates that a band pass filter of information for the resonator parameter sets can be observed. The coherence function by using the pyramidal parameter set (Fig. 4.4c1) is a decreasing function with increasing frequency. Therefore, the pyramidal cell (non-resonator) acts as a low pass filter on information (similar to the IF neuron models discussed in sec. 2). Comparing the

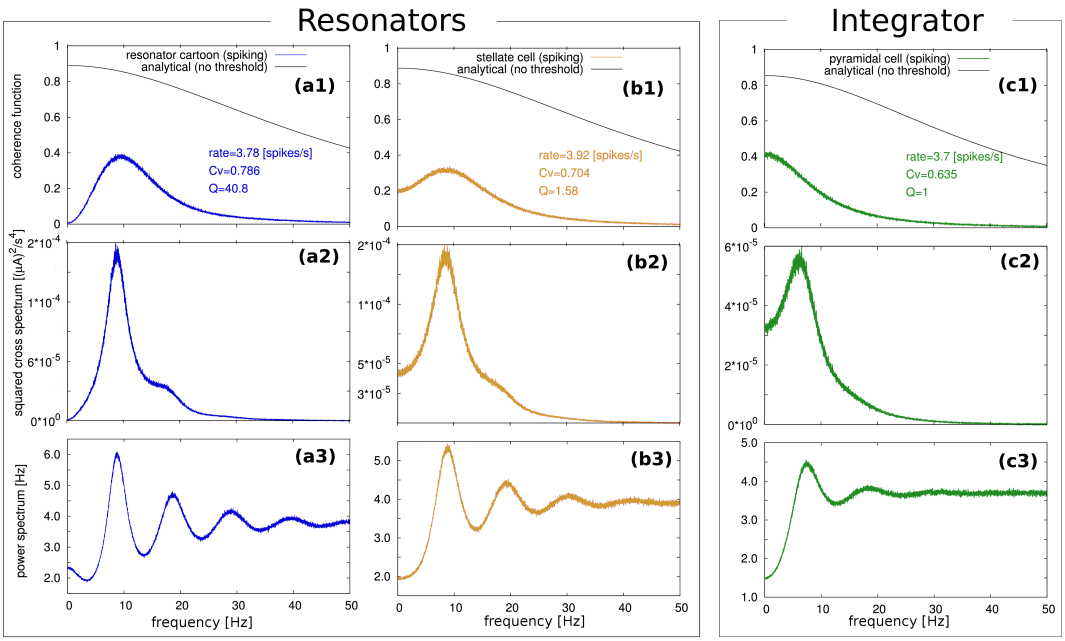

Figure 4.4: Example spectral measures concerning the information filtering for the resonate-and-fire neuron model. Shown are: coherence function for the resonator cartoon (a1), stellate cell (b1) and pyramidal cell (c1). The theoretical results (black solid lines in a1,b1,c1) for the purely subthreshold dynamics (without fire-and-reset) are given in Eq.(4.27). Cross-spectra between the input-signal (OU-process) and the output spike train for the resonator cartoon (a2), the stellate cell (b2) and for the pyramidal cell (c2). The associated power spectra of the output spike train are shown in a3, b3, c3 respectively (for parameters see Tab. C.1).

information filtering characteristic of the purely subthreshold response (see black solid line in Fig. 4.4) with the spiking response suggest that the interplay between neuronal nonlinearities (spiking response) and subthreshold resonances leads to a frequency selectivity in the signal transmission, i.e. a band pass filter on information. In contrast to the resonator parameter sets, the integrator parameter set (pyramidal cell) leads in both: subthreshold and spiking activity to a low pass filter on information. The most striking quantitative effect of the fire-and-reset rule on the information transmission characteristics is the reduction of the mutual information rate by a factor of ten (see Tab. 4.2). In the next section, we want to analyze the impacts of the various intrinsic and extrinsic parameters on the phenomenon of band-pass filtering on information.

Effects of varying the fixed point V_{FP} by changing I_0

By varying the input-DC I_0 one influences the fixed point V_{FP} of the linear system (see Eq.(4.17a) and Eq.(4.17b)). Therefore, the input-DC plays the crucial role and acts as

a control parameter in the deterministic system because it separates the two distinct neuronal activity regimes

- if the DC is below the critical DC value then the system is within the none excitability state and does not show spikes,
- if the DC is above the critical DC value then the autonomous deterministic system can elicit tonic spikes, i.e. with regular spike times.

The transition from the non-excitable to the excitable regime is described in terms of nonlinear dynamics as a Hopf bifurcation (in the presence of subthreshold resonances) or as a Saddle-Node (SN) bifurcation (in the absence of a resonance).

Because of intrinsic noise in the system, the clear separation between excitable and non-excitable regimes of the neuronal system is not possible. In the presence of noise one can classify three regimes of neuronal activity (shown in Fig. 4.5):

- low DC leads to phasic firing (high irregular firing activity (C_V around one)),
- moderate DC leads to a spiking activity of the system with irregular firing activity, i.e. a $C_V \leq 1$,
- high DC results in a tonic firing activity of the system ($C_V \approx 0$).

For the sake of comparability between the three model parameter sets (resonator cartoon, stellate cell and pyramidal cell) we will use rather the fixed point of the membrane voltage V_{FP} instead of the DC-input. The monotonic relationship between V_{FP} and I_0 is given in Eq.(4.17a).

In Fig. 4.6a,b the dependency of the dynamical statistics, i.e. the firing rate (a) and the coefficient of variation C_V (b) with respect to V_{FP} for the three model parameter sets is shown. One can see that the firing rate increases with increasing DC-input, or put differently with increasing V_{FP} (as stated above). The coefficient of variation decreases monotonically for all three parameter sets (the resonator cartoon in blue, the stellate cell in red, and the pyramidal cell in green). One can see that that the DC-input, i.e. the position of the fixed point of membrane voltage compared to the voltage threshold) acts as a control parameter of the system for all three parameter sets.

The question then arises how these dynamical statistics influence the information theoretical statistics like then coherence quality and the lower bound of the mutual information rate? Fig. 4.6c and Fig. 4.6d display the coherence quality and the frequency position of the maximum of the coherence function (band-pass filter frequency) with respect to the control parameter I_0, or put differently V_{FP}. These numerical results suggest that the band pass filter on information, by the resonator parameter sets (resonator cartoon and stellate cell), is most pronounced within the phasic firing regime, i.e. at low firing rates and very irregular spike timings (see Fig. 4.6c). Within this phasic firing regime, the band-pass filter frequency is almost constant, i.e. the position of the peak of the coherence function does not change drastically (see Fig. 4.6d). Even if the fixed point of the subthreshold dynamics (without threshold) is above the threshold of the spiking

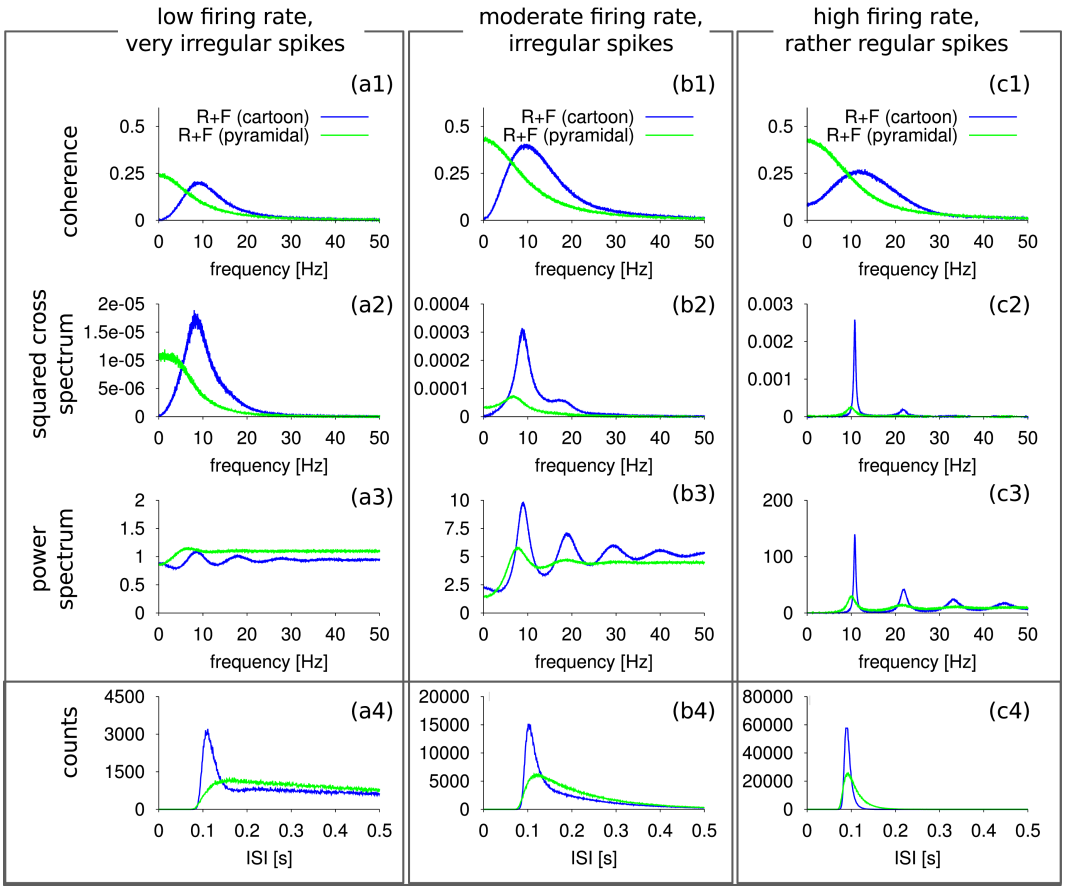

Figure 4.5: Example spectra for the RF neuron model (resonator cartoon and pyramidal cell parameter set) at three different input DC values. Shown are power spectrum (a3,b3,c3), squared cross-spectrum (a2,b2,c2), coherence function (a1,b1,c1) and the ISI histogram (a4,b4,c4) for a fixed point well below the threshold (a1–a4), nearby the threshold (b1–b4) and above the threshold (c1–c4). The band-pass filtering on information for the resonator cartoon (shown in blue) parameter set is visible in a large range of DC inputs. The pyramidal cell (shown in green) parameter set corresponds to a low pass filter on information.

resonate-and-fire model, we observe a band pass filter on information in the resonator parameter sets. Although diminished (compared to the phasic firing regime), the quality factor of the coherence function of the resonator cartoon parameter set is on the order of ten and decreases with increasing DC input. The peak frequency of the coherence function is close to the subthreshold resonance frequency (see Tab. 4.1 and Fig. 4.6d). The transition from the phasic to the tonic firing activity regime is accompanied by a further decrease of the coherence quality for the resonator parameter set, and thus with a decrease of the peakedness of the coherence function. In addition to the attenuation

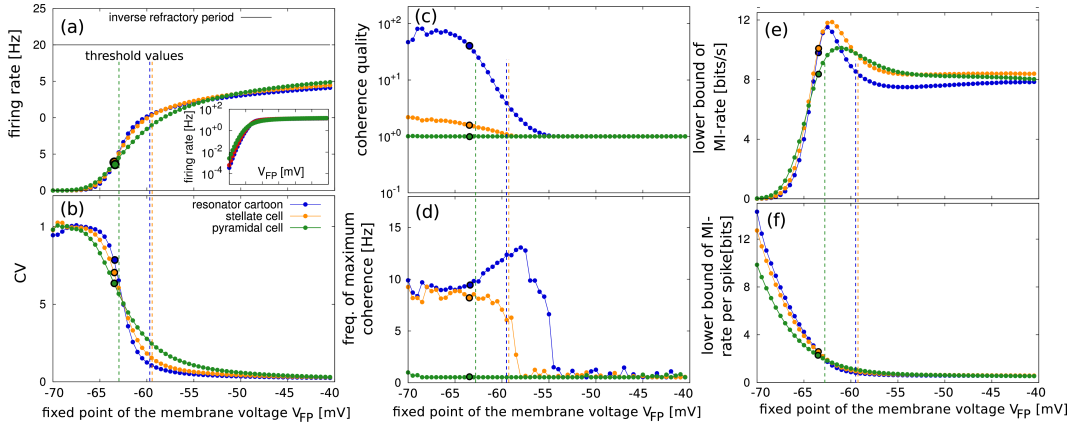

Figure 4.6: Variation of input-DC leads to the translation of V_{FP} of the linear resonator neuron model. The dependence of the dynamical parameter (firing rate (a), coefficient of variation (b)) as well as the information theoretic measures coherence quality (c), the frequency of maximum coherence (d), the lower bound of the mutual information rate (e) and for the lower bound of the mutual information rate per spike (f) for the three model parameter sets is shown. The dashed lines indicate the respective threshold values given in Tab. C.1 and the marked data points designate the parameter set listed in see Tab. C.1 and the corresponding spectra are shown Fig. 4.4
.

of the bandpass filter on information, the band-pass filter frequency in the resonator parameter sets changes drastically in the phasic and the tonic firing regime.

If one further increases the DC-input, and thus driving the neuron model (for all three parameter sets) into the tonic activity regime, leads to firing rates close to the inverse absolute refractory period (here: 50 ms leads to a maximum firing rate of 20 Hz) as well as a decrease of the quality of the bandpass filter characteristics (in the resonator parameter set).

In the very tonic firing regime, which is reflected in high firing rates (see Fig. 4.6a) and a coefficient of variations $C_V s$ close to zero (see Fig. 4.6b), all three parameter sets leads to a low pass filter on information, irrespective of the presence of absence of subthreshold resonances. This effect can be well understood by regarding the fact, that high DC-inputs increases the deterministic drift of the neuron model. Consequently, the voltage trajectory will go very quickly from the reset to the threshold value. Thus in the tonic firing regime, voltage threshold crossings are due to the deterministic drift, and the influence of MPOs on threshold crossings is drastically diminished. Within this tonic firing regime, the discrimination between resonators and integrators (pyramidal cell) becomes more difficult and ultimately leads to an indistinguishability between resonators and integrators (with respect to the dynamical statistics (see Fig. 4.6a,b) as well as the information theoretical statistics (see Fig. 4.6c,d and Fig. 4.6e,f)).

In contrast to the resonator parameter set, the integrator parameter set (green line in Fig. 4.6) demonstrates always a low pass filter on information (green line in Fig. 4.6c,d).

Having demonstrated the crucial role of the phasic firing regime (similar insights were found in a completely different neuron model, see sec. 3) to establish a band pass filter on information for the resonator parameter sets, the question arises, whether a band pass filter on information is accompanied by a loss or gain of the total transmitted information per time, approximated by the lower bound of the mutual information rate. Does the trade-off between band-pass filtering characteristics and mutual information (as was demonstrated in the presence of positive ISI correlations, see sec. 3) holds true for this mechanism, i.e. subthreshold resonance induced band pass filter on information?

In Fig. 4.6e it is shown that within the rather phasic firing regime, all three parameter sets act almost similar, irrespective of the presence or absence of subthreshold resonances. The increase of the mutual information per time is due to an increase of the firing rate (see Fig. 4.6a) and is a fact of increased firing rate and consequently for a higher coding capability. In contrast to the total mutual information rate (lower bound), if one studies the mutual information per spike instead of the mutual information per time, one can observe a decrease of the coding capabilities per spike (see Fig. 4.6f). This effect is because a single spike cannot carry as much information about the time-dependent input signal as the firing rate increases (in the tonic regime) compared to the low firing rate regime (phasic activity). This effect originated from the presence of an absolute refractory period (here of 5.0 ms, a typical value for the duration of an action potential). One can also observe that the lower bound of mutual information rate has a maximum within the rather phasic regime (see Fig. 4.6e), while the location of the maximum seems to be identical with the position of the inflection point of the firing rate as well as the coefficient of variation (see Fig. 4.6a).

The lower bound of mutual information per spike decreases monotonically as one drives the neuron model from the phasic to the tonic firing regime (see Fig. 4.6f). Within the tonic firing regime, the three neuron model parameter sets (resonator cartoon, stellate cell, pyramidal cell) become more and more similar with respect to dynamical statistics as well as all information theoretical statistics like the filtering properties, described by the coherence quality and the band-pass filter frequency, as well as the lower bound of mutual information rate.

One can conclude that the presence of subthreshold resonances in conjunction with a fire-and-reset rule (discontinuous nonlinearity) leads to the characteristics of a band pass filter on information within the low and moderate activity regime, where the quality of the band pass filter on information seems to be positively correlated with the quality of the subthreshold resonances (compare the information theoretic measures between the resonator cartoon and the stellate cell in Fig. 4.6). This effect of band-pass filtering on information due to subthreshold resonances is accompanied with a minor loss on mutual information rate if one compares integrators from resonators (with threshold).

Thus, a nonlinearity in terms of a fire-and-reset rule leads to a translation of the frequency preference on power (impedance function) to a preferred frequency of signal transmission (information filtering), whereas the information loss due to the nonlinear-

ity is for both cell types (integrators/non-resonators and resonators) of almost equal amount, namely a strong reduction of mutual information rate compared to the purely subthreshold response (without threshold). The excitable neuron model with subthreshold resonances can show both: i) low-pass (tonic) and band-pass (phasic) filtering characteristics on information.

The effects of the signal strength D_{OU}

As we have seen in in sec. 4.4.1, the DC-input acts as a control parameter with respect to the firing regime (phasic versus tonic), which is also reflected in the signal transmission characteristics, like the coherence quality. Here we will study numerically the effects of the strength of the stochastic input signal (Ornstein-Uhlenbeck process) on the signal transmission characteristics of the spiking resonate-and-fire neuron model.

One can abundantly assume that the strength of the external stochastic input current has the same effect on the dynamical characteristics, like the firing rate and the coefficient of variation, as the strength of the input-DC. Because a larger signal strength of the stochastic signal leads to larger excursions in the phase space from the steady state value, and thus a larger signal strength dominates the dynamics of the model, while contributions to the dynamics due to cell-intrinsic mechanisms (like the presence of subthreshold resonances) can always be neglected in the presence of a strong stochastic signal $s(t)$. Thus, one can expect that the arguments given in sec. 4.4.1 are also valid here, i.e. an increase of input strength leads to a monotonic increase in the firing rate and is accompanied by a monotonic decrease of the variability of the spiking output (see fig:5a,b). As was pointed out in sec. 4.4.1, the information characteristics are correlated with the dynamical (spiking) measures and therefore with the regime of spiking activity of the neuronal model. One can easily anticipate (by the arguments given above) that the strength of the external stochastic input current D_{OU} affects the band pass filter on information in a similar way as the DC-input I_0 (constant drift).

This 'intuition' is confirmed in Fig. 4.7 for the coherence quality (c) and the band-pass filter frequency (d). One can see that the irregular and low firing rate activity (phasic) can lead to a band pass filter on information in the presence of subthreshold resonances. The quality of the band pass filter on information decreases monotonically if one drives the system towards to tonic activity, i.e. high firing rates and low variability of the spiking response (see fig:5 c,d). This tonic firing activity leads to large values of the lower bound of the mutual information rate (see fig:5 e), whereas the mutual information per spike (see fig:5 f) decreases monotonically with increasing signal strength D_{OU}.

Thus, one can conclude that the strength of the time-dependent input current $s(t)$, here modeled with the help of an Ornstein-Uhlenbeck process with fixed correlation time of 10 ms, has the same effect of the neuronal dynamics (rate and CV) as well as the information theoretic measures (coherence quality, lower bound mutual information rate) as the DC-input I_0. Phasic firing regimes are distinguished by very pronounced band bass filter on information (in the presence of subthreshold resonances). This effect is diminished if the neuronal dynamics is overwhelmingly affected by the signal and thus by the neuronal absolute refractory period (here $\tau_{\mathrm{abs}} = 50.0$ ms).

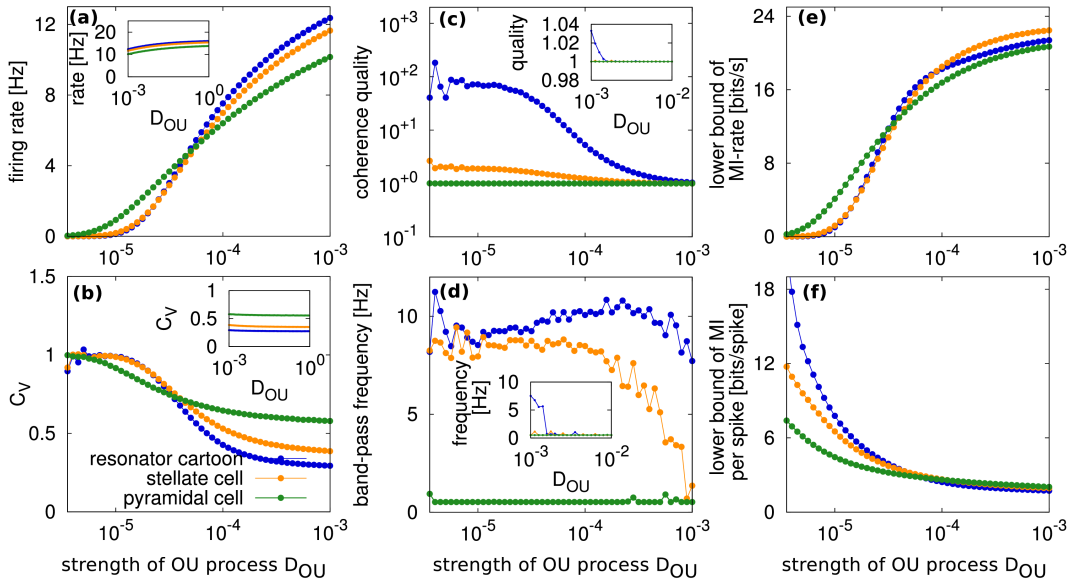

Figure 4.7: Effects of the signal strength on information filtering. Shown are: firing rate (a), coefficient of variation C_V (b), coherence quality (c), frequency of maximum coherence (d), lower bound of mutual information rate (e) and mutual information rate per spike (f) as functions of the external signal strength D_{OU} for the three model parameter sets (resonator cartoon in blue, stellate cell in orange, and the pyramidal cell in green) (parameters are given in Tab. C.1.). Insets show the respective statistics for a larger range of signal strength D_{OU}.

The effects of reset value and absolute refractory period

Two important neural parameters that vary among neurons are the reset value V_{reset} (reflecting the depth of afterhyperpolarization) and the absolute refractory period τ_{abs}, reflecting the presence of intervals of non-excitability. Here we study the effects of the absolute refractory period as well as the reset value on the signal transmission characteristics (information filtering) of the spiking resonate-and-fire neuron model.

In the left column of Fig. 4.8, the coherence function (Fig. 4.8a1), the squared cross-spectrum (Fig. 4.8a2) and the power spectrum of the spike train response (Fig. 4.8a3) for three values of reset values V_{reset} by using the resonator cartoon parameter set of the spiking resonate-and-fire neuron model are shown. One can infer from (Fig. 4.8a3) that lower reset values lead the higher firing rates and slightly higher CVs (compare the black ($V_{\mathrm{reset}} = -55$ mV) curve with the green ($V_{\mathrm{reset}} = -65$ mV) and blue ($V_{\mathrm{reset}} = -70$ mV) curve in Fig. 4.8a3). Thus, the higher harmonics in the power spectrum of the spiking response (due to the presence of subthreshold resonances at approx. 10 Hz) become more pronounced if one decreases the membrane voltage reset value V_{reset}.

The variation of the reset values alters the dynamics of the neuronal model as can be clearly seen by looking at the power spectra in Fig. 4.8a3. Please note, that this

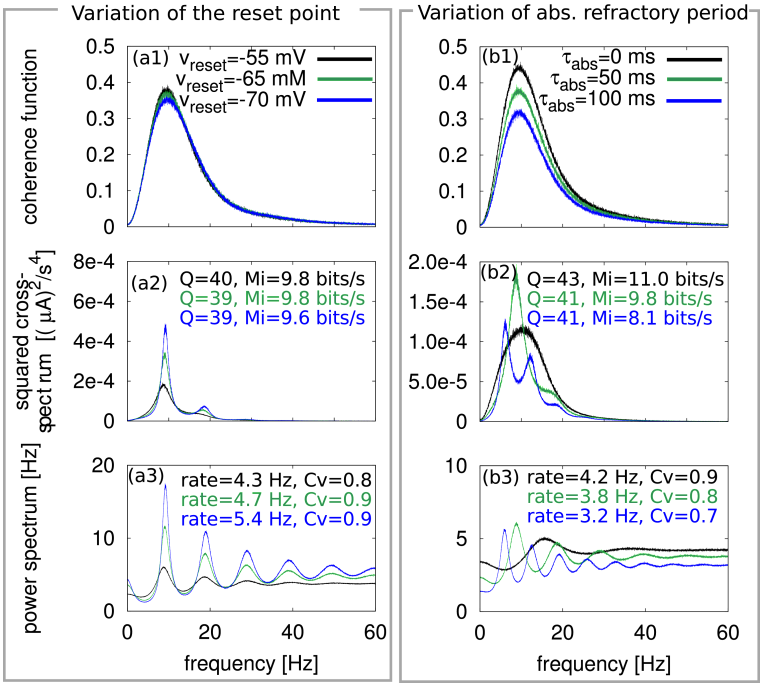

Figure 4.8: Effects of the voltage reset and the abs. refractory period. The effects of the voltage reset (a1–a3) value and on the coherence function (a1), cross-spectrum (a2), and power spectrum (a3) are shown. The effects of the absolute refractory period on the spectra are shown in (b1–b3) respectively. Variations are placed in the vicinity of the standard parameters of the resonator cartoon parameter set (stated in Tab. C.1).

changes the squared cross-spectrum in almost the same way, i.e. the dominant peak in the squared cross-spectrum between the spiking response and the input signal becomes more pronounced if one lowers the membrane voltage reset value (see Fig. 4.8a2).

The effect of V_{reset} on the signal transmission characteristics is therefore very small compared to the effects obtained by varying the DC-current (see sec. 4.4.1), for example.

The numerical results lead to the conclusion that the modification of the discontinuous nonlinearity (the fire-and-reset rule), by lowering the reset value (within biologically plausible regimes) and therefore effectively increasing the distance between reset and threshold, does not affect particularly the signal transmission characteristics (information filtering) of the resonate-and-fire neuron model. Variations of the absolute refractory period have more profound effects on the information transmission characteristics of the resonator cartoon neuron model.

In the right column of Fig. 4.8 one can see the spectra of interest of the resonate-and-fire neuron model (by using the resonator cartoon parameter set) for three different values of the absolute refractory period. One can expect that the inclusion of an absolute

refractory period lowers the firing rate of the neuronal model, and the output spike train will become more irregular (more phasic). The power spectrum of the spike train is shown in Fig. 4.8b3 for absolute refractory periods of $\tau_{\rm abs} = 0$ ms (black line), $\tau_{\rm abs} = 50$ ms (green line), and $\tau_{\rm abs} = 100$ ms (blue line). One can clearly see that the power spectrum is affected in a nontrivial way by the variation of the absolute refractory period. The higher harmonics changes as well as their 'markedness'.

As expected, the firing rate decreases with increasing absolute refractory period (see data shown in Fig. 4.8b3), and the spike train becomes more regular, i.e. the CV decreases (and approaches zero for very large absolute refractory periods) with increasing absolute refractory period. By changing the absolute refractory period, one does change the dynamics of the system profoundly. These strong effects are visible in the power spectrum of the spike train as well as in the cross-spectrum (see Fig. 4.8b2). However, the modifications in the squared cross-spectrum and the power spectrum (due to the presence of an absolute refractory period) cancel each other on the level of the coherence function (which is the ratio between the two spectra). Thus, the coherence function (see Fig. 4.8b1) is only affected by a frequency independent factor, which reflects the effects of the absolute refractory period on the firing rate. This leads to an overall reduction of the coherence[5]. Consequently, the quality factor of the coherence function (see numerical values in Fig. 4.8b2) are within numerical accuracy (due to a finite number of independent realizations) constant and not affected by variations of the absolute refractory period. Because of the overall reduction (for all frequencies) of the coherence function with increasing $\tau_{\rm abs}$, the lower bound of the mutual information rate $MI_{\rm LB}$ (see numerical values in Fig. 4.8b2) decrease with increasing $\tau_{\rm abs}$.

To conclude, the numerical results indicate that variation of the reset value and the absolute refractory period does affect the quality of the band pass filter on information. The absolute refractory period reduces the coherence function for all frequencies equally and thus reduces the lower bound of the mutual information rate but not the quality of the bandpass filter. The effects of the reset value and the absolute refractory period make small contributions in shaping the coherence function.

The effects of subthreshold resonances

In sec. 4.4.1 we came to the conclusion that a band pass filter on information is exclusively observed by using the resonator parameter sets in the presence of a strong nonlinearity, i.e. a fire-and-reset rule (resonate-and-fire). Besides, it was pointed out that the explorations via numerical computer simulations of the stochastic neuron models suggest a positive correlation between the quality of power filtering, measured by the quality of the impedance function, and the quality of the band pass filter on information, measured by the quality of the coherence function.

Here we will study this hypothesis in a more systematic and extensive procedure. Thus, we systematically change the quality value of the impedance function (keeping the resonance frequency $f_{\rm res}$ fixed) by changing R, R_L, L in a way detailed in sec. C.2.

[5]This effect has been shown theoretically for the stochastic LIF neuron model by Lindner (2012).

Secondly, for each value of impedance quality (in the range between 1 and 10), we vary the output firing rate[6] between $0.5 - 15$ Hz by changing the DC I_0.

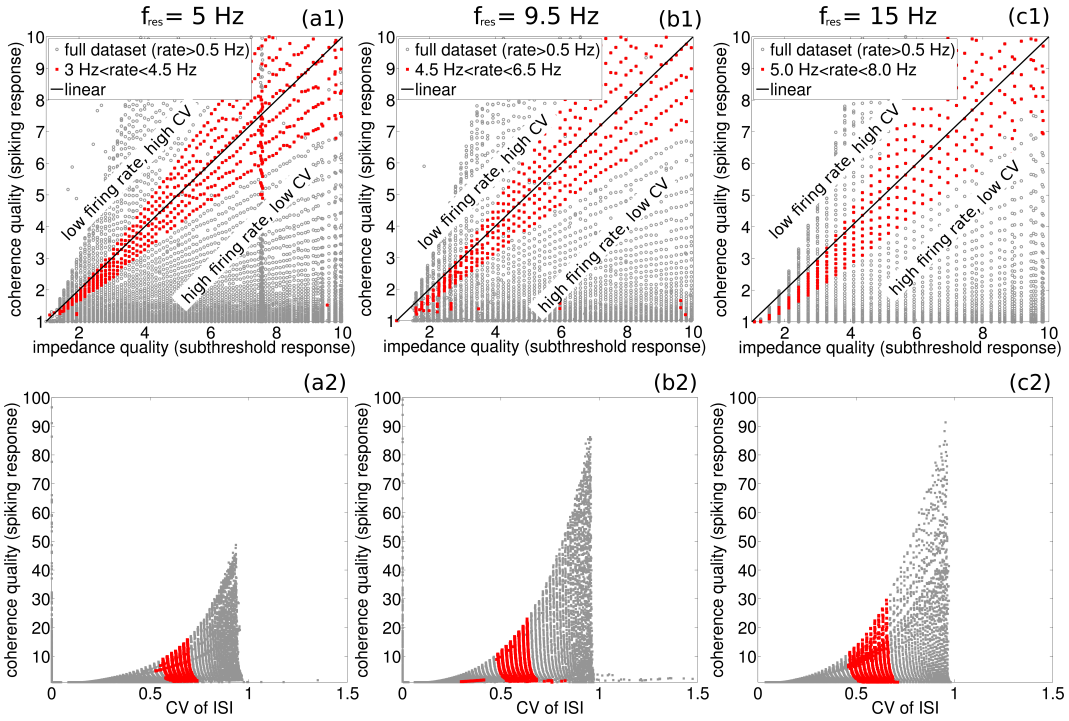

Figure 4.9: Correlations between the impedance quality of the purely subthreshold response and the quality of the coherence of the spiking RF model. Shown are numerical results of the spiking response of RF neuron model (3 x 25.000 parameter sets) at different resonance frequencies: $f_{\rm res} = 5$ Hz (a1), $f_{\rm res} = 9.5$ Hz (b1) and $f_{\rm res} = 15$ Hz (c1). If the firing rate is close the natural frequency of the resonator, then impedance quality and coherence quality are one-to-one related to each other (red points in a1,b1 and c1), which implies a rather irregular spiking activity $C_V \approx 0.6$ (see red points in a2, b2, and c2). A pronounced band pass filter on information is associated with very irregular ($C_V \approx 1$) spiking activity (see a2, b2, and c2) at low firing rates.

In Fig. 4.9 the numerical results for three different resonance frequencies are shown. In Fig. 4.9a1,a2 the peak of the impedance function is fixed to $f_{\rm res} = 5$ Hz. The quality factor of the impedance function was then varied systematically and is compared to the quality of the coherence function of the spiking RF model. Fig. 4.9a1 displays that the coherence quality, i.e. the quality of the band pass filter on information is positively correlated with the quality of the impedance function of the purely subthreshold response if the firing rate of the RF model (with threshold) is restricted to a certain region (see red data point in Fig. 4.9a1). This effect is observable even for different resonance

[6]Note that due to the absolute refractory period of 50 ms the output firing rate is bounded by 20 Hz

frequencies as shown in Fig. 4.9b1 and Fig. 4.9c1.

As we have seen previously, a pronounced band pass filter on information is associated with a very irregular firing rate regime, i.e. a $C_{\mathrm{V}} \approx 1$ (phasic firing activity). This is shown in Fig. 4.9a2 for a resonance frequency of $f_{\mathrm{res}} = 5$ Hz. The red data points are associated with a firing activity of the RF model restricted to a certain region. Interestingly, the regime in which the firing rate of the RF model is close to the natural frequency of the MPOs, is closely related to a coefficient of variation $C_V \approx 0.6$ for all resonance frequencies (see Fig. 4.9a2,b2 and c2).

In addition to Fig. 4.9, Fig. 4.10 shows the same data set used in Fig. 4.9. The first row shows the dependence of the coherence quality of the spiking RF model with respect to the quality of the impedance function (of the purely subthreshold response), i.e. the quality of the subthreshold resonance for three different resonance frequencies. The second row of Fig. 4.10a2,b2,c3 displays that the mutual information rate is negatively correlated with the coherence quality (trade-off). The mutual information rate of the spiking RF model has been normalized with respect to the mutual information rate of the purely subthreshold response (see Eq.(4.29)).

Thus, Fig. 4.10a2,b2,c2 display that the mutual information rate of the spiking output is reduced by a factor of 10 (for very low coherence qualities, i.e. integrator-like characteristics) or more (for pronounced band pass filter on information). The red data points correspond to firing rates of the spiking RF model within a certain region. These regions are connected to a moderate loss of mutual information rate (compared to the purely subthreshold response) by a factor of 13. The third row of Fig. 4.10a3,b3,c3 shows the frequency, at which the coherence function of the spiking RF model attains its maximal value with respect to the coherence quality (center-frequency or resonance frequency of the coherence function). One can see that for all three impedance resonance frequencies, the peak of the coherence function is in the vicinity of the peak of the impedance function, i.e. the resonance frequency (dashed line in Fig. 4.10a3,b3,c3).

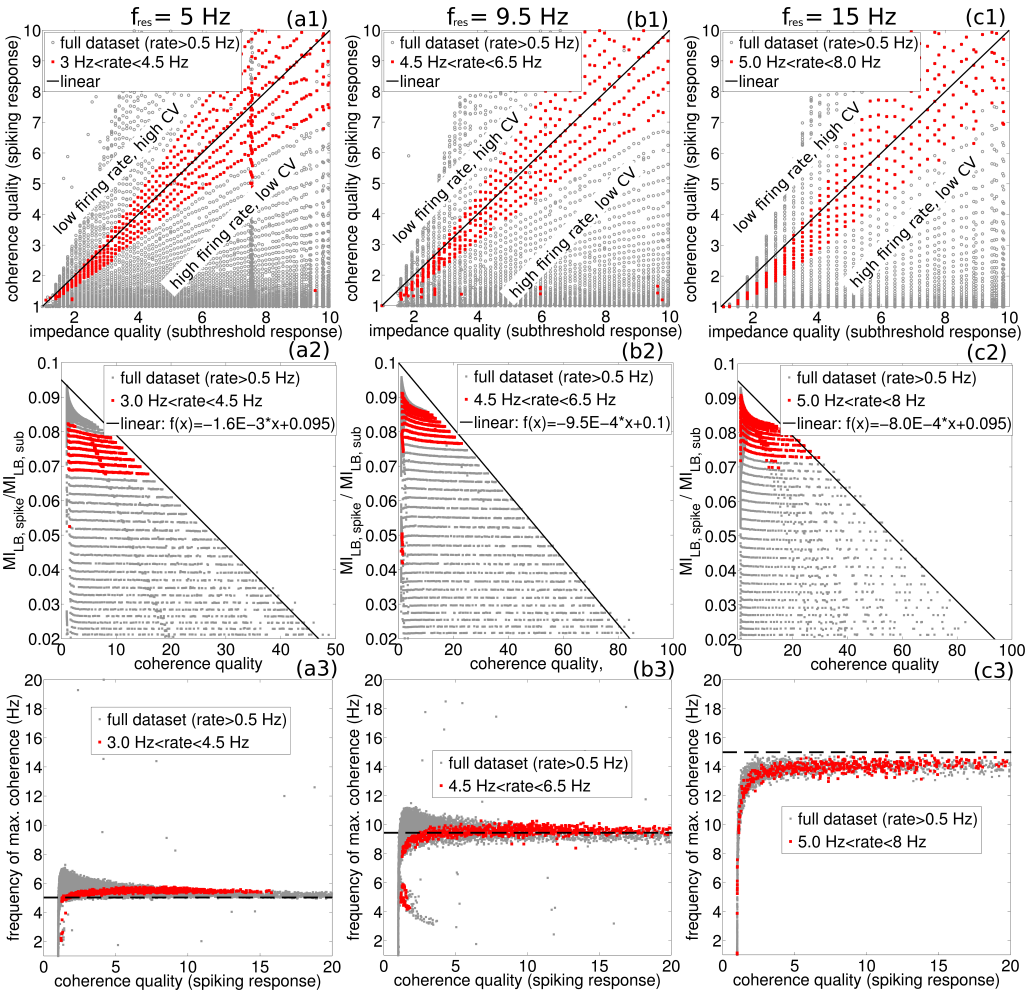

Figure 4.10: Correlations between the impedance quality of the purely subthreshold response and the quality of the coherence of the spiking RF model. Shown are numerical results of the spiking response of RF neuron model (3 x 25.000 parameter sets) at different resonance frequencies: $f_{\mathrm{res}} = 5$ Hz (a1), $f_{\mathrm{res}} = 9.5$ Hz (b1) and $f_{\mathrm{res}} = 15$ Hz (c1). Pronounced band-pass filtering on information implies a reduction of the mutual information rate, which is characterized in a negative correlation between mutual information rate (normalized by the mutual information rate without threshold) and the coherence quality of the spiking activity (a2, b2, and c2). Typically, the spiking activity contains less than ten percent of the mutual information rate of the purely subthreshold response. The frequency of maximum coherence is nearby the impedance resonance frequency (dashed line in a3, b3, and c3) and is almost constant for a large range of coherence qualities (see a3, b3, and c3). The red points correspond to spiking activities, for which the firing rate is bounded to a certain region.

4.5 Signal transmission with continuous nonlinearities

As I have described in sec. 4.4.1 the interplay between subthreshold resonances and a discontinuous nonlinearity in form of a fire-and-reset rule leads to a frequency-dependent signal transmission (information filtering) such that frequency components of the time-dependent (stochastic) current input signal, which are in the vicinity of the subthreshold resonance frequency [7] are preferentially transmitted.

We have seen in sec. 4.4.1 that this emergence of a band pass filter on information transmission comes to the cost of a reduction of the total transmitted information, or put differently the trade-off between qualitative (frequency-selective) and quantitative (lower bound of mutual information rate) signal transmission was established. The effect of band-pass filtering on information is most pronounced in the phasic firing regime, characterized by a low to moderate firing rate and a rather irregular spiking activity, or put differently a coefficient of variation CV close to one (see Fig. 4.6 and Fig. 4.7 for example).

Here, we will investigate the effects of a second kind of nonlinearity: a continuous nonlinearity in the form of a biophysical realistic action potential mechanisms, which reflected in nonlinear activation and deactivation functions of ion channel activity in conductance-based neuron models. These conductance-based neuron models can differ drastically from the resonate-and-fire (RF) neuron model.

We will focus on two continuous nonlinear neuron models: the two-dimensional Morris-Lecar (Eq.(4.21) and Eq.(4.21)) and the four-dimensional Hodgkin-Huxley neuron model (see sec. 4.2.4). Especially the Hodgkin-Huxley neuron model, as classical conductance-based neuron model allows us to study numerically different noise sources (current noise and biophysical realistic ion channel noise) and their effects on the signal information characteristics.

First, we will discuss in sec. 4.5.1 basic information filtering properties of the nonlinear two-dimensional Morris-Lecar neuron model and will complete this exploration on the effects of subthreshold resonances in conjunction with different kind of nonlinearities by analyzing the nonlinear four-dimensional Hodgkin-Huxley neuron model with a detailed description of ion-channel noise in sec. 4.5.2.

4.5.1 Morris-Lecar neuron model with current noise

The conductance-based Morris-Lecar neuron model is described by two nonlinear differential equations given in sec. 4.2.3. Depending on the choice of parameters, this spiking neuron model can be type I (integrator cell) or type II (resonator cell) (Rinzel and Ermentrout, 1989). In the resonator regime below the Hopf bifurcation, the model displays pronounced subthreshold resonances similar to the linearized (purely subthreshold) resonate-and-fire (RF) model at appropriate parameters. The main difference to the latter is that the Morris-Lecar (ML) model possesses a dynamical nonlinear mechanism

[7] Note, that the subthreshold resonance frequency of the chosen current-based RF model solely depends on its intrinsic characteristics and is not affected by the characteristics of external stimulus or the DC-input I_0, in contrast to conductance-baded models.

of spike generation and does not need a fire-and-reset rule. Here, we inspect whether the band-pass filtering effect on information is also present in this biophysical more realistic neuron model by using a type II parameter set(Schreiber et al., 2004). The numerical values for the type I and type II parameter set of the ML model are shown in Tab. 4.3. In

Table 4.3: Intrinsic model parameters (Schreiber et al., 2004) and spike train and information transmission characteristics (below the dashed line) for the Morris-Lecar.

parameter	type II (resonator)	type I (integrator)	parameter description
V_1 $[mV]$	-1.0	-1.0	calcium activation midpoint
V_2 $[mV]$	$+15$	$+15$	calcium activation slope factor
V_3 $[mV]$	$+0$	$+10$	potassium activation midpoint
V_4 $[mV]$	$+30$	$+14$	potassium activation slope factor
g_{Ca} $[mS/cm^2]$	1.1	1.1	max. conductance of Ca^{++} channels
g_K $[mS/cm^2]$	2.0	2.0	max. conductance of potassium channels
g_L $[mS/cm^2]$	0.5	0.5	max. conductance of leakage channels
E_{Ca} $[mV]$	$+100$	$+100$	reversal potential of Ca gated channels
E_K $[mV]$	-70	-70	reversal potential of potassium channels
E_L $[mV]$	-50	-50	reversal potential of leakage channels
C $[\mu F/cm^2]$	1	1	normalized membrane capacitance
ϕ	$\frac{1}{5}$	$\frac{1}{3}$	dimensionless reference frequency
I_0 $[\mu A/cm^2]$	20.21	7.252	DC input
D	5.0	10.0	strength of the intrinsic current noise
D_{OU}	5.0	2.0	strength of the OU current input signal
τ_{OU} $[ms]$	1.0	10.0	correlation time of OU input signal

order to compare the coherence function for the integrator(non-resonator) and resonator versions of the model we choose parameter sets used before by (Rinzel and Ermentrout, 1989) (see Tab. 4.3).

Fig. 4.11 shows the numerical results of the ML neuron model by using the two parameter sets: integrator (shown in black) and resonator (shown in red) in three different spiking activity regimes i) low firing rate and very irregular spike trains (Fig. 4.11a1–a3), ii) moderate firing rate and irregular spike trains (Fig. 4.11b1–b3) and iii) high firing rate and rather regular spike trains (Fig. 4.11c1–c3). The DC input was adjusted such that the model parameters results in similar firing rates and CV. The stochastic input signal was chosen to be an Ornstein-Uhlenbeck process with a correlation time of 10 ms (as was used in the RF neuron model, see sec. 4.4.1).

In Fig. 4.11a1,b1,c1) coherence function, which takes into account the squared cross-spectrum (seen in Fig. 4.11a2,b2,c2) and the power spectrum of the spike train (presented in Fig. 4.11a3,b3,c3) is shown. One can see from Fig. 4.11a1–c1 (red lines) that the type

II parameter set (resonator) leads to a band pass filter on information because the respective coherence function has a pronounced peak in the vicinity of the subthreshold resonance frequency (here around 60 Hz). This effect is robust in the sense that the band-pass filter effect is visible in all three spiking activity regimes (from phasic to tonic spiking activity). In the ML model the appearance of the band pass filter on information within the type two parameter regime is due to a pronounced peak in the squared cross-spectrum (see red line in Fig. 4.11a2,b2,c2) and the local minimum in the spike train power spectrum (Fig. 4.11a3, b3, c3, red curve). Upon increasing the DC-input, the peaks in the squared cross-spectrum as well as in the power spectrum become narrower because the output spike train becomes more regular.

Very interestingly, because different from the RF neuron model (discussed in sec. 4.4.1), the ML neuron model (type II parameter set) displays a band pass filter on information across different activity regimes, ranging from very irregular firing activity ($C_V \approx 1$) to rather regular firing activity ($C_V \approx 0$). The ML neuron model (type II parameter set) exhibits a different information filtering characteristics than the RF neuron model inasmuch that the coherence quality of the ML model (type II parameter set) is a non-monotonically function with respect to the DC-input and displays a resonance for band-pass filtering on information at rather irregular firing activities (compare red curves in Fig. 4.11a1, b1, c1).

In contrast to the ML type II parameter set (resonator), the ML type I parameter set (integrator) displays in all three spiking activity regimes a low pass filter on information (see black curve in Fig. 4.11a1,b1,c1). This effect is rather surprising if one compares the power and the squared cross-spectrum of the two parameter sets. Although the spectra look qualitatively very similar, the ratio, i.e. the coherence function differs dramatically between these two parameter sets (low pass filter characteristics for the type I ML parameter set and band pass filter on information for the type II ML parameter set). Hence, the ML model in the type I regime can be regarded as a low pass filter on information across different spiking activity regimes.

Thus, we conclude that subthreshold resonances can affect the frequency preference on information of the suprathreshold spiking response in the conductance-based ML neuron model with continuous nonlinearity. This insight establishes the vital role of neuronal nonlinearities to establish a band pass filter on information.

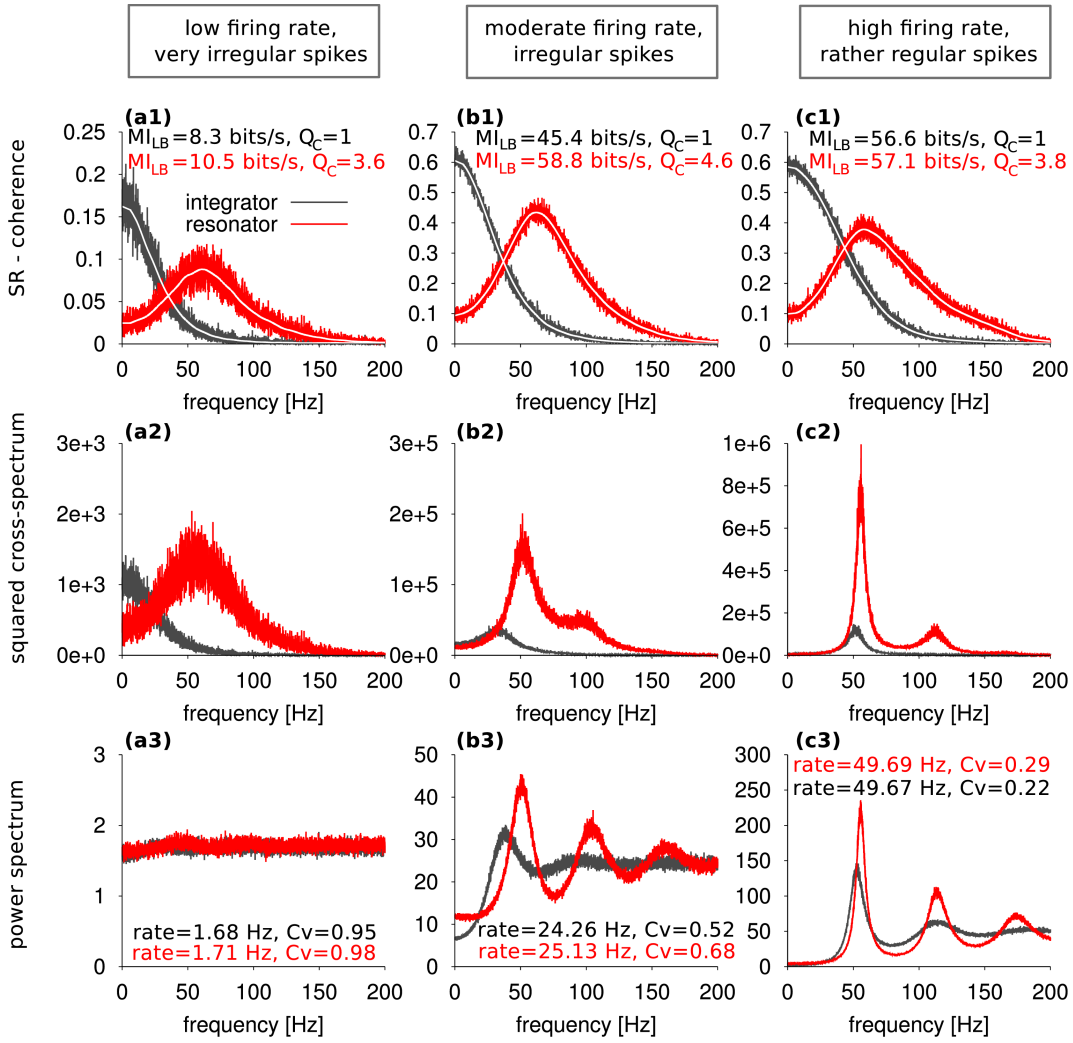

Figure 4.11: Spectral measures for the stochastic Morris-Lecar neuron model for different firing regimes. Shown are spectra of two distinct parameter sets (integrator-like, shown in black and resonator, shown in red) for low firing rate (a1-3), intermediate activity (b1-3) and high spiking activity (c1-3). Irrespective of the firing rate, the resonator parameter set exhibits always a band pass filter on information, whereas the integrator-like parameter set results in a low pass filter on information. In this continuous nonlinear neuron model, the peak in the coherence function is due to a maximum in the squared cross-spectrum, in contrast to the origin of the band pass filter on information in the RF neuron model described in 4.4.1. Parameter sets and numerical details can be found in Tab. 4.3.

4.5.2 Hodgkin-Huxley neuron model with ion channel noise

Here we study the information transmission characteristics of the stochastic Hodgkin-Huxley neuron model (HH) (Hodgkin and Huxley, 1952e), which incorporates realistic ion-channel stochasticity. Because of the continuous nonlinearities incorporated in the original Hodgkin-Huxley (HH) equations, which enters as nonlinear activation and inactivation functions of ion channels, the HH neuron model is a spiking neuron model. The HH model is usually utilized as a biophysically realistic neuron model for type II spiking activity. However, the HH model can be either type I or type II neuron model(Lundstrom et al., 2008), i.e. the can undergo a saddle-node on an invariant circle (SNIC) or a Hopf bifurcation upon increasing the DC-input. The sodium ion channel conductance or put differently the density of sodium conducting ion channels is a critical control parameter between the two bifurcation characteristics (type I and type II). Therefore an adjusted the type II parameter set(Schmandt and Galán, 2012) (see Tab. 4.4) was used by increasing the sodium ion channel conductance from $g_{\mathrm{Na}} = 20$ pS/μm^2 (type II) to $g_{\mathrm{Na}} = 130$ pS/μm^2 (type I). An efficient numerical Monte-Carlo-Markov-Chain (MCMC) implementation proposed by Schmandt and Galán (2012) was used to study the HH neuron model and its information filter characteristics in the presence of subthreshold resonances (type II HH parameter set) and the absence of subthreshold resonances (type I HH parameter set).

Spiking response with current input

In order to study the information filtering properties of the HH neuron model within the type I and type II parameter regime we have estimated numerically the coherence function between the spike train output and the input signal, which is modeled by an Ornstein-Uhlenbeck process with a correlation time of 10 ms (see Tab. 4.4).

Because the DC-input acts as a bifurcation parameter in the HH neuron model, we have used three different DC-input values (see Tab. 4.4) to study three different spiking activity regimes (similar to the ML neuron model in sec. 4.5.1): i) low firing rate and very irregular spike trains (Fig. 4.12a1–a3), ii) moderate firing rate and irregular spike trains (Fig. 4.12b1–b3), and iii) high firing rate and rather regular spike trains (Fig. 4.12c1–c3). In Fig. 4.12a1,b1,c1 the coherence function for the HH type I parameter set (blue curve) is shown. Similar to the ML neuron model type II parameter set, the HH type II parameter set displays a band pass filter on information characteristics, i.e. a pronounced peak of the coherence function in all three spiking activity regimes. This observation is in contrast to phenomena seen in the spiking RF neuron model and is due to biophysical realistic continuous nonlinearity, inherent in the HH neuron model (as well as in the ML neuron model). The preferred frequency of information transmission is close to the resonance frequency (here in the range from $40 - 60$ Hz, depending on the DC-input) of the purely subthreshold dynamics (obtained by linearizing the HH neuron model equations around the fixed point numerically). The power and the squared cross-spectra of the HH neuron model are very similar to the spectra obtained by using the ML neuron model (compare Fig. 4.12 and Fig. 4.11).

On the contrary to the type II parameter set, the HH type I parameter set show always a low pass filter on information characteristic, i.e. a monotonically decreasing coherence function, irrespective of the neuronal spiking activity (low, moderate or high firing rate regime) (see green line in Fig. 4.12a1,b1,c1).

Table 4.4: Intrinsic model parameters adopted from (Schmandt and Galán, 2012). Resonator and the integrator parameter set were obtained by increasing the sodium conductance per channel(Lundstrom et al., 2008). Listed are spike train and information transmission characteristics (below the dashed line) for the stochastic Hodgkin-Huxley model within the stochastic shielding approximation.

parameter	type II (resonator)	type I (integrator)	parameter description
A $[m^2]$	500.0	500.0	simulated membrane patch size
C $[pF/\mu m^2]$	0.01	0.01	membrane capacitance
E_L $[mV]$	-54.387	-54.387	leak reversal potential
g_L $[pS/\mu m^2]$	3.0	3.0	leak channel conductance
E_{Na} $[mV]$	45.0	45.0	sodium reversal potential
g_{Na} $[pS/\mu m^2]$	20.0	130.0	sodium channel conductance
E_K $[mV]$	-77.0	-77.0	potassium reversal potential
g_K $[pS/\mu m^2]$	20.0	20.0	potassium channel conductance
ρ_{Na} $[1/\mu m^2]$	25.0	25.0	sodium channel density
ρ_K $[1/\mu m^2]$	5.0	5.0	potassium channel density
I_0 []	-2.0	-3.45	DC-input (low firing rate)
I_0 []	-0.5	-2.56	DC-input (moderate firing rate)
I_0 []	0.9	-1.45	DC-input (high firing rate)
D_{OU}	10.0^{-10}	10.0^{-10}	strength of OU signal
τ_{OU} $[ms]$	10.0	10.0	correlation time of OU signal
T [s]	30.0	30.0	simulation time
dt [ms]	0.01	0.01	time step
N	1000	1000	number of independent trials

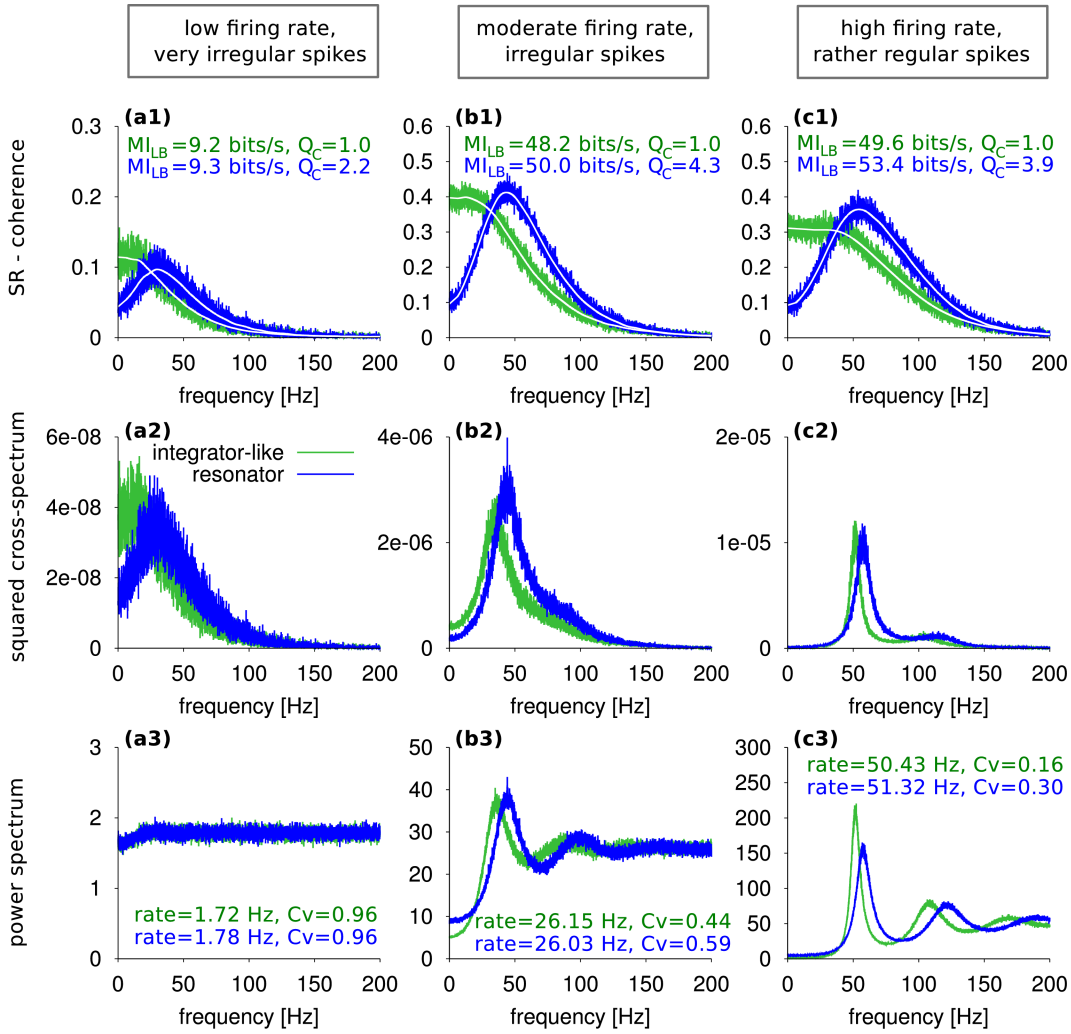

Figure 4.12: Spectral measures for the stochastic Hodgkin-Huxley neuron model for different firing regimes. Shown are spectra of two distinct parameter sets (integrator-like, shown in green and resonator, shown in blue) for low firing rate (a1-3), intermediate activity (b1-3) and high spiking activity (c1-3). Irrespective of the firing regime, the resonator parameter set exhibits always a band pass filter on information, whereas the integrator-like parameter set results in a low pass filter on information. In this continuous nonlinear neuron model, the peak in the coherence function is due to a maximum in the squared cross-sprectrum (as for example observed also in the continuous nonlinear ML model, discussed in 4.5.1). Parameter sets and numerical details can be found in Tab. 4.4.

4.6 Summary and Discussion

Here, the main findings on the effects of subthreshold resonances in conjunction with neuronal nonlinearities on the frequency-dependent signal transmission (information transmission) are summarized and discussed.

Linear voltage response versus nonlinear spiking response. The rather surprisingly finding was shown, that subthreshold resonances alone (without nonlinearities) does not lead to band-pass filtering on information about a time-dependent input signal. However, if the linear neuron model is extended with a non-linearity, either in the form of a fire-and-reset rule or as inherent nonlinear ion channel dynamics, subthreshold resonances can be 'translated' to the level of information transmission based on spiking neuronal responses. This effect is reflected in a peak of the coherence function between the current input signal (Ornstein-Uhlenbeck process) and the neuronal spiking response (spike train). The phenomenon of band-pass filtering on information was demonstrated in several nonlinear neuron models, which show different kind of nonlinearities, ranging from the simple resonate-and-fire model (see sec. 4.4.1) to more biological plausible conductance based models like the Morris-Lecar (see sec. 4.5.1) and the Hodgkin-Huxley (see sec. 4.5.2) model. The effect of band-pass filtering on information in nonlinear neuron models with subthreshold resonances is a rather robust because it does not depend on the nature of the nonlinearity.

Detailed numerical studies of the RF neuron model suggest, that the band-pass filtering effect on information (based on subthreshold resonances) is most pronounced for firing activities that are characterized by a low firing rate and very rather irregular firing activities, described by the coefficient of variation ($C_V < 0.6$). This effect can be understood by the intuition that the presence of subthreshold resonances divides the dynamics of the nonlinear neuron model in roughly two types of trajectories: i) trajectories which go directly from the reset to the threshold value (without any excursion), and ii) trajectories which 'spiral' around the fixed point. The integrator parameter set of the RF model does not show subthreshold resonances, and therefore all trajectories go directly from the reset to the threshold (minor excursion are just due to the presence of noise in the system). In contrast to the integrator parameter set, the resonating parameter set of the RF model is characterized by the fact that these two types of trajectories occur. In the regime of low baseline current, i.e. within the phasic firing regime, most of the trajectories 'spiral' around the fixed point and can be 'kicked' above the voltage threshold by a suitable signal deflection if the trajectory of the neuron model is close the voltage threshold. This effect is manifested by a potentially multimodal[8] and long-tailed ISI density in the phasic regime (see Fig. 4.5a4). The oscillation frequency of the trajectory around the fixed point is closely related to the subthreshold resonance frequency. Therefore, information transmission about the time-dependent input signal is (in this phasic regime) frequency-dependent and shows a resonance in the spectral coherence function close to the subthreshold resonance frequency. This effect of signal transmis-

[8]The density can become multimodal in the presence of very strong oscillations and weak intrinsic current noise, because the trajectory can be kicked after multiple circulations around the fixed point.

sion is diminished within the regime of tonic firing because this regime is characterized by a strong baseline current such that neither the stochastic input signal nor the intrinsic noise influences threshold crossings. This is manifested by a very sharp unimodal ISI density (see Fig. 4.5c4). Therefore, the filtering properties between integrators (without subthreshold resonances) and resonators (presence of subthreshold resonances) are described by low-pass filtering on information within the tonic firing regime.

Information filtering is a robust phenomenon. This statement is true in the sense that it requires neither a fine tuning of the correlation time of the Ornstein-Uhlenbeck process nor a fine tuning of the model intrinsic parameter (like absolute refractory period or the reset value). It was demonstrated through extensive numerical studies, that the resonance frequency of information filtering (based on the spectral SR coherence function) is closely related to the subthreshold resonance frequency. However, a one-to-one dependency between the impedance quality and the coherence quality can only be observed within a restricted firing rate regime.

The 'costs' of information filtering. The advantage of the presence of subthreshold resonances is the potential realization of a frequency-dependent signal transmission and consequently of a band pass filter on information transmission. However, this feature comes to the cost of a reduction of the mutual information rate between the signal and the spike train. Thus, the more pronounced the band pass filter on information is the less information about a time-dependent input signal is transmitted. This was shown in sec. 4.4.1 through extensive numerical studies of the RF neuron model. This trade-off between qualitative (frequency-specific) and quantitative (mutual information rate) signal transmission was demonstrated and is in line with results obtained in a complete different neuron model (see sec. 3).

Analytical approaches to resonate-and-fire neuron models. In this chapter, we discussed exclusively numerical results concerning the information filtering properties of resonate-and-fire (RF) neuron models. Analytical studies of the filtering properties of complex conductance-based neuron models (Morris-Lecar, Hodgkin-Huxley) are foredoomed to fail. However, analytical approaches for the RF neuron model were developed by Verechtchaguina et al. (2006) and Brunel et al. (2003).

In Verechtchaguina et al. (2006), an analytical approach was developed to estimate the first-passage-time of resonate-and-fire neuron models driven by Gaussian white noise using Fokker-Planck equations (FPEs). These expression can be used in connection with the renewal formula for the power spectrum: $S(f) = r_0 \frac{1-|\tilde{F}_1(f)|^2}{|1-\tilde{F}_1(f)|^2}$, which connects the spike train power spectrum ($S(f)$) to the Fourier transform of interspike interval (ISI) density ($\tilde{F}_1(f)$) in the absence of correlations. However, this approach leads only to semi-analytical results, because the expressions involved are very complicated and only in special cases in a closed form derived.

The same argument holds true for the approach developed by Brunel et al. (2003) to estimate the cross-spectrum between the input signal (Gaussian white noise) and the output spike train. Apart from the complexity of the involved expressions to estimate the power and cross spectrum, different models of resonating neurons were explored analytically by Verechtchaguina et al. (2006) and Brunel et al. (2003); Richardson et al.

(2003). Both theoretical approaches(Brunel et al., 2003; Verechtchaguina et al., 2006) were analyzed separately (not shown in this thesis).

An alternative approach to estimate the spectra of noisy oscillators analytically using FPEs can be obtained by using the so-called phase-response-curve (PRC)(Ermentrout et al., 2007; J. R. Schleimer, 2009). This approach assumes that the neuron model operates in the limit-cycle regime, i.e. the tonic firing regime. However, We have seen in this chapter that the most pronounced effects of the subthreshold resonances on the information filtering occur in the phasic regime and are attenuated in the tonic firing regime. For this reason, the effects of subthreshold resonances in single neuron models (excitable/non-excitable) were examined and discussed with the help of numerical computer simulations.

Band-pass filtering in more biological plausible neuron models. The effects of subthreshold resonances in conjunction with more biological plausible conductance-based neuron models were discussed in sec. 4.5.1 and sec. 4.5.2. The band pass filter on information becomes apparent across different neuronal activity regimes (ranging from low firing rate and very irregular spiking activity to high firing rate and rather regular spiking activity) in these conductance-based neuron models. These models allow studying the effects of biophysical realistic intrinsic neuronal noise sources like ion-channel noise, modeled with the help of Monte-Carlo-Markov-Chain methods.

I have demonstrated that the effect of band-pass filtering in conductance-based neuron models does not does not depend on the specific nature of the nonlinearity (continuous, discontinuous) but rather on the combination of subthreshold resonances with nonlinearities. Thus, this chapter highlights the importance of nonlinearities to establish a frequency-dependent signal transmission, i.e. a band-pass filtering on information.

Non-linear coding and band-pass filtering on information. The effects of subthreshold resonances in conjunction with non-linearities (continuous and discontinuous) were analyzed in this chapter utilizing the spectral stimulus-response (SR) coherence. It is known that the SR coherence can be used to construct a lower bound on the mutual information rate between an input signal and the neuronal output. This approach presumes that the neuron model linearly encodes information about a time-dependent stimulus. Here, it will be briefly discussed, how the information filtering properties of the neuron model changes, if one uses the response-response (RR) coherence function instead. Fig. 4.13 shows the numerical results for the SR and RR coherence function for the most biological plausible neuron model studied in this chapter: the Hodgkin-Huxley model with realistic stochastic ion channel noise in different firing rate regimes. As one can infer from Fig. 4.13, the filtering properties of the stochastic HH neuron model within the resonator parameter regime, i.e. in the presence of subthreshold resonances, do not change drastically in the sense that the RR coherence also describes band-pass filtering on information (similar to the SR coherence) (see Fig. 4.13a2,b2,c2). Although the qualitative changes between the SR and the RR coherence function are subtle, the SR coherence function strongly underestimates the total transmitted information rate. The same observation can be seen in the integrator-like parameter set of the stochastic HH neuron model (shown in Fig. 4.13a1,b1,c1). The discrepancy between SR and RR

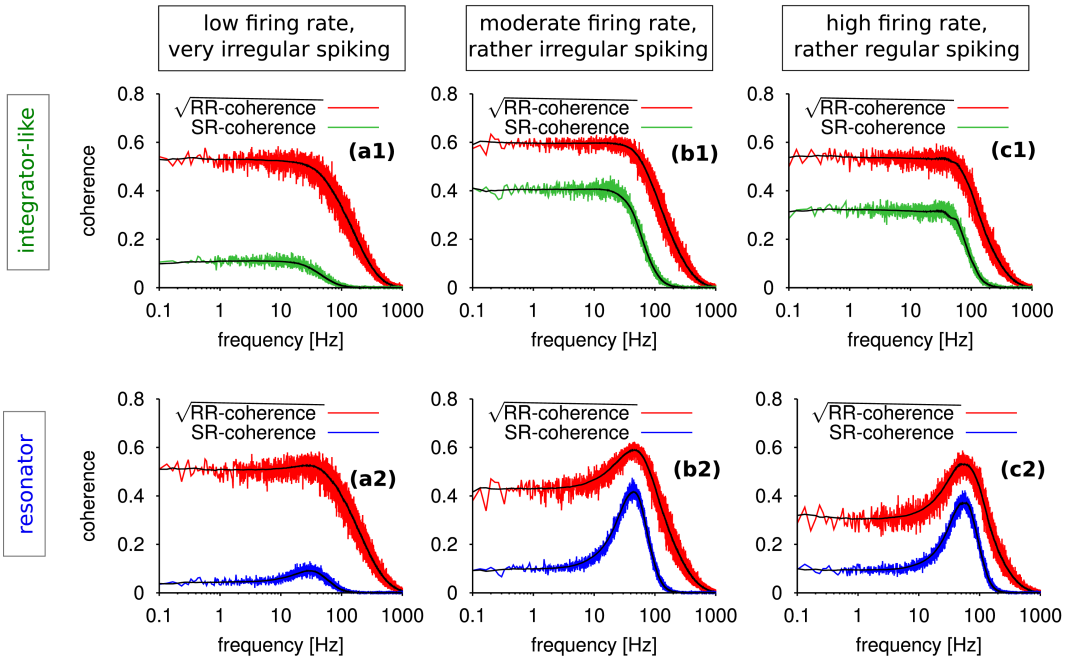

Figure 4.13: Stimulus-response versus response-response coherence function of the stochastic ion channel (MCMC) Hodgkin-Huxley neuron model. Shown are: numerical results of the HH neuron model driven by an Ornstein-Uhlenbeck current input signal in different firing rate regimes (controlled by the baseline current) for two model parameter sets (integrator-like, resonator): at low firing rates of $r \approx 1.7$ Hz and $C_V \approx 1.0$ (a1,a2), at moderate firing rates of $r \approx 26$ Hz and $C_V \approx 0.5$ (b1,b2), and at high firing rates of $r \approx 50$ Hz and $C_V \approx 0.25$. The RR coherence function (shown in red) describes a weaker band pass filter on information based on the coherence quality factor compared to the spectral SR coherence (shown in blue and green). The solid black lines represent the smooth versions of the spectra to calculate information theoretic measures (the quality of the coherence, the resonance frequency of coherence, the mutual information rate) reliably. The parameter sets and numerical details can be found in Tab. 4.4. 200 independent signal realizations and 50 independent intrinsic noise realizations to estimate the RR coherence function numerically were used.

coherence becomes smaller in the regime of very high and very regular firing activity (compare Fig. 4.13a1, b1, and c1, c2). This convergence between SR and RR coherence is expected because the linear coding assumption becomes justified in the tonic firing regime. Thus, my numerical results (shown in Fig. 4.13) suggest that subthreshold resonances in conjunction with non-linearities can lead to band-pass filtering on information in both: i) linear and ii) non-linear coding regimes.

The numerical results, presented in the chapter, are in line with previous numerical results on integrator neuron models (see sec. 2) for the integrator parameter set of all three analyzed neuron models (resonate-and-fire, Morris-Lecar, and Hodgkin-Huxley

with stochastic ion channel dynamics). Integrator neuron models preferentially encode information about slow components of a time-dependent input signal, whereas the presence of subthreshold resonances leads to band-pass filtering on information. This effect can be observed in both spectral measures: i) the stimulus-response coherence function, and ii) the response-response coherence function. Thus, subthreshold resonances are a model-intrinsic theoretical mechanism, besides ISI correlations (see sec. 3), which lead to frequency-dependent information transmission about a time-dependent current input signal with the help of nonlinear neuronal responses, i.e. output spike trains.

5 Information filtering in linear-nonlinear cascades

Abstract | The roles of a special kind of continuous nonlinearities: static nonlinearities and their effects on the signal transmission characteristics are explored in this chapter. Here, different forms of static nonlinearities: a) exponential, b) hard-threshold, and c) soft threshold (sigmoidal) are used to investigate so-called linear-nonlinear neuron models and their filtering characteristics numerically as well as analytically. This study completes the survey of information filtering effects based on neuronal nonlinearities.

5.1 Introduction

We have seen in the previous chapters that nonlinearities in the form of a fire-and-reset rules (see sec. 4.4.1) as well as in the shape of continuous neuronal spike mechanisms (see sec. 4.5) can 'transfer' subthreshold frequency selectivity on power (measured by the impedance function) to the level of spiking information transmission. The disadvantage of using either fire-and-reset or more complicated neuron models (Morris-Lecar or Hodgkin-Huxley) is that these neuron models cannot be investigated analytically.

Here, a third nonlinear neuron model and its information filtering characteristics will be explored using numerical simulation and with the help of analytical expressions for the power and cross spectrum. We will use an approximate classifier, the curvature of the coherence function, to distinguish between low pass and band/high pass filter on information.

The concept of the static nonlinearity (SNL) involves a passive transformation of the response $x(t)$ of the linear model (without fire-and-reset rule) via a distortion function $z(t) = g(x(t))$ (see Fig. 5.1). A suitable distortion of the membrane potential of the linear system that captures the upstroke of a spike is an exponential distortion function of the following form:

$$z(t) = e^{\gamma(x(t)-\mu)}. \tag{5.1}$$

This results in a suppression of values $x(t) < \mu$ and a positive distortion (action potential

like) for values $x(t) > \mu$. Thus, the parameter μ acts like a 'threshold'. Here γ models the speed of the spike upstroke and μ measures the 'threshold' at which 'spikes' (pulsatile distortions) are initiated.

Although very simple, the exponential static nonlinearity does not respect the finite response of a neuron. Therefore, sigmoidal functions are often used in order to model a rapid firing rate onset as well as the limitedness of the firing rate (see Fig. 5.1). In

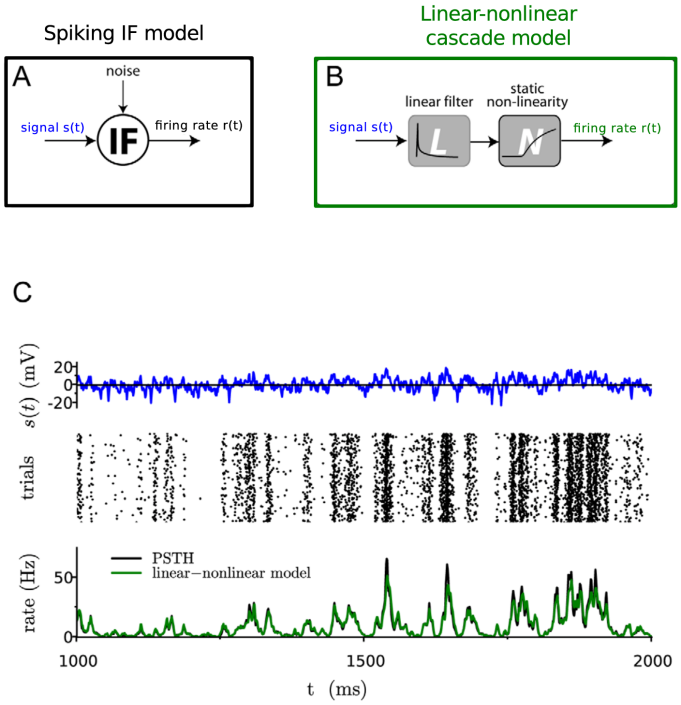

Figure 5.1: Linear-nonlinear neuron models can successfully describe output statistics of spiking IF models. Schematic view of the spiking IF neuron model (A) in comparison to the linear-nonlinear (NL) cascade model (B). Using a proper static non-linearity (SNL), one can match the time-dependent output firing rate (C) of the IF (black curve) to the output of the LN cascade (green curve). Figure adopted and modified from Ostojic and Brunel (2011).

Fig. 5.1A the general dynamics of a spiking neuron model is shown. The input signal $s(t)$ influences the dynamics of the spiking neuron model and thus, by employing a discontinuous or continuous nonlinearity, its spiking response (see raster plot in the middle of Fig. 5.1C). Linear-Nonlinear (LN) neuron models are used to model the firing rate (rate models) instead of modeling the subthreshold or spiking neuronal dynamics in detail. LN cascade models are purely phenomenological models.

The basic concept of a LN cascade model is shown in Fig. 5.1B. An input signal enters a linear neuron model (for example the resonate-and-fire model without a threshold, see sec. 4). A subsequent SNL is then used to distort the output of the linear (L) component

of the LN cascade. The utilization of a SNL 'translates' the linear subthreshold dynamics (L) to a firing statistics: the instantaneous firing rate (shown in Fig. 5.1C). LN cascade models can be used to reproduce to high precision the spiking behavior(Ostojic and Brunel, 2011).

Here, four different SNLs are used to study the information filtering characteristics of the LN cascade model (Fig. 5.1B) for different subthreshold dynamics, i.e. in the presence or absence of subthreshold resonances (see sec. 4.3).

5.1.1 Example static nonlinearities

In the following we will study four different static nonlinearities:
the **identity SNL** (for reasons of consistency check) given by:

$$z_1(t) = g_0(x(t)) = x(t), \tag{5.2}$$

the **exponential SNL** given by:

$$z_2(t) = g_1(x(t)) = e^{\gamma(x(t)-\mu)}, \tag{5.3}$$

and the **erf-sigmoidal SNL** of the form:

$$z_3(t) = g_3(x(t)) = \frac{\left(1 + \mathrm{erf}\left(\frac{\gamma}{\sqrt{2}}\left(x(t) - \mu\right)\right)\right)}{2}, \tag{5.4}$$

as well as the **Heaviside SNL** written as:

$$z_4(t) = g_4(x(t)) = \Theta\left(x(t) - \mu\right). \tag{5.5}$$

The parameter γ determines in the first two cases how 'strong' the static nonlinearity distorts the output of undistorted Gaussian process $x(t)$ (see sec. 5.1.2 for a more refined notion of 'strenght' of a static nonlinearity).

Of course, the identity SNL is used to validate analytical results. The Heaviside SNL (Eq.(5.5)) can be regarded as the limit: $\gamma \to \infty$ of the error-function-sigmoidal (erf-sigmoidal SNL, see Eq.(5.4)). The influence of the SNL on the 'firing rate', or put differently the response of the LN cascade, is determined by its location μ and its slope-factor γ. In the next section, we will develop a measure of 'nonlinearity', i.e. a measure of the 'strength' of the LN cascade. Throughout this chapter, it is assumed that the linear output is a stochastic Gaussian process.

5.1.2 A measure of 'nonlinearity'

The 'strength' of the 'nonlinearity' of the LN-cascade model depends on: **i)** the location of the SNL with respect to the mean value of the linear system (L), and **ii)** the slope factor of the SNL. A measure ($\Gamma_{\mathrm{g(V)}}$) that respects both influences can be given by:

$$\Gamma_{\mathrm{F(V)}} = \int_{-\infty}^{+\infty} \frac{e^{-\frac{V^2}{2\sigma^2}}}{\sqrt{2\pi}\sigma} g'^2(\gamma;\mu,V)dV - \left(\int_{-\infty}^{+\infty} \frac{e^{-\frac{V^2}{2\sigma^2}}}{\sqrt{2\pi}\sigma} g'(\gamma;\mu,V)dV \right)^2, \tag{5.6}$$

where for simplicity we assume that the linear output has zero mean value, i.e. $< V >= V_{\mathrm{FP}} = 0$. As pointed out earlier, the effect of a static nonlinearity depends solely on the relative distance between the mean value of the linear output and the offset (μ) of the static nonlinearity, and thus a non-zero mean value can be absorbed in the offset parameter μ of the SNL.

We note that the distribution of local slope values of the nonlinearity sampled by the voltage distribution, $g'(V,\gamma,\mu) = \frac{\partial}{\partial V} g(V,\gamma,\mu)$, is indicative of the amount of nonlinearity Eq.(5.6). If the variance of this distribution of local slopes is very small, then the transformation is nearly linear (including also a constant transformation), whereas if the variance of the slope distribution is very large, then the transformation is strongly nonlinear.

In the following, we will calculate analytically $\Gamma_{\mathrm{g(V)}}$ for the different SNLs (see Eq.(5.2)–Eq.(5.5)).

The **identity function** as a static nonlinearity leads to a nonlinearity measure Γ according to Eq.(5.6) of the following form

$$\Gamma_{\mathrm{linear}} = 0. \tag{5.7}$$

Using a **exponential function** SNL results in a nonlinearity measure Γ:

$$\Gamma_{\mathrm{exp}} = \gamma^2 \left(e^{\gamma^2\sigma^2} - 1 \right) e^{\gamma(\gamma\sigma^2 - 2\mu)}. \tag{5.8}$$

The application of an **erf-sigmoidal** SNL results in a nonlinearity measure of the form:

$$\Gamma_{\mathrm{erf}} = \frac{\gamma^2}{2\pi} \left(\frac{e^{-\frac{\gamma^2\mu^2}{2\gamma^2\sigma^2+1}}}{\sqrt{2\gamma^2\sigma^2+1}} - \frac{e^{-\frac{\gamma^2\mu^2}{\gamma^2\sigma^2+1}}}{\gamma^2\sigma^2+1} \right). \tag{5.9}$$

and is illustrated in Fig. 5.2 for various combinations of slope factor γ and offset μ.

The **Heaviside sigmoidal** as a static nonlinearity leads to a nonlinearity measure Γ of the following form

$$\Gamma_{\mathrm{Heaviside}} = \lim_{\gamma\to\infty} \Gamma_{\mathrm{erf}} = \infty. \tag{5.10}$$

The two extreme cases: i) the linear SNL, and the ii) Heaviside SNL justifies the notation of a 'nonlinearity' measure. For the linear SNL, the nonlinearity measure attains its minimal value (zero), whereas for a very strong 'distortion' of the linear output by using a Heaviside SNL is reflected in an infinite amount of 'nonlinearity'. Thus,the nonlinearity measure Eq.(5.6) indeed captures the nonlinear nature of the static nonlinearity and therefore measures the nonlinearity of the LN cascade. A value close to zero can be interpreted as a rather linear transformation of the Gaussian output, whereas a large value ($\Gamma >> 1$) indicates a more nonlinear transformation. In Fig. 5.2, the nonlinearity

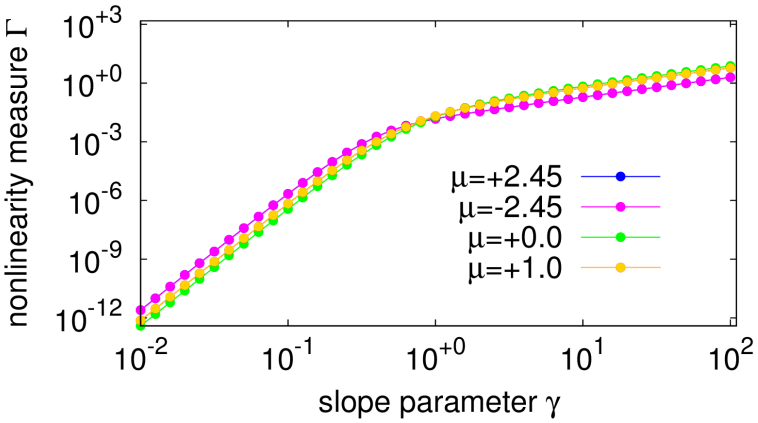

Figure 5.2: The nonlinearity measure of the erf-sigmoidal SNL as a function of the slope parameter γ. Shown for four different offsets μ for the resonator cartoon parameter set without threshold (model parameters are stated in Tab. C.1).

measure for the erf-sigmoidal distortion function is shown. Different offset values, or put differently different mean values of the stochastic Gaussian process (L), are used to show their impact on the nonlinearity measure (Eq.(5.9)). The resonator cartoon parameter set of the resonate-and-fire neuron model (without a threshold, see sec. 4) was used to evaluate (Eq.(5.9)). The offset of the SNL was varied in the region of the threshold of the resonate-and-fire model. One can infer from Fig. 5.2 that the nonlinearity measure Γ is very sensitive to the slope parameter of the SNL. For very small slope parameter values, the SNL can be well approximated by a linear function and consequently, its nonlinearity measure approaches zero. In contrast, in the limit of a hard threshold (Heaviside SNL), i.e. at very large values of slope factors, the nonlinearity measure diverges. One can draw the second conclusion from Fig. 5.2: the nonlinearity measure of the erf-sigmoidal is a monotonically increasing function for increasing slope factors (γ).

In the next section, we will explore the effects of the erf-sigmoidal SNL as a proxy of 'realistic' SNLs (limited LN cascade output, i.e. firing rate) by using the linear resonator neuron model (see sec. 4.2.1), i.e. the resonate-and-fire without a threshold and reset). We will call this model: resonator-LN-cascade model. This numerical study will motivate the subsequent analytical investigation (see sec. 5.3) on so-called integrator-LN-cascade

models, based on subthreshold leaky integrate-and-fire models.

5.2 Numerical results for resonator neurons

In sec. 4.4.1 we have learned that the discontinuous fire-and-reset rule leads to a very nonlinear response of the neuron model, which resulted in a different information transmission characteristics in the presence of subthreshold resonances, i.e. a band-pass filter on information (measured by the coherence function) nearby the resonance frequency (peak position of the impedance function by stimulating the neuron model with a ZAP-current). Thus, this discontinuous nonlinearity allowed the neuron model to 'pass on' a frequency selectivity within the subthreshold response (continuous membrane voltage response) to frequency selectivity of information of the suprathreshold response (discontinuous spike train). The emergence of a band-pass filter on information for resonant neurons was also true for a continuous nonlinearity in the form of a biophysical spike mechanism described in conductance-based neuron models (see sec. 4.5).

Here, we will investigate a different kind of nonlinearity: continuous static nonlinearities (SNL). The term "static" refers to the fact that it just depends explicitly on the input (linear model) values and *not* on time. The concept of static nonlinearities (SNL) involves the transformation of the response of the linear neuron model Eq.(4.1a) and Eq.(4.1b) (without any threshold) with a suitable function that depends on the value of the response (see Fig. 5.3).

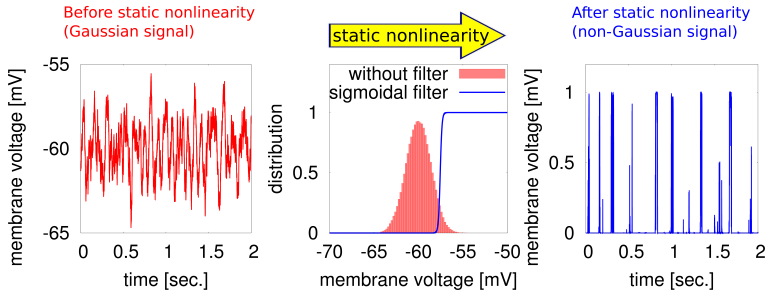

Figure 5.3: Sketch of the action a sigmoidal static nonlinearity. An erf-sigmoidal SNL is used with a slope factor $\gamma = 100.0$ and offset $\mu = 2.45$ mV, which is the distance between voltage fixed point V_{FP} and the threshold V_{thresh} of the resonator cartoon parameter set of the resonate-and-fire model (see Tab. C.1), on the membrane voltage trace.

This soft-threshold, i.e. the erf-sigmoidal SNL takes into account that the distorted neuronal response (firing rate) is limited. Here, we use specifically a sigmoidal SNL in terms of the error-function, i.e. the erf-sigmoidal SNL given in Eq.(5.4). In addition we will compare the results of the sigmoidal SNL with a Heaviside step function $F(V) = \Theta(V(t) - \mu)$ centered around $V = \mu$, which corresponds to the limit $\gamma \to \infty$ in Eq.(5.4).

Fig. 5.4 shows example distributions before (Fig. 5.4a,b,c) and after (Fig. 5.4d,e,f) the erf-sigmoidal SNL. The output of the erf-sigmoidal-LN-cascade is always non-Gaussian, due to the non-linear transformation by the SNL. In Fig. 5.5 we show example spectra for

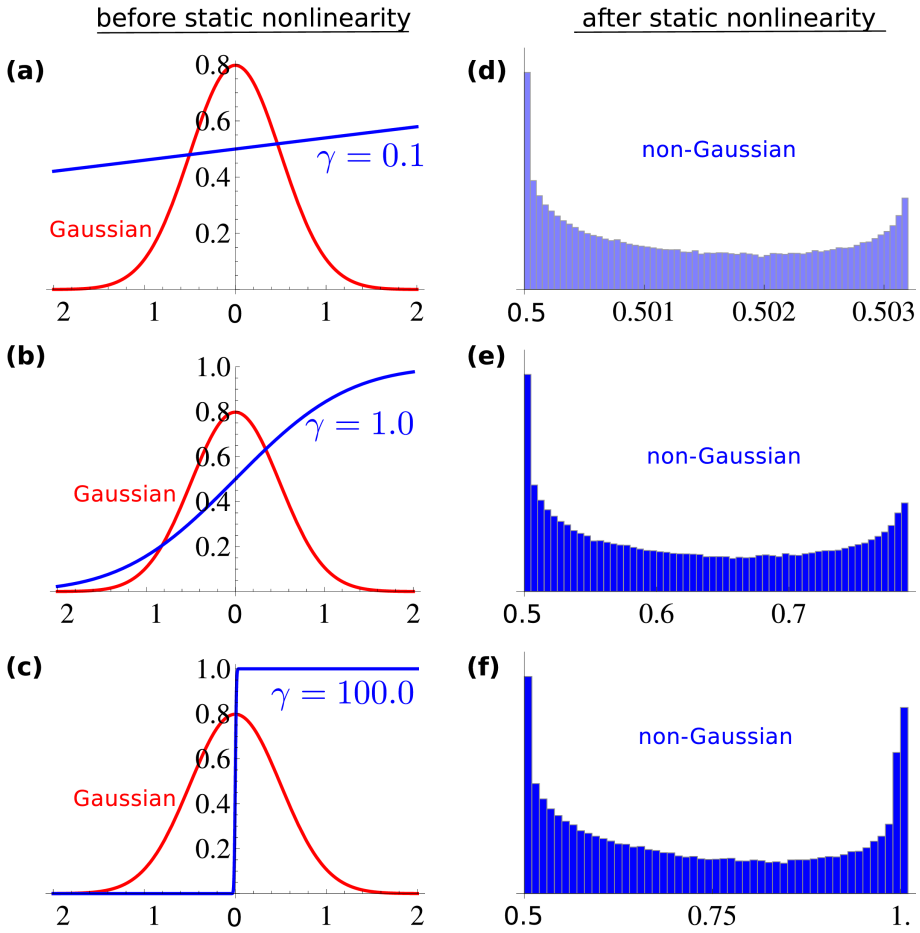

Figure 5.4: Output distribution of an erf-sigmoidal-LN cascade. Shown are: the Gaussian probability distributions of a linear system with zero mean and variance $\sigma_x = 0.5$ (red line in a,b,c), the static nonlinearities corresponding to $\gamma \in \{0.1, 1, 100\}$ (blue line in a,b,c), and the corresponding distribution out outputs after the SNL, i.e. outputs of the LN-cascade (blue line in d,e,f). 500.000 samples from a Gaussian distribution were used to obtain the distribution of outputs after the SNL.

the resonating neuron model (described by Eq.(4.1a) and Eq.(4.1b)) using the parameter sets listed in Tab. C.1 by using the sigmoidal SNL.

Fig. 5.5 (blue curve in a1–a3) displays the coherence function between the distorted output (by using an erf-sigmoidal SNL according to Eq.(5.4) with parameters $\mu = +2.45$ and $\gamma = 100.0$) and the input signal (OU-process with parameters given in Tab. C.1) for the **resonator cartoon** parameter set (see Tab. C.1). One can see that the coherence function exhibits a peak (Fig. 5.5a1,b1) nearby the resonance frequency of the linear

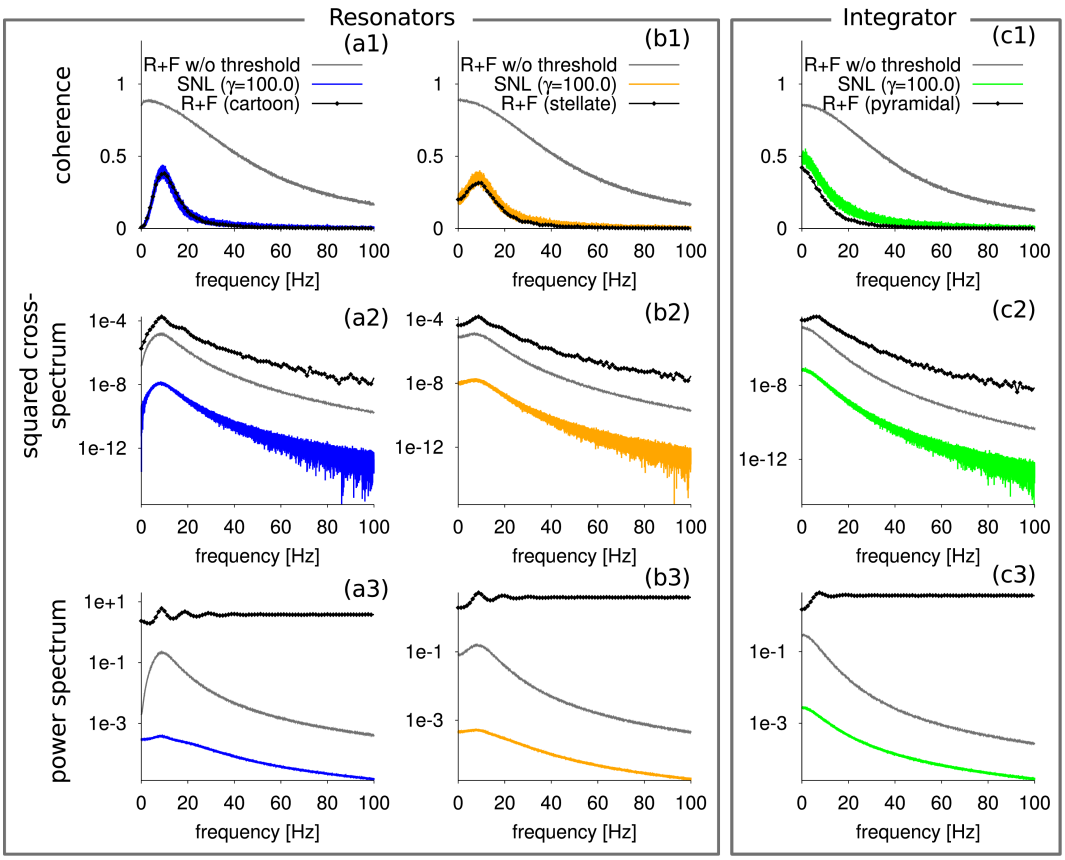

Figure 5.5: Example spectra of the resonator-LN-cascade neuron model for resonator cartoon parameter set (blue line, a1–a3), the stellate cell (orange line in b1–b3) and the pyramidal cell (green line in c1–c3). Coherence function (a1,b1,c1), squared cross spectrum (a2,b2,c2) and the power spectrum (a3,b3,c3) are compared with the spectra of the purely subthreshold response (resonate-and-fire without threshold) (shown in grey) and the spiking resonate-and-fire (R+F) neuron model at the same parameter sets (given in Tab. C.1). Here we have used an erf-sigmoid static nonlinearity (Eq.(5.4)) with a $\gamma = 100$ and $\mu = 2.45$ in order to obtain a reasonable 'degree' of nonlinearity.

system (Eq.(4.1a) and Eq.(4.1b)). For reasons of comparison, also shown are: i) the respective coherence function between the linear membrane potential output $V(t)$ and the input signal (grey curve in Fig. 5.5), and ii) the coherence function between the spiking resonate-and-fire neuron model and the input signal (black curve in Fig. 5.5). The specific choice of the erf-sigmoidal SNL parameter (μ and γ) leads to very similar coherence functions for the resonate-and-fire neuron model and the LN-cascade model.

Thus, Fig. 5.5 implies that the application of a suitable SNL (here a soft threshold) can lead to a band-pass filtering on information very similar to results obtained for the nonlinear spiking resonate-and-fire model.

Is this similarity between the two model systems (resonator-LN-cascade and resonate-and-fire) coincidental, or is this a general feature of the resonator-LN-cascade model? We will answer this question by means of a numerical exploration of the filtering effects of the chosen model.

5.2.1 Coherence shape and information rate depend on the nonlinearity

In Fig. 5.5 numerical evidences were shown that the utilization of an erf-sigmoidal static nonlinearity (Eq.(5.4)) could lead to band-pass filtering effects on information similar to the response of the spiking resonate-and-fire neuron model. In this section, we will investigate the effects of the erf-sigmoidal SNL parameter μ and γ on the i) quality of the band pass filter on information and ii) the lower bound of the mutual information rate. Before presenting the numerical results for the resonator-cartoon parameter set, we will briefly establish an intuition of the impact of both parameters, i.e. μ and γ.

First, if the inflection point μ of the erf-sigmoidal SNL is far away from the mean value of the linear membrane voltage trace $V(t)$ (here it was set to zero), then the distorted output will be almost constant and close zero. Consequently, the linear system would not 'feel' the nonlinearity of the SNL and the LN-cascade would almost act as a linear transformation of the membrane voltage trace $V(t)$, and thus would not change the frequency modulation of the power and cross-spectrum of the linear output $V(t)$. This would lead to a coherence function of the LN-cascade very similar to the coherence function of the linear model. In our case (see Eq.(4.27)), the linear model acts as a low pass filter on information.

Second, if the SNL is not very steep ($\gamma \approx 0$) then the effect of the SNL would also be well approximated by using a linear transformation (in the case of the erf-sigmoidal, see Eq.(5.4), this linear transformation will become a constant, i.e. 0.5, see Fig. 5.4a,d and Eq.(5.5)). The effect would be similar to the application of a linear static linearity. Thus, the same argument that was presented above holds true in this case: coherence function of the LN-cascade is very similar to the coherence of the linear system, i.e. in our case a low-pass filter on information.

In Fig. 5.6 the numerical results of the purely subthreshold response of the resonator-LN-cascade (erf-sigmoidal SNL and Heaviside-limit-SNL) with different slope factors γ as well as different offset values of the static nonlinearity (inflection point of the sigmoidal SNL) are shown. Fig. 5.6a displays the functional relation between the coherence quality of the resonator-LN-cascade and the offset of the erf-sigmoidal SNL. As mentioned above, if the sigmoidal is very linear ($\gamma << 1$) (within one SD (standard deviation) of the linear Gaussian stochastic system), then the quality factor of the coherence function is independent of the location of the SNL (see magenta data points in Fig. 5.6a). This is plausible because the output of the erf-sigmoidal-SNL becomes a constant in this limit and does not dependent on the value of the input, i.e. $V(t)$. If the SNL becomes very nonlinear in the vicinity of the mean value of the subthreshold membrane voltage $V(t)$ (see Fig. 5.4b,c), then the emergence of a band pass filter on information, i.e. a peak in the coherence function and thus a quality factor of the coherence function above one, can be observed (see orange, green and blue data sets in Fig. 5.6a).

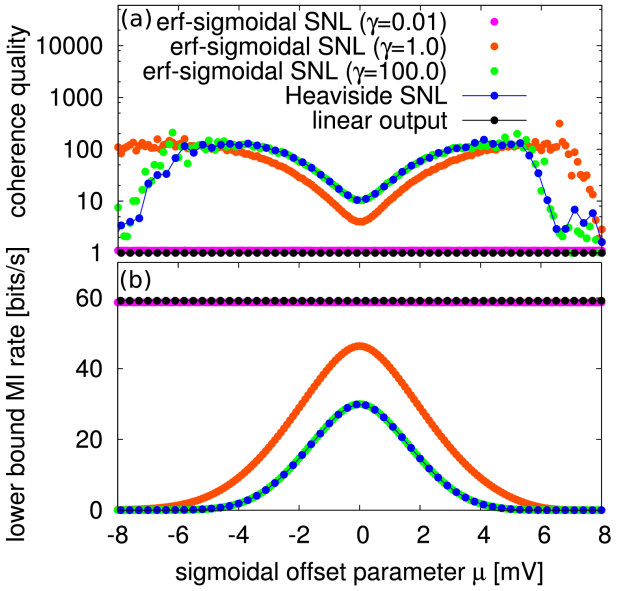

Figure 5.6: Variation of the sigmoidal offset-parameter μ of the erf-sigmoidal static nonlinearity for three different slope parameters $\gamma \in \{0.01, 1, 100\}$. Shown are the quality of the coherence function (a), and the lower bound of the mutual information rate (b) as functions of the sigmoidal offset value μ for the erf-sigmoidal SNL, the Heaviside SNL.

If the erf-sigmoidal SNL is very steep ($\gamma >> 10$) and is far away from the mean value ($\mu >> 1$) of the subthreshold Gaussian membrane potential distribution, then the effect of the nonlinearity is diminished and vanishes finally. The symmetry between negative and positive SNL-offsets are due to the symmetric probability distribution of the linear stochastic membrane voltage system (linear resonator neuron model), i.e. a Gaussian centered at zero.

Additionally, Fig. 5.6b shows the dependency of the lower bound of the mutual information rate (Eq.(1.12)) of the resonator-LN-cascade model with respect to the location of the sigmoidal SNL at different slope factors γ. The highest information transmission has the almost linear resonator-LN-cascade model (see magenta data point Fig. 5.6b), which is (of course) very similar to the mutual information rate of the linear resonator model (see black data points in Fig. 5.6b). For moderate and high slope factors of the SNL, the mutual information rate of the resonator-LN-cascade model attains its maximal value at offsets, which corresponds to the mean value of the purely subthreshold membrane potential $V(t)$, i.e. the maximum of the subthreshold Gaussian membrane potential distribution (see Fig. 5.6b). Again, the symmetric structure of the dependency of the lower bound of the mutual information rate with respect to the offset parameter μ can be understood by noticing that the distribution of membrane voltages of the linear system (linear resonator model) is symmetric with respect to its mean value, here zero.

Thus, we can conclude that the offset of the erf-sigmoidal-SNL plays a vital role in establishing a band pass filter on information of the resonator-LN-cascade model. The similarity between the coherence functions of the spiking resonate-and-fire neuron model and the resonator-LN-cascade, depicted in Fig. 5.5a1,b1,c1 is not a robust phenomenon, because of the sensitivity of the coherence function of the LN-cascade model with respect to the offset of the erf-sigmoidal-SNL (see Fig. 5.6a,b.

5.2.2 Subjecting voltage values to different degrees of nonlinearities

Fig. 5.5a1–c1 showed the remarkable similarity between the coherence function of the linear resonator neuron model and the resonator-LN-model (using an erf-sigmoidal SNL). Although their underlying nonlinearity (fire-and-reset rule and sigmoidal distortion) is very different, reflected by the observation that the power and cross spectra are very different from each other (see Fig. 5.5a2–c2 and Fig. 5.5a3–c3). We have seen in sec. 5.2.1 that the information theoretical meta statistics, reflecting qualitative (coherence quality) and quantitative (lower bound of mutual information) signal transmission, is very sensitive to variations of the offset μ of the erf-sigmoidal SNL. Here, we want to explore the effects of the slope factor γ of the SNL on the signal transmission characteristics of the resonator-LN-cascade model.

As demonstrated in Fig. 5.7, for low slope factors γ of the sigmoidal SNL, the information transmission properties of the resonator-LN-cascade are similar to the linear resonator neuron model (see Fig. 5.7a1-c1). This similarity holds true for all three parameter sets (resonator cartoon Fig. 5.7a1, stellate cell Fig. 5.7b1 and pyramidal cell Fig. 5.7c1), and was discussed above.

Upon increasing the slope of the sigmoidal SNL, the effect of the nonlinearity components of the sigmoidal SNL will become stronger. Consequently, the spectra of the resonator-LN-cascade model differ from the spectra of the purely subthreshold response. Thus, the sigmoidal SNL shapes the power spectrum (seen in Fig. 5.7c1-c3) and the squared cross spectrum (seen in Fig. 5.7b1-b3) in a non-trivial way for all parameter sets, such that the coherence function of the resonator-LN-cascade model displays a peak (see Fig. 5.7a1,b1).

One can observe the general phenomenon that the peak in the power spectrum of the distorted output is diminished upon increasing the slope factor γ of the sigmoidal SNL (see Fig. 5.7a3,b3). In contrast to the power spectrum of the resonator-LN-cascade model, the shaping of the squared cross-spectrum between the input signal (OU-process) and the output of the resonator-LN-cascade is not observable. The squared cross-spectrum changes with an overall (for all frequencies) factor. Thus, the shaping of the coherence function, by changing the slope factor γ of the erf-sigmoidal SNL, is solely due to the shaping of the power spectrum by the static nonlinearity.

For non-resonating parameter sets like the pyramidal cell (see Tab. C.1), power (see Fig. 5.7c2) and cross-spectrum (see Fig. 5.7c3) do not exhibit any peaks and consequently, the coherence function is a decreasing function with increasing frequency, i.e. the hallmark of a low pass filter on information (see Fig. 5.7c1-c3).

Thus, we can conclude here, that the phenomenon of band-pass filtering on information

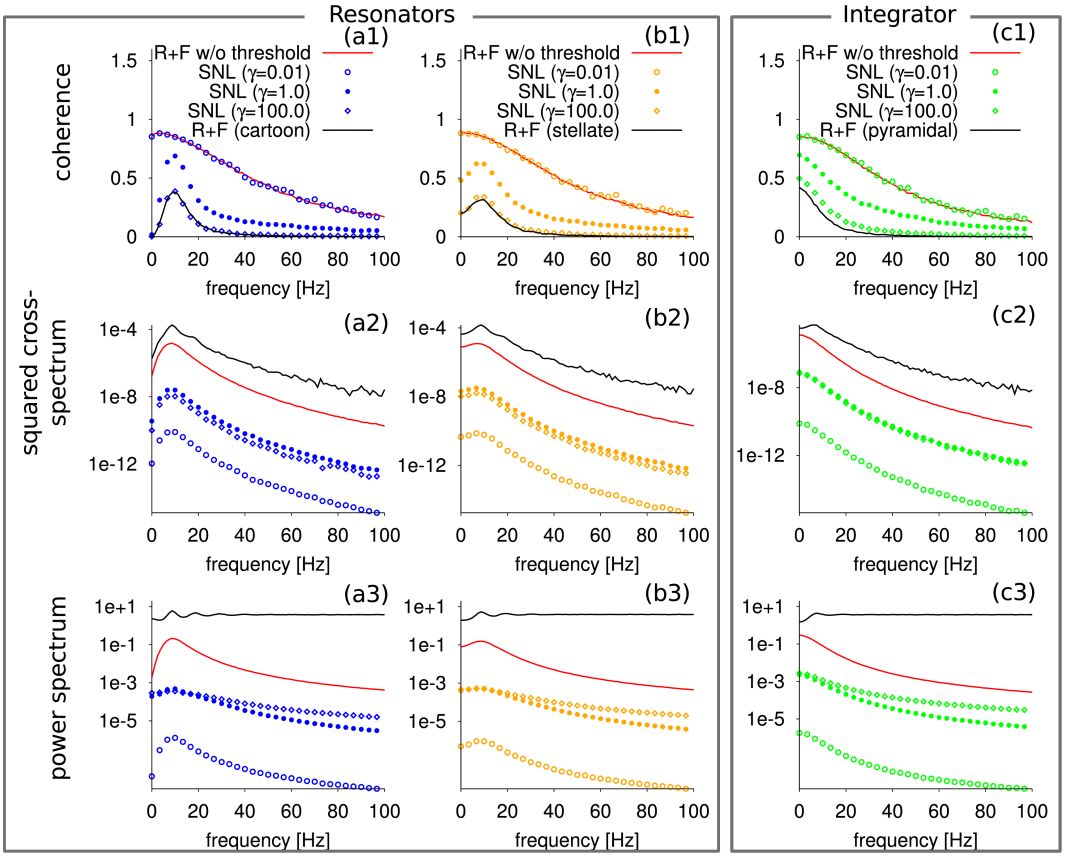

Figure 5.7: Spectral measures for the resonator neuron model subjected to a different sigmoidal static nonlinearity ($\gamma \in \{0.01, 1, 10.0\}$ and $\mu = 2.45$). Shown are coherence function (a1,b1,c1), squared cross spectrum (a2,b2,c2), and the power spectrum (a3,b3,c3) for the resonator cartoon parameter set (blue line), the stellate cell (orange line) and the pyramidal cell (green line). Coherence functions of the spiking RF model (red solid line) as well as the linear resonator model (without threshold) are shown.

in the resonator-LN-cascade model is robust under variations of the slop factor, i.e. the 'nonlinearity', of the erf-sigmoidal SNL. The center-frequency, at which the coherence function attains its maximum, does not change drastically under variations of the slope factor γ (see for example Fig. 5.7a1) and is close to the frequency of the subthreshold resonance of the linear system. The numerical results suggest that if the distortion of the linear system is strong enough (large slope factor γ, for example), then the resonator-LN-cascade model can act as a band pass filter on information very similar to the resonate-and-fire neuron model, i.e. in the presence of a discontinuous nonlinearity.

What does the term 'distortion is large enough' mean? The intuition considered at the beginning of the section leads to a measure of nonlinearity that captures the 'effective'

nonlinearity which takes the subthreshold dynamics into account. Using this measure (as described in sec. 5.1.2) for a fixed offset value μ of the sigmoidal SNL and different slope factors γ, leads to different values of nonlinearity Γ. Here, Γ is a monotonically increasing function of γ. The spectra shown in Fig. 5.7a1–c1 suggest that high nonlinearity values Γ lead to high coherence qualities.

Additionally, we have seen in Fig. 5.7a1–c1 that the coherence function of the resonate-LN-cascade model converges almost to the coherence function of the resonate-and-fire model (for high values of the slope factor γ and appropriate choice of μ). Thus, the coherence quality of the distorted output should be a sigmoidal-shaped function with respect to the nonlinearity measure Γ.

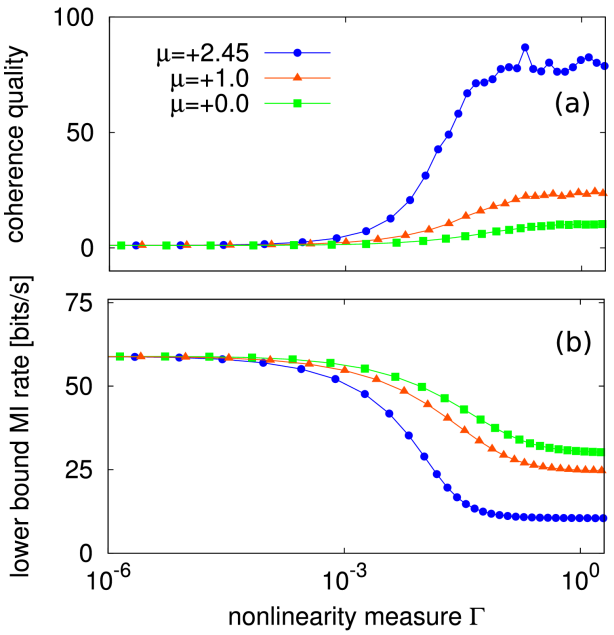

Figure 5.8: Information characteristics with respect to SNL nonlinearity measure. Shown are the coherence quality (a) and the mutual information rate (b) of the resonate-LN-cascade model as functions of the effective nonlinearity Γ for the resonator cartoon parameter set (see Tab. C.1). Values of Γ depend on the slope factor γ of the erf-sigmoidal-SNL. For each curve, the offset μ was fixed (see legend), but γ – and consequently the effective nonlinearity – was varied. The coherence quality (a) increases monotonically with nonlinearity and saturates at a value which depends on the offset μ. Conversely, the lower bound mutual information rate (b) decreases.

In Fig. 5.8a the coherence function of the resonator-LN-cascade model is shown with respect to the nonlinearity measure of the sigmoidal SNL (using different offset values μ of the sigmoidal SNL) for the resonator cartoon parameter set (see Tab. C.1).

Fig. 5.8a shows clearly the anticipated S-shaped dependency between coherence quality (Q_C) and nonlinearity measure of the sigmoidal SNL (Γ). Fig. 5.8a suggests that

higher offset values lead to larger coherence qualities and thus to more pronounced band pass filter on information of the resonator-LN-cascade model (within resonating parameter sets). A tendency, which we have observed already in the spiking spiking resonate-and-fire neuron model (see Fig. 4.10), is also visible here: higher Q-values of the coherence function imply smaller values of the lower bound of the mutual information rate. Therefore, the resonate-LN-cascade model exhibits a trade-off between qualitative (band pass filter) and quantitative (lower bound of mutual information rate) signal transmission. This trade-off phenomenon was demonstrated in spiking neuron models with continuous (sec. 4.5) and discontinuous (sec. 4.4.1) nonlinearities as well as in the perfect-integrate-and-fire neuron model, equipped with positive ISI correlations (sec. 3.5.4).

Because LN-cascade models connect phenomenologically subthreshold membrane dynamics to firing rates, a band-pass filtering effect in resonate-LN-cascade models corresponds to a band pass filter based on the firing rate, i.e. rate coding. This information filtering based on the firing rate is of vital biological importance for information filtering in feed-forward networks, because neurons 'communicate' via transmitter release. The amount of transmitter release depends among other things on the firing rate of the pre-synaptic neuron.

Having explored numerically the interesting effects of static nonlinearities on the information filtering characteristics of the neuron model, we next turn to an analytic approach for the power and cross-spectrum of the LN-cascade models. This culminates in exact expressions for the spectral measures of an integrator-LN-model.

5.3 Theoretical approaches

If one assumes (for sake of simplicity) that both stochastic Gaussian processes $x(t), y(t)$ has zero mean and unit variance, then the auto- and cross-correlation between the distorted output (by using the distortion function $z(t) = g(x(t))$) and the signal $s(t)$ can be written as(Bussgang, 1952):

$$r_{\mathrm{z,z}}(\tau) = \frac{1}{2\pi\sqrt{1-r^2}} \int_{-\infty}^{+\infty}\int_{-\infty}^{+\infty} g(x)g(y)e^{-\frac{x^2+y^2-2rxy}{2(1-r^2)}}dxdy, \tag{5.11a}$$

$$r_{\mathrm{z,s}}(\tau) = \left(\frac{1}{\sqrt{2\pi}}\int_{-\infty}^{+\infty} xg(x)e^{-\frac{x^2}{2}}dx\right) r_{\mathrm{x,s}}(\tau), \tag{5.11b}$$

where $r = r_{\mathrm{x,x}}(\tau)$ denotes the normalized auto correlation before the static nonlinearity $g(x)$. A simple calculation shows that the effect of the static nonlinearity $g(x)$ on the cross-correlation between the distorted output $z(t)$ and the current input signal $s(t)$ is given by a constant factor, which depends **solely** on the form of the static nonlinearity (Bussgang, 1952) and is not **not** shaped by the static nonlinearity. This phenomenon is regarded as the 'Bussgang-theorem'(Bussgang, 1952). The interested reader might be

referred to sec. D.2, where general expressions for the cross-correlation between current signal and distorted output are stated.

The normalized auto correlation of the distorted output $z(t) = g(x(t))$ then takes the form:

$$r_{\mathrm{z,z}}(\tau) = \frac{1}{2\pi\sqrt{1-r^2}} \int_{-\infty}^{+\infty}\int_{-\infty}^{+\infty} g(x)g(y)e^{-\frac{x^2+y^2-2rxy-2(1-r)\mu_{\mathrm{x}}(x+y-\mu_{\mathrm{x}})}{2(1-r^2)\sigma_{\mathrm{x}}^2}} dxdy, \quad (5.12)$$

where we have used the abbreviation $r = r_{\mathrm{x,x}}(\tau)$ for the auto correlation before the static nonlinearity. $\sigma_{\mathrm{y}} = \sigma_{\mathrm{x}}$ as well as $\mu_{\mathrm{y}} = \mu_{\mathrm{x}}$, because $x(t)$ and $y(t)$ are identical.

From the analytical expressions of the auto and cross-correlation and the help of the Wiener-Khinchin theorem (see for example Gardiner (1985)), one can derive analytical expressions of the respective power and cross-spectrum.

5.3.1 Analytical cross-spectrum

The cross-spectrum between the input signal and the distorted output is the Fourier transform of the cross correlation $r_{\mathrm{z,s}}(\tau)$ written in Eq.(D.12). Therefore the cross spectrum can be expressed simply as:

$$\begin{aligned}\frac{S_{\mathrm{z,s}}(f)}{\sigma_{\mathrm{z}}\sigma_{\mathrm{s}}} = \quad & \sqrt{\frac{1}{2\pi\sigma_{\mathrm{x}}^2}}\Bigg[\left(\mu_{\mathrm{s}}\int_{-\infty}^{\infty} dx g(x)e^{-\frac{(x-\mu_{\mathrm{x}})^2}{2\sigma_{\mathrm{x}}^2}}\right)\delta(f) + ... \\ & + \left(\frac{\sigma_{\mathrm{s}}}{\sigma_{\mathrm{x}}}\int_{-\infty}^{\infty} dx(x-\mu_{\mathrm{x}})g(x)e^{-\frac{(x-\mu_{\mathrm{x}})^2}{2\sigma_{\mathrm{x}}^2}}\right)\frac{S_{\mathrm{x,s}}(f)}{\sigma_{\mathrm{x}}\sigma_{\mathrm{s}}}\Bigg]. \end{aligned} \quad (5.13)$$

The effect of the variance of the signal σ_{s}^2 as well as the mean value of the signal μ_{s} on the cross-spectrum between the distorted output $z(t)$ and the input signal $s(t)$ is just in the form of a multiplicative factor, whereby the mean value of the signal just contributes to the DC-component, i.e. the zero frequency bin of the cross-spectrum. This is plausible, because the offset of the signal can also be absorbed directly into the mean value of the stochastic process $x(t)$, which then would only effect the zero-frequency component of the cross-spectrum.

The general expression Eq.(5.13) for the cross-spectrum between the distorted output and the input signal can be written as:

$$\frac{S_{\mathrm{z,s}}(f)}{\sigma_{\mathrm{z}}\sigma_{\mathrm{s}}} = \left(\frac{\sigma_{\mathrm{x}}\mu_{\mathrm{s}}}{\sqrt{2\pi}}\int_{-\infty}^{\infty} dy g(\sigma_{\mathrm{x}}y+\mu_{\mathrm{x}})e^{-\frac{y^2}{2}}\right)\delta(f) + \left(\frac{\sigma_{\mathrm{s}}\sigma_{\mathrm{x}}}{\sqrt{2\pi}}\int_{-\infty}^{\infty} dy y g(\sigma_{\mathrm{x}}y+\mu_{\mathrm{x}})e^{-\frac{y^2}{2}}\right)\frac{S_{\mathrm{x,s}}(f)}{\sigma_{\mathrm{x}}\sigma_{\mathrm{s}}}. \quad (5.14)$$

Eq.(5.14) can be further simplified by using the zero mean and unit variance assumption

for both stochastic processes (neural response $x(t)$ and signal $s(t)$) to(Bussgang, 1952):

$$S_{\mathrm{z,s}}(f) = \left(\frac{1}{\sqrt{2\pi}} \int_{-\infty}^{+\infty} x g(x) e^{-\frac{x^2}{2}} dx \right) S_{\mathrm{x,s}}(f). \tag{5.15}$$

We conclude that the utilization of a static nonlinearity does not shape the cross-spectrum of the distorted output.

5.3.2 Analytical power spectrum

The power spectrum of the distorted output can be expressed as an infinite series of multiple convolutions of the power spectrum of the undistorted signal. This insight stems from the expansion of the integral kernel in Eq.(5.12):

$$p(x,y) = \frac{e^{\frac{2rxy - x^2 - y^2}{2(1-r^2)}}}{2\pi\sqrt{1-r^2}}, \tag{5.16}$$

in terms of r (the auto-correlation function before the SNL). This expansion leads to(Abramowitz and Stegun, 1970):

$$p(x,y) = \frac{e^{\frac{2rxy - x^2 - y^2}{2(1-r^2)}}}{2\pi\sqrt{1-r^2}} = \sum_{l=0}^{\infty} \frac{1}{l!} \frac{1}{2\pi} e^{-x^2/2} H_{e_l}(x) e^{-y^2/2} H_{e_l}(y) r^l, \tag{5.17}$$

where $H_{e_l}(x)$ are the lth-order probabilists' Hermite polynomials(see sec. D.1). Using this expression in the equation for the autocorrelation function of the distorted output Eq.(5.12) leads to:

$$r_{\mathrm{z,z}}(\tau) \;=\; \sum_{l=0}^{\infty} \frac{1}{l!} \left(\frac{1}{\sqrt{2\pi}} \int_{-\infty}^{\infty} dx g(x) e^{-x^2/2} H_{e_l}(x) \right)^2 r_{\mathrm{x,x}}(\tau)^l.$$

One can easily generalize the above expansion, if one loses the zero mean and unit variance restriction for the stochastic processes $x(t), y(t)$. The corresponding bivariate (2-dimensional) Gaussian joint probability distribution then reads:

$$p(x,y) = \frac{e^{\frac{\frac{2r(x-\mu_{\mathrm{x}})(y-\mu_{\mathrm{y}})}{\sigma_{\mathrm{x}}\sigma_{\mathrm{y}}} - \frac{(x-\mu_{\mathrm{x}})^2}{\sigma_{\mathrm{x}}^2} - \frac{(y-\mu_{\mathrm{y}})^2}{\sigma_{\mathrm{y}}^2}}{2(1-r^2)}}}{2\pi\sigma_{\mathrm{x}}\sigma_{\mathrm{y}}\sqrt{1-r^2}}, \tag{5.18}$$

where $\mu_{x,y}$ denotes the mean of x or y and $\sigma_{x,y}$ is the standard deviation of x or y and r is the cross-correlation between x and y, i.e. $r = r_{\mathrm{x,y}}(\tau)$.

Using the fact that the two-dimensional Gaussian distribution is the generating function of the product of probabilist's Hermite polynomials(Abramowitz and Stegun, 1970),

one arrives at:

$$\frac{e^{\frac{\frac{2r(x-\mu_{\mathrm{x}})(y-\mu_{\mathrm{y}})}{\sigma_{\mathrm{x}}\sigma_{\mathrm{y}}}-\frac{(x-\mu_{\mathrm{x}})^2}{\sigma_{\mathrm{x}}^2}-\frac{(y-\mu_{\mathrm{y}})^2}{\sigma_{\mathrm{y}}^2}}{2(1-r^2)}}}{2\pi\sigma_{\mathrm{x}}\sigma_{\mathrm{y}}\sqrt{1-r^2}} = \frac{1}{2\pi\sigma_{\mathrm{x}}\sigma_{\mathrm{y}}}\sum_{l=0}^{\infty}\frac{1}{l!}e^{-\hat{x}^2/2}H_{e_l}(\hat{x})e^{-\hat{y}^2/2}H_{e_l}(\hat{y})r^l, \quad (5.19)$$

where $\hat{x} = (x-\mu_{\mathrm{x}})/\sqrt{2\sigma_{\mathrm{x}}^2}$, $\hat{x} = (y-\mu_{\mathrm{y}})/\sqrt{2\sigma_{\mathrm{y}}^2}$, and $r = r_{\mathrm{x,y}}(\tau)$ denotes the cross correlation between the two Gaussian stochastic processes $x(t)$ and $y(t)$. Using this expansion of the 2-dimensional Gaussian probability distribution and the expression for the auto correlation function of the distorted output $z(t)$ leads to:

$$\begin{aligned} r_{\mathrm{z,z}}(\tau) &= \int_{-\infty}^{+\infty}\int_{-\infty}^{+\infty} g(x)g(y)\frac{\exp\left(-\frac{2(r-1)\mu_{\mathrm{x}}(-\mu_{\mathrm{x}}+x+y)-2rxy+x^2+y^2}{2(1-r^2)\sigma_{\mathrm{x}}^2}\right)}{2\pi\sqrt{1-r^2}\sigma_{\mathrm{x}}^2}dxdy \\ &= \sum_{l=0}^{\infty}\frac{1}{l!}\left(\frac{1}{\sqrt{2\pi\sigma_{\mathrm{x}}^2}}\int_{-\infty}^{\infty}dxg(x)e^{-(x-\mu_{\mathrm{x}})^2/2\sigma_{\mathrm{x}}^2}H_{e_l}\left(\frac{x-\mu_{\mathrm{x}}}{\sigma_{\mathrm{x}}}\right)\right)^2 r_{\mathrm{x,x}}(\tau)^l. \quad (5.20) \end{aligned}$$

By simply Fourier transform the expression of the autocorrelation function (Eq.(5.20)) and using the fact that multiplications in time-space leads to convolutions in Fourier-domain, i.e

$$\mathfrak{F}\left(r_{\mathrm{x,x}}(\tau)^l\right) = \underbrace{S_{\mathrm{x,x}}(f)\otimes ...\otimes S_{\mathrm{x,x}}(f)}_{\substack{\texttt{(l-1)-fold convolutions of}\\ \texttt{the power spectrum of}\\ \texttt{the undistorted output}}} \frac{1}{\sigma_{\mathrm{x}}^{2l}}, \quad (5.21)$$

one can arrive at an expression for the power spectrum of the distorted output in terms of multiple convolutions of the power spectrum of the undistorted output:

$$\frac{S_{\mathrm{z,z}}(f)}{\sigma_{\mathrm{z}}^2} = G_0(\gamma,\mu)\cdot\delta(f) + \sum_{l=1}^{\infty}\frac{G_l(\gamma,\mu)}{\sigma_{\mathrm{x}}^{2l}}\cdot \underbrace{S_{\mathrm{x,x}}(f)\otimes ...\otimes S_{\mathrm{x,x}}(f)}_{\substack{\texttt{(l-1)-fold convolutions of}\\ \texttt{the power spectrum of}\\ \texttt{the undistorted output}}}. \quad (5.22)$$

Note, that the frequency dependence is solely due to the multiple convolutions of the power spectrum of the undistorted output $x(t)$.

Eq.(5.22) can be used twofold: i) in terms of a perturbative expression of the power spectrum by a truncation of the infinite series in Eq.(5.22), and ii) as a starting point for exact calculations of the power spectrum of the distorted output and its derivatives at zero frequency in order to calculate the curvature of the coherence function as a proxy classifier between low and band pass filtering on information.

In the following, we will use the the zero mean and unit variance approach for sake of simplicity. By using the expression for the DC-component contribution $G_0(\gamma,\mu)$ one

can simplify expression Eq.(5.22) to:

$$\frac{S_{\mathrm{z,z}}(f)}{\sigma_{\mathrm{z}}^2} = \left(\frac{1}{\sqrt{2\pi\sigma_{\mathrm{x}}^2}} \int_{-\infty}^{\infty} dx g(x) e^{-(x-\mu_{\mathrm{x}})^2/2\sigma_{\mathrm{x}}^2} \right)^2 \delta(f) + \\ + \sum_{l=1}^{\infty} \frac{1}{l!} \left(\frac{\int_{-\infty}^{\infty} dx g(x) e^{-(x-\mu_{\mathrm{x}})^2/2\sigma_{\mathrm{x}}^2} H_{e_l}\left(\frac{x-\mu_{\mathrm{x}}}{\sigma_{\mathrm{x}}}\right)}{\sqrt{2\pi\sigma_{\mathrm{x}}^2}} \right)^2 \underbrace{\frac{S_{\mathrm{x,x}}(f) \otimes ... \otimes S_{\mathrm{x,x}}(f)}{\sigma_{\mathrm{x}}^{2l}}}_{\substack{\texttt{(l-1)-fold convolutions} \\ \texttt{of the power spectrum of} \\ \texttt{the undistorted output}}} . \quad (5.23)$$

This expression for the power spectrum of a distorted output $z(t) = g(x(t))$ in terms of multiple convolutions of the power spectrum of the undistorted output $x(t)$ is crucial for the understanding of the results obtained in this chapter (see Fig. 5.9 and the discussion therein).

For sake of completeness we will write out the first three contributions to the power spectrum of the distorted output in Eq.(5.23) with $\mu_{\mathrm{x}} = 0$, $\sigma_{\mathrm{x}} = 1$:

$$\begin{aligned} S_{\mathrm{z,z}}(f) = \quad & \left(\frac{1}{\sqrt{2\pi}} \int_{-\infty}^{\infty} dx e^{-\frac{x^2}{2}} g(x) \right)^2 \delta(f) + \\ & + \left(\frac{1}{\sqrt{2\pi}} \int_{-\infty}^{\infty} dx e^{-\frac{x^2}{2}} x g(x) \right)^2 S_{\mathrm{x,x}}(f) + \\ & + \frac{1}{2} \left(\frac{1}{\sqrt{2\pi}} \int_{-\infty}^{\infty} dx e^{-\frac{x^2}{2}} \left(x^2 - 1\right) g(x) \right)^2 S_{\mathrm{x,x}}(f) \otimes S_{\mathrm{x,x}}(f) + \\ & + \quad \cdots . \end{aligned} \quad (5.24)$$

The effect of the SNL on the power spectrum is now reduced to solutions of the two mathematical problems: i) evaluation of the integrals of the coefficients, and ii) finding an expression for multiple convolutions of the power spectrum of the undistorted output. The first problem is independent of the stochastic system (as long as it is a Gaussian process) and depends solely on the nature of the distortion function, i.e. the static nonlinearity $g(x)$. The second mathematical problem depends just on the nature of the stochastic process before the static nonlinearity,i.e. the knowledge of its power spectrum and its multiple convolutions, and does not depend on $g(x)$. Note, that the the contribution from the static nonlinearity enters quadratically and therefore, a symmetric or antisymmetric SNL results in a symmetric contribution to the power spectrum. This explains the symmetries observed in previously (see for example Fig. 5.6 in sec. 5.2.1).

In Fig. 5.9, the effects of multiple convolutions on the power spectrum of a linear resonator neuron model (resonator cartoon parameter set) is shown.

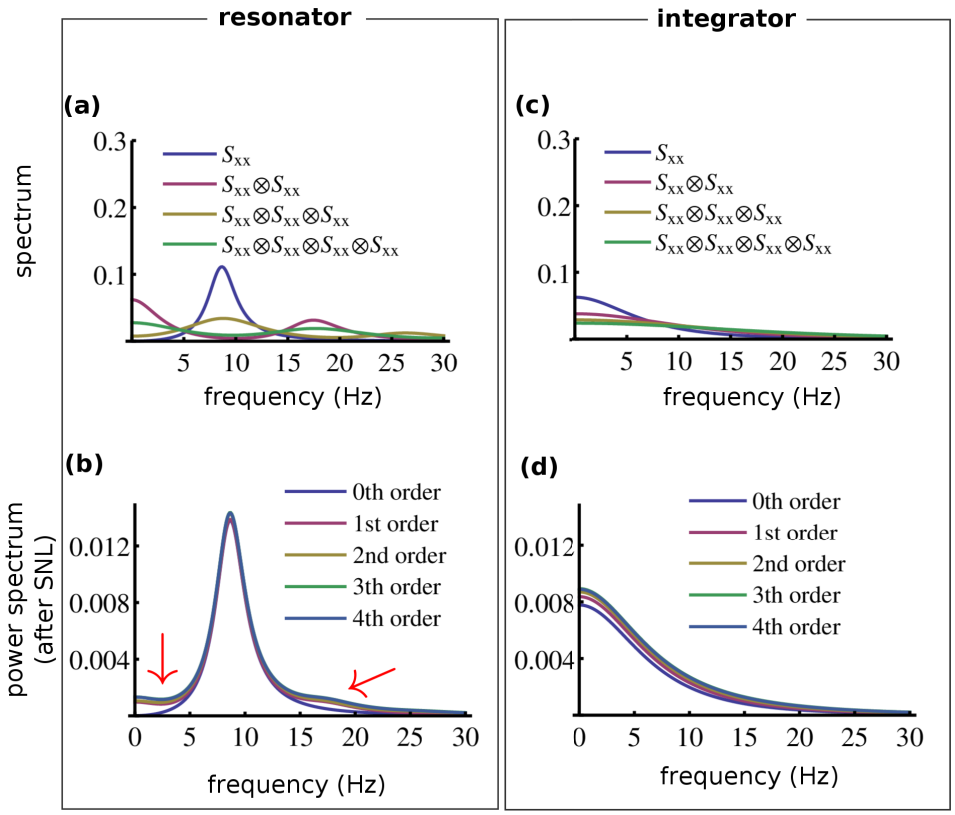

Figure 5.9: Effects of a erf-sigmoidal SNL on the power spectrum of the LN-cascade model. Shown are: multiple convolutions of the power spectrum for the resonator cartoon (a) and pyramidal cell (c) parameter set (Tab. C.1) for the linear RF-model (Eq.(4.1a) and Eq.(4.1b), without threshold), and the perturbative contributions Eq.(5.24) of the power spectrum of the LN-cascade model. An erf-sigmoidal SNL (Eq.(5.4)) was used with parameters: $\mu = 0.5$ and $\gamma = 100$. The output of the linear RF-model has zero mean and unit variance for sake of simplicity.

Fig. 5.9a displays the consequence of multiple convolutions of the power spectrum of the linear RF-model (see Eq.(4.1a) and Eq.(4.1b)), i.e. without threshold for the resonator cartoon parameter set (see Tab. C.1). The main effect of the weighted sum of multiple convolutions of the power spectrum of the output of a linear resonator neuron model is the enhancement of power at low frequencies and high frequencies, or put differently, in frequency bands outside the resonance frequency (marked by the red arrows in Fig. 5.9b). This enhancement leads to a peak in the coherence function in the vicinity of the subthreshold resonance frequency (see for example Fig. 5.7).

Multiple convolutions of the power spectrum of a linear integrator model (see Tab. C.1) do not shape the global frequency-dependence (see Fig. 5.9c). Consequently, the perturbative approach for power spectrum (Eq.(5.24)) of an integrator-LN-cascade (shown in

Fig. 5.9d) does not show any frequency selectivity.

5.4 Example spectra by using different static nonlinearities

5.4.1 The identity static nonlinearity

The **identity static nonlinearity** $z(t) = x(t)$ leads to a **cross-spectrum** of the distorded output $z(t)$ and the input signal of the following form:

$$S_{\mathrm{z,s}}(f) = \mu_{\mathrm{s}}\mu_{\mathrm{x}}\delta(f) + S_{\mathrm{x,s}}(f), \tag{5.25}$$

thus, the DC-component of the cross-spectrum between the input signal $s(t)$ and the 'distorted' output $z(t) = x(t)$ is formed by the mean values of the input signal μ_{s} and of the undistorted output μ_{x} alone. Whereas the non-zero frequency contribution is identical to the power spectrum of the undistorted output, i.e.

$$S_{\mathrm{z,z}}(f) = S_{\mathrm{x,x}}(f), \tag{5.26}$$

where we used the fact that only $G_1(\gamma, \mu) = 1$ and for all other values $G_{l\neq 1}(\gamma, \mu) = 0$. Thus, Eq.(5.12) describes the trivial identity distortion correct.

5.4.2 The exponential static nonlinearity

The first non-trivial distortion, the **exponential static nonlinearity** leads to a **cross-spectrum** of the distorted output $y(t)$ and the input signal of the following form:

$$S_{\mathrm{z,s}}(f) = \gamma e^{\frac{1}{2}\gamma^2 - \gamma\mu} S_{\mathrm{x,s}}(f). \tag{5.27}$$

The **exponential static nonlinearity** leads to a **power spectrum** of the distorded output $y(t)$ in terms of the power spectrum of the undistorted output $x(t)$ of the following form:

$$S_{\mathrm{z,z}}(f) = e^{\gamma^2 - 2\mu\gamma}\delta(f) + e^{\gamma^2 - 2\mu\gamma} \sum_{l=1}^{\infty} \frac{\gamma^{2l}}{l!} \underbrace{S_{\mathrm{x,x}}(f) \otimes ... \otimes S_{\mathrm{x,x}}(f)}_{\substack{\texttt{(l-1)-fold convolutions of} \\ \texttt{the power spectrum of} \\ \texttt{the undistorted output}}} . \tag{5.28}$$

The coherence function between the distorted output and the input signal can be expressed as (neglecting the explicit DC-contribution ($l = 0$)):

$$C_{\mathrm{z,s}}(f) = \frac{|S_{\mathrm{z,s}}(f)|^2}{S_{\mathrm{z,z}}(f)S_{\mathrm{s,s}}(f)} = \frac{|S_{\mathrm{x,s}}(f)|^2 / S_{\mathrm{s,s}}(f)}{S_{\mathrm{x,x}}(f) + \frac{1}{2}\gamma^2 S_{\mathrm{x,x}}(f) \otimes S_{\mathrm{x,x}}(f) + ...}.$$

Therefore, the coherence function of the exponentially distorted output and the input signal is independent of the position of the 'threshold' μ, or put differently it is independent of the mean value μ_{x} of the Gaussian stochastic process $x(t)$. We can also see that

in the limit $\gamma \to 0$, the coherence function between the distorted output and the input signal is equal to the coherence between the undistorted output $x(t)$ and the signal $s(t)$, i.e.

$$\lim_{\gamma \to 0} C_{\mathrm{z,s}}(f) = C_{\mathrm{x,s}}(f). \tag{5.29}$$

This is a very remarkable result, because both squared cross and power spectrum by itself vanish in this limit, but the ratio of the two remains finite.

5.4.3 The Heaviside static nonlinearity

The **Heaviside static nonlinearity** $g(x) = \Theta(x - \mu)$ leads to a **cross-spectrum** of the distorted output $z(t)$ and the input signal of the following form:

$$S_{\mathrm{z,s}}(f) = \frac{e^{-\frac{\mu_{\mathrm{eff}}^2}{2}}}{\sqrt{2\pi}} S_{\mathrm{x,s}}(f), \tag{5.30}$$

and to a **power spectrum** of the distorted output $z(t)$ according to Eq.(5.23) of the following form:

$$\begin{aligned} S_{\mathrm{z,z}}(f) = & \left(\frac{1}{2}\mathrm{erfc}(\mu_{\mathrm{eff}}^2/\sqrt{2})\right)^2 \delta(f) + \\ & + \sum_{l=1}^{\infty} \frac{1}{l!} \left(\frac{1}{\sqrt{2\pi}} e^{-\frac{\mu_{\mathrm{eff}}^2}{2}} H_{e,l-1}(\mu_{\mathrm{eff}})\right)^2 \underbrace{S_{\mathrm{x,x}}(f) \otimes \ldots \otimes S_{\mathrm{x,x}}(f)}_{\substack{\texttt{(l-1)-fold convolutions of} \\ \texttt{the power spectrum of} \\ \texttt{the undistorted output}}} , \end{aligned} \tag{5.31}$$

where $\mathrm{erfc}(x)$ denotes the complementary error function and $\mu_{\mathrm{eff}} = \frac{\mu - \mu_{\mathrm{x}}}{\sigma_{\mathrm{x}}}$.

Because the offset μ of the SNL enters the power spectrum of the distorted output as well as the cross-spectrum between only quadratically and $H_{l-1}(\mu_{\mathrm{eff}})$ describes a polynomial in terms of μ_{eff}^2 with degree $(l-1)/2$, the sign of the offset of the SNL does not play any role. Thus, the coherence function and therefore all its characteristics like the quality factor or the lower bound of the mutual information rate of the distorted output will be symmetric with respect to the offset μ of the SNL. This theoretical result is supported by numerical computer simulations (see for example Fig. 5.6). For sake of completeness, we will present the result for the power spectrum of the distorted output explicitly in terms of the first three convolution contributions ($l = 0, 1, 2$):

$$\begin{aligned} S_{\mathrm{z,z}}(f) = & \left(\frac{1}{2}\mathrm{erfc}(\mu^2/\sqrt{2})\right)^2 \delta(f) + \left(\frac{e^{-\frac{\mu^2}{2}}}{\sqrt{2\pi}}\right)^2 S_{\mathrm{x,x}}(f) \\ & + \frac{1}{2}\left(\frac{e^{-\frac{\mu^2}{2}}\mu}{\sqrt{2\pi}}\right)^2 S_{\mathrm{x,x}}(f) \otimes S_{\mathrm{x,x}}(f) + \cdots \end{aligned} \tag{5.32}$$

In the limit of very large SNL offset values μ, the power spectrum of the distorted output vanishes identically:

$$\lim_{\mu\to\pm\infty} S_{\mathrm{z,z}}(f) = 0. \tag{5.33}$$

5.4.4 The erf-sigmoidal static nonlinearity

Assuming zero mean and unit variance of the undistorted output, the cross-correlation takes the form:

$$r_{\mathrm{z,s}}(\tau) = \left(\frac{\gamma e^{-\frac{\gamma^2\mu^2}{2\gamma^2+2}}}{\sqrt{2\pi}\sqrt{\gamma^2+1}} \right) r_{\mathrm{x,s}}(\tau), \tag{5.34}$$

and the auto correlation function(Bedenbaugh and Gerstein, 1994) reads:

$$r_{\mathrm{z,z}}(\tau) = \frac{1}{4} + \frac{1}{2\pi} \sin^{-1}\left(\frac{\gamma^2}{\gamma^2+1} r_{\mathrm{x,x}}(\tau) \right). \tag{5.35}$$

The latter expression is very surprising, because the relation for the erf-sigmoidal-SNL is very similar to the expression for a hard threshold. In the limit of $\gamma \to \infty$, i.e. the Heaviside step-function limit, one arrives at the well-known expression(Baum, 1957):

$$\lim_{\gamma\to\infty} r_{\mathrm{z,z}}(\tau) = \frac{1}{4} + \frac{1}{2\pi} \sin^{-1}\left(r_{\mathrm{x,x}}(\tau) \right). \tag{5.36}$$

5.5 Closed-form expressions for the spectra of LN-cascades

Here, we will use a very simple one-dimensional stochastic process, i.e. an Ornstein-Uhlenbeck process, which can be used to mimic subthreshold behavior of integrator-like neuron models. This model has the advantage that the perturbative approach can be solved exactly, i.e. it leads to a closed-form expression of all linear spectra of the distorted output.

5.5.1 Integrator-LN-cascade

Here, we consider the following one-dimensional linear stochastic process(Ricciardi and Sacerdote, 1979):

$$\tau_{\mathrm{x}} \frac{d}{dt} x(t) = -\delta x(t) + \sqrt{2\left(1-c\right)D}\eta_1(t) + \sqrt{2cD}\eta_2(t), \tag{5.37}$$

where $x(t)$ denotes the passive membrane voltage and τ_{x} its associated membrane time constant of the neuron, which is described as a leaky ($\delta > 0$) integrator (without a spiking mechanism or spiking rule, i.e. without any nonlinearity) with intrinsic Gaussian white noise $\eta_1(t)$. The signal $s(t) = \sqrt{2cD}\eta_2(t))$ is modeled as Gaussian white noise with intensity cD, mean $< \eta_2(t) >= 0$, and autocorrelation function $< \eta_{1,2}(t)\eta_{1,2}(t') >= \delta(t')$ and cross-correlation $< \eta_{1,2}(t)\eta_{2,1}(t') >= 0$.

The power spectrum of such an Ornstein-Uhlenbeck process is well known(Wang and Uhlenbeck, 1945) and reads:

$$S_{\mathrm{x,x}}(f) = \frac{2D}{\delta^2 + (2\pi f \tau_{\mathrm{x}})^2}. \tag{5.38}$$

The squared cross-spectrum between linear output $x(t)$ and the input signal $s(t)$ takes the form:

$$|S_{\mathrm{x,s}}(f)|^2 = \frac{2cD}{\delta^2 + (2\pi f \tau_{\mathrm{x}})^2}. \tag{5.39}$$

Multiple convolutions of the power spectrum of the undistorted linear output

Multiple convolutions of the power spectrum given in Eq.(5.38) can be expressed analytically as:

$$\begin{aligned} \underbrace{S_{\mathrm{x,x}}(f) \otimes \ldots \otimes S_{\mathrm{x,x}}(f)}_{\substack{\texttt{l-fold convolutions of} \\ \texttt{the power spectrum of} \\ \texttt{the undistorted output}}} &= \int_{-\infty}^{+\infty} d\tau_1 \ldots d\tau_l S_{\mathrm{x,x}} \left(f - \sum_{j=1}^{l} \tau_j \right) \prod_{j=1}^{l} S_{\mathrm{x,x}}(\tau_j) \\ &= \frac{l+1}{(2\tau_{\mathrm{x}}\delta)^l} \cdot \frac{(2D)^{l+1}}{(l+1)^2 \delta^2 + (2\pi f \tau_{\mathrm{x}})^2}. \end{aligned} \tag{5.40}$$

Thus, multiple convolutions of these spectra result in a Lorentzian spectrum (Fig. 5.9c).

Spectra of the distorted output

Cross-spectrum The **exponential static nonlinearity** leads to a **cross-spectrum** of the distorted output $y(t)$ and the input signal of the following form:

$$S_{\mathrm{z,s}}(f) = \gamma e^{\frac{1}{2}(\gamma^2 - 2\mu\gamma)} S_{\mathrm{x,s}}(f). \tag{5.41}$$

Power spectrum The **exponential static nonlinearity** leads to an auto correlation function as follows:

$$r_{\mathrm{z,z}}(\tau) = e^{\gamma^2 - 2\mu\gamma} e^{\gamma r_{\mathrm{x,x}}(\tau)}. \tag{5.42}$$

Expanding this expression in terms of $r_{\mathrm{x,x}}(\tau)$ and Fourier transform the resulting relation, leads to a **power spectrum** of the distorted output $y(t)$ in terms of the power

spectrum of the undistorted output $x(t)$ of the following form:

$$S_{\mathrm{z,z}}(f) = e^{\gamma^2-2\mu\gamma}\delta(f) + e^{\gamma^2-2\mu\gamma}\sum_{l=1}^{\infty}\frac{\gamma^{2l}}{l!}\underbrace{S_{\mathrm{x,x}}(f)\otimes\ldots\otimes S_{\mathrm{x,x}}(f)}_{\substack{\texttt{(l-1)-fold convolutions of}\\ \texttt{the power spectrum of}\\ \texttt{the undistorted output}}}$$

$$= e^{\gamma^2-2\mu\gamma}\left(\delta(f) + \sum_{l=1}^{\infty}\frac{\gamma^{2l}}{l!}\frac{l}{(2\tau_{\mathrm{x}}\delta)^{l-1}}\cdot\frac{(2D)^l}{l^2\delta^2+(2\pi f\tau_{\mathrm{x}})^2}\right). \tag{5.43}$$

The infinite sum on the r.h.s. can be further simplified with the help of generalized incomplete Gamma functions $\Gamma(a,z_0,z_1)$, and reads

$$\sum_{l=1}^{\infty}\frac{\gamma^{2l}}{l!}\frac{l}{(2\tau_{\mathrm{x}}\delta)^{l-1}}\frac{(2D)^l}{l^2\delta^2+(2\pi f\tau_{\mathrm{x}})^2} = \frac{\tau\nu^{-\kappa}\Gamma(1+\kappa,0,\nu)-\nu^{2\kappa}\Gamma(1-\kappa,0,\nu)}{\delta\kappa} \tag{5.44}$$

where we have used the abbreviations $\nu = -\frac{\gamma^2 D}{\delta\tau}$ and $\kappa = \frac{2\pi f\tau}{\delta}i$ as well as the definition of the generalized incomplete Gamma functions: $\Gamma(a,z_0,z_1)$

$$\Gamma(a,z_0,z_1) = \Gamma(a,z_0) - \Gamma(a,z_1). \tag{5.45}$$

Thus, the power spectrum of the exponentially distorted output ($z(t)$) can be written compactly as:

$$S_{\mathrm{z,z}}(f) = e^{\gamma^2-2\mu\gamma}\left(\delta(f) + \frac{\tau\nu^{-\kappa}\gamma(1+\kappa,0,\nu)-\nu^{2\kappa}\Gamma(1-\kappa,0,\nu)}{\delta\kappa}\right). \tag{5.46}$$

The offset μ modifies the power spectrum just in terms of the frequency-independent prefactor $e^{\gamma^2-2\mu\gamma}$.

In the limit of a very weak exponentially distortion, the power spectrum reads:

$$\lim_{\gamma\to 0} S_{\mathrm{z,z}}(f) = \delta(f) + 0 = \delta(f). \tag{5.47}$$

This indicates that the power spectrum of the exponentially distorted output vanishes in the limit of weak distortion. Although the cross-spectrum and the power spectrum of the distorted output vanishes in this limit, the ratio, i.e. the coherence function remains finite and approaches in this weak distortion limit to the coherence function of the undistorted output (by neglecting the DC-peak):

$$\lim_{\gamma\to 0} C_{\mathrm{z,s}}(f) = C_{\mathrm{x,s}}(f). \tag{5.48}$$

A second interesting limit of the distorted power spectrum is the low frequency limit, i.e.

$$\lim_{f\to 0} S^{(0)}_{\mathrm{z,z}}(f) = -\frac{2\tau e^{\gamma(\gamma-2\mu)}\left[\log(\nu)+\Gamma(0,\nu)+\tilde{\gamma}\right]}{\delta^2}, \tag{5.49}$$

where $\tilde{\gamma}$ is Euler's constant, i.e. $\tilde{\gamma} \approx 0.577216$. In order to calculate the curvature of the spectral coherence function at zero frequency, I also computed the second derivative of the power spectrum of the exponentially distorted output as

$$\lim_{f\to 0} S^{(2)}_{\mathrm{z,z}}(f) = \frac{16\pi^2\nu\tau^3 e^{\gamma^2-2\gamma\mu}\,{}_4F_4(1,1,1,1;2,2,2,2;-\nu)}{\delta^4}, \tag{5.50}$$

where ${}_pF_q\left(a_1,...,a_p;b_1,...,b_q;x\right)$ denotes the generalized hypergeometric function (see sec. D.1).

Curvature of the coherence function at zero frequency By having analytical expressions for the cross- and power spectrum, one can easily calculate the curvature of the coherence function at zero frequency, which acts as a discriminator between low pass (negative curvature) and band/high pass (positive curvature) filtering on information.

In the presence of a Gaussian white noise input, one can write the curvature of the coherence function as:

$$C^{(2)}_{\mathrm{z,s}}(0) \propto \frac{S_{\mathrm{z,z}}(0)S^{(2)}_{z,s}(0) - S_{\mathrm{z,s}}(0)S^{(2)}_{\mathrm{z,z}}(0)}{S_{\mathrm{z,z}}(0)^2}. \tag{5.51}$$

The sign of the curvature of the coherence at zero frequency is determined solely by the numerator in Eq.(5.51). Using Eq.(5.49), Eq.(5.50),Eq.(5.41) in Eq.(5.51), the sign of the curvature of the coherence between the output of the integrator-LN-cascade (see Eq.(5.37)) and the input signal (stochastic Gaussian white noise) takes the form:

$$C^{(2)}_{\mathrm{z,s}}(0) \propto -\frac{32\pi^2 c\tau^4 e^{3\gamma(\gamma-2\mu)}}{\delta^6}\nu\left[-\nu\,{}_4F_4(1,1,1,1;2,2,2,2;-\nu) + \log(\nu) + \Gamma(0,\nu) + \tilde{\gamma}\right]. \tag{5.52}$$

The parameters c,τ,γ,μ,δ are defined as positive real numbers. Thus, the curvature can take positive values, only if the following inequality holds true:

$$G(\nu) < 0, \tag{5.53}$$

with

$$G(\nu) := \nu\left[-\nu\,{}_4F_4(1,1,1,1;2,2,2,2;-\nu) + \log(\nu) + \Gamma(0,\nu) + \tilde{\gamma}\right]. \tag{5.54}$$

The parameter $\nu = -\frac{\gamma^2 D}{\delta\tau}$, which was introduced to simplify the expression of the power spectrum (see Eq.(5.46)), can only take negative real values. Numerical evaluation of $G(\nu)$ demonstrates, that the above stated inequality for positive curvature of the coherence function at zero frequency is not fulfilled. Consequently, one can conclude, that the integrator-LN model with an exponential static nonlinearity shows always negative curvature of the coherence function at zero frequency, which indicates low-pass filtering on information, irrespective of the model parameters (for example, with or without a leakage term in the linear system (L), or for arbitrary signal-to-noise ratios).

Although the exponential static nonlinearity can mimic the transfer function of single

neurons for small signal strengths, it lacks a description of a finite response. For this reason, one often uses sigmoidal shape distortion or transfer functions, which relate the linear response $x(t)$ to a measure of activity $y(t)$ and feature finite responses, i.e. saturation effects. For this reason, we will analyze in the following theoretically the effects of a very strong sigmoidal SNL by using the Heaviside step function $\Theta(x(t)-\mu)$, where $x(t)$ denotes again the undistorted output (of the linear system) and μ the offset of the SNL is set to zero, i.e. $\mu = 0$ for sake of simplicity.

The **Heaviside static nonlinearity** $\Theta(x)$ leads to a **cross-spectrum** of the distorted output $y(t)$ and the input signal of the following form:

$$S_{\mathrm{z,s}}(f) = \sqrt{\frac{1}{2\pi}} S_{\mathrm{x,s}}(f), \tag{5.55}$$

where we have used the Bussgang theorem in order to obtain the cross-spectrum. Thus, The autocorrelation of the distorted output can be calculated analytically in terms of the autocorrelation of the undistorted output $r_{\mathrm{x,x}}(\tau)$ and reads(Baum, 1957):

$$r_{\mathrm{y,y}}(\tau) = \frac{1}{4} + \frac{1}{2\pi} \sin^{-1}\left(r_{\mathrm{x,x}}(\tau)\right). \tag{5.56}$$

This expression can be expanded in terms of a power series in $r_{\mathrm{x,x}}(\tau)$ as:

$$r_{\mathrm{z,z}}(\tau) = \frac{1}{4} + \frac{1}{2\pi} \sum_{k=0}^{\infty} \frac{(2k-1)!!}{(2k)!!} \frac{1}{2k+1} r_{\mathrm{x,x}}(\tau)^{2k+1}. \tag{5.57}$$

By applying the Fourier transform, one can express the power spectrum of the distorted output ($y(t)$) in terms of multiple convolutions of the power spectrum of the undistorted output ($x(t)$) as:

$$\frac{S_{\mathrm{z,z}}(f)}{\sigma_{\mathrm{y}}^2} = \frac{1}{4}\delta(f) + \frac{1}{2\pi} \sum_{k=0}^{\infty} \frac{(2k-1)!!}{(2k)!!} \frac{1}{2k+1} \left(\frac{1}{\sigma_{\mathrm{x}}^2}\right)^{2k+1} \underbrace{S_{\mathrm{x,x}}(f) \otimes ... \otimes S_{\mathrm{x,x}}(f)}_{\substack{\texttt{(2k+1)-fold convolutions of} \\ \texttt{the power spectrum of} \\ \texttt{the undistorted output}}}$$

Inserting the expression of multiple convolutions of the power spectrum of an OU-process with itself (Eq.(5.40)), results in

$$\begin{aligned}\frac{S_{\mathrm{z,z}}(f)}{\sigma_{\mathrm{y}}^2} &= \frac{1}{4}\delta(f) + \frac{1}{2\pi} \sum_{k=0}^{\infty} \frac{(2k-1)!!}{(2k)!!} \frac{1}{2k+1} \left(\frac{1}{\sigma_{\mathrm{x}}^2}\right)^{2k+1} \underbrace{S_{\mathrm{x,x}}(f) \otimes ... \otimes S_{\mathrm{x,x}}(f)}_{\substack{\texttt{(2k+1)-fold convolutions of} \\ \texttt{the power spectrum of} \\ \texttt{the undistorted output}}} \\ &= \frac{1}{4}\delta(f) + \frac{1}{2\pi} \sum_{k=0}^{\infty} \frac{(2k-1)!!}{(2k)!!} \frac{1}{2k+1} \left(\frac{1}{\sigma_{\mathrm{x}}^2}\right)^{2k+1} \frac{2(2k+1) D^{2k+1} \left(\delta\tau_{\mathrm{x}}\right)^{-2k}}{4\pi^2 f^2 \tau_{\mathrm{x}}^2 + (\delta + 2\delta k)^2}\end{aligned} \tag{5.58}$$

The sum on the r.h.s. can be performed analytically and results in a closed-form expres-

sion for the power spectrum of the Heaviside distorted output $y(t) = \Theta(x(t))$ as follows:

$$\frac{S_{\mathrm{z,z}}(f)}{\sigma_{\mathrm{z}}^2} = \frac{1}{4}\delta(f) - \frac{\tau_{\mathrm{x}} \left(\psi^2\right)^{\omega} B_{\psi^2}\left(1-\omega, \frac{1}{2}\right) - \psi^2 \tau_{\mathrm{x}} \Gamma(\omega)\, {}_2\tilde{F}_1\left(\frac{1}{2}, \omega; \omega+1; \psi^2\right)}{4\pi\delta\psi\,(1-2\omega)}, \quad (5.59)$$

with the abbreviations $\psi = D/(\tau_{\mathrm{x}}\delta\sigma_{\mathrm{x}}^2) = 1/2$, $\omega = (1 - i2\pi\tau_{\mathrm{x}} f/\delta)/2$ and $B_z(a,b)$ is the incomplete beta function and ${}_2\tilde{F}_1\left(a,b;c;x\right)$ denotes the regularized hypergeometric function (see sec. D.1). The distorted power spectrum has therefore the following low- and high frequency limits:

$$\lim_{f\to 0} S_{\mathrm{z,z}}^{(0)}(f) = \frac{\psi\tau_{\mathrm{x}}\, {}_3F_2\left(\frac{1}{2}, \frac{1}{2}, \frac{1}{2}; \frac{3}{2}, \frac{3}{2}; \psi^2\right)}{\pi\delta}, \quad (5.60)$$

$$\lim_{f\to 0} S_{\mathrm{z,z}}^{(2)}(f) = -\frac{8\pi\psi\tau_{\mathrm{x}}^3\, {}_5F_4\left(\frac{1}{2}, \frac{1}{2}, \frac{1}{2}, \frac{1}{2}, \frac{1}{2}; \frac{3}{2}, \frac{3}{2}, \frac{3}{2}, \frac{3}{2}; \psi^2\right)}{\delta^3}, \quad (5.61)$$

$$\lim_{f\to\infty} S_{\mathrm{z,z}}^{(0)}(f) = 0. \quad (5.62)$$

The curvature of the coherence function at zero frequency (see Eq.(5.51)) can thus be written as:

$$C_{\mathrm{s,z}}^{(2)}(0) = 0. \quad (5.63)$$

Thus, the integrator-LN-cascade with a Heaviside static nonlinearity acts as an 'all' pass filter on information, i.e. does not show any frequency preferences at all, and is consequently not able to process information by means of filtering methods.

The **erf-sigmoidal static nonlinearity** leads to a **cross-spectrum** of the distorted output $z(t)$ and the input signal of the following form:

$$S_{\mathrm{z,s}}(f) = \left(\frac{\gamma e^{-\frac{\gamma^2\mu^2}{2\gamma^2+2}}}{\sqrt{2\pi}\sqrt{\gamma^2+1}}\right) S_{\mathrm{x,s}}(f), \quad (5.64)$$

where Bussgang's theorem was applied in order to obtain the cross-spectrum. The autocorrelation of the distorted output ($r_{\mathrm{z,z}}(\tau)$) can be calculated analytically in terms of the autocorrelation of the undistorted output $r_{\mathrm{x,x}}(\tau)$ as follows(Bedenbaugh and Gerstein, 1994):

$$r_{\mathrm{z,z}}(\tau) = \frac{1}{4} + \frac{1}{2\pi}\sin^{-1}\left(\frac{\gamma^2}{1+\gamma^2} r_{\mathrm{x,x}}(\tau)\right), \quad (5.65)$$

where γ is the slope of the erf-sigmoidal (σ_{x} is the standard deviation of the undistorted Gaussian process $x(t)$). This expression can be written in terms of a power series in

$r_{\mathrm{x,x}}(\tau)$ as follows:

$$r_{\mathrm{z,z}}(\tau) = \frac{1}{4} + \frac{1}{2\pi}\sum_{k=0}^{\infty}\frac{(2k-1)!!}{(2k)!!}\frac{1}{2k+1}\left(\frac{1}{\sigma_{\mathrm{x}}^2}\right)^{2k+1}\left(\frac{\gamma^2}{1+\gamma^2}\right)^{2k+1} r_{\mathrm{x,x}}(\tau)^{2k+1}. \quad (5.66)$$

By applying the Fourier transform, one can express the power spectrum of the distorted output ($y(t)$) in terms of multiple convolutions of the power spectrum of the undistorted output ($x(t)$) as:

$$\frac{S_{\mathrm{z,z}}(f)}{\sigma_{\mathrm{z}}^2} = \frac{1}{4}\delta(f) + \frac{1}{2\pi}\sum_{k=0}^{\infty}\frac{(2k-1)!!}{(2k)!!}\frac{1}{2k+1}\left(\frac{1}{\sigma_{\mathrm{x}}^2}\frac{\gamma^2}{1+\gamma^2}\right)^{2k+1} \underbrace{S_{\mathrm{x,x}}(f)\otimes ...\otimes S_{\mathrm{x,x}}(f)}_{\substack{\texttt{(2k+1)-fold convolutions of}\\ \texttt{the power spectrum of}\\ \texttt{the undistorted output}}}$$

Inserting the expression of multiple convolutions of the power spectrum of an OU-process with itself (Eq.(5.40)), results in:

$$\frac{S_{\mathrm{z,z}}(f)}{\sigma_{\mathrm{z}}^2} = \frac{1}{4}\delta(f) - \frac{\tau_{\mathrm{x}}\left(\psi^2\right)^{\omega} B_{\psi^2}\left(1-\omega,\frac{1}{2}\right) - y^2\tau_{\mathrm{x}}\Gamma(\omega)\,{}_2\tilde{F}_1\left(\frac{1}{2},\omega;\omega+1;\psi^2\right)}{4\pi\delta\psi\,(1-2\omega)}, \quad (5.67)$$

with $\psi := \frac{D}{\tau_{\mathrm{x}}\delta\sigma_{\mathrm{x}}^2}\frac{\gamma^2}{1+\gamma^2} = \frac{1}{2}\frac{\gamma^2}{1+\gamma^2}$, $\omega := (1 - i2\pi\tau_{\mathrm{x}}f/\delta)/2$. By comparing Eq.(5.59) with Eq.(5.67), one can see that the analytical expression for the power spectrum of the erf-sigmoidal (centered at zero, i.e. $\mu = 0$) distorted output is very similar to the power spectrum of the Heaviside distorted output (Eq.(5.59)).

The frequency-limits of the power spectrum and its second derivative are as follows:

$$\lim_{f\to 0} S_{\mathrm{z,z}}^{(0)}(f) = \frac{\psi\tau_{\mathrm{x}}\,{}_3F_2\left(\frac{1}{2},\frac{1}{2},\frac{1}{2};\frac{3}{2},\frac{3}{2};\psi^2\right)}{\pi\delta}, \quad (5.68)$$

$$\lim_{f\to 0} S_{\mathrm{z,z}}^{(2)}(f) = -\frac{8\pi\psi\tau_{\mathrm{x}}^3\,{}_5F_4\left(\frac{1}{2},\frac{1}{2},\frac{1}{2},\frac{1}{2},\frac{1}{2};\frac{3}{2},\frac{3}{2},\frac{3}{2},\frac{3}{2};\psi^2\right)}{\delta^3}. \quad (5.69)$$

The curvature of the coherence function at zero frequency (see Eq.(5.51)) can thus be written as:

$$C_{\mathrm{s,z}}^{(2)}(0) \propto -\frac{8\left(\beta^2+1\right)c\psi^2\tau_{\mathrm{x}}^4\left[{}_3F_2\left(\frac{1}{2},\frac{1}{2},\frac{1}{2};\frac{3}{2},\frac{3}{2};\psi^2\right) - {}_5F_4\left(\frac{1}{2},\frac{1}{2},\frac{1}{2},\frac{1}{2},\frac{1}{2};\frac{3}{2},\frac{3}{2},\frac{3}{2},\frac{3}{2};\psi^2\right)\right]}{\beta^2\delta^5}. \quad (5.70)$$

It can be shown that this curvature is always negative, because the term in the square brackets ([...]) in Eq.(5.70) is always positive for positive ψ. Thus, we conclude that the integrator-LN-cascade with an error-function sigmoidal leads to a negative curvature of the coherence function at zero frequency, and thus acts primarily as low pass filter on

information, irrespective of model parameters. Note that the limit:

$$\lim_{\gamma\to\infty} C^{(2)}_{\mathrm{s,z}}(0) = 0, \tag{5.71}$$

is in accordance with previous results obtained by using a centered Heaviside SNL (see Eq.(5.63)).

To conclude, the integrator-LN-cascade always shows a negative curvature of the coherence function at zero frequency, irrespective of the specific shape of the nonlinearity: i) exponential increasing, ii) hard threshold (Heaviside SNL), and iii) soft threshold (sigmoidal SNL) and the model parameters: membrane time constant τ_{x}, leakage term δ, signal-to-noise strength c or signal intensity D, and thus shows low pass filter characteristics on information. The integrator-LN-cascade models offer an exact analytic treatment of the information filtering properties because all necessary spectra for the coherence function can be derived in closed-form expressions. As it was observed in sec. 2, integrator neuron models act primarily as low pass filters on information. Therefore, an additional mechanism is needed (see sec. 3) to shape their filtering properties.

5.6 Summary & Discussion

In this chapter, it was demonstrated that the concept of a static nonlinearity (SNL), which are a key component of so-called linear-nonlinear cascades (LN), leads to band-pass filtering on information in the presence of subthreshold resonances. Three different non-trivial SNLs were presented: i) exponential, ii) hard-threshold, and iii) soft-threshold (sigmoidal). A measure of the effective nonlinearity of the LN model was derived and applied.

Based on the biological importance of soft-threshold nonlinearities, the error function based sigmoidal SNL were analyzed in detail numerically in models with subthreshold oscillations, i.e. the linear resonator neuron model, which was presented in sec. 4.2.1. It was shown that the band pass filter on information requires: a) subthreshold resonances, and b) a rather 'nonlinear' transformation of the linear response. The band-pass filter frequency in a so-called resonate-LN cascade neuron model is close to the resonance frequency of the impedance function. The resonate-LN cascade model can be tuned such that the similarity between band-pass filtering of the resonate-LN cascade model and the resonate-and-fire (RF) neuron model (sec. 4.2.2) appears. This similarity relies on the facts that the SNL should be 'nonlinear' and located close to the membrane threshold of the RF model.

Based on Bussgang's theorem, a simple approach was presented to calculate the power and cross-spectrum of a generic LN-cascade neuron model in terms of multiple convolutions of the power spectrum of the linear (L) output. This approach was used to describe numerically observed symmetries in the information filtering characteristics of the LN-cascade model.

For the class of integrate-LN-cascade neuron models, closed-form expressions for the spectra, necessary to study the spectral coherence function, were derived. Based on

the exponential, hard-, and soft-threshold SNL, it was shown that integrate-LN-cascade models exhibit a negative curvature of the coherence function at zero frequency. This analytical finding suggests that integrate-LN-cascade neuron models act as low pass filter on information, i.e. they preferentially transmit information about slow components of a time-dependent input current signal.

This study finalises the survey of this thesis regarding theoretical neural mechanisms that can manifest in a band pass filter on information (based on the spectral coherence function).

Alternative analytical approaches. Basically, Bussgang's theorem was applied in this chapter to derive analytical expressions for the spectra of the LN-cascade model. It should be mentioned here, that several alternative approaches to obtain analytical expressions for the statistics of a LN-cascade model were developed independently. Several reasons are accountable for this.

First, the notion of LN-cascade neuron models is quite novel(Chichilnisky, 2001) and to the best of the author's knowledge, the following notations are equivalent:

- LN-cascade neuron models(Chichilnisky, 2001),
- non-linear amplitude distortion functions(Bussgang, 1952),
- (non-linear) amplitude transformation(Banelli, 2011),
- zero memory continuous nonlinearity(Masry and Cambanis, 1978),
- zero memory clipper(Price, 1958),
- limiters(Davenport, 1953),
- rectification of noise processes(Bedenbaugh and Gerstein, 1994),
- smoothly limited Gaussian noise(Baum, 1957),
- (non-linear) instantaneous device(Wiener, 1942),
- static nonlinearities(Marmarelis, 1972),
- Wiener system(Wiener, 1966).

Major contributions to analytical approaches of these LN-cascades were developed by Bussgang (1952); Malahov (1978); Marmarelis (1972); Middleton et al. (1960). Especially the work by Malahov (1978)[1] was almost forgotten because of a missing English translation of the Russian original[2].

[1]The author, S.B., wants to thank Alexander (Shura) Neiman, Ohio University (USA), who pointed out this work.

[2]S.B. wants to thank Sergej Voronenko and Alexandra Kruscha, Humboldt-Universität zu Berlin (Germany), who helped enormously in order to conceive the Russian original book.

6 Summary and concluding remarks

'When the work is done - so, I'm done with it.'[1]

In this thesis, several single neuron models were investigated, ranging from very simplified integrate-and-fire (IF) models to more realistic conductance-based Hodgkin-Huxley-type neuron models. The underlying question was, how certain cell intrinsic mechanisms can shape the information transmission properties? This question was asked by studying the spectral stimulus-response (linear coding) and the response-response (non-linear coding) coherence function. Various mechanisms (subthreshold resonances and ISI correlations) in conjunction with several types of neuronal nonlinearities: i) a fire-and-reset rule (discontinuous nonlinearity), iii) biophysical spike mechanism (conductance-based neuron models), and iii) static nonlinearities (continuous nonlinearities) and their effects on the spectral signal transmission characteristics were discussed.

It was shown that neuronal nonlinearities, which are a key feature of excitable neuron models, are of a vital role in establishing a frequency-selective signal transmission (band pass filter) that solely relies on the single neuron model and is not induced by external parameters. Thus, spikes, in contrast to the purely subthreshold linear responses, generated by neuronal nonlinearities are essential for information filtering in single neuron models.

First, in sec. 2, the well established stochastic IF neuron models and their spectral information characteristics were studied using numerical (Monte-Carlo computer simulations) and semi-analytical approaches (Richardson's method). Both approaches are complementary and suggest that within a wide parameter range, all IF neuron models (perfect IF, leaky IF, quadratic IF, and the exponential IF) act as a low pass filter on information. Thus, transmitting preferentially information about slow components of a time-dependent input signal. This finding is in-line with the notation of integrators, because only slow components of the input signal, or put differently low-frequency components, pushes the membrane voltage above a certain threshold. Although highly nonlinear, IF neuron models do not show a frequency preference on information. Thus, passive single neuron mechanisms, described by the IF neuron models, do not provide

[1] 'Wenn die Arbeit fertig ist - ja, dann bin ich damit fertig.'(Hannah Arendt, 26.10.1964)

a source of band-pass filtering on information. The biological relevance of this study stems from the fact that pyramidal neurons in the cortex (in vivo and in-vitro) can be well described by IF models.

Secondly, the information filtering effects of interspike interval (ISI) correlations was put into focus. Such ISI correlations are often modeled with the help of an active feedback mechanism, which is due to the interplay of different types of ion channels in the membrane of the neuron. In sec. 3, the simplest IF neuron model, the perfect IF (PIF) was modified by a stochastic threshold-and-reset concept, which leads to positive ISI correlations of adjacent ISIs. Two model variants (renewal and non-renewal version), which differ solely by the presence of ISI correlations, which can be gradually tuned between zero and one-half were discussed. By choosing the threshold distribution appropriately, a single neuron model with positive ISI correlations and realistic ISI distributions (here modeled with the help of an Inverse Gaussian) was constructed. Due to the mathematical simplicity of the neuron model, it offers an analytical study (complemented with numerically obtained results) on its information filtering properties. The main finding of this study is that those positive ISI correlations always lead to a preferred frequency in information transmission, i.e. a more or less pronounced peak in the spectral coherence function, whereas the renewal model acts dominantly as low pass filter on information. The frequency of preferred information transmission was found numerically to be close to half of the spontaneous firing rate (firing rate without an external signal). Thus, positive ISI correlations, resulting from cell intrinsic feedback mechanisms (adaptation mechanisms) can shape the coherence function from low to band pass filter on information. Analytically this was underpinned by evaluating the curvature of the coherence function at zero frequency. The curvature of the renewal model variant is dominantly negative, whereas the curvature of the coherence function of the non-renewal variant (with positive ISI correlations) is always positive, which suggests a band pass filter on information. The trade-off between band-pass filtering on information and the total amount of transmitted information (approximated by the lower bound of the mutual information rate) was investigated and confirmed by extensive numerical computer simulations (50.000 parameter sets).

Then, in sec. 4, the effects of subthreshold resonances on the information filtering properties of the linear and non-linear response of the neuron models were brought into focus. To analyze the information transmission in the spiking response, the neuron model was subjected to a fire-and-reset rule (resonate-and-fire, RF). The RF model was investigated by employing three parameter sets: i) resonator cartoon (highly resonant), ii) stellate cell (moderately resonant), and iii) pyramidal (non-resonant) cell. The main finding of this study is that subthreshold resonances can show a frequency preference on information, if the response of the neuron is nonlinear, i.e. spiking response. In contrast to the spiking response, the purely linear subthreshold response does not show a frequency preference on information and its signal transmission characteristics is not affected by the presence of subthreshold resonances at all. Thus, subthreshold resonances in conjunction with nonlinearities (resonant neurons) can act as a band-pass filter on information (based on the spectral coherence function). Numerical findings of the RF

model suggest that the band pass filter on information is very pronounced if the neuron operates in the low firing and irregular firing regime (phasic firing) and is diminished in the high firing rate and very regular firing region (tonic firing). With the help of extensive computer simulations (75.000 parameter sets), it was shown that the frequency of preferred information transmission does not necessarily coincide with the subthreshold resonance frequency.

The one-to-one relationship between the quality of the subthreshold resonance and the quality of the band pass filter on information was achieved, only if the neuron's firing rate is restricted to a particular region. Thus, subthreshold resonances in conjunction with a fire-and-reset rule can lead to band-pass filtering on information about a time-dependent current stimulus. In the RF neuron model, this phenomenon of band-pass filtering on information is a rather robust one and always exhibits a trade-off between markedness of the filter on the lower bound of the mutual information rate. Similar numerical studies were performed for conductance-based neuron models, which are equipped with a dynamical spike-mechanism. It was shown that generic conductance-based neuron models, like the well-established Morris-Lecar (ML) and the Hodgkin-Huxley (HH) models, can show band-pass filtering effects on information in the presence of subthreshold resonances. Numerical computer simulations of stochastic versions of the ML and the HH neuron model demonstrate this filtering property, based on subthreshold resonances, is more robust and extends to the tonic firing regime of these models. The subject of linear versus non-linear coding in the RF, ML, and HH neuron model was discussed by using the response-response coherence function as an estimate of the upper bound of mutual information. It was shown that the neuron models encode information about a time-dependent input current rather non-linearly within the phasic firing regime, manifested by a significant discrepancy between the stimulus-response and the response-response coherence function. This deviation between the two spectral measures becomes diminished within the tonic firing regime. Both spectral measures show a preferred frequency selectivity on information in the presence of subthreshold resonances. However, the band pass filter described by the response-response coherence function is less pronounced than the filter described by the stimulus-response coherence.

Finally (see sec. 5), the effects of continuous nonlinearities in conjunction with subthreshold resonances were investigated using linear-nonlinear (LN) cascade neuron models. The usage of static nonlinearities (SNLs) allows an analytical treatment of the spectral characteristics of the (continuous) neuron model in terms of a perturbation approaches.

The stronger the nonlinearity distorts the response of the underlying linear (L) model, the more 'pulsatile' is the resulting distorted output. The main finding of this study is twofold. First, by the observation that SNLs in conjunction with subthreshold resonances can lead to band-pass filtering on information. The preferred frequency of information transmission is close to the subthreshold resonance and depends on the 'strength' of the SNL. A measure was proposed, which captures the effective nonlinearity ('strength') of the linear-nonlinear cascade (see sec. 5.1.2). This measure depends on the parameters and the shape of the SNL as well as the neuron model parameters (mean value and

variance of the membrane voltage). This measure was analytically calculated and resulted in simple closed form expressions for the i) exponential, ii) hard-threshold, and iii) soft-threshold SNLs. The second incentive for using LN models lies in their mathematical simplicity. They allow an analytical exploration of the signal transmission properties of the model. Exact results for the power spectrum of the LN-cascade model and the cross spectrum between LN-cascade output and input signal were derived for the linear integrator dynamics subjected to i) exponential, ii) hard threshold (Heaviside function), and iii) soft-threshold (error-function sigmoidal) static nonlinearities. It was proven analytically that these integrator-LN-cascades exhibit a negative curvature of the coherence function at zero frequency, and therefore act primarily as low pass filter on information. Based on numerical results, it was shown that resonator-LN-cascades could show band-pass filtering characteristics. This filtering effect was presented exemplary for the error-function sigmoidal SNL, because it captures in essence realistic single neuron transfer functions, i.e. respecting exponential shape within the phasic regime and a finite response (firing rate) within the tonic firing regime.

Thus, the effects of several theoretical mechanisms on the information filtering characteristics in single neuron models were analyzed. Mechanisms that lead to potentially band-pass filtering characteristics on information are: i) subthreshold resonances in conjunction with nonlinearities that lead to spiking activity, ii) positive ISI correlations.

Alternative mechanisms for achieving band-pass filtering on information, that were not the subject of this thesis are for example:

- the interplay between facilitating and depressing synapses(Droste et al., 2013),
- synchronous spiking activity in networks(Sharafi et al., 2013).

A further investigation on the spectral signal transmission of linear-nonlinear-cascade (LN) neuron models based on analytical approaches for resonate-LN-cascade models seems very promising. Based on the theoretical work of Malahov (1978); Middleton et al. (1960), it would seem reasonable that a curvature analysis of the coherence function at zero frequency of these resonate-LN-cascade models (similar to the analysis performed in sec. 3) would lead to analytical insights on the information-filtering properties of LN-cascade models in the presence of subthreshold resonances.

Throughout this thesis, two measures of information filtering were utilized: i) the spectral stimulus-response coherence (SR), and ii) the response-response coherence (RR). The validity of the SR coherence function relies on the assumption that the neuron model encodes information about a time-dependent input signal linearly. This assumption was tested by the RR coherence function, which is at best, a good approximation for an upper bound of the mutual information rate. The obtained numerical results for the RR coherence function appeared plausible because RR and SR coherence function become similar in the tonic firing regime. In cases, in which the SR coherence function exhibits a peak, the corresponding RR coherence function displayed a similar peak, but less pronounced. This comparison between SR and RR coherence function leads to the conclusion, that in both regimes (linear and non-linear coding), the filtering properties of the single neuron models were qualitatively similar.

A more rigorous approach to study the spectral signal transmission in the non-linear coding regime was developed by Bernardi and Lindner (2014) based on the work of Strong et al. (1998). However, this numerical approach is more involved and was not utilized in this thesis. Future work should include these approaches to investigate the non-linear coding characteristics of the chosen neuron models.

A Richardson's integration method

A.1 Introduction

Richardson's integration method(Richardson, 2007, 2008) was developed for calculating numerically the spectra of the stochastic integrate-and-fire (IF) neuron models driven by Gaussian white noise without simulating single trajectories (Monte-Carlo methods, MC). This approach is, therefore, less computationally demanding than MC techniques and offers a powerful method to study the information filtering aspects of IF models on large model parameter sets. Here, the basic approaches of Richardson's integration method are reviewed.

The stochastic IF model driven by Gaussian white noise with intensity D is given by:

$$\frac{dV(t)}{dt} = \underbrace{\left(E(t) - V(t) + \psi(V)\right)/\tau}_{=:\mu(V,t)} + \underbrace{\sqrt{2\sigma^2/\tau}}_{=:\sqrt{2D(V,t)}}\ \eta(t), \tag{A.1}$$

where $\mu(V,t)$ is called the **drift** and $D(V,t)$ the **diffusion**. The nonlinearity function $\psi(V)$ defines the specific IF model variant, for example the exponential-integrate-and-fire neuron model is given by:

$$\psi_{\mathrm{EIF}}(V) = \Delta_T e^{(V-V_T)/\Delta_T}. \tag{A.2}$$

A.2 Calculation of the power spectrum via spike triggered rate

The associated Focker-Planck equation(Risken, 1989) (FPE):

$$\frac{\partial P(V,t)}{\partial t} = -\frac{\partial}{\partial V}\left[\mu\left(V,t\right)P(V,t)\right] + \frac{\partial^2}{\partial V^2}\left[D(V,t)P(V,t)\right]. \tag{A.3}$$

One can define a probability flux $J(V,t)$ as follows:

$$\tau J(V,t) = \left(E(t) - V(t) + \psi(V)\right)P(V,t) - \sigma^2\frac{\partial P}{\partial V}, \tag{A.4}$$

with the following **boundary values**:

$$J(V_{\mathrm{th}}, t) = r(t),\ J(V_{\mathrm{lb}}, t) = 0, \tag{A.5}$$

where V_{th} denotes the membrane threshold voltage and V_{lb} an appropriate lower bound of the membrane voltage, at which $P(V_{lb}, t) \approx 0$.

The flux satisifes the following time-dependent continuity equation:

$$-\frac{\partial J(V,t)}{\partial V} = \frac{\partial P(V,t)}{\partial t} + \rho(t)\delta(V - V_{\mathrm{th}}) - \rho(t - \tau_{\mathrm{r}})\delta(V - V_{\mathrm{re}}) - \delta(t - t_0)\delta(V - V_0), \tag{A.6}$$

where τ_{r} denotes the absolute refractory period and V_{re} the reset value after threshold crossing. Taking the Fourier transform (denoted by a tilde) of the probability function $P(V,t)$, the Fokker-Planck equation can be written as:

$$-\frac{\partial \tilde{P}(V,t)}{\partial V} = \frac{1}{\sigma^2}\left(\tau \tilde{J}(V,t) + (V - E_0 - \psi(V))\,\tilde{P}(V,t)\right). \tag{A.7}$$

Using the following decomposition-Ansatz for the Fourier transform of the probability function $\tilde{P}(V,t)$ as well as the probability flux $\tilde{J}(V,t)$:

$$\tilde{P} = \tilde{\rho}\tilde{p}_\rho + \tilde{p}_i,\ \ \tilde{J} = \tilde{\rho}\tilde{j}_\rho + \tilde{j}_i, \tag{A.8}$$

one can rewrite the continuity equation Eq.(A.6) and the FPE Eq.(A.7) as:

$$-\frac{\partial \tilde{j}_\rho}{\partial V} = i\omega\tilde{p}_f(\omega) + \delta(V - V_{\mathrm{th}}) - e^{-i\omega\tau_{\mathrm{r}}}\delta(V - V_{\mathrm{re}}), \tag{A.9}$$

$$-\frac{\partial \tilde{p}_\rho}{\partial V} = \frac{1}{\sigma^2}\left(\tau\tilde{j}_\rho(\omega) + (V - E_0 - \psi(V))\,\tilde{p}_\rho(\omega)\right), \tag{A.10}$$

where $\tilde{\rho}$ is the Fourier transform of the spike triggered rate (STR). The initial conditions (for fixed frequency ω) are:

$$\tilde{p}_\rho(V_{th}, \omega) = 0,\ \ \tilde{j}_\rho(V_{th}, \omega) = 1. \tag{A.11}$$

The associated **initial value problem** for $\tilde{j}_i(V)$ and $\tilde{p}_i(v)$ reads:

$$-\frac{\partial \tilde{j}_i}{\partial V} = i\omega\tilde{p}_i + e^{-i\omega t_i}\delta(V - V_i), \tag{A.12}$$

and

$$-\frac{\partial \tilde{p}_i}{\partial V} = \frac{1}{\sigma^2}\left(\tau\tilde{j}_i(\omega) + (V - E_0 - \psi(V))\,\tilde{p}_i(\omega)\right), \tag{A.13}$$

with the **inital value problem** (for fixed frequency ω):

$$\tilde{p}_i(V_{\mathrm{th}}, \omega) = 0,\ \ \tilde{j}_i(V_{\mathrm{th}}, \omega) = 0. \tag{A.14}$$

The Fourier transform of STR can be written as follows:

$$\tilde{\rho}(\omega) = -\frac{\tilde{j}_i(V_{\rm lb}, \omega)}{\tilde{j}_\rho(V_{\rm lb}, \omega)}. \tag{A.15}$$

The spike train power spectrum $S_{\rm x,x}(\omega)$ can be obtained by the spike train autocorrelation function $C_{\rm x,x}(\tau)$:

$$C_{\rm x,x}(\tau) =< x(t)x(t+\tau) >= r_0\delta(\tau) + r_0\rho(|\tau|), \tag{A.16}$$

and the help of the Wiener-Khinchin theorem(Gardiner, 1985; Risken, 1989):

$$S_{\rm x,x}(\omega) = \int_{-\infty}^{+\infty} d\tau e^{-i\omega\tau} C_{\rm x,x}(\tau), \tag{A.17}$$

and reads (renewal model):

$$S_{\rm x,x}(\omega) = r_0 \left(1 + \tilde{\rho}(\omega) + \tilde{\rho}^*(\omega)\right). \tag{A.18}$$

Therefore, integrating Eq.(A.9),Eq.(A.10),Eq.(A.12),Eq.(A.13) using inital values Eq.(A.11),Eq.(A.14) from $V_{\rm th}$ to an appropriate $V_{\rm lb}$ and employing Eq.(A.15) and Eq.(A.18) leads to a numerical value of the spike train power spectrum for fixed frequency ω. By repeating this inital value problem for frequency $\omega + d\omega$, one can sample numerically the power spectrum of the spiketrain at a finite frequency grid. Similarly procedures can be derived to calculate the cross-spectrum between in input signal and the spike train.

B Information filtering effects of positive ISI correlations

B.1 Raw and standardized moments of the inverse Gaussian ISI density

One can define the ISI standardized moments of a given distribution by its raw moments $\mu_n = \langle T^n \rangle$. In this study I have used in Eq.(3.27) and Eq.(3.33) the first standardized moments: squared coefficient of variation ($\beta_0 = C_{\rm V}^2$), the skewness (β_1) and the kurtosis (β_2) of the ISI distribution as follows:

$$\begin{aligned}
\beta_0 &= C_{\rm V}^2 = \frac{\mu_2}{\mu_1^2} - 1, \\
\beta_1 &= \frac{\mu_3 - 3\mu_1\left(\mu_2 - \mu_1^2\right) - \mu_1^3}{\left(\mu_2 - \mu_1^2\right)^{3/2}}, \\
\beta_2 &= \frac{\mu_4 - 4\mu_1\mu_3 + 6\mu_1^2\mu_2 - 3\mu_1^4}{\mu_1^4 - 2\mu_1^2\mu_2 + \mu_2^2}.
\end{aligned} \tag{B.1}$$

Due to the importance (see Eq.(3.27) and Eq.(3.33)) of the raw moments (μ_n) of an inverse Gaussian (IG) distribution (given in Eq.(3.5)) in this study, I state here its raw moments as well as its standardized moments β_0, β_1 and β_2 for sake of completeness. The first four *raw* moments $\mu_1, \cdots, \mu_4$ reads:

$$\begin{aligned}
\mu_{1,\rm IG} &= 1/r_0, \\
\mu_{2,\rm IG} &= \left(1 + C_{\rm V}^2\right)/r_0^2, \\
\mu_{3,\rm IG} &= \left(1 + 3C_{\rm V}^2 + 3C_{\rm V}^4\right)/r_0^3, \\
\mu_{4,\rm IG} &= \left(1 + 3C_{\rm V}^2 + 15C_{\rm V}^4 + 15C_{\rm V}^6\right)/r_0^4.
\end{aligned} \tag{B.2}$$

Using the above mentioned raw moments, one can express the skewness and kurtosis of the IG ISI density in terms of its $C_{\rm V}$ as:

$$\beta_{1,\rm IG} = 3C_{\rm V}, \quad \beta_{2,\rm IG} = 3 + C_{\rm V}^2. \tag{B.3}$$

B.2 Approximation of the coherence function at low frequencies

Here, we want to approximate the coherence function of the renewal/non-renewal model variant in the following way:

$$C(f) \approx C(0) + C^{(2)}(0)\frac{f^2}{2} + C^{(4)}(0)\frac{f^4}{24}, \tag{B.4}$$

in which $C(0), C^{(2)}(0), C^{(4)}(0)$ are frequency independent coefficients. Thus, the derivative of the quartic expansion of the coherence at zero frequencies is given by:

$$C'(f) \approx C^{(2)}(0)f + C^{(4)}(0)\frac{f^3}{6} = f\left(C^{(2)}(0) + C^{(4)}(0)\frac{f^2}{6}\right). \tag{B.5}$$

A condition for a global maximum of the coherence function is that the derivative of the coherence function with respect to the frequency is zero at the resonance frequency $\hat{f}$, i.e.

$$C'(\hat{f}) = \hat{f}\left(C^{(2)}(0) + C^{(4)}(0)\frac{\hat{f}^2}{6}\right) = 0. \tag{B.6}$$

We are interested solely in real, non-zero and positive resonance frequencies and thus, the only non-trivial solution of Eq.(B.6) is given by:

$$\hat{f} = \sqrt{-6\frac{C^{(2)}(0)}{C^{(4)}(0)}}. \tag{B.7}$$

We already know that a *first* condition of band-pass filtering of information is that $C^{(2)}(0) \geq 0$ (i.e. positive curvature condition). Therefore, in order to obtain a positive resonance frequency $\hat{f}$ (see Eq.(B.7)) of the coherence function we obtain a second condition of band-pass filtering: $C^{(4)}(0) \leq 0$. The quality factor (see Eq.(1.19)) of the coherence function can be approximated as:

$$Q_{\mathrm{C}} = \frac{C(f_{res})}{C(f=0)} = 1 - \frac{3}{2}\frac{C^{(2)}(0)^2}{C(0)C^{(4)}(0)}. \tag{B.8}$$

We note here that the quality Q_{C} of the coherence function is greater than one if the first and second band-pass filter condition (i.e $C^{(4)}(0) \leq 0 \leq C^{(2)}(0)$) holds true.

B.3 Analytics & numerics for triangular ISI distributions

B.3.1 Moments of the triangular ISI density

Although mathematically more elegant than the inverse Gaussian distributions for thresholds and resets, the resulting ISI density is less realistic than the inverse Gaussian density

and has never been observed in experiments so far by my knowledge. However, it is of interest as an analytical stochastic neuron model because it offers closed form expressions of the power spectrum of the spontaneous spiking activity.

If one samples the magnitude of the threshold and reset values independently from each other from a uniform distribution in the range $[T_-, T_+]$ one obtains a triangular ISI distribution[1] of the form: (Lindner, 2005):

$$F_{1,0}(T) = \frac{1}{16\pi^2\beta^2} \begin{cases} T - 2T_-, & 2T_- < T < \frac{\Theta_0}{\mu}, \\ 2T_+ - T, & \frac{\Theta_0}{\mu} < T < 2T_+, \\ 0, & \text{else.} \end{cases} \tag{B.9}$$

With the abbreviations $T_\pm = \frac{\Theta_0/2 \pm D}{\mu}$. Carrying out the corresponding integrals of the ISI density (Eq.(B.9)) multiplied with monomials T^n analytically, I obtain a closed form expression for the n-th moments ($\mu_n :=< T^n >$) of the triangular ISI distribution as follows:

$$\mu_{\text{n,tria}} = \left(\frac{\Theta_0}{\mu}\right)^2 \frac{(2T_-)^n \left(1 - \frac{2D}{\Theta_0}\right)^2 + (2T_+)^n \left(1 + \frac{2D}{\Theta_0}\right)^2 - 2\left(\frac{\Theta_0}{\mu}\right)^n}{(n+1)(n+2)}. \tag{B.10}$$

Using this expression for $n = 1$ and $n = 2$, I can express the first two moments of the ISI density, namely the firing rate r_0 and CV, in the compact form:

$$\begin{aligned} 1/r_0 &= \frac{\Theta_0}{\mu}, \\ C_V^2 &= \frac{2}{3}\left(\frac{D}{\Theta_0}\right)^2. \end{aligned} \tag{B.11}$$

Thus, one can easily reparametrize Eq.(B.9) in terms of firing rate r_0 and coefficient of variation C_V of the spike train of the spontaneous activity by:

$$\begin{aligned} D &= \sqrt{\frac{3}{2}} C_V \Theta_0, \\ \mu &= r_0 C_V^2. \end{aligned} \tag{B.12}$$

By using this reparameterization (Eq.(B.12)), I can express the n-th moments of the triangular ISI distribution in terms of its first two moments (rate and CV) as follows:

$$\mu_{\text{n,tri}} = \frac{\left(1 - \sqrt{6}C_V\right)^n \left(1 - 2C_V\left(\sqrt{6} - 3C_V\right)\right) + \left(1 + \sqrt{6}C_V\right)^n \left(1 + 2C_V\left(\sqrt{6} + 3C_V\right)\right)}{(n+1)(n+2)\, r_0^{n+2}}. \tag{B.13}$$

[1] This is basically due to the fact that the convolution of two uniform distributions results in a triangular distribution (see Eq.(3.11) for $n = 1$).

B.3.2 Exact spontaneous power spectrum (max. correlations)

Using a uniform distribution for threshold and reset voltage, the power spectrum of the spontaneous activity (without signal) can be written as (Lindner, 2005):

$$S_{\mathrm{R},0}(f) = r_0 \frac{(\beta f)^4 - \sin^4(\beta f)}{(\beta f)^4 - 2(\beta f)^2 \sin^2(\beta f)\cos^2(2\pi f/r_0) + \sin^4(\beta f)}, \tag{B.14}$$

with the abbreviation $\beta = 2\pi D/\mu$.

As described above, the special model variant in which the reset value is the mirrored version of the preceding threshold value leads to positive correlations between subsequent ISIs of one-half. Using a uniform distribution of thresholds as well as the fact that the ISI distribution $F_{1,0}(T)$ of the renewal variant is a triangular distribution, the spontaneous power spectrum (in the absence of an external signal) can be written as:

$$S_{\mathrm{NR},0}(f) = r_0 \left(1 + \frac{2\,\mathrm{sinc}^2(\beta f)\left(\cos(2\pi f/r_0) - \mathrm{sinc}(2\beta f)\right)}{1 + \mathrm{sinc}^2(2\beta f) - 2\,\mathrm{sinc}^2(2\beta f)\cos(2\pi f/r_0)}\right), \tag{B.15}$$

where I have used $\beta = 2\pi D/\mu$ (as in the renewal case) and $\mathrm{sinc}(x) = \sin(x)/x$.

B.3.3 The effects of threshold and reset variability

As I have shown in sec. B.3.3, the intrinsic neuronal variability due to the threshold and reset fluctuations plays an important role in establishing a band-pass filtering effect on information in the more realistic model by using an inverse Gaussian distribution for threshold and reset values. Here, I will consider the same setup, but by using the less realistic triangular ISI density, i.e. a uniform distribution of threshold and resets.

Fig. B.1 display the meta statistics of the numerical analysis of the two model variants (renewal, non-renewal) by using a uniform distribution of threshold and reset values, which lead to a triangular ISI distribution. The results shown in Fig. B.1 are very similar to the investigation above, where I have used the inverse Gaussian density (see Fig. 3.12). Fig. B.1a, e show the coherence quality with respect to the CV of the evoked activity for the two model variants (renewal, non-renewal with max. positive ISI correlations of one-half). As we have seen in Fig. 3.12 in sec. B.3.3, the renewal model variant acts within this parameter regime ($0 \leq CV \leq 0.5$) as a low pass filter on information. This phenomenon is manifested by a coherence quality of one (see Fig. B.1a).

In contrast to the renewal model variant, the non-renewal variant can act as a band pass filter on information, i.e. coherence quality values larger than one (see Fig. B.1e). As pointed out in sec. 3.5.1 and Fig. 3.12, the coherence quality of the non-renewal version reaches a maximum at a rather regular firing activity ($CV \approx 0.2$) for weak signals (red data points in Fig. B.1). For moderate and strong signals (see blue and magenta data points in Fig. B.1), the maximum of the coherence quality with respect to the evoked CV becomes less pronounced (compare red, blue, magenta, and black data points in Fig. B.1).

As pointed out earlier, the maximum of the coherence function of the non-renewal

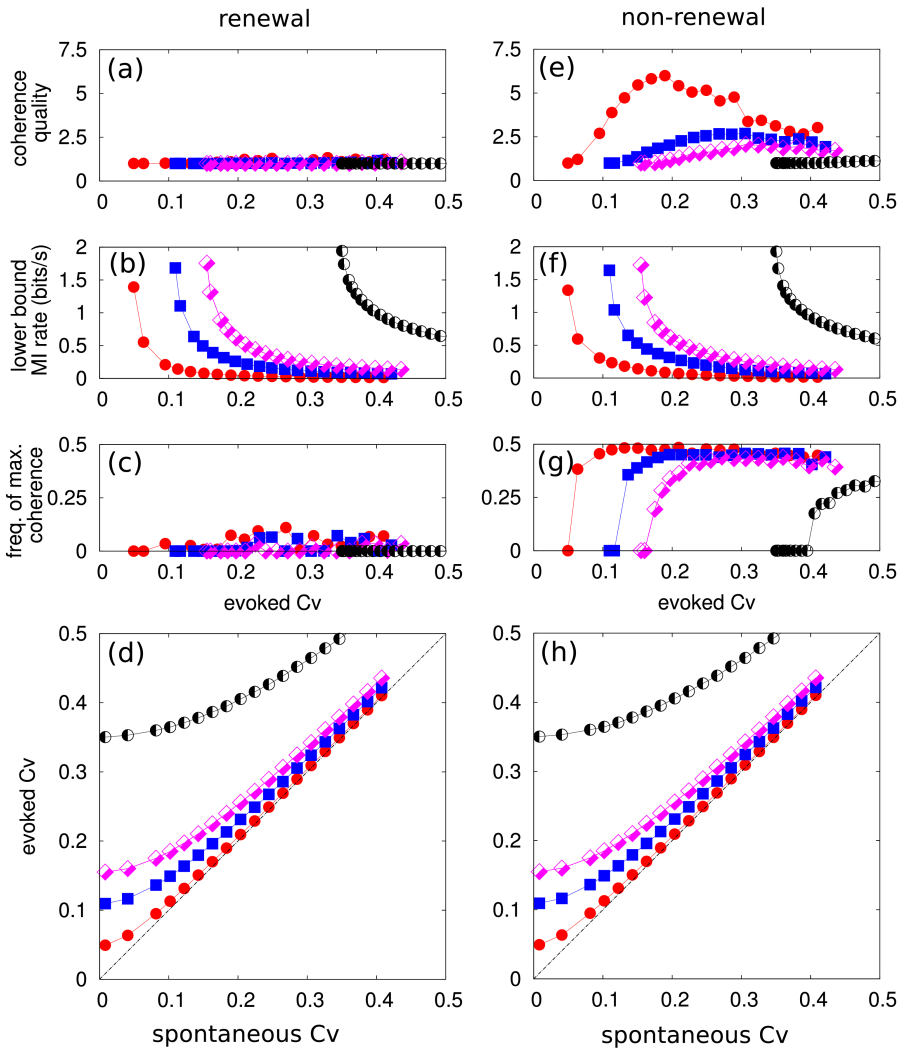

Figure B.1: Characteristics of the information transmission and filtering as functions of spiking variability for renewal model (left) and non-renewal model (right) using a uniform distribution of thresholds and resets. Shown are: the frequency at which the coherence has its global maximum (a, e), quality of coherence, Eq.(1.19) (b, f), and lower bound on the mutual information rate, Eq.(1.12) (c, g). All statistics are determined from simulation data and plotted vs evoked coefficient of variation (CV in the presence of broadband stimulus), which is also measured in simulations. The evoked CV was varied by changing the CV of the spontaneous activity, a parameter that enters the model through the distributions of threshold and reset, Eq.(3.6). The evoked CV is shown as a function of spontaneous CV in (d, h). All results were obtained from numerical Monte-Carlo simulations of the models.

version is close to half the firing rate (here $r_0 = 1$) of the spontaneous activity (see Fig. B.1g). The renewal model version leads to coherence function, which attains its maximum value at zero frequency. This indicates a quality factor of one, and consequently, a low pass filter on information (see Fig. B.1c). Although the band-pass filter effect (in the non-renewal variant, see Fig. B.1e) is very prominent for weak signals and a rather regular firing regime, the mutual information rate is very small within this parameter regime (see Fig. B.1b, f). As expected, the mutual information rate decreases with increasing variability of the evoked activity (see Fig. B.1b, f).

We conclude here, that the numerical results suggest that the presence of positive correlations between neighboring ISIs, although very weak, establishes a band pass filter on information. This filtering effect is most pronounced for pronounced ISI correlations (here the correlation between adjacent ISIS are restricted to the range $\rho_1 = [0; 0.5]$ via construction because the threshold and reset distribution should not overlap). The results obtained by using a triangular ISI density Fig. B.1, rather than an inverse Gaussian ISI density, suggest that the specific choice of threshold and reset distribution does not play a significant role in establishing a frequency-dependent signal transmission, i.e. a band-pass filter on information.

This filtering phenomenon is very similar to the filtering property of the more realistic model (see Fig. 3.12 in sec. 3.5.1), in which an Inverse Gaussian ISI distribution was used. Thus, the band-pass filtering characteristic on information is robust under variations of the shape of the ISI distribution.

C Information filtering in resonator neuron models

C.1 Numerical values of the model parameter sets

Here, the three parameter sets (resonator cartoon, stellate cell, and pyramidal cell) for the resonate-and-fire neuron model, as discussed in sec. 4, are presented.

Table C.1: Parameters of the neuron model for three distinct regimes (for stellate and pyramidal cells, R, R_L, L, C adopted from Schreiber et al. (2004)) and input and noise parameters (below the dashed line).

parameter	resonator cartoon	stellate cell (EC-II)	pyramidal cell (EC-III)	parameter description
R $[M\Omega]$	51.6	56.7	69.9	membrane resistance
R_{L} $[M\Omega]$	4.4	46.1	34661.0	coil resistance
L $[MH]$	0.97	1.26	173.0	coil inductance
C $[pF]$	310	310	310	membrane capacitance
V_{thresh} $[mV]$	-59.2	-59.5	-60.5	voltage threshold for spiking
V_{resting} $[mV]$	-63.5	-63.5	-63.5	voltage steady state
V_{reset} $[mV]$	-75.0	-75.0	-75.0	voltage reset after spiking
τ_{abs} $[ms]$	50	50	50	absolute refractory period
$I_0[nA]$	4.1017	0.65	0.236	DC-input
D $[10^{-6}(nA/s)^2]$	6.40	6.97	4.44	strength of intrinsic current noise
D_{OU} $[10^{-5}(nA/s)^2]$	5.18	5.53	2.60	strength of OU current input

C.2 Gradually changing the impedance quality

In order to differentiate gradually between resonators and integrators, I have implemented a numerical scheme, which permits to tune the impedance quality gradually. This will be of great importance, because the impedance quality in the described three parameter sets (resonator cartoon, stellate cell, pyramidal cell, see Tab. C.1 in sec. 4) is fixed, and does not dependent on the external parameters (like baseline current or signal strength). Thus, in order to reveal the general impact of subthreshold resonances on the suprathreshold signal transmission, one has to be able to fine tune the quality of the impedance function at fixed resonance frequency. I will use the following experimentally motivated constraints under variation of the impedance resonance Q_{ZAP}:

a) natural frequency of the MPOs is smaller than resonance frequency of the impedance (see Fig. 10 in Erchova et al. (2004)), here I use $\frac{f_{\mathrm{nat}}}{f_{\mathrm{res}}} \approx 0.8$,

b) band-with of the impedance resonance is proportional to the impedance resonance freq. (see Fig. 7B in Erchova et al. (2004)).

I have implemented a numerical scheme to parameterize the impedance quality gradually, and respects the above given constraints. It turned out that the quality of the impedance function is is most sensitive to variations of the resistance of the inductor R_{L} (by respecting the above-stated constraints). Additionally to the constraints (which are respected by the stellate cell parameter set), the resonator cartoon parameter set was chosen according to the above-given constraints, and can be therefore referred as 'biologically plausible' resonator cartoon (see Fig. C.1). In Fig. C.1, an example parameterization manifold (iso-resonance-frequency manifold) is shown for a resonance frequency of $f_{\mathrm{res}} = 9.5$ Hz (see Tab. C.1). The used standard parameter set for resonator cartoon and stellate cell are marked on the parametrization manifold (see blue and red data points in Fig. C.1).Fig. C.1c shows that an increase of the inductor resistance R_{L} leads to a monotonic increase of the damping factor and consequently, to a monotonic decrease of the impedance quality (shown in Fig. C.1d). The dependency between inductor resistance R_{L} and membrane resistance R as well as the inductance L are non-monotonic in nature (see Fig. C.1a,b). In sec. 4.4.1, we will use three different iso-resonance-frequency parameterization manifolds ($f_{\mathrm{res}} = 5$ Hz, $f_{\mathrm{res}} = 9.5$ Hz, and $f_{\mathrm{res}} = 15$ Hz) to investigate the effects of subthreshold resonances on suprathreshold frequency-dependent signal transmission (information filtering) by employing extensive numerical Monte-Carlo simulations (75.000 different parameter sets) of the spiking RF neuron model ranging from very regular to very irregular spiking activity (controlled by the baseline current). This leads to the observation of a trade-off between the quality factor of the bandpass filter on information and the mutual information rate (lower bound) and reveals the relationship between the coherence quality (spiking activity) and the impedance quality (purely subthreshold response).

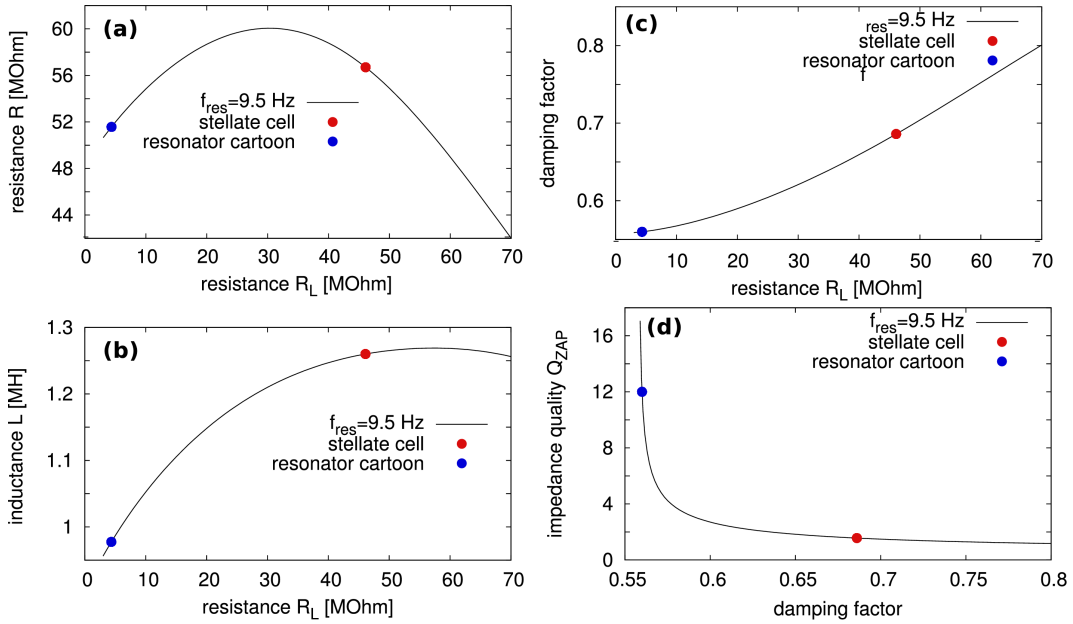

Figure C.1: Parameter sets yielding the same resonance frequency of the impedance in the linear, subthreshold dynamics. By fixing the resonance frequency and changing the resistance of the inductor R_L, one can systematically vary the impedance quality. This way gradual transitions from resonators to integrators (including the physiological parameter set of the stellate cell, red data point) were obtained. a–c Lines of equal resonance frequency in subspaces of parameters of the subthreshold dynamics of the RF model (resistance R versus the resistance of the inductor R_L, inductance L, and the damping factor, respectively). d Impedance quality decreases with an increasing damping factor

D Information filtering in linear-nonlinear cascades

D.1 Frequently used functions

Here, we will list frequently used special function in order to derive analytical expressions for the spectra of the integrate-LN-cascade in sec. 5.5. A complete list of definitions can be found in Abramowitz and Stegun (1970) for example.

D.1.1 Pochhammer symbols

The Pochhammer symbols are defined as(Abramowitz and Stegun, 1970):

$$(x)_n = x(x-1)(x-2)...(x-n+1). \tag{D.1}$$

D.1.2 Hermite polynomials

In physics textbooks, one often encounters (eigenfunctions of the quantum harmonic oscillator) the so-called **physicist's Hermite polynomials**, which are defined as(Abramowitz and Stegun, 1970):

$$H_n(x) = (-1)^n \, e^{x^2} \, \frac{d^n}{dx^n} e^{-x^2}. \tag{D.2}$$

The **probabilist's Hermite polynomials** are can be written as(Abramowitz and Stegun, 1970):

$$H_{e_n}(x) = (-1)^n \, e^{x^2/2} \frac{d^n}{dx^n} e^{-x^2/2}. \tag{D.3}$$

probabilist's and physicist's Hermite polynomials are related via the following equation:

$$H_n(x) = 2^{n/2} H_{e_n}(\sqrt{2}x). \tag{D.4}$$

In sec. 5.3, we made use of the so-called probabilist's Hermite polynomials. The first

five probabilist's Hermite polynomials are as follows:

$$H_{e_0}(x) = 1, \tag{D.5a}$$
$$H_{e_1}(x) = x, \tag{D.5b}$$
$$H_{e_2}(x) = x^2 - 1, \tag{D.5c}$$
$$H_{e_3}(x) = x^3 - 3x, \tag{D.5d}$$
$$H_{e_4}(x) = x^4 - 6x^2 + 3. \tag{D.5e}$$
$$\tag{D.5f}$$

D.1.3 Gamma function

The Gamma function can be expressed as(Abramowitz and Stegun, 1970):

$$\Gamma(y) = \int_0^\infty x^{y-1} e^{-x} dx. \tag{D.6}$$

D.1.4 Error functions

The error function is defined as(Abramowitz and Stegun, 1970):

$$\mathrm{erf}(x) = \frac{2}{\sqrt{\pi}} \int_0^x e^{-t^2} dt. \tag{D.7}$$

The associated complementary error function can be expressed as(Abramowitz and Stegun, 1970)

$$\mathrm{erfc}(x) = 1 - \mathrm{erf}(x). \tag{D.8}$$

D.1.5 Hypergeometric functions

The generalized hypergeometric function is defined as:

$${}_pF_q(a_1, ..., a_p; b_1, ..., b_q; x) = \sum_{k=0}^{\infty} \frac{(a_1)_k (a_2)_k ... (a_p)_k}{(b_1)_k (b_2)_k ... (b_q)_k} \frac{x^k}{k!}. \tag{D.9}$$

The associated regularized hypergeometric function can be obtained via(Abramowitz and Stegun, 1970):

$${}_p\tilde{F}_q(a_1, ..., a_p; b_1, ..., b_q; x) = \frac{{}_pF_q(a_1, ..., a_p; b_1, ..., b_q; x)}{\Gamma(b_1) ... \Gamma(b_q)}. \tag{D.10}$$

D.1.6 Incomplete beta function

The definition of the incomplete beta function reads:

$$\begin{aligned} B\left(z;a,b\right) = & \int_0^z u^{a-1}(1-u)^{b-1}du \\ = & z^a\Gamma\left(a\right){}_2\tilde{F}_1\left(a,1-b;a+1;z\right). \end{aligned} \tag{D.11}$$

D.2 Generalized expression

D.2.1 Cross-correlation

The expression Eq.(5.11b) for the cross-correlation between a current input signal $s(t)$ and the distorted output $z(t) = g(x(t) + s(t))$ can be further generalized for arbitrary Gaussian stochastic processes (non-zero mean and non-unit variance) to:

$$r_{\mathrm{z,s}}(\tau) = \left(\frac{\sigma_s\mu_s}{\sqrt{2\pi}}\int_{-\infty}^{\infty} g(x)e^{-\frac{(x-\mu_x)^2}{2\sigma_x^2}}\right) + \left(\frac{\sigma_s^2}{\sqrt{2\pi}\sigma_x}\int_{-\infty}^{\infty}(x-\mu_x)g(x)e^{-\frac{(x-\mu_x)^2}{2\sigma_x^2}}\right) r_{\mathrm{x,s}}(\tau), \tag{D.12}$$

where $\sigma_{x,s}$ denotes the standard deviation of the stochastic Gaussian process x or s. The respective mean values are denoted by $\mu_{x,s}$. One can infer from Eq.(D.12) that a non-zero input signal causes a constant offset in the cross-correlation.

Bibliography

B. Abraham and N. Balakrishna. Inverse Gaussian autoregressive models. *J. Time Ser. Anal.*, 20:605, 1999.

M. Abramowitz and I. A. Stegun. *Handbook of Mathematical Functions.* Dover, New York, 1970.

E. D. Adrian. The impulses produced by sensory nerve endings: Part I. *J. Physiol.*, 61: 49, 1926.

E. D. Adrian and Y. Zotterman. The impulses produced by sensory nerve-endings: Part II. the response of a Single End-Organ. *J. Physiol.*, 61:151, 1926a.

E. D. Adrian and Y. Zotterman. The impulses produced by sensory nerve endings: Part III. impulses set up by Touch and Pressure. *J. Physiol.*, 61:465, 1926b.

C. D. Aizenman, C. J. Akerman, K. R. Jensen, and H. T. Cline. Visually driven regulation of intrinsic neuronal excitability improves stimulus detection in vivo. *Neuron*, 39:831, 2003.

A. Alonso and R. R. Llinás. Subthreshold Na^+-dependent theta-like rhythmicity in stellate cells of entorhinal cortex layer II. *Nature*, 342:175, 1989.

O. Avila-Akerberg and M. J. Chacron. Nonrenewal spike train statistics: causes and consequences on neural coding. *Exp. Brain Res.*, 210:353, 2011.

R. Azouz and C. M. Gray. Cellular mechanisms contributing to response variability of cortical neurons in vivo. *J. Neurosci.*, 19:2209, 1999.

R. Azouz and C. M. Gray. Dynamic spike threshold reveals a mechanism for synaptic coincidence detection in cortical neurons in vivo. *Proc. Nat. Acad. Sci.*, 97:8110, 2000.

R. Baddeley, L. Abbott, M. Booth, F. Sengpiel, T. Freeman, E. Wakeman, and E. Rolls. Responses of neurons in primary and inferior temporal visual cortices to natural scenes. *Proc. R. Soc. Lond. B*, 264:1775, 1997.

L. Badel, S. Lefort, T. K. Berger, C. C. H. Petersen, W. Gerstner, and M. J. E. Richardson. Extracting non-linear integrate-and-fire models from experimental data using dynamic I-V curves. *Biol. Cybern.*, 99:361, 2008a.

L. Badel, S. Lefort, R. Brette, C. C. H. Petersen, W. Gerstner, and M. J. E. Richardson. Dynamic I-V curves are reliable predictors of naturalistic pyramidal-neuron voltage traces. *J. Neurophysiol.*, 99:656, 2008b.

L. Badel, S. Lefort, R. Brette, C. C.H. Petersen, W. Gerstner, M. J. E. Richardson, et al. Dynamic IV curves are reliable predictors of naturalistic pyramidal-neuron voltage traces. *J. Neurophysiol.*, 99:656, 2008c.

D. Baecker. *Form und Formen der Kommunikation*. Suhrkamp Frankfurt am Main, 2005.

P. Banelli. Non-linear transformations of Gaussians and Gaussian-mixtures with implications on estimation and information theory. *arXiv preprint arXiv:1111.5950*, 2011.

C. Bauermeister, T. Schwalger, D. Russell, A. B. Neiman, and B. Lindner. Characteristic effects of stochastic oscillatory forcing on neural firing: Analytical theory and comparison to paddlefish electroreceptor data. *PLoS Comput. Biol.*, 9:e1003170, 2013.

R. Baum. The correlation function of smoothly limited Gaussian noise. *IRE T. Inform. Theor.*, 3:193–197, 1957.

P. Bedenbaugh and G. L. Gerstein. Rectification of correlation by a sigmoid nonlinearity. *Biol. Cybern.*, 70:219–225, 1994.

D. Bernardi and B. Lindner. A Frequency-Resolved Mutual Information Rate and its Application to Neural Systems. *J. Neurophysiol.*, 113:1342, 2014.

J. Bernstein. Über den zeitlichen Verlauf der negativen Schwankung des Nervenstroms. *Pflueg. Arch. Eur. J. Phy.*, 1:173, 1868.

J. Bernstein. Untersuchungen zur Thermodynamik der bioelektrischen Ströme. *Pflueg. Arch. Eur. J. Phy.*, 92:521, 1902.

L. Boltzmann. Weitere Studien ueber das Waermegleichgewicht unter Gasmolekuelen. *Wien. Ber*, 66, 1872.

L. Boltzmann. Further studies on the thermal equilibrium of gas molecules. *The Kinetic Theory Of Gases. Series: History of Modern Physical Sciences*, 1:262–349, 2003.

A. Borst and F. Theunissen. Information theory and neural coding. *Nat. Neurosci.*, 2: 947, 1999.

H. P. Bowditch. On the peculiarities of excitability which the fibres of cardiac muscle. *Leipzig: Physiological Institute*, 1871.

R. Brette and W. Gerstner. Adaptive exponential integrate-and-fire model as an effective description of neuronal activity. *J. Neurophysiol.*, 94:3637, 2005.

N. Brunel and V. Hakim. Fast global oscillations in networks of integrate-and-fire neurons with low firing rates. *Neural Comput.*, 11:1621, 1999.

N. Brunel, V. Hakim, and M. J. E. Richardson. Firing-rate resonance in a generalized integrate-and-fire neuron with subthreshold resonance. *Phys. Rev. E*, 67:051916, 2003.

A. N. Burkitt. A review of the integrate-and-fire neuron model: I. homogeneous synaptic input. *Biol. Cyber.*, 95:1, 2006a.

A. N. Burkitt. A review of the integrate-and-fire neuron model: II. inhomogeneous synaptic input and network properties. *Biol. Cyber.*, 95:97, 2006b.

J. J. Bussgang. *Crosscorrelation functions of amplitude-distorted Gaussian signals*. Research Laboratory of Electronics, Massachusetts Institute of Technology, 1952.

G. Buzsáki. *Rhythms of the Brain*. Oxford University Press, New York, Oxford, 2006.

G. Buzsáki and A. Draguhn. Neural oscillations in cortical networks. *Science*, 304:1926, 2004.

W. H. Calvin. Three modes of repetitive firing and the role of threshold time course between spikes. *Brain Res.*, 69:341, 1974.

H. Câteau and A. D. Reyes. Relation between single neuron and population spiking statistics and effects on network activity. *Phys. Rev. Lett.*, 96:058101, 2006.

M. J. Chacron. Nonlinear information processing in a model sensory system. *J. Neurophysiol.*, 95:2933, 2006.

M. J. Chacron, A. Longtin, M. St-Hilaire, and L. Maler. Suprathreshold stochastic firing dynamics with memory in P-type electroreceptors. *Phys. Rev. Lett.*, 85:1576, 2000.

M. J. Chacron, B. Doiron, L. Maler, A. Longtin, and J. Bastian. Non-classical receptive field mediates switch in a sensory neuron's frequency tuning. *Nature*, 423:77, 2003.

M. J. Chacron, L. Maler, and J. Bastian. Electroreceptor neuron dynamics shape information transmission. *Nat.Neurosci.*, 8:673, 2005.

M. J. Chacron, B. Lindner, and A. Longtin. Threshold fatigue and information transfer. *J. Comput. Neurosci.*, 23:301, 2007.

R. Chhikara. *The Inverse Gaussian Distribution: Theory: Methodology, and Applications*, volume 95. CRC Press, Boca Raton, Florida, 1988.

E. J. Chichilnisky. A simple white noise analysis of neuronal light responses. *Network-Comp. Neural.*, 12:199–213, 2001.

K. S. Cole and R. F. Baker. Longitudinal impedance of the squid giant axon. *J. Gen. Physiol.*, 24:771, 1941.

M. Costandi. The Discovery Of The Neuron, 2006. URL `https://neurophilosophy.wordpress.com/2006/08/29/the-discovery-of-the-neuron/`.

T. Cover and J. Thomas. *Elements of Information Theory*. Wiley, New-York, 1991.

D. R. Cox. *Renewal Theory*. Methuen, London, 1962.

D. R. Cox and V. Isham. *Point Processes*. Chapman and Hall, London, 1980.

D. A. Darling and A. J. F. Siegert. The 1st passage problem for a continuous Markov process. *Ann. Math. Stat.*, 24:624, 1953.

W. B. Davenport. Signal-to-Noise Ratios in Band-Pass Limiters. *J. Appl. Phys.*, 24: 720–727, 1953.

P. J. W. Debye, W. Nernst, M. Smoluchowski, A. Sommerfeld, and H. A. Lorentz. *Vorträge über die kinetische Theorie der Materie und der Elektrizität: gehalten in Göttingen auf Einladung der Kommission der Wolfskehlstiftung*. BG Teubner, Leipzig, 1914.

A. Destexhe and M. Rudolph-Lilith. *Neuronal noise*, volume 8. Springer US, New York, 2012.

A. D. Dorval. The rhythmic consequences of ion channel stochasticity. *Neuroscientist*, 12:442, 2006.

A. D. Dorval and J. A. White. Channel noise is essential for perithreshold oscillations in entorhinal stellate neurons. *J. Neurosci.*, 25:10025, 2005.

F. Droste, T. Schwalger, and B. Lindner. Interplay of two signals in a neuron with short-term synaptic plasticity. *Front. Comp. Neurosci.*, 7:86, 2013.

A. K. Engel, P. König, and T. B. Schillen. Why does the cortex oscillate? *Curr. Biol.*, 2:332, 1992.

T. A. Engel, L. Schimansky-Geier, A. V. M. Herz, S. Schreiber, and I. Erchova. Subthreshold membrane-potential resonances shape spike-train patterns in the entorhinal cortex. *J. Neurophysiol.*, 100:1576, 2008.

I. Erchova, G. Kreck, U. Heinemann, and A. V. Herz. Dynamics of rat entorhinal cortex layer II and III cells: characteristics of membrane potential resonance at rest predict oscillation properties near threshold. *J. Physiol.*, 560:89, 2004.

B. Ermentrout. Type I membranes, phase resetting curves, and synchrony. *Neural Comput.*, 8:979, 1996.

G. Ermentrout, R. Galán, and N. Urban. Relating neural dynamics to neural coding. *Phys. Rev. Lett.*, 99:248103, 2007.

M. A. Escabí, R. Nassiri, L. M. Miller, C. E Schreiner, and H. L. Read. The contribution of spike threshold to acoustic feature selectivity, spike information content, and information throughput. *J. Neurosci.*, 25:9524, 2005.

A. A. Faisal, J. A. White, and S. B. Laughlin. Ion-channel noise places limits on the miniaturization of the brain's wiring. *Curr. Biol.*, 15:1143, 2005.

A. A. Faisal, L. P. J. Selen, and D. M. Wolpert. Noise in the nervous system. *Nat. Rev. Neurosci.*, 9:292, 2008.

F. Farkhooi, M. F. Strube-Bloss, and M. P. Nawrot. Serial correlation in neural spike trains: Experimental evidence, stochastic modeling, and single neuron variability. *Phys. Rev. E.*, 79:021905, 2009.

R. M. Fazlollah. *An introduction to information theory*. Courier Corporation, 1961.

K. Fisch. *The contribution of spike-frequency adaptation to the variability of spike responses in a sensory neuron*. PhD thesis, LMU, 2011.

K. Fisch, T. Schwalger, B. Lindner, A. Herz, and J. Benda. Channel noise from both slow adaptation currents and fast currents is required to explain spike-response variability in a sensory neuron. *J. Neurosci.*, 32:17332, 2012.

J. L. Folks and R. S. Chhikara. The inverse Gaussian distribution and its statistical application–a review. *J. R. Stat. Soc. B*, page 263, 1978.

N. Fourcaud-Trocme, D. Hansel, C. van Vreeswijk, and N. Brunel. How spike generation mechanisms determine the neuronal response to fluctuating inputs. *J. Neurosci.*, 23: 11628, 2003.

R. F. Fox and Y. N. LU. Emergent collective behavior in large numbers of globally coupled independently stochastic ion channels. *Phys. Rev. E.*, 49:3421, 1994.

M. Frigo and S.G. Johnson. The design and implementation of FFTW3. *Proc. IEEE*, 93:216, 2005.

F. Gabbiani. Coding of time-varying signals in spike trains of linear and half-wave rectifying neurons. *Network: Comput. Neural Syst.*, 7:61, 1996.

C. W. Gardiner. *Handbook of Stochastic Methods*. Springer-Verlag, Berlin, 1985.

G. L. Gerstein and B. Mandelbrot. Random walk models for the spike activity of a single neuron. *Biophys. J.*, 4:41, 1964.

W. Gerstner and R. Naud. How good are neuron models? *Science*, 326:379, 2009.

J. W. Gibbs. *Elementary principles in statistical mechanics*. Courier Corporation, 2014.

S. Gielen, M. Krupa, and M. Zeitler. Gamma oscillations as a mechanism for selective information transmission. *Biol. Cybern.*, 103:151, 2010.

B. Gimbarzevsky, R. M. Miura, and E. Puil. Impedance profiles of peripheral and central neurons. *Can. J. Physiol. Pharm.*, 62:460, 1984.

T. Gloveli, D. Schmitz, R. M. Empson, and U. Heinemann. Frequency-dependent information flow from the entorhinal cortex to the hippocampus. *J. Neurophysiol.*, 78: 3444, 1997.

J. H. Goldwyn and E. Shea-Brown. The what and where of adding channel noise to the Hodgkin-Huxley equations. *PLoS Comput. Biol.*, 7:e1002247, 2011.

J. H. Goldwyn, N. S. Imennov, M. Famulare, and E. Shea-Brown. Stochastic differential equation models for ion channel noise in Hodgkin-Huxley neurons. *Phys. Rev. E*, 83: 041908, 2011.

B. S. Gutkin and G. B. Ermentrout. Dynamics of membrane excitability determine interspike interval variability: a link between spike generation mechanisms and cortical spike train statistics. *Neural Computation*, 10:1047, 1998.

S. Hagiwara. On the fluctuation of the interval of the rhythmic excitation. *Rep. Physiol. Sci. Inst. Tokyo Univ.*, 3:19, 1949.

J. D. Hamilton. *Time series analysis*, volume 2. Princeton University Press, Princeton, 1994.

D. Hansel and G. Mato. Existence and stability of persistent states in large neuronal networks. *Phys. Rev. Lett.*, 86:4175, 2001.

R. V. L. Hartley. Transmission of Information. *Bell Syst. Tech. J.*, 7:535, 1928.

A. M. Hattox and S. B. Nelson. Layer V neurons in mouse cortex projecting to different targets have distinct physiological properties. *J. Neurophysiol.*, 98:3330, 2007.

D. A. Henze and G. Buzsaki. Action potential threshold of hippocampal pyramidal cells in vivo is increased by recent spiking activity. *Neuroscience*, 105:121, 2001.

L. Hermann. Beiträge zur Physiologie und Physik des Nerven. *Pflü. Arch. Ges. Phys.*, 109:95–144, 1905.

A. V. M. Herz, T. Gollisch, C. K. Machens, and D. Jaeger. Modeling single-neuron dynamics and computations: a balance of detail and abstraction. *Science*, 314:80, 2006.

B. Hille. *Ion channels of excitable membranes*. Sinauer, Sunderland, 2001.

A. L. Hodgkin and A. F. Huxley. Action potentials recorded from inside a nerve fibre. *Nature*, 144:710, 1939.

A. L. Hodgkin and A. F. Huxley. The components of membrane conductance in the giant axon of Loligo. *J. Physiol.*, 116:473, 1952a.

A. L. Hodgkin and A. F. Huxley. Currents carried by sodium and potassium ions through the membrane of the giant axon of Loligo. *J. Physiol.*, 116:449, 1952b.

A. L. Hodgkin and A. F. Huxley. The dual effect of membrane potential on sodium conductance in the giant axon of Loligo. *J. Physiol.*, 116:497, 1952c.

A. L. Hodgkin and A. F. Huxley. Propagation of electrical signals along giant nerve fibres. *P.Roy. Soc. Lond. B Bio.*, page 177, 1952d.

A. L. Hodgkin and A. F. Huxley. A quantitative description of membrane current and its application to conduction and excitation in nerve. *J. Physiol.*, 117:500, 1952e.

D. Hoffmann, H. Laitko, and S. Müller-Wille. *Lexikon der bedeutenden Naturwissenschaftler*, volume 2. Spektrum Akademischer Verlag, Heidelberg, 2004.

A. Holden. *Models of the stochastic activity of neurones*, volume 12. Springer Science US, New York, 2013.

A. V. Holden. *Models of the Stochastic Activity of Neurones*. Springer-Verlag, Berlin, 1976.

J. I. Hubbard, D. Stenhouse, and R. M. Eccles. Origin of synaptic noise. *Science*, 157: 330, 1967.

B. Hutcheon and Y. Yarom. Resonance, oscillation and the intrinsic frequency preferences of neurons. *Trends in Neurosciences*, 23:216, 2000.

Y. Yarom I. Lampl. Subthreshold oscillations of the membrane potential: a functional synchronizing and timing device. *J. Neurophysiol.*, 70:2181–2186, 1993.

Y. Yarom I. Lampl. Subthreshold oscillations and resonant behavior: two manifestations of the same mechanism. *Neuroscience*, 78:325–341, 1997.

E. M. Izhikevich. *Dynamical Systems in Neuroscience: The Geometry of Excitability and Bursting*. The MIT Press, Cambridge, London, 2007.

N. Burgess J. Huxter and J. O'Keefe. Independent rate and temporal coding in hippocampal pyramidal cells. *Nature*, 425:828–832, 2003.

M. Stemmler J. R. Schleimer. Coding of information in limit cycle oscillators. *Phys. Rev. Lett.*, 103:248105, 2009.

T. Jaeger. Neuronal coding of pacemaker neurons - a random dynamical systems approach. *Commun. Pur. Appl. Anal.*, 10:995, 2011.

E. T. Jaynes. Information theory and statistical mechanics. *Physical review*, 106(4):620, 1957.

P. I. M. Johannesma. Diffusion models for the stochastic activity of neurons. In E. R. Caianiello, editor, *Neural networks*, page 116. Springer, 1968.

D. H. Johnson. Point process models of single-neuron discharges. *J. Comput. Neurosci.*, 3:275, 1996.

J. B. Johnson. Thermal agitation of electricity in conductors. *Phys. Rev.*, 32:97, 1928.

R. Jolivet, A. Rauch, H.-R. Lüscher, and W. Gerstner. Predicting spike timing of neocortical pyramidal neurons by simple threshold models. *J. Comput. Neurosci.*, 21:35, 2006.

W. M. Kistler, W. Gerstner, and J. L. van Hemmen. Reduction of the Hodgkin-Huxley equations to a single-variable threshold model. *Neural Comput.*, 9:1015, 1997.

B. W. Knight. Dynamics of encoding in a population of neurons. *J. Gen. Phys.*, 59:734, 1972.

C. Koch. *Biophysics of Computation - Information Processing in Single Neurons.* Oxford University Press, New York, Oxford, 1999.

C. Koch, O. Bernander, and R. J. Douglas. Do neurons have a voltage or a current threshold for action potential initiation? *J. Comput. Neurosci.*, 2:63, 1995.

A. F. Kohn. Computer simulation of noise resulting from random synaptic activities. *Computers in biology and medicine*, 27:293, 1997.

L. Kostal, P. Lánský, and C. Zucca. Randomness and variability of the neuronal activity described by the Ornstein-Uhlenbeck model. *Network: Comput. Neural Systems*, 18: 63, 2007.

A. K. Kreiter and W. Singer. Oscillatory neuronal responses in the visual cortex of the awake macaque monkey. *Eur.J. Neurosci.*, 4:369, 1992.

P. Lánský and J. P. Rospars. Ornstein-Uhlenbeck model neuron revisited. *Biol. Cybern.*, 72:397, 1995.

L. Lapicque. Recherches quantitatives sur l'excitation électrique des nerfs traitéecomme une polarization. *J. Physiol. Pathol. Gen.*, 9:620, 1907.

P. E. Latham, B. J. Richmond, P. G. Nelson, and S. Nirenberg. Intrinsic dynamics in neuronal networks. i. theory. *J. Neurophysiol.*, 83:808, 2000.

H. Lecar and R. Nossal. Theory of threshold fluctuations in nerves: I. relationships between electrical noise and fluctuations in axon firing. *Biophys. J.*, 11:1048, 1971a.

H. Lecar and R. Nossal. Theory of threshold fluctuations in nerves: II. Analysis of various sources of membrane noise. *Biophys. J.*, 11:1068, 1971b.

C. D. Lewis, G. L. Gebber, P. D. Larsen, and S. M. Barman. Long-term correlations in the spike trains of medullary sympathetic neurons. *J. Neurophysiol.*, 85:1614, 2001.

B. Lindner. Interspike interval statistics of neurons driven by colored noise. *Phys. Rev. E.*, 69:022901, 2004.

B. Lindner. Correlations in sequences of first-passage times. volume 800, page 323. AIP, 2005.

B. Lindner. Low-pass Filtering of Information in the Leaky Integrate-and-Fire Neuron Driven by White Noise. In I. Visarath, A. Palacios, and P. Longhini, editors, *International Conference on Theory and Application in Nonlinear Dynamics (ICAND 2012)*, page 249. Springer, 2012.

B. Lindner, L. Schimansky-Geier, and A. Longtin. Maximizing spike train coherence or incoherence in the leaky integrate-and-fire model. *Phys. Rev. E.*, 66:031916, 2002.

B. Lindner, A. Longtin, and A. Bulsara. Analytic expressions for rate and CV of a type I neuron driven by white gaussian noise. *Neural. Comp.*, 15:1761, 2003.

B. Lindner, M. J. Chacron, and A. Longtin. Integrate-and-fire neurons with threshold noise - a tractable model of how interspike interval correlations affect neuronal signal transmission. *Phys. Rev. E.*, 72:021911, 2005.

R. R. Llinás. The contribution of Santiago Ramon y Cajal to functional neuroscience. *Nat. Rev. Neurosci.*, 4:77, 2003.

A. Longtin. Effect of noise on the tuning properties of excitable systems. *Chaos, Solitons and Fractals*, 11:1835, 2000.

A. Longtin and D. M. Racicot. Spike train patterning and forecastability. *Biosystems*, 40:111, 1997.

K. Lucas. The all or none contraction of the amphibian skeletal muscle fibre. *J. Physiol.*, 38:113, 1909.

B. N. Lundstrom, S. Hong, M. H. Higgs, and A. L. Fairhall. Two computational regimes of a single-compartment neuron separated by a planar boundary in conductance space. *Neural Comput.*, 20:1239, 2008.

A. N. Malahov. *Kumulyantnyıanaliz sluchaınykh negaussovskikh protsessov i ikh preobrazovanii.* Moskva, 1978.

P. Z. Marmarelis. *Nonlinear dynamic transfer functions for certain retinal neuronal systems.* PhD thesis, California Institute of Technology, 1972.

P. Z. Marmarelis and V. Z. Marmarelis. *Analysis of physiological systems.* Springer US, New York, 1978.

P. Z. Marmarelis and K.-I. Naka. White-noise analysis of a neuron chain: an application of the Wiener theory. *Science*, 175:1276, 1972.

P. Z. Marmarelis and F. E. Udwadia. The identification of building structural systems II. the nonlinear case. *B. Seismol. Soc. A.*, 66:153, 1976.

V. Z. Marmarelis. *Advanced methods of physiological system modeling*, volume 2. Springer US, New York, 2012.

G. Marsat and G. S. Pollack. Differential temporal coding of rhythmically diverse acoustic signals by a single interneuron. *J. Neurophysiol.*, 92:939, 2004.

E. Masry and S. Cambanis. Signal reconstruction after noisy nonlinear transformations. Technical report, DTIC Document, 1978.

C. Massot, M. J. Chacron, and K. E. Cullen. Information transmission and detection thresholds in the vestibular nuclei: single neurons vs. population encoding. *J. Neurophysiol.*, 105:1798, 2011.

J. C. Maxwell. A dynamical theory of the electromagnetic field. *Philos. T. R. Soc. Lond.*, page 459, 1865.

D. Middleton, Institute of Electrical, and Electronics Engineers. *An introduction to statistical communication theory.* McGraw-Hill, New York, 1960.

J. W. Middleton, M. J. Chacron, B. Lindner, and A. Longtin. Firing statistics of a neuron model driven by long-range correlated noise. *Phys. Rev. E.*, 68:021920, 2003.

J. W. Middleton, A. Longtin, J. Benda, and L. Maler. Postsynaptic receptive field size and spike threshold determine encoding of high-frequency information via sensitivity to synchronous presynaptic activity. *J. Neurophysiol.*, 101:1160, 2009.

R. Moreno, J. de la Rocha, A. Renart, and N. Parga. Response of spiking neurons to correlated inputs. *Phys. Rev. Lett.*, 89:288101, 2002.

C. Morris and H. Lecar. Voltage oscillations in the barnacle giant muscle fiber. *Biophys. J.*, 35:193, 1981.

B. Naundorf, F. Wolf, and M. Volgushev. Unique features of action potential initiation in cortical neurons. *Nature*, 440:1060, 2006.

M. P. Nawrot, C. Boucsein, V. Rodriguez-Molina, A-. Aertsen, S. Grün, and S. Rotter. Serial interval statistics of spontaneous activity in cortical neurons in vivo and in vitro. *Neurocomputing*, 70:1717, 2007.

A. Neiman and D. F. Russell. Stochastic biperiodic oscillations in the electroreceptors of paddlefish. *Phys. Rev. Lett.*, 86:3443, 2001.

A. Neiman and D. F. Russell. Models of stochastic biperiodic oscillations and extended serial correlations in electroreceptors of paddlefish. *Phys. Rev. E.*, 71:061915, 2005.

A. B. Neiman and D. F. Russell. Two distinct types of noisy oscillators in electroreceptors of paddlefish. *J. Neurophysiol.*, 92:492, 2004.

A. B. Neiman and D. F. Russell. Sensory coding in oscillatory electroreceptors of paddlefish. *Chaos*, 21:047505, 2011.

A. B. Neiman, D. F. Russell, and M. H. Rowe. Identifying temporal codes in spontaneously active sensory neurons. *Plos One*, 6:e27380, 2011.

H. Nyquist. Thermal agitation of electric charge in conductors. *Phys. Rev.*, 32:110, 1928.

S. Ostojic and N. Brunel. From spiking neuron models to linear-nonlinear models. *PLoS Comp. Biol.*, 7:e1001056, 2011.

A.-M. M. Oswald, M. J. Chacron, B. Doiron, J. Bastian, and L. Maler. Parallel processing of sensory input by bursts and isolated spikes. *J. Neurosci.*, 24:4351, 2004.

E. Overton. Beiträge zur allgemeinen Muskel-und Nervenphysiologie. *Pflueg. Arch. Eur. J. Phy.*, 92:115, 1902.

G. Pareti. The 'all-or-none' law in skeletal muscle and nerve fibres. *Arch. Ital. Biol.*, 145:39, 2007.

D. H. Perkel, G. L. Gerstein, and G. P. Moore. Neuronal spike trains and stochastic point processes: I. the single spike train. *Biophys. J.*, 7:391, 1967.

J. Platkiewicz and R. Brette. A threshold equation for action potential initiation. *PLoS Comput. Biol.*, 6:e1000850, 2010.

R. Price. A useful theorem for nonlinear devices having Gaussian inputs. *Information Theory, IRE Transactions on*, 4:69–72, 1958.

N. J. Priebe and D. Ferster. Inhibition, spike threshold, and stimulus selectivity in primary visual cortex. *Neuron*, 57:482, 2008.

A. Rauch. Neocortical pyramidal cells respond as integrate-and-fire neurons to in vivo-like input currents. *J. Neurophysiol.*, 90:1598, 2003.

A. Rauch, G. La Camera, H.-R. Luscher, W. Senn, and S. Fusi. Neocortical pyramidal cells respond as integrate-and-fire neurons to in vivo-like input currents. *J. Neurophysiol.*, 90:1598, 2003.

L. M. Ricciardi and L. Sacerdote. The Ornstein-Uhlenbeck process as a model for neuronal activity. *Biol. Cybernetics*, 35:1, 1979.

S. O. Rice. Mathematical analysis of random noise. *Bell Syst Tech J*, 23:282, 1944.

M. J. E. Richardson. Firing-rate response of linear and nonlinear integrate-and-fire neurons to modulated current-based and conductance-based synaptic drive. *Phys. Rev. E.*, 76:021919, 2007.

M. J. E. Richardson. Spike-train spectra and network response functions for non-linear integrate-and-fire neurons. *Biol. Cybern.*, 99:381, 2008.

M. J. E. Richardson, N. Brunel, and V. Hakim. From subthreshold to firing-rate resonance. *J. Neurophysiol.*, 89:2538, 2003.

F. Rieke, D. Warland, and W. Bialek. Coding efficiency and information rates in sensory neurons. *Europhys. Lett.*, 22:151, 1993.

F. Rieke, D. Warland, R. de Ruyter van Steveninck, and W. Bialek. *Spikes: Exploring the neural code*. MIT Press, Cambridge, Massachusetts, 1996.

J. Rinzel and B. Ermentrout. Analysis of Neural Excitability and Oscillations. In C. Koch and I. Segev, editors, *Methods in Neuronal Modeling: From Ions to Networks*, page 251. MIT Press, Cambridge, Mass., 1989.

H. Risken. *The Fokker-Planck Equation* (second edition, see appendix A.12). Springer, Berlin, 1989.

J. C. Roddey, B. Girish, and J. P. Miller. Assessing the performance of neural encoding models in the presence of noise. *J. Comp. Neurosci.*, 8:95, 2000.

K. Rogers. Scientific modeling, Encyclopædia Britannica. Encyclopædia Britannica Online, 2006. URL `http://www.britannica.com/science/scientific-modeling`.

C. Rossant, D. Goodman, B. Fontaine, J. Platkiewicz, A. Magnusson, and R. Brette. Fitting neuron models to spike trains. *Front. Neurosci.*, 5:9, 2011.

M. Rudolph and A. Destexhe. A fast-conducting, stochastic integrative mode for neocortical neurons in vivo. *J. Neurosci.*, 23:2466, 2003.

E. Salinas and T. J. Sejnowski. Correlated neuronal activity and the flow of neural information. *Nat. Rev.Neurosci.*, 2:539, 2001.

R. Schaette, T. Gollisch, and A. V. M. Herz. Spike-train variability of auditory neurons in vivo: Dynamic responses follow predictions from constant stimuli. *J. Neurophysiol.*, 93:3270, 2005.

W. R. Schlue, D. W. Richter, K. H. Mauritz, and A. C. Nacimiento. Responses of cat spinal motoneuron somata and axons to linearly rising currents. *J. Neurophysiol.*, 37: 303, 1974.

N. T. Schmandt and R. F. Galán. Stochastic-shielding approximation of Markov chains and its application to efficiently simulate random ion-channel gating. *Phys. Rev. Lett.*, 109:118101, 2012.

S. Schreiber, I. Erchova, U. Heinemann, and A. V. M. Herz. Subthreshold resonance explains the frequency-dependent integration of periodic as well as random stimuli in the entorhinal cortex. *J. Neurophysiol.*, 92:408, 2004.

S. M. Schuetze. The discovery of the action potential. *Trends Neurosci.*, 6:164, 1983.

T. Schwalger and B. Lindner. Theory for serial correlations of interevent intervals. *Eur. Phys. J. Spec. Topics*, 187:211, 2010.

T. Schwalger and B. Lindner. Patterns of interval correlations in neural oscillators with adaptation. *Front. Comp. Neurosci.*, 7:164, 2013.

T. Schwalger, K. Fisch, J. Benda, and B. Lindner. How noisy adaptation of neurons shapes interspike interval histograms and correlations. *PLoS Comp. Biol.*, 6:e1001026, 2010.

T. Schwalger, F. Droste, and B. Lindner. Statistical structure of neural spiking under non-Poissonian or other non-white stimulation. *J. Comput. Neurosci.*, 39:29, 2015.

C. J. Schwiening. A brief historical perspective: Hodgkin and Huxley. *J. Physiol.*, 590: 2571, 2012.

P. C. Schwindt and W. E. Crill. Factors influencing motoneuron rhythmic firing: results from a voltage-clamp study. *J. Neurophysiol.*, 48:875, 1982.

B. Sengupta, S. B. Laughlin, and J.E. Niven. Comparison of Langevin and Markov channel noise models for neuronal signal generation. *Phys. Rev. E*, 81:011918, 2010.

D. L. Sengupta and T. K. Sarkar. Maxwell, Hertz, the Maxwellians, and the early history of electromagnetic waves. *IEEE Antennas Propag. Mag.*, 45:13, 2003.

C. E. Shannon. Communication in the presence of noise. *P. Ire.*, 37:10, 1949.

C. E. Shannon. A mathematical theory of communication. *ACM SIGMOBILE Mobile Computing and Communications Review*, 5:3, 2001.

R. Shannon. The mathematical theory of communication. *Bell. Syst. Tech. J.*, 27:379, 1948.

N. Sharafi, J. Benda, and B. Lindner. Information filtering by synchronous spikes in a neural population. *J. Comp. Neurosci.*, 34:285, 2013.

L. Shiau, T. Schwalger, and B. Lindner. Interspike interval correlation in a stochastic exponential integrate-and-fire model with subthreshold and spike-triggered adaptation. *J. Comput. Neurosci.*, 38:589, 2015.

S. Shinomoto, Y. Sakai, and S. Funahashi. The Ornstein-Uhlenbeck process does not reproduce spiking statistics of neurons in prefrontal cortex. *Neural Comp.*, 11:935, 1999.

H. Sompolinsky, H. Yoon, K. Kang, and M. Shamir. Population coding in neuronal systems with correlated noise. *Phys. Rev. E.*, 64:051904, 2001.

T. L. Sourkes and L. G. Stevenson. *Nobel Prize winners in medicine and physiology, 1901-1965*. Number 45. Abelard-Schuman, London, 1967.

L. R. Squire. *The history of neuroscience in autobiography*, volume 4. Oxford University Press, New York, Oxford, 2011.

C. E. Stafstrom, P. C. Schwindt, J. A. Flatman, and W. E. Crill. Properties of subthreshold response and action potential recorded in layer v neurons from cat sensorimotor cortex in vitro. *J. Neurophysiol.*, 52:244, 1984.

R. B. Stein. A theoretical analysis of neuronal variability. *Biophys. J.*, 5:173, 1965.

R. B. Stein. Some models of neuronal variability. *Biophys. J.*, 7:37, 1967.

R. L. Stratonovich. *Topics in the Theory of Random Noise.* Gordon and Breach, New York, 1967.

S. P. Strong, R. Koberle, R. R. D. van Steveninck, and W. Bialek. Entropy and information in neural spike trains. *Phys. Rev. Lett.*, 80:197, 1998.

H. C. Tuckwell. *Introduction to Theoretical Neurobiology.* Cambridge University Press, Cambridge, 1988.

H. C. Tuckwell. *Stochastic Processes in the Neuroscience.* SIAM, Philadelphia, Pennsylvania, 1989.

H. C. Tuckwell and D. K. Cope. Accuracy of neuronal interspike times calculated from a diffusion approximation. *J. Theor. Biol.*, 83:377, 1980.

M. C. K. Tweedie. Statistical Properties of Inverse Gaussian Distributions. I. *Ann. Math. Stat.*, page 362, 1957.

F. E. Udwadia and P. Z. Marmarelis. The identification of building structural systems I. the linear case. *B. Seismol. Soc. A.*, 66:125, 1976.

G. E. Uhlenbeck and L. S. Ornstein. On the theory of the Brownian motion. *Phys. Rev.*, 36:823, 1930.

R.R. De Ruyter van Steveninck, G. D. Lewen, S. P. Strong, R. Koberle, and W. Bialek. Reproducibility and variability in neural spike trains. *Science*, 275:1805, 1997.

T. Verechtchaguina, I. M. Sokolov, and L. Schimansky-Geier. First passage time densities in resonate-and-fire models. *Phys. Rev. E*, 73:031108, 2006.

R. D. Vilela and B. Lindner. A comparative study of three different integrate-and-fire neurons: spontaneous activity, dynamical response, and stimulus-induced correlation. *Phys. Rev. E.*, 80:031909, 2009.

V. Volterra. *Theory of functionals and of integral and integro-differential equations.* Courier Corporation, Chicago, Illinois, 2005.

W. von Waldeyer-Hartz. *Über einige neuere Forschungen im Gebiete der Anatomie des Centralnervensystems.* G. Thieme, Leipzig, 1891.

M. C. Wang and G. E. Uhlenbeck. On the theory of Brownian motion II. *Rev. Mod. Phys.*, 17:323, 1945.

X-J. Wang. Ionic basis for intrinsic 40 Hz neuronal oscillations. *Neuroreport*, 5:221, 1993.

X. J. Wang and G. Buzsáki. Gamma oscillation by synaptic inhibition in a hippocampal interneuronal network model. *J. Neurosci.*, 16:6402, 1996.

T. F. Weiss. A model of the peripheral auditory system. *Kybernetik*, 3:153, 1966.

J. A. White, J. T. Rubinstein, and A. R. Kay. Channel noise in neurons. *Trends Neurosci.*, page 131, 2000.

N. Wiener. Response of a non-linear device to noise. Technical report, DTIC Document, 1942.

N. Wiener. *Nonlinear problems in random theory.* MIT Press, Cambridge, Massachusetts, 1966.

Publications concerning this thesis

Articles in scientific journals

- S. Blankenburg, W. Wu, B. Lindner, and S. Schreiber
  Information filtering in resonant neurons,
  J. Comp. Neurosci. **(39)**, Issue 3 (2015), p. 349-370

- S. Blankenburg and B. Lindner
  The effect of positive interspike interval correlations on neuronal information transmission,
  Math. Biosci. Eng. **(3)**, Issue 13 (2016), p. 461-481

Danksagung / Acknowledgments

An dieser Stelle möchte ich mich bei all den Personen bedanken, die mich in den letzten Jahren, während diese Arbeit entstanden ist, unterstützt und getragen haben.

An erster Stelle möchte ich mich bei meinen beiden Betreuern bedanken:

Frau Prof. Dr. Susanne Schreiber
&
Herrn Prof. Dr. Benjamin Lindner

Susanne hat maßgeblich dazu beigetragen, dass ich mich der computergestützten Neurowissenschaft in Form einer Dissertation genähert habe. Für diese Möglichkeit, die vielen Ratschläge und die Einbindung in das Kollegium des ITBs bin ich Ihr sehr dankbar. **Benjamin** gebürt eine Riesenportion Dank, da er mich vor allem wissenschaftlich förderte und forderte. Von Benjamin & Susanne habe ich gelernt, zielstrebiger und ausdauernder an einer wissenschaftlichen Fragestellung zu arbeiten, als ich es vorher für möglich hielt. Dafür vielen Dank!

Unendlich großer Dank gebürt auch meinen Kollegen: Nikola Schrenk, Alexandra Kruscha, Felix Droste, Jens Doose, Sergej Voronenko, Davide Bernardi, Florian Fruth, Tilo Schwalger, Stefan Wieland, Leonidas Eleftheriou, Jordi Giner-Baldó, Lucian Willareth und Rinaldo Betkiewicz; die in den letzten Jahren zu wichtigen (teilweise auch zu sehr wichtigen) Menschen in meinem Leben wurden.

Danke **Nikola**, für Deine Organisationstalente und Deine unmittelbar wärmende Mitmenschlichkeit, ohne die ich oftmals einfach versteinert gewesen wäre (*'out of competition'* heißt es bei den Filmfestspielen in Cannes); **Felix**, für die vielen wissenschaftlichen Diskussionen und Deine beispiellose Lässigkeit; **Sergej**, für die vielen humorvollen Momente in der Teeküche; **Jens**, für Deine nette und angenehme Art und den wohlduftenden Geruch von Chai auf dem Flur; **Alexandra**, für Deine Durchhalteparolen und vieles mehr; **Davide**, für Deine musikalische und charmante Art; **Tilo**, für Deine Begeisterung für die Neurowissenschaften, die theoretische Physik und für die vielen Tipps am Anfang meiner PhD-Zeit; **Leonidas**, für die vielen interessanten Diskussionen.

Ohne euch und eure Hilfe wäre diese Arbeit nicht denkbar gewesen. Man ist doch nie 'nur' wissenschaftlicher Miktarbeiter in einem Projekt, sondern vor allem auch *inter hominess esse*[1]. Habt vielen Dank dafür.

[1] Mir gefällt, wie das Wort hominess durch inter und esse (*Interesse*) umgeben ist.

Selbständigkeitserklärung

Ich erkläre, dass ich die vorliegende Arbeit selbständig und nur unter Verwendung der angegebenen Literatur und Hilfsmittel angefertigt habe.

Berlin, den 15. August 2016 Sven Blankenburg

Index

A

action potential 3
adaptation currents 36
all pass 145
all-or-none principle 3
asymmetry approach 43
attractor network model 81

B

band pass 52, 109, 130
band pass filter 15, 109
band-limited Gaussian white noise 47, 48
baseline current 20
Bussgang-theorem 132

C

characteristic function 43
circuit description 83
coefficient of variation 6
complementary error function 170
conditional entropy 11
conductance-based 88, 107
continuity equation (flux) 156
continuous nonlinear neuron models . 107
continuous nonlinearities 119
convolution of the probability densities 44
cross-correlation 83
cross-spectrum 10
curvature (coherence) . 16, 46, 143, 145, 146
cut-off frequency f_c 48

D

damped harmonic oscillator 81
damping factor 84, 167
diffusion approximation 21
distortion function 119

E

entropy 10, 11
entropy (conditional) 11
entropy (joint) 11
erf-sigmoidal SNL 121
erf-sigmoidal static nonlinearity . 140, 145
error function 170
evoked activity 47
exponential distortion function 119
exponential IF (EIF) 20
exponential integrate-and-fire 25
exponential SNL 121
exponential static nonlinearity . 120, 138, 141

F

fire-and-reset rule 81
firing rate 6
firing-rate resonances 81
fixed points 86
flux (probability) 156
Fokker-Planck equation 155
frequency preference 81
frequency-dependent signal transmission 11, 79
frequency-filtering characteristics 15

G

Gamma function 170
Gaussian process 121
generalized hypergeometric function . 170
generalized incomplete Gamma functions 142
generalized integrate-and-fire (GIF) .. 86
gradual transitions 167

H

Heaviside SNL 121
Hermite polynomials 134, 169
high pass filter 15
Hopf bifurcation 111
hypergeometric functions 170

I

identity static nonlinearity 121, 138
impedance function 84
incomplete beta function 171
information theory 9
information theory (Shannon) 11
information transmission 9
Integrate-and-fire 19
integrate-and-fire 155
integrator-LN-cascade 124, 143
inverse Gaussian 35, 38, 41
ion channels 3

J

joint entropy 11

K

kurtosis (inverse Gaussian) 159

L

leaky IF (LIF) 20
linear resonator model 82, 123
linear response 47
linear-nonlinear cascades 119, 169
linear-nonlinear neuron models 119
long term memory 36
Lorentzian spectrum 141
low pass 15, 51, 109, 127, 143, 146

M

measure of 'nonlinearity' 122
membrane potential 89
memory 36
mirroring rule 44
Monte-Carlo (MC) method 25
Monte-Carlo-Markov-Chain 111
Morris-Lecar (ML) 88
multiple convolutions 135, 144
mutual information 11
mutual information rate (lower bound) 12, 99

N

natural frequency 84
neural excitability 3
neural oscillators 81
non-renewal variant 35
nonlinearity functions 20

O

Ornstein-Uhlenbeck process 82

P

perfect IF (PIF) 20
phase-response-curve 116
physicist's Hermite polynomials 169
Pochhammer symbols 169
point processes 87
power spectrum 10
probabilist's Hermite polynomials 169
pyramidal cell 93

Q

quadratic IF (QIF) 20
quality factor 15, 84
quality factor (impedance) 85, 166

R

recovery variable 89
regularized hypergeometric function 145, 170
renewal variant 35
resonate-and-fire 86
resonator cartoon 89, 93, 166
resonator neuron models 79, 165
resonator-cartoon 127
resonator-LN-cascade model 123
response-response coherence 13, 117
reversal potentials 89
reverse construction approach 9
rhythmic activity 80
Richardson's integration method .25, 155

S

saddle-node bifurcation 88
saddle-node on an invariant circle (SNIC) 111
scaling factor α 44
serial correlation coefficient 40
signal-to-noise ratio 12
skewness (inverse Gaussian) 159
slope factor of the SNL 122
spectral stimulus-response coherence .12
spike train 6, 87
spike triggered rate (STR) 156
spontaneous activity 40, 162
static nonlinearities 119
stellate cell 93, 166

stochastic Hodgkin-Huxley model ... 111
stochastic IF neuron models 20
stochastic threshold and reset concept 37
stochastic threshold models 38
subcritical Hopf bifurcation 88
subthreshold membrane potential oscillations (MPOs) 79
subthreshold resonances 79, 81, 103, 111
susceptibility (PIF) 47
synchronous spiking behavior 81

T

theory I (power spectrum) 47
theory II (power spectrum) 48
threshold variability 35
threshold-and-reset concept 20
trade-off 105, 107, 132, 166
triangular ISI distributions 160, 162
tuning curve approach 7
type I neuron models 88, 107, 111
type II neuron models 88, 107, 111

V

variable spike-thresholds 37

W

Wiener method 9
Wiener-Khinchin theorem 157